Facies analysis and diagenetic evolution of the Dinantian carbonates in the Dutch subsurface: overview and synthesis

Report by SCAN

September 2019

Ministerie van Economische Zaken en Klimaat

ebn

TNO

Interreg
North-West Europe
DGE-ROLLOUT

This page intentionally left blank

Facies analysis and diagenetic evolution of the Dinantian carbonates in the Dutch subsurface: overview and synthesis

Written by:

Mahtab Mozafari[1], Peter Gutteridge[2], Alberto Riva[3], Kees Geel[4], Joanna Garland[2] and Julie Dewit[2]

September 2019

1- Energie Beheer Nederland (EBN), Daalsesingel 1, 3511 SV Utrecht, the Netherlands

2- Cambridge Carbonates Ltd, No. 4 The Courtyard, 707 Warwick Road, Solihull, B91 3DA, UK

3- G.E.Plan Consulting srl, Via L. Ariosto 58, 44121 Ferrara, Italy

4- Geological Survey of the Netherlands (TNO), Princetonlaan 6, 3584 CB Utrecht, the Netherlands

Version 1 (September 2019)
Version 2 (November 2019) – minor textual edits

This page intentionally left blank

Acknowledgements

This page intentionally left blank

Table of contents

List of figures and tables

1. Samenvatting/Executive summary

1.1 Doelstellingen van het onderzoek

Een eerste doelstelling van het onderzoek was het beoordelen van de bestaande gepubliceerde en commercieel verkrijgbare geologische gegevens met betrekking tot de bekkenevolutie, stratigrafie, sedimentologie en reservoirkwaliteit van het Dinantien in Nederland en aanpalende gebieden. Een tweede doel was het maken van een sedimentologische interpretatie van het Dinantien van onshore Nederland en aanpalende gebieden inclusief Zuidelijke offshore. De hiertoe onderzochte gegevens omvatten boorkernen, boorgruis, 'side-wall cores' en boorgatmetingen van bestaande boringen. die in het verleden geboord zijn voor de opsporing en produktie van koolwaterstoffen, water, aardwarmte of andere delfstoffen. Hiervan zijn sedimentaire facies beschreven en interpretaties van afzettingsmilieus gemaakt. Uit de boorkernen zijn monsters genomen voor specifieke analyses. De hieruit verkregen resultaten en eerder gepubliceerde data voor iedere boring zijn samengebracht in Appendix A. Deze Appendix bevat ook een lijst van de meest relevante referenties voor de betreffende boringen. De geproduceerde sedimentaire logs zijn als pdf en als CoreCAD-bestand als bijlage bij de individuele putrapporten bijgevoegd (Appendix B). Een derde doelstelling was het evalueren en, waar nodig, herzien van de bestaande biostratigrafische dateringen en correlaties teneinde de bestaande stratigrafische schema's van het Dinantien te verbeteren en te verfijnen. Hiertoe werden aanvullende biostratigrafische gegevens verkregen door bemonstering van geselecteerde kernen (Appendix A). Een vierde doel was het maken van een sequentie-stratigrafische correlatie van het Dinantian op basis van putgegevens en het extrapoleren van deze correlatie door de gehele ondergrond van Nederland, zowel onshore als (Zuidelijke) offshore (Appendix C). De stratigrafische gegevens worden gepresenteerd in drie correlatiepanelen: in zuidwest, zuidoost, en noord-Nederland. Een vierde paneel laat een regionale correlatie door het hele land zien. Om de geologische interpretatie in de gebieden tussen de putten te kunnen doen werden er seismische gegevens gebruikt, voor zo ver die beschikbaar waren. Seismiek werd eveneens gebruikt om, waar mogelijk, de verspreiding en evolutie van de geïsoleerde carbonaatplatforms en het voorkomen van karst in kaart te brengen. Een vijfde doel was het construeren van een serie paleogeografische kaarten met de verdeling van afzettingsmilieus op verschillende stratigrafische niveaus binnen het Dinantien. Er zijn ook kaarten geproduceerd met de verspreiding van de verschillende generaties van verkarsting. De paleogeografische kaarten worden aangeleverd middels een GIS-project. Een zesde doel was het begrijpen van de factoren die de reservoirkwaliteit bepalen van het Dinantien. Hiervoor zijn er gedetailleerde diagenetische studies op monsters uit boorkernen en ontsluitingen uitgevoerd met behulp van technieken zoals kathodeluminescentie, stabiele C, O en S isotopen, vloeistofinsluitingsanalyses en thermische metingen, waaronder vitrinietreflectie en palynomorfenverkleuringsindex. Tenslotte was verder een belangrijke doelstelling van deze studie het verstrekken van geologische informatie en feedback aan andere disciplines die bij deze studie betrokken waren, zoals petrofysica, geofysica, bekkenmodellering en reservoirsimulatie.

1.2 Conclusies

Bekkenevolutie: Het Nederlandse deel van het Noordwest-Europese Carboonbekken werd tijdens het laat-Devoon - vroeg-Dinantien gevormd door tektonische extensie, dat de belangrijkste structurele elementen creëerde die de daaropvolgende sedimentatie bepaalden. Eerst werd er tijdens het laat-Devoon - vroeg-Tournaisien terrestrisch klastisch materiaal

afgezet in Nederland, terwijl er tegelijkertijd carbonaatafzetting plaatsvond in het gebied ten zuidoosten van Nederland, het tegenwoordige Rijnlands leisteenplateau. Als gevolg van de veelvuldig optredende NE-SW/NNE-SSW-extensie tijdens het Dinantian vond er rifting plaats. Tijdens het Tournaisian - vroeg-Viséen begon de afzetting van carbonaat op verschillende tijdstippen vanwege de verschillende tijdstippen waarop onlap op de onderliggende basement structuren gebeurde. Het laat-Viseen was een tijd van opheffing rond de randen van het Londen-Brabant Massief wat, gecombineerd met een zeespiegeldaling, resulteerde in blootstelling en karstificatie van de Dinantische carbonaten. Het laat-Carboon was een periode van regionale bekkendaling, waarin een dikke sequentie klastische sedimenten van de Limburg Groep werd afgezet. Het laat-Carboon/vroeg-Perm was een periode van opheffing die samenviel met een thermische gebeurtenis die in een aantal putten terug te vinden is als diagenetische gebeurtenis. Verdere rifting tijdens het vroege Trias leidde tot regionale daling die doorging tot het einde van de Jura toen een fase van opheffing gepaard ging met een tweede thermische gebeurtenis. Tijdens het Krijt werden vroegere structuren geïnverteerd en opgeheven, met een belangrijke fase van verkarsting langs de noordelijke rand van het Londen-Brabant Massief. Dit werd gevolgd door algehele bekkendaling met de afzetting van chalk tijdens het laat-Krijt. De bodemdaling ging door tijdens het Tertiair, maar werd af en toe onderbroken door uplift events tijdens het laat-Krijt – vroeg-Paleoceen en het laat-Eoceen - vroeg-Oligoceen.

Sedimentologie: In deze studie werd de depositionele facies bepaald door middel van het bestuderen van boorkernen, ondersteund door de beschrijvingen van microfacies van side-wall cores en boorgruis. Het materiaal was afkomstig van 11 putten. In Zuid-Nederland ontwikkelden zich van laat-Tournaisien tot midden-Viseen "carbonate ramps" (carbonaathellingen) langs de noordelijke rand van het Londen-Brabant Massief. De afzettingsmilieus van deze ondiep-mariene hellingen omvatten 1) cyclische perimariene carbonaten die in de luwte achter "carbonate shoals" (ondieptes) werden afgezet; 2) gebioturbeerde packstone/wackestones die halverwege de helling werden afgezet; en 3) die gradueel overgaan in een diepwater distale hellingsfacies met daarin 'Waulsortian mud mounds'. Deze carbonaathellingen hadden een relatief flauwe helling van ongeveer 8-9°. Tijdens het laat-Viséen ontwikkelden deze hellingen zich tot carbonaatplatforms met een vlakke top en steil hellende randen bovenaan de helling (tot 30°) die bekkenwaarts overgaan in kleïige carbonaten. In Noord-Nederland werd tijdens het laat-Tournaisien - vroeg-Viséen een aantal geïsoleerde carbonaatplatforms gevormd op structurele hogen in een gebied wat gedomineerd werd door fijnkorrelige bekkensedimentatie. Deze carbonaatplatforms werden op verschillende tijden gevormd.

Sequentiestratigrafie: Er is een hoog-resoluut sequentie-stratigrafisch schema ontwikkeld op basis van log-, kern-, en biostratigrafische gegevens. Het schema is gebaseerd op de carbonaat 'ramp'- en 'shelf' systemen in zuidwest Nederland, omdat dit gebied de hoogste concentratie putten heeft. Er werden drie regionale sequenties herkend, die ieder bestaan uit 10 afzettingscycli die ieder een 3e orde sedimentaire sequentie representeren. Deze depositionele cycli werden ook herkend en gecorreleerd met bekkenopeenvolgingen in zuidoost en midden-Nederland en met de geïsoleerde carbonaatplatforms in noord-Nederland. Dankzij de biostratigrafische resolutie kunnen deze afzettingscycli worden gegroepeerd in drie reeksen van lagere orde van laat-Tournaisien tot het vroegste Molinacien, midden- tot laat-Molinacien en Warnantien.

Seismische stratigrafie: Er is een seismisch-stratigrafische studie uitgevoerd om de aanwezigheid van mogelijke carbonaatplatforms op structurele hogen in Noord-Nederland te identificeren. De structurele hogen van Uithuizermeeden en Luttelgeest bevatten carbonaatplatforms die aangeboord zijn. Interne reflectoren die te zien zijn op 3D-seismiek van

het Uithuizermeeden-platform geven de indruk dat de carbonaatsedimentatie begon op de zuidwestelijke rand van de structuur, waarbij het carbonaatplatform geleidelijk over het hoog migreert naar het noordoosten. Waarschijnlijk zijn er carbonaatplatforms aanwezig op een deel van de Fryslân en Nagele structuren, maar andere structurele hogen in Noord- en Midden-Nederland zijn bedekt door fijnkorrelige Dinantien bekkensedimenten, of het zijn kale structuren zonder Dinantien sediment. Een uitgebreide seismische interpretatie is uitgevoerd als afzonderlijk project waarvan het rapport beschikbaar is op de NLOG-website, Ten Veen *et al.*, 2019.

Karst: Er zijn drie hoofdfases van karst geïdentificeerd uit kern- en seismische gegevens. Intra-Dinantien karst (3e orde of hoger) komt voor aan de top van de sedimentaire cycli en kan in boorkernen worden herkend door de aanwezigheid van Dinantien bioclasten in karstholtes. Karst is ook aanwezig in de Dinantien carbonaten op de overgang Viséen-Namurien langs de noordelijke rand van het London-Brabant Massif. In boorkernen manifesteert deze karst zich als opvulling van breuken en holtes in de vorm van donkere 'mudstone' en als intervallen van breccie-conglomeraten. Deze laatste worden geïnterpreteerd als karstinstorting of karstopvulling.

Er is ook seismiek gebruikt om de karstverschijnselen in kaart te brengen. Ze worden gekenmerkt door chaotische reflectoren en door indicaties voor dolines. Onder de Basis Krijt discordantie zijn er ook goed ontwikkelde karstsystemen aanwezig, die in boorkernen kunnen worden herkend door de aanwezigheid van holtes en scheuren die zijn opgevuld met glauconitische en bioclastische sedimenten van Campanien-Maestrichtien ouderdom. De verticale penetratie van dit karstsysteem is minstens 177 m onder de Basis Krijt discordantie.

Paleogeografische kaarten: Er zijn paleogeografische kaarten geconstrueerd voor elk van de drie regionale depositionele sequenties. De kwaliteit van deze kaarten wordt dusdanig bepaald door de kwaliteit en beschikbaarheid van de seismische gegevens, dat er aparte kaarten zijn gemaakt met de betrouwbaarheid van de faciesinterpretaties voor elk van de drie depositionele sequenties. De facieskaarten worden nog verder beperkt door het voorkomen van karst, truncatie door de Basis Namurien en Basis Krijt discordanties, en door seismische geometrieën die geassocieerd zijn met onlap tegen carbonaatplatformranden en carbonaat buildups.

Diagenese en reservoirkwaliteit:

o Vroege neerslag van mariene en meteorische calciet in de matrix van de kalksteen resulteert in verstopping of vermindering van de primaire poriën.

o Uitgebreide karstificatie: veel van de karstholtes zijn opgevuld met sediment waardoor er nauwelijks toename van porositeit zichtbaar is in boorkernen. Daarentegen is karst zeer heterogeen en gezien het feit dat er in Loenhout (België) gasopslag plaatsvindt in verkarst (en verbreukt) Dinantien, lijkt het redelijk om aan te nemen dat er grote poreuze karstsystemen aanwezig kunnen zijn in de Dinantien carbonaten van zuidwest en zuidoost Nederland.

o Over het algemeen is de porositeit en permeabiliteit in niet-gedolomitiseerde kalksteen laag. In putten waar dolomitisatie is waargenomen, b.v. O18-01, KTG-01, BHG-01 en LTG-01, wordt matige tot goede interkristal- en 'biomouldic' porositeit aangetroffen en deze putten hebben naar verwachting een matige tot goede reservoirkwaliteit, in ieder geval in delen van de Dinantien sectie. Dolomitisatie kan resulteren in zeer variabele matrixreservoireigenschappen (2-6% en in sommige intervallen tot 15%) en is soms lokaal aanwezig onder afdichtende lagen. Ook kunnen aders met 'saddle' dolomiet wijzen op de aanwezigheid van lokale vuggy porositeit. Hoewel de

reservoireigenschappen van dolomietlichamen slecht kunnen zijn, zal de grotere brosheid van dolomiet in vergelijking met kalksteen kunnen resulteren in een hogere hoeveelheid 'fractures' (scheuren) in dolomietlichamen. Bovendien kunnen aders met 'saddle' dolomietcement wijzen op de mogelijke aanwezigheid van breukzones die de permeabiliteit aanzienlijk zouden kunnen verhogen.

o De reservoirkwaliteit in zowel kalksteen als dolomiet neemt behoorlijk toe door de aanwezigheid van scheurtjes die samenhangen met het voorkomen van breuken en karstverschijnselen, vooral geassocieerd met de Basis Krijt en Basis Namurien discordanties langs de noordoostelijke rand van het London-Brabant Massief. Het grootste risico is dat de karstporositeit opgevuld is met impermeabel sediment en cement. De beste geothermische reservoireigenschappen worden gevormd door een combinatie van scheuren in breukzones en karst onder de Basis Permische Discordantie in de putten in Californië.

o De reservoirkwaliteit van de Dinantien fijnkorrelige bekkensedimenten is in een klein gebied van Limburg door de intensieve verwering onder de Basis Krijt discordantie sterk verbeterd. De resulterende porositeit loopt op tot 50%, maar het Dinantien ligt zeer dicht bij het oppervlak en en bestaat voornamelijk uit microporositeit waardoor de matrixpermeabiliteit laag is.

1.3 Aanbevelingen

De belangrijkste doelen voor geothermische exploratie in het Dinantien Kalksteen zijn de Basis Namurien en Basis Krijt verkarsting en de aanwezigheid van scheuren en oplossingsholtes geassocieerd met breukzones. De Basis Namurien karst is ook geassocieerd met sulfidemineralisatie die, samen met de verhoogde porositeit, aantoont dat Basis Namurien karstsystemen fungeerden als doorvoerkanalen voor vloeistofstromen uit dieper gelegen formaties. Dolomietlichamen zouden wellicht wat extra opslagcapaciteit bieden voor een geothermisch reservoir, maar moeten dan wel aangesloten zijn op een breuksysteem om effectief te zijn.

Wij doen de volgende aanbevelingen voor verdere definitie van deze geothermische plays: Om depositionele geometrieën in het Dinantien vast te leggen en karstfenomenen zoals dolines, karstinstorting en karsttopografie te identificeren en in kaart te brengen is meer en betere seismiek nodig. Seismische attributen van 3D seismiek zouden gebruikt kunnen worden om breukentrends te identificeren en in kaart te brengen. Meer (3D) seismiek en een hogere kwaliteit van de seismiek zou met name belangrijk zijn voor het gebied rondom de Winterswijk put, ten noorden van de geothermische installaties van Californië en in de Roerslenk in zuid-Nederland, waar de omvang van het carbonaatplatform (of platforms) nog zeer onzeker is.

Er is tot nu toe geen gedetailleerde studie verricht naar de factoren die de goede reservoirkwaliteit van de Californië-putten bepalen. Een dergelijke studie zou zich moeten richten op de aanwezigheid en herkomst van de dolomitisatie, het voorkomen van matrix- en fracture porositeit en permeabiliteit en de interactie tussen karst en breuken. Een dergelijk onderzoek vraagt om meer seismische data in dat gebied. Onderzoek naar microfacies, diagenese en reservoirkwaliteit is zeer wenselijk en zou uitgebreid kunnen worden met de overige, nog niet publieke, Californië putten.

Om een goed model van de ondergrond te bouwen dat geschikt is voor de diepe geothermische exploitatie is het in de eerste plaats noodzakelijk om goede gegevens te hebben, zoals seismiek, maar ook een complete reeks boorgatmetingen en een goede bemonsteringsstrategie voor

stratigrafie en diagenese. We raden daarom voor nieuwe boringen in Dinantien een uitgebreid gegevensacquisitieprogramma aan met 'borehole image logs' om niet alleen informatie te verzamelen over de facies, maar ook over scheur- en breukpatronen. Ook het nemen van boorkernen, 'side wall cores', samen met gedetailleerde bemonstering van cuttings wordt van harte aanbevolen.

De gegevens van de ondergrond zouden kunnen worden aangevuld met analoge studies in ontsluitingen van breuken, paleo- en huidige stressregimes en karst-gerelateerde diagenese. Dit zou onze kennis van de verspreiding en bepalende factoren op reservoirkwaliteit voor zo ver die gerelateerd zijn aan breuken, enorm doen toenemen. Deze analogen moeten zowel gescheurde en verbreukte dolomieten bevatten als kalksteen. Het doel van deze studies is om de scheurenpopulatie en hun verspreiding te voorspellen in relatie tot breuken die op seismiek zichtbaar zijn, en om het verband te begrijpen tussen diagenetische processen, breuken en reservoirkwaliteit. Analogen van breuken die door karst worden verbreed, kunnen ook worden bestudeerd om meer grip te krijgen op de geometrie van dergelijke reservoirs.

Gegevens uit omringende landen kunnen zeer nuttig zijn om het gedrag te begrijpen van Dinantien carbonaten bij het produceren van vloeistoffen. Gegevens uit België zijn in dit geval bijzonder belangrijk, omdat er al enkele ondergrondse projecten zijn die deze aquifers/reservoirs exploiteren voor aardwarmte en gasopslag.

Executive summary

1.4 Aims of study

A first aim of the study was to review the existing published and commercially available geological data on the basin evolution, stratigraphy, sedimentology and reservoir quality distribution of the Dinantian carbonates of the Netherlands and surrounding areas. A second aim was to undertake a sedimentological interpretation of the Dinantian carbonates of the Netherlands and surrounding areas. Data examined included cores, cuttings, sidewall cores and log data from existing wells drilled for hydrocarbons, water, geothermal resources and other purposes. Descriptions and interpretations of sedimentary facies and depositional environments were undertaken. Additional samples were collected from core for selected analyses. The obtained results and the pre-existing published data on each well is presented in the Appendix A. This appendix also includes a list of the most relevant references on the studied wells. Core logs are presented as pdf and as CoreCAD files in appendices (Appendix B) to the individual well reports. A third goal was to review and revise existing biostratigraphic dating and correlations to improve and refine existing Dinantian stratigraphic schemes. This included obtaining additional biostratigraphic information (Appendix A) by sampling selected cores. A fourth aim was to establish a sequence stratigraphic correlation (Appendix C) of the Dinantian carbonates based on log data and to extrapolate this correlation to the whole of the Netherlands subsurface including offshore as well as onshore. Stratigraphic data are presented in an associated Petrel project that includes 3 correlation panels of the SW, SE and N Netherlands and a fourth panel to show a regional correlation across the whole country. Seismic data (if available) were used to constrain the geological interpretation in areas between wells. Seismic data were additionally used to map the distribution and evolution of isolated carbonate platforms and the occurrence of karst. A fifth aim was to construct a series of palaeogeographic maps showing the distribution of depositional environments at selected stratigraphic levels within the Dinantian carbonates. Maps showing the distribution of various karst generations were also produced. A sixth aim was to understand the controls and distribution of reservoir quality through the Dinantian. This involved detailed diagenetic studies on selected core and outcrop samples using techniques including cathodoluminescence, stable C, O and S isotopes, fluid inclusion analyses and thermal measurements including vitrinite reflectance and spore colouration. Finally, a further aim of this study was to provide geological information and feedback to other groups involved in this study including petrophysics, geophysics, basin modelling and reservoir simulation.

1.5 Conclusions

Basin evolution: The Dutch part of the Northwest European Carboniferous Basin formed during an extensional tectonic event throughout the Late Devonian to early Dinantian. This event created the main structural elements that controlled subsequent sedimentation. There was initial deposition of terrestrial clastics over the Netherlands during the Late Devonian to early Tournaisian with carbonate depositional systems of equivalent age present in the Rhenish Mountains to the south of the Netherlands. Rifting took place in response to NE-SW/NNE-SSW extension that episodically occurred throughout the Dinantian time. Carbonate deposition was initiated at different times during the Tournaisian to early Visean owing to differing times of local onlap of the basement structures. The end Visean was a time of uplift around the margins of the London-Brabant Massif that, combined with a sea-level drop, resulted in exposure and karstification of the Dinantian carbonates. The Late Carboniferous was a period of regional subsidence during which, the thick Limburg Group clastics were deposited. The Late Carboniferous/Early Permian was a period of uplift associated with a thermal event recorded as various diagenetic events in a number of wells. Further rifting during Early Triassic

lead to regional subsidence that continued until the end of Jurassic when a phase of uplift accompanied by a second thermal event occured. During the Cretaceous, pre-existing structures were inverted and uplifted, with a major phase of karstic exposure along the northern margin of the London-Brabant Massif. This was followed by general subsidence and deposition of the Late Cretaceous chalk. Subsidence continued during the Tertiary punctuated by uplift events during the late Cretaceous/early Palaeocene and late Eocene/early Oligocene.

Sedimentology: Depositional facies defined in this study were supported by microfacies study of the cores, sidewall cores and cuttings from 11 wells. In the southern Netherlands, Late Tournaisian to mid Visean carbonate ramps developed along the northern margin of the London-Brabant Massif. Shallow ramp depositional settings include cyclic peritidal carbonates sheltered behind carbonate shoals, bioturbated packstone/wackestone were deposited in mid ramp settings passing into deep-water distal ramp facies with speculated Waulsortian carbonate mud mounds. These carbonate ramps had relatively gentle depositional slopes of some 8-9°. During the late Visean, these ramps developed into flat-topped carbonate platforms with more steeply-dipping margins at the uppermost slope (up to 30°) that passed down dip into basinal argillaceous carbonates. In the northern Netherlands, a number of isolated carbonate platforms were initiated at various times during the late Tournaisian to early Visean over structural highs in an area of overall basinal sedimentation. These isolated platforms had relatively higher depositional slopes of up to 12°.

Sequence stratigraphy: A high resolution sequence stratigraphic scheme based on log and core data, constrained by biostratigraphic data was based around the carbonate ramp and shelf systems in SW Netherlands since this area has the highest concentration of wells data. Three regional sequences consist of 10 depositional cycles were recognised. These depositional cycles were also identified and correlated with basinal successions in SE and central Netherlands and with isolated carbonate platforms in the northern Netherlands. Biostratigraphic resolution allows these depositional cycles to be grouped into three lower order sequences (3rd order) of late Tournaisian to earliest Molinacian, mid- to late-Molinacian and Warnantian ages.

Seismic stratigraphy: A seismic stratigraphic study was undertaken to identify the presence of possible carbonate platforms over structural highs in the northern Netherlands. Carbonate platforms, confirmed by cored wells, are present over Uithuizermeeden and Luttelgeest structures. Internal reflectors seen on the 3D seismic grid over the Uithuizermeeden platform suggest that the carbonate sedimentation was initiated over the southwestern margin of the structural high with the carbonate platform progressively onlapping the exposed high to the northeast. A carbonate platform is likely to be present over at least part of the Fryslân and Nagele Highs, however, other positive structures in the northern and central Netherlands are considered to be either draped by basinal Dinantian sediments or are highs with no deposition during the Dinantian time. A comprehensive seismic image analysis has been conducted as a separate project and report is available on the NLOG website.

Karst: Three main phases of karst were identified from core and seismic data. Intra-Dinantian karst (3rd order or higher) occur at the tops of depositional cycles and is recognised in core by the presence of Dinantian bioclasts that infill karst cavities. Karst is also present in Dinantian carbonates at the Visean-Namurian (sub-Namurian) boundary along the northern margin of the London-Brabant Massif. This is identified in core as infills of enlarged fractures and cavities by dark mudstone and intervals of breccio-conglomerates interpreted as karst collapse or karst fill. Seismic data, although limited, were also used to map the distribution of karst collapse features characterised by chaotic and rugose reflectors and the presence of doline collapse structures. Karst systems are also developed beneath the sub-Cretaceous unconformity, which was recognised in core by the presence of cavities and enlarged fractures infilled by glauconitic

and bioclastic sediments dated as Campanian-Maastrichtian. The vertical penetration of this karst system may be at least 177 m beneath the sub-Cretaceous unconformity.

Palaeogeographical mapping: Palaeogeographical maps were constructed for each of the three lower order regional depositional sequences. These maps were constrained by the quality of the seismic data and aerial coverage such that maps showing the confidence of interpretation of facies distribution were produced for each sequence. The facies maps were also constrained by the distribution of karst features, truncation at the sub-Namurian and Cretaceous unconformities and seismic geometries associated with onlap against carbonate platform margins and carbonate build-ups.

Diagenesis and reservoir quality:

- o Early marine and meteoric calcite precipitation observed in the matrix of the limestone results in the occlusion or reduction of primary pores.
- o Extensive karstification: Much of the karst cavities are filled with sediment and no major net porosity enhancement is observed in core. However, karst is known to be highly heterogenous and given the fact that in Loenhout (Belgium) a gas storage facility is developed in karstified Dinantian it is reasonable to assume that large porous karst bodies can potentially be present in the Dinantian carbonates of the SW and SE Netherlands.
- o In general, porosity and permeability in non-dolomitised limestones is poor. Dolomitisation observed in some wells, e.g. O18-01, KTG-01 (Kortgene-01), BHG-02 (Brouwershavense Gat-01) and LTG-01 (Luttelgeest-01), contains moderate to good intercrystal and biomouldic porosity and is expected to have moderate to good reservoir quality. However, dolomitisation can result in highly variable matrix reservoir properties (2-6% and in some limited intervals up to 15%) and may be developed locally below sealing units. Moreover, mineralised intervals in close association with saddle dolomitisation exhibit local vuggy porosity. While the matrix reservoir properties of dolomite bodies may be low, the more brittle nature of dolomite compared to limestone is expected to result in a higher fracture density in dolomite bodies. Additionally, veins cemented by saddle dolomites may testify to the possible presence of fractured zones allowing for a better reservoir flow.
- o Reservoir quality in both limestone and dolomite can be improved by the development of fractures associated with faults and karstic macropore systems, particularly associated with the sub-Namurian and sub-Cretaceous unconformities along the NE margin of the London-Brabant Massif. The main risk is the infill of karstic porosity by impermeable sediment and cement. The best geothermal reservoir properties are associated with a combination of fracturing associated with faulting and sub-Permian karst in the Californië wells.
- o Sub-Cretaceous weathering was able to improve reservoir quality of basinal Dinantian sediments in a restricted area of the Limburg province. The resulted porosity is up to 50%, but it is very close to surface and mostly consists of microporosity and hence matrix permeability is low.

1.6 Recommendations

The main targets for geothermal exploration could be the sub-Namurian and sub-Cretaceous karst systems in the Dinantian and fractures/dissolution development associated with fault corridors. The sub-Namurian karst is also associated with sulphide mineralisation that in addition to enhancing porosity, demonstrates that sub-Namurian karst systems acted as conduits for deep-seated fluid flow from basins. Dolomitised bodies may also provide some additional

storage capacity for a geothermal reservoir but may need to be connected to a fracture system to be an effective reservoir.

The recommendations for further definition of these geothermal plays:

Improved seismic imaging is required to capture Dinantian depositional geometries and to identify and map karst features such as dolines, karst collapse and karst topography. Seismic attributes from 3D seismic should be used to identify and map fault and fracture trends. Improved seismic data coverage and quality would be particularly important for the area towards the Winterswijk well, north of the Californië geothermal field and in the Roer Valley Graben in southern Netherlands, where the extent of the carbonate platform(s) is still uncertain.

There is, as yet, no detailed study on the controls on reservoir quality in the Californië wells that is a demonstrably successful geothermal system. Such a study may include an investigation into the distribution and origin of dolomitisation, the occurrence of matrix and fracture porosity and permeability and the interplay of karst and faulting. A study of microfacies, diagenesis and porosity and permeability is needed and could be extended to the additional Californië wells.

To build a proper subsurface model suitable for the deep geothermal exploitation, it is necessary at first to have good data, such as seismic, but also a complete suite of wireline logs and a proper sampling strategy for stratigraphy and diagenesis. We therefore recommend a comprehensive program of data acquisition that includes image logs to provide information not only on the facies, but also on fracture and fault patterns. Acquisition of core, sidewall cores, together with detailed sampling of cuttings.

Sub-surface data could be augmented by additional work on analogue studies of fault, palaeo- and current stress regimes, and karst-related diagenesis at outcrop and may improve our understanding of the distribution and controls on reservoir quality associated with faulting. Analogues should include faulted and fractured dolomites as well as limestone. The aims of these studies would be to predict the fracture population and their distribution in relation to seismic-scale faults, and to understand the link between diagenetic processes, faulting and reservoir quality. Analogues of faults exploited by karst could also studied to understand the geometry of such reservoirs.

Data from surrounding countries could be extremely useful to understand the behavior of Dinantian carbonates when producing fluids: Belgian data are particularly important in this case, as there are already some subsurface projects exploiting these aquifers/reservoirs for geothermal energy and gas storage.

2. Introduction

Geothermal energy systems have been considered as a potential alternative for the fossil energy use. Currently, geothermal projects are already in use in the Netherlands. However, the application of geothermal energy in existing projects is not adequate for the provision of high-temperature heat for, as an example, the process industry. It is anticipated that Ultra Deep Geothermal (UDG) energy could potentially make a substantial contribution to the transition towards a sustainable energy supply. To reach sufficiently high temperatures (>130°C) in the Netherlands, geothermal reservoirs at depths of over 4 km are required. The Dutch subsurface at these depths has not been explored extensively until now and is therefore relatively unknown. Based on the limited amount of subsurface data, the Lower Carboniferous (Dinantian) carbonates were identified by Boxem *et al*. (2016) as the most promising target matching the initial requirements for UDG.

The study reported in this document is a result of SCAN, a government funded program to scope out the potential of geothermal energy, including the Dinantian carbonates. This program includes a range of subsurface studies of the Dinantian carbonates. The results of the SCAN studies will be released and become available via www.nlog.nl.

The geological studies presented in this report assess the quality of the Dinantian carbonates as potential host rocks for development of UDG systems, and is supported by the detailed reports on individual well analyses presented as appendices. The aim is to provide insights into the factors controlling or pre-conditioning the reservoir characteristics, particularly porosity and permeability. Moreover, the data obtained will enable the prediction of their nature, e.g. fractured vs matrix porosity, and distribution of the potential reservoirs on local and regional scales. This report is based on an integrated approach evaluating a collection of published reports, data bases, seismic data, well logs and detailed core and thin sections analysis. Accordingly, the geometry and paleogeography of the Dinantian carbonates are depicted as maps. The lithology, facies analysis and depositional environments (e.g. inner platform, outer platform vs basinal) of the studied carbonates are defined. The diagenetic modifications enhancing or destroying the reservoir quality are pinpointed. Subsequently, by integration of the petrography, microthermometry data and constructed burial history curves, the diagenesis and fluid evolution are linked to the geodynamics of the area. To conclude, a regional trend for the carbonate depositional system, dominant diagenetic characteristics and regional reservoir quality is proposed.

3. Databases, literature and information available

This study benefited from the available data provided by 26 wells (Figures 3-1 and 3-2) that penetrated the Dinantian carbonates of the Netherlands (Tables 3-1 and 3-2). For a better constraint and larger geological extent of the data, a number of wells from UK and north Belgium (12 wells; Table 3-3) and west Germany (4 wells; Table 3-4) were also included in this study. However, some of the data were only partially publicly available (e.g. wells CAL-GT-04 and 05 were still confidential at the time of this study).

3.1 The Netherlands wells

Wireline logs were only available for 15 wells, while for nine wells, the data used were only from published literature. The (limited) data from two wells (CAL-GT-04 and CAL-GT-05) were confidential, so only the locations of the wells were available.

Table 3-1: Wells in the Netherlands that have been drilled within the Dinantian.

Code	Extended name	Availability of data
BHG-01	BROUWERSHAVENSE GAT-01	Yes
CAL-GT-01	CALIFORNIE-GT-01	Yes
CAL-GT-02	CALIFORNIE-GT-02	Yes
CAL-GT-03	CALIFORNIE-GT-03	Yes
CAL-GT-04	CALIFORNIE-GT-04	No, Confidential until 2021
CAL-GT-05	CALIFORNIE-GT-05	No, Confidential until 2021
DB-105	DIEPBORING-105 HOUTHEM	Partial, only literature data
DB-106	DIEPBORING-106 GULPEN	Partial, only literature data
DB-108	DIEPBORING-108 MESCH	Partial, only literature data
DB-109	DIEPBORING-109 CADIER EN KEER	Partial, only literature data
DB-123	DIEPBORING-123 KASTANJELAAN	Partial, only literature data
GVK-01	GEVERIK-01	Yes
HEU-01	HEUGEM-01	Yes
KSL-02	KASTANJELAAN-02	Yes
KTG-01	KORTGENE-01	Yes
LTG-01	LUTTELGEEST-01	Yes
O18-01	O18-01	Yes
P16-01	P16-01	Yes
S02-02	S02-02	Yes
S05-01	S05-01	Yes
THM-2000	THERMAE-2000	Partial, only literature data
THM-2001	THERMAE-2001	Partial, only literature data
THM-2001	THERMAE-2002	Partial, only literature data
UHM-02	UITHUIZERMEEDEN-02	Yes
WDR-01	WOENSDRECHT-01 (former DB-17)	Partial, only literature data
WSK-01	WINTERSWIJK-01	Yes

Table 3-2: Available data for the Dutch wells drilled in the Dinantian carbonates. The * and ** indicate the new performed analyses, and the wireline logs that were digitised during this study, respectively.

Well name	Well tops	Wireline logs	Biostrat	Litholog	Core Total length (m)	New core description	CCAL	Core thin sections	Cuttings TS	C and O Isotopes	S Isotopes	FI	VR	Purpose	Year of drilling
BHG-01	X	X	X*	X	25.8	X	X	74+6*	-	9*	3*	2	10+2*	HC- exploration	1978
CAL-GT-01	X	X	-	-	-	-	-	-	X	-	-	-	-	Geothermal energy	2012
CAL-GT-02	X	X	-	-	-	-	-	-	12	-	-	-	-	Geothermal energy	2012
CAL-GT-03	X	X	-	-	-	-	-	-	-	-	-	-	-	Geothermal energy	2012
DB-105	X	-	-	-	-	-	-	-	-	-	-	-	-	Exploration	1920
DB-106	X	-	-	-	-	-	-	-	-	-	-	-	-	Exploration	1920-1921
DB-109 Cadier en Keer	X	-	X	X	-	-	-	-	-	-	-	-	-	Exploration	1920-1921
DB-108 MESCH	X	-	X	-	-	-	-	-	-	-	-	-	-	Exploration	1922
DB-123 Kastanjelaan	X	-	X	-	-	-	-	-	-	-	-	-	-	Exploration	1927-1929
GVK-01	X	X	X	X	695	-	X+SCAL	-	-	2	-	1	31	Exploration	1986
HEU-01	X	X**	-	-	188	X	X	70	-	-	-	-	-	Mineral water	1981
HEU-01-S1	X	X**	-	-	193	X	X	33	-	-	-	-	13	Mineral water	1981
KSL-02	X	X**	-	-	164	X	X	43+5*	-	7*	-	1*	5	Mineral water	1981
KTG-01	X	X	X*	X	51	X	X	69+5*	-	18*	-	2*	-	HC- exploration	1982
LTG-01	X	X	X	-	5.5	X	X	9	16	-	-	-	-	HC- exploration	2004-2005
O18-01	X	X	X	X	53	X	X	23+2*	1	37+4*	-	2+1*	13	HC- exploration	1991
P16-01	X	-	X	X	-	-	-	-	-	-	-	-	18	HC- exploration	1991
S02-02	X	X	X	-	16	X	-	18	-	-	-	-	22	HC- exploration	1983
S05-01	X	X	X	-	127	X	X	228+4*	-	14*	-	-	5	HC- exploration	1981
THERMAE – 2000	X	-	-	-	-	-	-	-	N.A.	-	-	-	7	Mineral water	1985-1986
THERMAE – 2001	X	-	-	-	-	-	-	-	-	-	-	-	-	Mineral water	1985-1986
THERMAE – 2002	X	X	-	-	-	-	-	-	N.A.	-	-	-	9	Mineral water	1985-1986
UHM-02	X	X	X*	-	7	X	X	19	198	12	-	1	1*	HC- exploration	2001
WDR-01	X	-	X	X	N.A.	-	-	-	-	-	-	-	-	HC/coal- exploration?	1912-1914
WSK-01	X	X	X	X	7.4	X	X	11	-	-	-	-	5	HC- exploration	1977-1978

Figure 3-1: Map showing all the wells penetrating the Dinantian carbonates. The wells were studied either through direct observation or through reference to existing published literature and reports. The ones that are indicated in red have not been used in this study. The dashed rectangle includes the wells in the Limburge province and Belgium (shown in Figure 3-2).

3.2 Belgium, UK and Germany wells

In order to compare the Dutch wells with the geology of the surrounding regions, we included the data wells from Belgium (Table 3-3) and Germany (Table 3-4) in this study. For most of the wells, a full suite of data was not available and thus the study relied mostly on the publicly available literature. In some cases, only the wireline logs were available (e.g. MOL-GT-01).
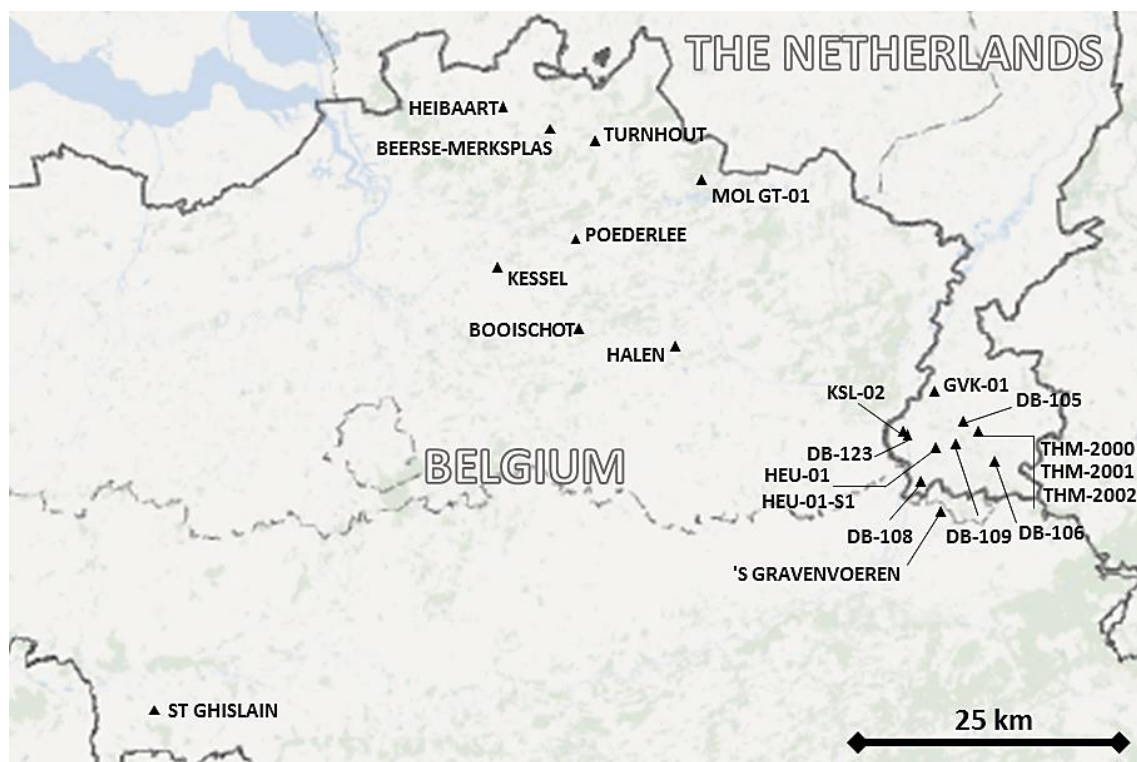
Figure 3-2: Magnified image of the Limburg province and Belgium showing the wells used in this study.

Table 3-3: The UK and Belgian wells included in this study.

Code	Extended name	Wireline Logs	Literature references
53/12-02 (UK)	-	X	Cameron, 1993
007E0178	HEIBAART	X	Bless *et al*., 1976; Dejonghe, 1983
030W0371	POEDERLEE	X	Muchez *et al*., 1990
017W0265	BEERSE MERKSPLAS	X	Vandenberghe *et al*., 2000
017E0225	TURNHOUT	X	Bless *et al*., 1976; Muchez *et al*., 1994
44W11 (KB38)	KESSEL	-	Bless *et al*., 1976
76E243 (KB131)	HALEN	-	Bless *et al*., 1976
59E146 (KB132)	BOOISCHOT	-	Bless *et al*., 1976
108W359 (KB192)	'S GRAVENVOEREN	-	Batten *et al*., 1987; Muchez and Viaene, 1987
DZH-01	HEIBAART	-	Bless *et al*., 1981; Muchez *et al*. 1987, 1994; Amantini *et al*., 2009
MOL GT-01	MOL GT-01	X	Bos and Laenen, 2017
150E0387	ST GHISLAIN	-	Groessens *et al*., 1979; De Putter *et al*., 1994

Table 3-4: German wells included in the study.

Extended name	Wireline Logs	Literature references
MUNSTERLAND-1	X	Bless *et al*., 1976, 1980
ISSELBURG-3	-	Bless *et al*., 1976, 1980
WACHTENDONK-1	-	Bless *et al*., 1976
SCHWALMTAL-1001	-	Mathes-Schmidt, 2000

14

4. Geological Setting

4.1 Structural Evolution

The tectonic evolution of the Netherlands is complex, and the flat topography hides a pattern of structural highs and lows (Figure 4-1) that have been explored for hydrocarbons during the past 50 years. The oldest rocks of the Netherlands were penetrated by the O18-01 and KTG-01 wells and consist of Silurian low grade dark turbiditic sandy claystone. The beginning of the structural evolution of the Netherlands (Figure 4-2) is marked by the Caledonian orogeny and the associated post-orogenic extension with a NE-SW/NNE-SSW orientation (Smit *et al.*, 2018). This structural grain was repeatedly reactivated by younger tectonic phases.
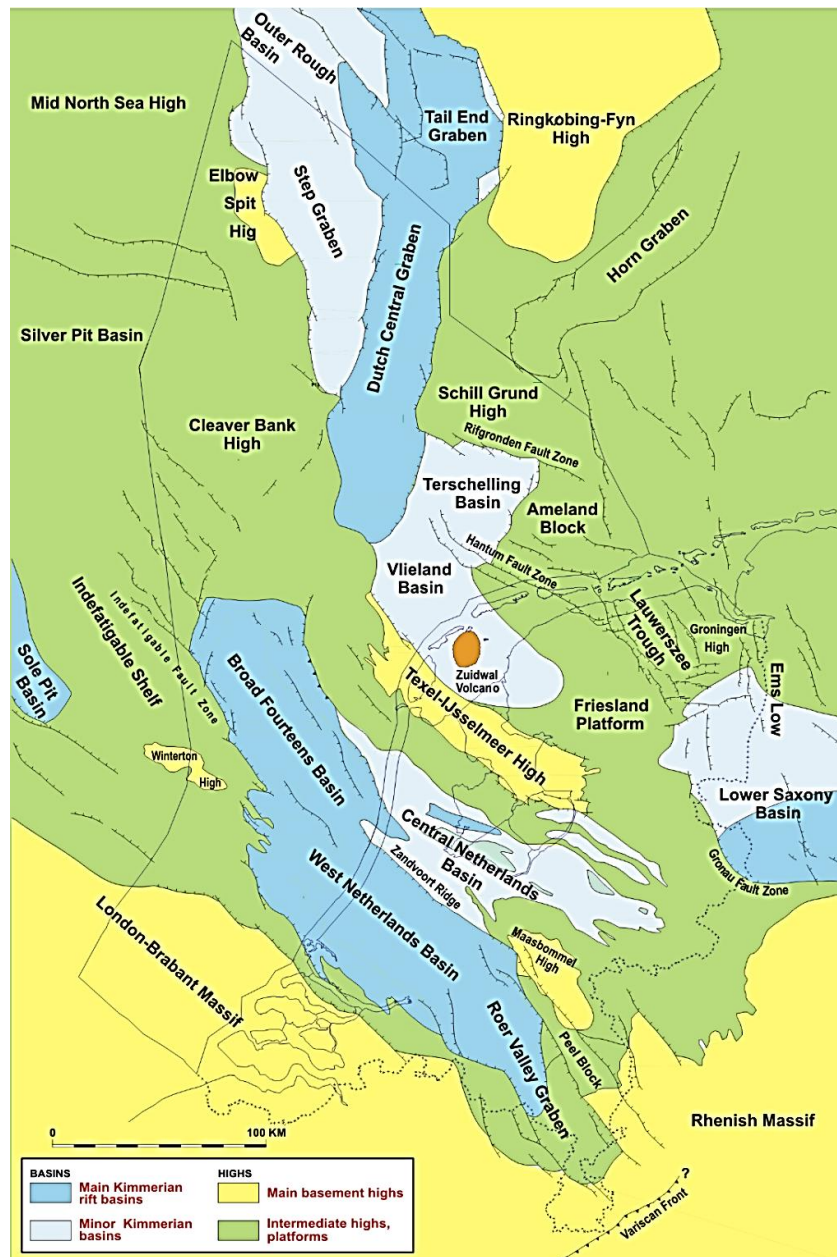
Figure 4-1: General tectonic outline of the Netherlands (from De Jager, 2007).
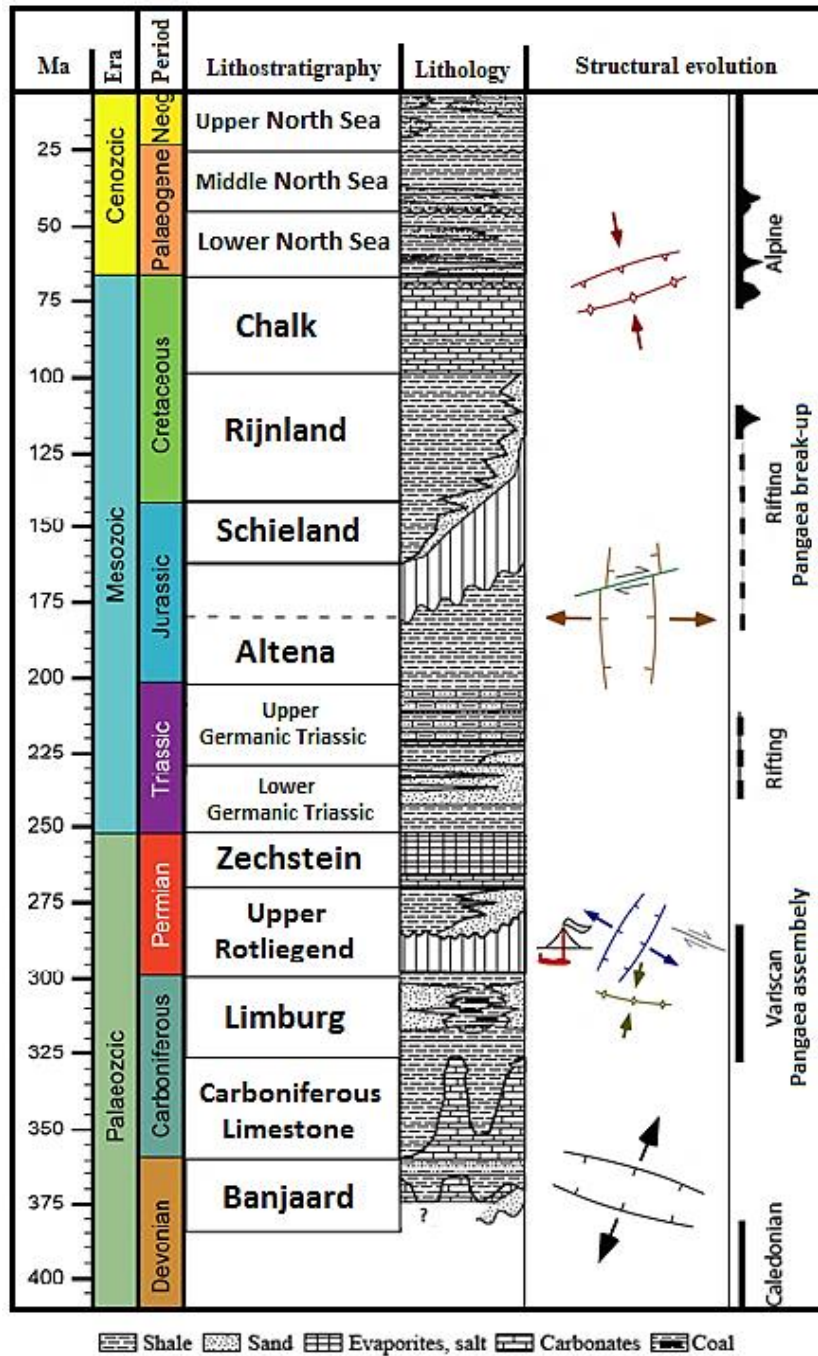
Figure 4-2: Stratigraphic table for the Netherlands presenting the major lithological units (Group level) and the tectonic events affecting them (modified from Van Hulten, 2012 and references there in; Ter Borgh *et al*., 2018). The Early Permian and Middle to Late Jurassic extensional tectonic regimes were synchronous with magmatism activities and thermal events (Van Bergen and Sissingh, 2007).
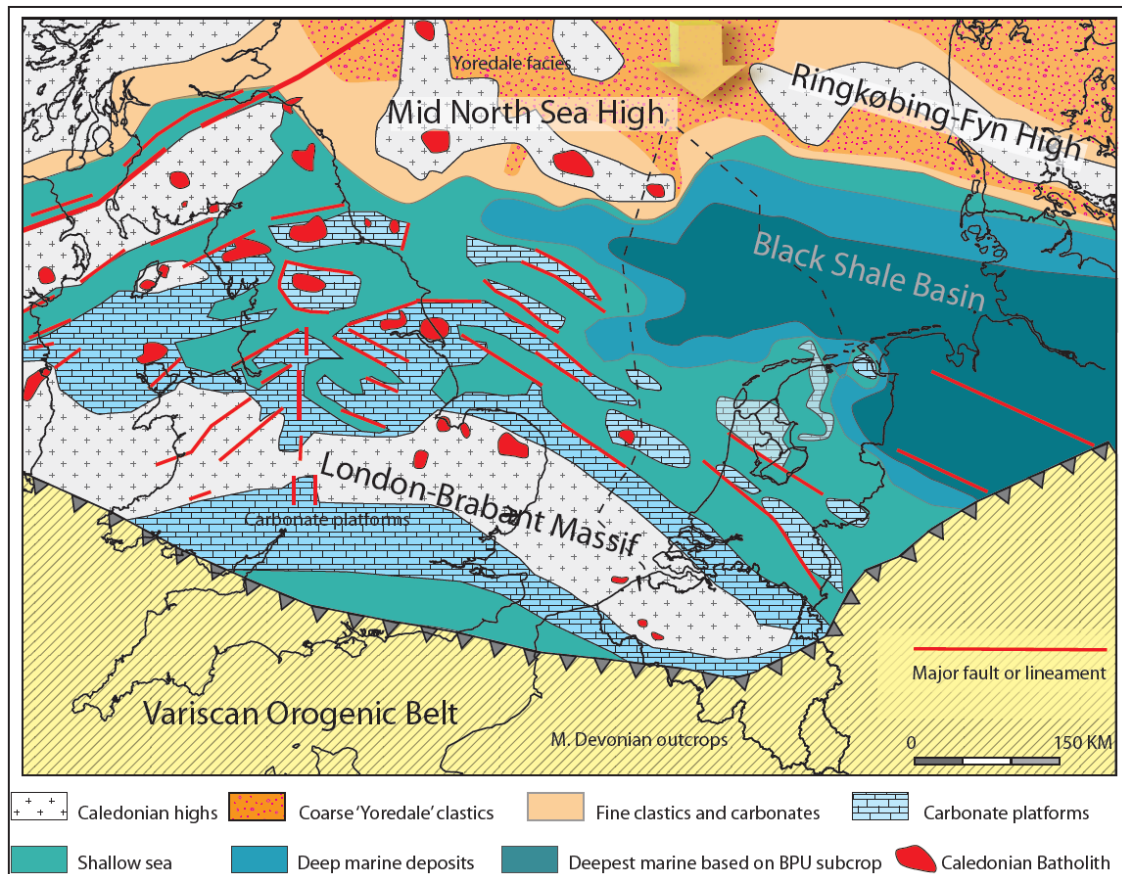
Figure 4-3: Paleogeography during the Early Carboniferous (from Van Hulten, 2012). Note that the outlines of the carbonate platforms presented in this map are schematic.

4.1.1 Devonian to Early Carboniferous Crustal Extension

During the Late Devonian, an extensional tectonic phase resulted in development of several basins along inverted structures. This tectonic phase was most likely linked to a partial inversion and collapse along the Thor suture that separates the Avalonia and Baltica terranes (Figure 4-1; Geluk *et al*., 2007; Smit *et al*., 2016).

In Belgium, the oldest sediments above the Caledonian basement that were penetrated by the Booischot and Heibaart boreholes are attributed to the Givetian and Frasnian, respectively. The Booischoot borehole recovered 203 m of continental clastics that were deposited in an active half graben, which became inactive during Late Devonian (Muchez and Langenaeker, 1993; Lagrou and Coen-Aubert, 2017). At the same time, development of Devonian carbonate buildups are reported in Belgium during the Frasnian (e.g. Boulvain, 2001). Based on studies performed on well A17-01 in the North Sea region, volcanism was associated with this tectonic phase, as reflected in intrusive and extrusive mafic rocks in of the Buchan Formation (e.g. Lundmark *et al*., 2018).

During the Late Devonian, clastic sedimentation persisted, except for on the Rhenish Mountains to the south of the Netherlands (Herbig and Mamet, 2014), where carbonate ramps were preserved. The distal facies of such carbonate ramp are probably represented in the Winterswijk-1 well.

This tectonic phase, with further reactivation of older Caledonian structures with a NE-SW/NNE-SSW oriented extension (Smit *et al*., 2018), continued with decreasing intensity from the Tournaisian to Visean. An asymmetric pattern of horsts and grabens developed as a result of this extension (Total UK, 1997; Schroot *et al*., 2006). Together with strong subsidence

during the Tournaisian, this tectonic phase shaped structural highs and basins, in some cases, deeper than 1 km. Structural highs were close to or above sea level, creating the conditions for shallow-water carbonate production and the start-up of Dinantian platforms in some parts of the northern Netherlands (Figure 4-3). The final event, in this extensional regime took place during the late Visean (mid-Brigantian; Total UK, 1997), and was marked by an unconformity associated with paleokarst on the flank of the London-Brabant Massif. To the central-north Netherlands the sedimentation was continuous with a probable paraconformity or drowning unconformities above the carbonate platforms (Reijmer *et al.*, 2017).

4.1.2 Variscan Compression

The late Visean/early Namurian period is marked as the onset of the Variscan tectonic phase (Figure 4-4; Ziegler, 1990; Pharaoh *et al.*, 1995; Geluk *et al.*, 2007) responsible for deepening and drowning of the Dinantian basin and the onset of clastic sedimentation along its southern and eastern margin (Kombrink *et al.*, 2008). The Variscan orogeny resulted from the continental collision of Gondwana with Laurentia and Iberia with the formation of the Pangea supercontinent. The main Variscan thrust front is located to the south of the Netherlands, close to the Limburg province. During this tectonic event, Late Devonian-Dinantian basins were inverted as far north as the Midland Valley in UK (Figure 4-4). Moreover, it is responsible for the development of an extensive, complex foredeep with a succession of Upper Carboniferous clastics up to 6-7 kilometers thick. The northern part of the Netherlands is located in a more distal part of the foredeep. Folding of the crust and lithosphere induced by the Variscan orogeny may have caused differential subsidence and local uplift (Bouroullec *et al.*, 2019 and references there in).
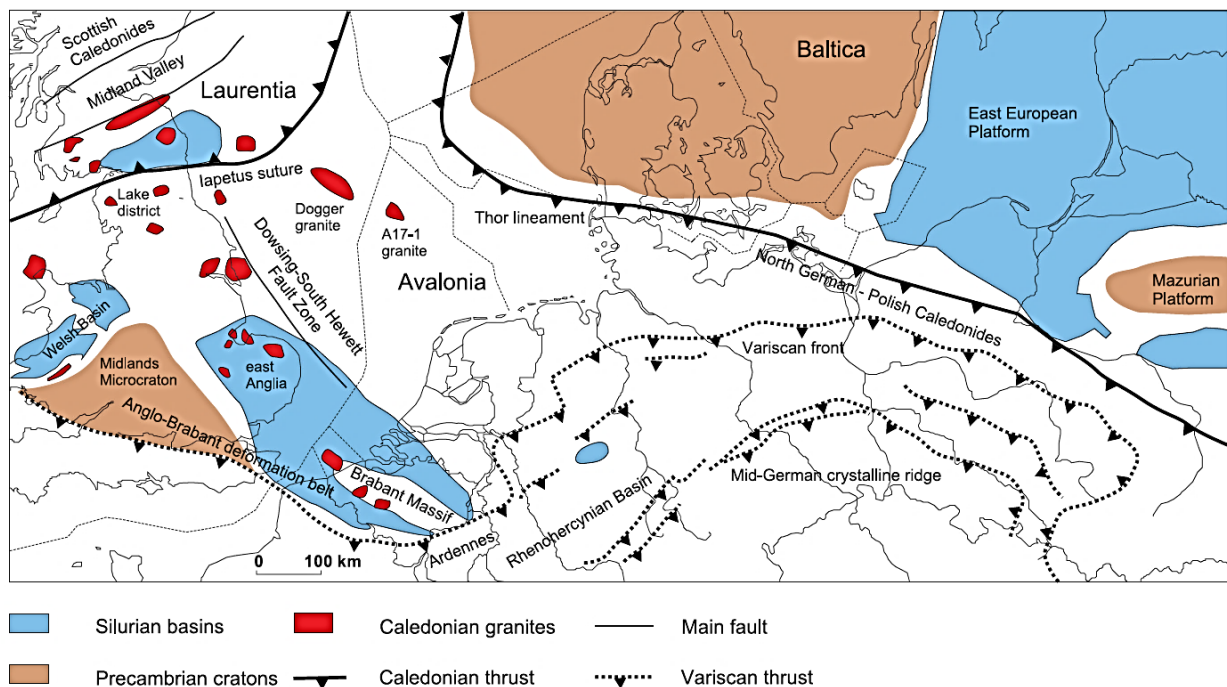
Figure 4-4: Map showing the location of the Variscan thrust front in northern Europe (from Geluk *et al.*, 2007 and references there in).

4.1.3 The Permian Uplift

During the uppermost Carboniferous-Lower Permian, a marked phase of uplift is associated with a strong thermal event attributed to the rise of an asthenospheric plume under large parts of the northern and southern Permian basins including the Netherlands (Abdul Fattah and Verweij, 2014; Bouroullec *et al*., 2019 and references there in). This caused variable erosion (i.e. base Permian unconformity), in the order of some kilometers, of the Carboniferous succession. The presence of thermal anomaly is documented across the region and is responsible for the elevated maturity recorded in many wells of the Netherlands (e.g. GVK-01, KSL-02 and HEU-01). This thermal event was distributed over more than half of the Netherlands. The size and the strength of the event suggest that it was associated with a regional tectono-magmatic event, sometimes linked with major pluton emplacement (Figure 4-5; Sissingh, 2004). The extent of the uplift linked to the heat flow event suggests the presence of a pronounced asthenospheric anomaly, but this was unable to develop broad effusive volcanic products in the Netherlands as seen in Germany and Denmark (Sissingh, 2004).

The aforementioned uplift is responsible for the development of the base-Permian (Saalian) unconformity, a major event that marks the beginning of rifting in the region. The decrease in the heat flow produced crustal thermal relaxation, allowing the development of the Southern Permian Basin and the sedimentation of the Zechstein Group (Ziegler, 1988, Van Wees *et al*., 2000).

Figure legend:
- INTRUSIVE ROCK
- EXTRUSIVE ROCK
- VOLCANICLASTICS
- BASEMENT

NETHERLANDS

Columns: F10-1, Q7-2, L13-3, GIESSENDAM-1, LOON OP ZAND-1, ANDEL-4, ZUIDWAL-1, DE WIJK-7, E6-1 (2415 m), E6-1 (2420 m), BERKEL-1, WANNEPERVEEN-1, WINTERSWIJK-1, F3-7, DROUWENERMOND-1, BAARLO-1, E18-2, DE WIJK-7, HARDENBERG-2, STEENWIJKERWOLD-1, DWINGELO-2, NAGELE-1, A17-1

FORTIES | UK C. GRABEN | EGERSUND BASIN | DANISH N. SEA | S. PERMIAN BASIN

Ma			
75	MESOZOIC	CRETACEOUS / LATE	MAASTRICHTIAN
			CAMPANIAN
			SANTONIAN
			CONIACIAN
			TURONIAN
100			CENOMANIAN
		EARLY	ALBIAN
			APTIAN
125			BARREMIAN
			HAUTERIVIAN
			VALANGINIAN
			RYAZANIAN
150		JURASSIC / LATE	VOLGIAN
			KIMMERIDGIAN
			OXFORDIAN
		MIDDLE	CALLOVIAN
			BATHONIAN
			BAJOCIAN
175			AALENIAN
		EARLY	TOARCIAN
			PLIENSBACHIAN
			SINEMURIAN
200			HETTANGIAN
		TRIASSIC EARLY+MIDDLE+LATE	RHAETIAN + NORIAN + CARNIAN +
225			LADINIAN +
			ANISIAN +
250			SKYTHIAN
	PALEOZOIC	PERMIAN / LATE	'ZECHSTEIN'
275		EARLY	'ROTLIEGEND'
300		CARBONIFEROUS / LATE	STEPHANIAN + WESTPHALIAN +
325			NAMURIAN +
		EARLY	VISEAN +
350			TOURNAISIAN

reworked

in Late Devonian

Figure 4-5: Magmatic events in the Netherlands (from Van Bergen and Sissingh, 2007).

4.1.4 Triassic-Jurassic Extension

The Early Triassic marks another extensive phase of subsidence in the region that is linked to a rifting phase (Total UK, 1997). The thermal subsidence continued until the end of the Late Jurassic, when a period of long-lasting uplift from 209-146 Ma, as recorded by apatite fission tracks of the flank of the London-Brabant Massif (Van den Haute and Vercoutere, 1990; Vercoutere and Van den Haute, 1993). This uplift, linked to the Kimmerian tectonic phase, was

20

accompanied by a thermal event, with a volcanic climax giving rise to the development of the Zuidwal Volcano (152-144 Ma; Sissingh, 2004), which is synchronous with gas emplacement in the Groningen Field (150-120 Ma; Lee *et al*., 1985).

4.1.5 Cretaceous-Tertiary Inversion

During the Cretaceous, the tectonic regime shifted from a dominantly extensional towards a compressional or strike slip system. From the Late Jurassic onwards, subsidence was mostly thermal, but many areas remained subaerially exposed during the Early Cretaceous developing pronounced erosion and associated karstification. A subsequent first phase of inversion, attributed to the Sub-hercynian tectonic phase, occurred after the Turonian with a peak during the Campanian (Total UK, 1997; De Jager, 2007). However, this inversion is not often properly recorded in the sedimentary successions, as the associated unconformity is included within the Upper Jurassic unconformity. The Santonian marine conditions were re-established in most parts of the NW Europe, represented by the deposition of chalk facies that onlap the underlying Jurrasic unconformity. The uppermost Cretaceous-Paleocene inversion (Laramide tectonic phase) marks the end of chalk deposition and the beginning of siliciclastic sedimentation of the North Sea supergroup, with erosion occurring in the western and central Netherlands and in the Broad Fourteens Basin (Figure 4-1; De Jager, 2007). A broad uplift also occurred during the Upper Eocene until the Lower Oligocene as a result of the Pyrenean tectonic phase. The latest inversion, during the Upper Oligocene (Savian tectonic phase), except for the West Netherlands Basin, is poorly developed in the Netherlands, yet is more evident towards UK (De Jager, 2007).

4.2 General Dinantian Carbonate Models and Analogues

4.2.1 Dinantian carbonate buildups

A series of global anoxic events during the Late Devonian are responsible for mass extinctions that caused the demise of existing skeletal reef-building communities (e.g. corals; McGhee, 1996). This leads to the proliferation and dominance of microbially-produced carbonate mud mounds that form the main type of global carbonate buildups throughout the Dinantian (Bridges *et al*., 1990; Yao *et al.,* 2016). These carbonate mud mounds show a progressive evolution in their depositional settings, size and geometry during the Dinantian (Aretz and Chevalier, 2007; Bridges *et al*., 1995). They contain a common microfacies that is dominated by carbonate mud with a distinctive micropeloidal texture. The carbonate mud is thought to have been produced on the buildup by a microbial community. This community is also thought to have formed adhesive mats that bound the surface of the mud mound allowing steep depositional slopes to be supported and to protect the micritic carbonate substrate against erosion in high energy conditions (Gutteridge, 1995). These carbonate mud mounds contain a network of complex depositional cavities (known as stromatactis or stromatactoid cavities) that are lined by thick crusts of marine radial fibrous calcite cement often overlain by geopetal fills of internal peloidal sediment. The development of early marine fibrous calcite cements associated with mud mounds is a typical early diagenetic feature also reported from the Carboniferous deposits of the Cantabrian platform in Spain (Van der Kooij *et al*., 2007, 2009, 2010) and the Devonian carbonates of the SW Czech Republic (Hladil, 2005). *In situ* and recumbent intact sheets of fenestrate bryozoans are often associated with these cavities which are interpreted as shelter cavities that were initially formed around fenestrate bryozoan sheets but modified by collapse of the surrounding unlithified micropeloidal carbonate muds and by internal erosion (Gutteridge, 1990, 1995).

A wide variety of patch reefs were constructed by a diverse range of microfossils throughout the Dinantian. Adams (1984) described late Molinacian (Arundian) patch reefs, some 1 m in height and 1.5 m across that were formed by tabulate corals. Other biota include *Aphralysia* (a

possible encrusting foraminifera), calcareous worm tubes, *Renalcis, Girvanella, Garwoodia* (encrusting blue-green algae), vermetid gastropods, Solenoporid algae that formed a framestone inhabited by other benthic bioclasts such as brachiopods, echinoderms and bryozoans (Bridges *et al*., 1995). These build-ups are associated with medium-bedded bioclastic and peloidal packstone with occasional grainstone deposited near normal wave base on the middle part of a carbonate ramp.

Arezt and Herbig (2003) described patch reefs within the Livian (Holkerian) Hunts Bay Oolite from South Wales, a cross-bedded oolitic grainstone deposited in an inner carbonate ramp setting. These are constructed by colonial rugose corals forming a bafflestone with a matrix of stromatolitic and thrombolitic carbonate mud with encrusting bioclasts such as bryozoans, agglutinating foraminifera and blue green algae; marine cement is also present as a stabilising component.

Bancroft *et al.* (1988) found an early Warnantian (Asbian) patch reef constructed by bryozoans that formed a bafflestone and framestone associated with the early Warnantian (Asbian) carbonate platform margin facies association in the North Wales.

Bridges *et al*. (1995) recognised five types of Dinantian carbonate buildups (Table 4-1) from North America and NW Europe, 1, 3 and 4; the types represented in NW Europe are described below and shown in Figure 4-6:

Type 1 represents the type 'Waulsortian' mud mounds of Tournaisian to early Molinacian (Chadian) age and are dominated by microbial carbonate muds with stromatactoid cavities. They were deposited in deep carbonate ramp settings forming large single build-ups several hundred of meters in size and relief or as off lapping complexes. Lees *et al*. (1995), Lees and Miller (1995) and Lees (1997), defined a depth-related microfacies zonation that implies these mounds were deposited in water depths deeper than 130 m.

Type 3 represents the carbonate mud mounds that contain a more diverse bioclast assemblage than the Waulsortian (i.e. Type 1 buildups) including numerous brachiopods, foraminifera, calcareous algae and abundant crinoids. These were deposited in shallower carbonate platform interior settings and are often associated with carbonate platform margin facies. These carbonate mud mounds form smaller structures in comparison with the Waulsortian carbonate mud mounds and are found in carbonate shelf depositional systems of Holkerian to Brigantian age (Pickard, 1992; Gutteridge, 1995; Aretz and Herbig, 2003).

Type 4 includes coralgal *Aphralysia* and bryozoan coralgal buildups which refer to patch reefs that occur in shelf interior or inner carbonate ramp settings of various ages. They are generally made up of an assemblage of specialist encrusting microfossils. These structures are typically only a few meters in size.

Table 4-1: Relative abundance of skeletal components in the five types of buildup. Relative abundance notation: VA, very abundant; A, abundant; C, common; R, rare (modified from Bridges *et al.*, 1995).

Build-up	Principal component	Relative abundance	Minor components	Relative abundance
Type 1	Fenestrate bryozoans	A-C	Molluscs	R
	Sponge spicules	A-C	Brachiopods	R
	Crinoids	A-C	Ostracodes	R
Type 2	Crinoids	VA	Brachiopods/gastropodes	C-R
	Fenestrate bryozoans	A	Corals/trilobites	R/R
			Ostracodes/dasycladaceans	R/R
Type 3	Crinoids	A-C	Ostracodes	C-R
	Brachiopods	A-C	Plurilocular foraminifera	C-R
	Fenestrate bryozoans	A-C	Corals/trilobites	R/R
	Molluscs	A-C	Calcified algae	R
	Sponge spicules	A-R		
Type 4	Calcified	A-C	Plurilocular foraminifera	C-R
	algae/cyanobacteria	A-R	Ostracodes	C-R
	Bryozoans	C-R	Brachiopods	C-R
	Corals	C-R	Bivalves	R
	Aphralysia			
Type 5	Trepostome bryozoans	A-C	Spirorbids	C-R
	Microthrombolite	A-C	Bivalves	C-R
	Brachiopods	VA	Gastropodes	R
	Worm tubes	C-R		
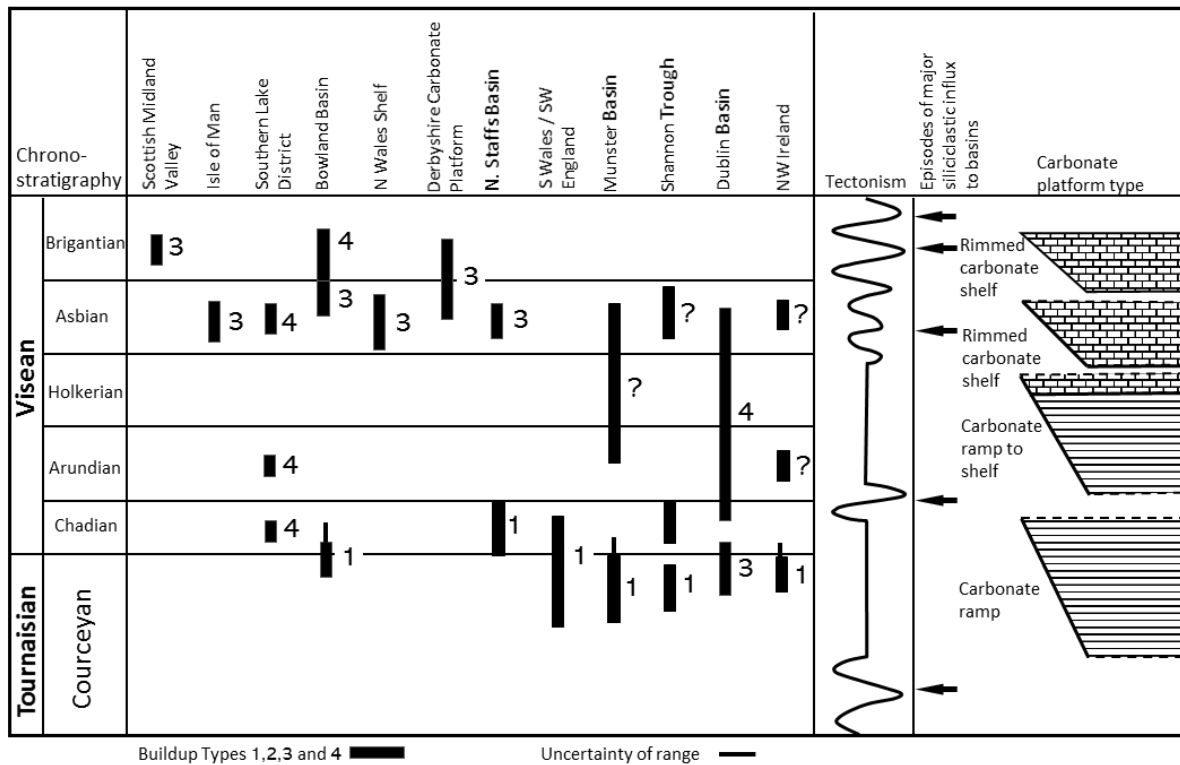
Figure 4-6: Distribution of the carbonate buildup types in NW Europe and their abundance during evolution of the carbonate platform types. Types 2 and 5 buildups described by Bridges *et al.* (1995) are not represented in NW Europe.

4.2.2 Tournaisian to mid Visean carbonate ramp systems along the southern Laurussian margin

Carbonate ramp systems of Tournaisian to mid Visean age occur along the southern margin of the Laurussian continent, south of the London-Brabant Massif. Examples are exposed in southern Belgium, South Wales, southern Ireland and are also known from the subsurface of southern England. Deposition of these large-scale carbonate systems took place in several hundred metres water depth in their distal parts, passing into shallow water or emergent conditions over a distance of at least 100-200 km, not allowing for Variscan shortening across the Rheic Ocean.

The deepest part of the depositional system known as the "Kulm" facies that consists of very fine-grained black shale and radiolarian chert with high organic and minor carbonate content deposited in very deep water, sediment-starved, stratified basins (Uffmann *et al.*, 2012; Vachard *et al.*, 2017).

A south-dipping carbonate ramp of late Tournaisian age is described by Lees (1997) from southern Belgium. The distal parts of the carbonate ramps are characterised by the presence of large isolated, stacked or offlapping complexes of Waulsortian carbonate mud mounds deposited in sub-photic conditions at water depths estimated at some 300 m (e.g. MacCarthy and Gardiner, 1987). The Waulsortian mounds show a progressive down-ramp increase in size and degree of amalgamation (Figure 4-7).
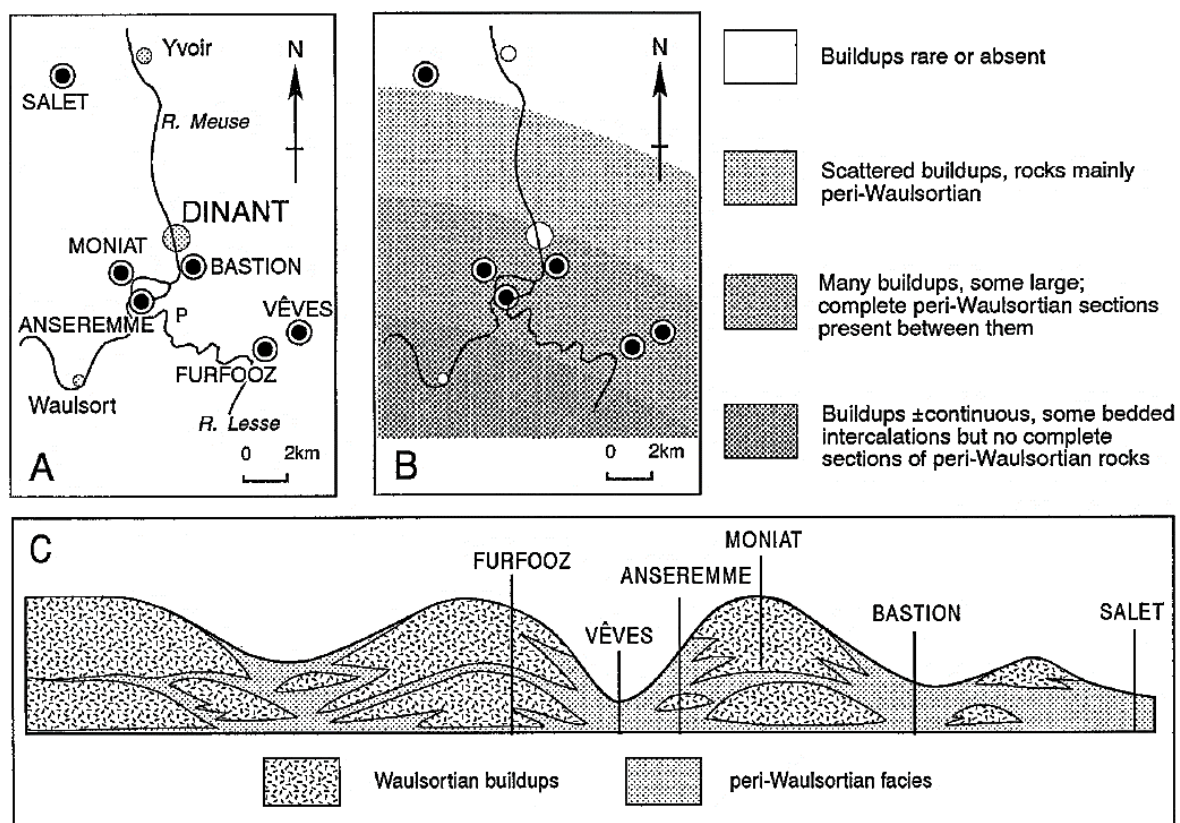
Figure 4-7: Down ramp change in carbonate mud mound morphology; Tournaisian to early Visean carbonate ramp, southern Belgium, from Lees (1997).

The proximal lateral equivalents of the Waulsortian mounds consists of the following facies (Figure 4-8):

Bayard facies: This facies is the lateral equivalent of mid- to late Tournaisian Waulsortian mounds, and consists of crinoid fenestrate bryozoan packstone with minor wackestone and

24

grainstone. It is interpreted as resedimented bioclastic carbonates derived from shallow water settings on the carbonate ramp.

Leffe facies: This facies forms the lateral equivalent of late Tournaisian Waulsortian mounds, and consists of wackestone with lesser amounts of crinoids and bryozoans than in the Bayard facies. Ostracods, moravamminids, calcispheres, sponge spicules and, locally, foraminiferans, increase in importance. Many allochems are micritised and some are coated. The intraclasts and skeletal grains commonly have a micritic, sometimes laminated, coating interpreted as microbial. This facies is interpreted as a mixture of resedimented bioclastic carbonates derived from shallow water settings on the carbonate ramp or from the Waulsortian carbonate mud mounds. The Leffe facies may also contain a component of fine-grained peri-platform carbonates.

Molignée facies: This facies represents a post- Waulsortian mound basinal facies of early Visean age, and consists of very fine grained, thinly bedded, black wackestone or carbonate mudstone with very finely comminuted bioclasts. These are interpreted as peri-platform carbonate deposited in a very low energy setting, probably 100+m water depth.

Stratigraphy				Lithofacies	Relative thickness
Conodont zonation					
Visean	Molinatian	*G. homopunctatus*		Molignée	M
Tournaisian	Freyrian	*M. Beckmanni* *M. praebeckmanni*		transition	
Tournaisian	Ivorian	*Scaliognathus anchoralis*	*P. bischoffi*	Leffe	③
			D. latus	Waulsortian	②
		Polygnathus Communis carina	*Do. bouckaerti*	transition	①
			E. bultyncki		
			E. cf. bultyncki	Bayard	L
			Do. hassi		B
	Hastarian	*Siphonodella*		Calcschistes de Maurenne	

Figure 4-8: Tournaisian to early Visean distal carbonate ramp facies of the southern Belgium (Dinant area), from Lees (1997). The lines labelled 1, 2 and 3 on the relative thickness diagram correspond to the base of the Moliniacian stage, and the base of the Visean respectively. Do. Dollymae; E. Eotaphrus; D. Doliognathus; P. Polygnathus; M. Mestognathus; G. Gnathodus.

Mid- to outer carbonate ramp facies are represented by the 'Petit Granit' of southern Belgium (Figure 4-9) that consists of variably argillaceous dark grey bioclastic limestone dominated by crinoids (Figure 4-10). Grainstone, packstone, wackestone and other bioclasts include fauna adapted to a weakly agitated environment and relatively soft substrate (e.g. brachiopods, bryozoans, tabulate and rugose corals). Some beds of bioclastic wackestone or packstone contain well-preserved *in situ* colonial and solitary rugose and tabulate corals. Rare nektonic and benthonic feeders such as trilobites and cephalopods are also preserved (Debout and Denayer, 2018). Beds of bioclastic grainstone and packstone are common, these are often amalgamated, graded and sometimes show hummocky cross-stratification. Intensive bioturbation is often also present. The depositional setting is interpreted as a very broad inner

to middle carbonate ramp below normal wave base as a result of storm reworking and redeposition (Figure 4-10).
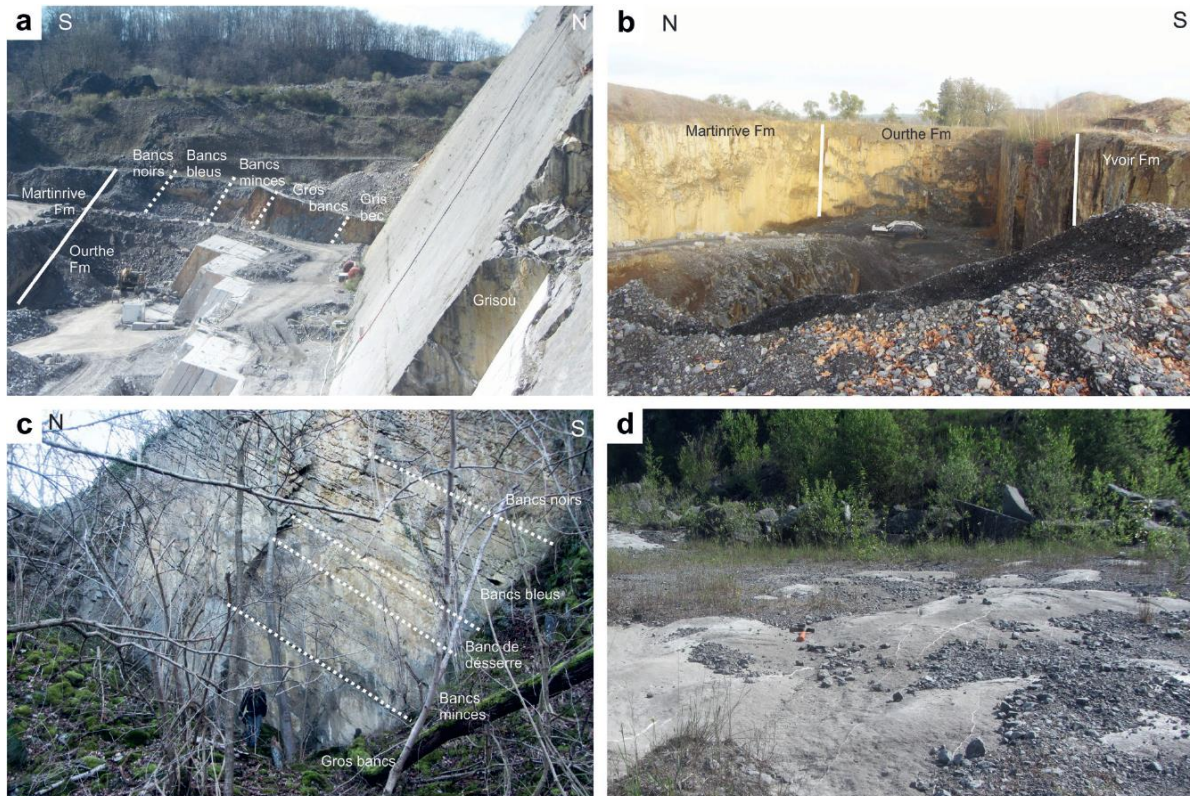
Figure 4-9: Field photographs showing the outcrops of upper Tournaisian mid- to outer ramp facies known as the 'Petit Granit' (southern Belgium): a) View of the La Préalle quarry (Chanxhe) with denomination of the quarried beds. b) View of the Jenneret quarry showing base and top of the beds. c) View of the Royseux disused quarry with denomination of associated beds. d) Hummocky crossstratifications at the top of the "Pas de Loup" bed, Gauthier-Wincqz quarry in Soignies (Debout and Denayer, 2018).
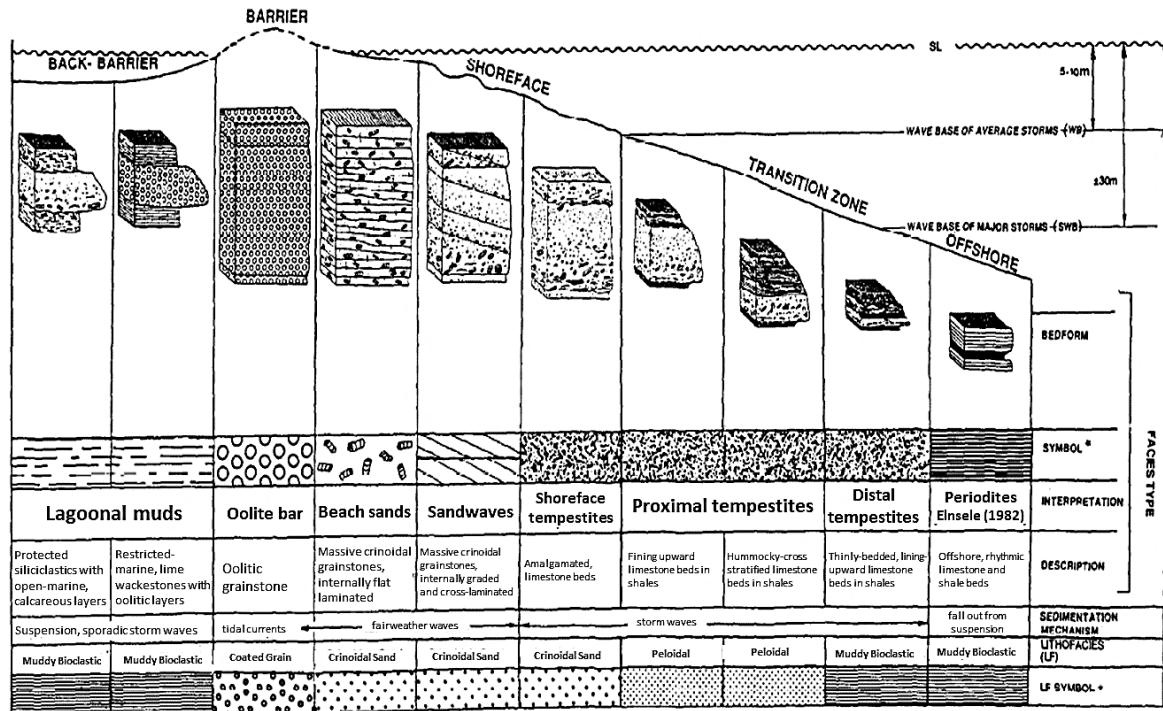
Figure 4-10: Tournaisian carbonate ramp facies profile from southern Belgium (Van Steenwinkel, 1990).

Wright (1982, 1986) and Van Steenwinkel (1990) described inner carbonate ramp facies in South Wales and southern Belgium, respectively, forming a number of offlapping progradational packages separated by erosional surfaces in proximal areas (Figure 4-11). Mid- to outer ramp facies include bioturbated bioclastic and oolitic storm deposits with hummocky cross-stratification with occasional Waulsortian mud mounds. These pass up-dip into oolitic and bioclastic barrier with associated high energy beach, sand wave and shore face facies. The barrier sheltered muddy bioclastic lagoonal and peritidal facies (Figure 4-11). Supratidal areas are associated with erosional surfaces, calcrete, karst and some influx of sandstone (Figure 4-11; Wright, 1982, 1986, 1987).

27
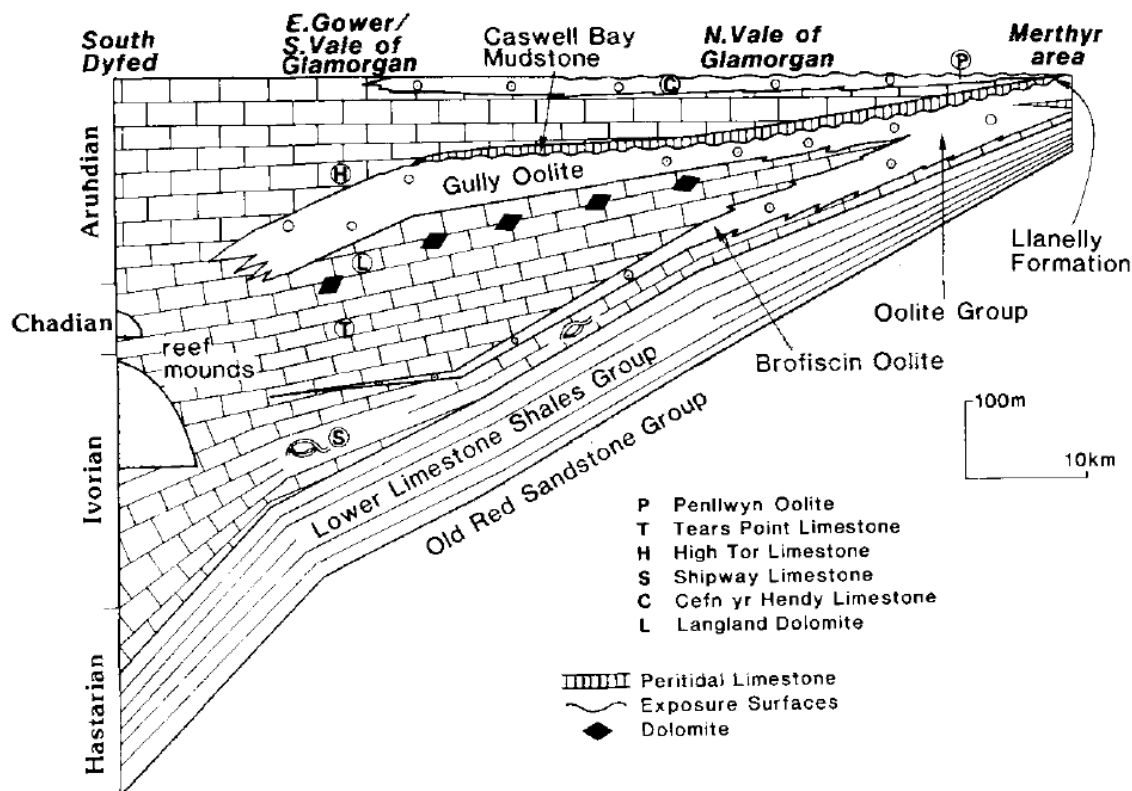
Figure 4-11: Tournaisian to mid Visean carbonate ramp facies profile from South Wales (Wright, 1986).

4.2.3 Tournaisian to mid Visean carbonate ramp systems north of the London-Brabant Massif

The Tournaisian to mid-Visean carbonate ramp systems (shown by Pickard and Gutteridge, 1997; Reijmer *et al.*, 2017) present north of the London-Brabant Massif are located in a mega-basin between the London-Brabant Massif and the Caledonide orogenic belt to the north; this includes the Netherlands, the southern North Sea, northern England and North Wales and the central and northern part of Ireland. This basin complex has a very different tectonic setting and evolution from the larger-scale carbonate ramp systems located to the south of the London-Brabant Massif. The structural architecture and evolution of the sub-basins is controlled by the distribution and size of underlying basement blocks and their response to re-activation during a number of rifting and inversion events during the Dinantian time (Gawthorpe *et al.*, 1989). The contrasting sedimentary response during alternating episodes of rifting and passive subsidence has produced a recognisable seismic stratigraphy (Fraser and Gawthorpe, 1990; Ebdon *et al.*, 1990; Fraser *et al.*, 1990).

Carbonate depositional systems of Tournaisian to earliest Visean age are preserved only in basins that underwent subsidence during the Late Devonian or early Dinantian. The onset of carbonate sedimentation in these sub-basins and the timing of carbonate platform nucleation around structural highs is therefore diachronous and depends on the local structural template, the amount of subsidence and the timing of arrival of the Dinantian transgression. The dimensions of these carbonate ramp systems are controlled by the basin architecture and are generally on the order of several tens of km down dip with 10s-100+m depositional relief between proximal and distal facies.

The persistence of carbonate ramps during Tournaisian to mid Visean is attributed to progressive onlap of basement topography and the ability of the carbonate systems to keep up with subsidence and sea level rise. Molinacian to Livian (Arundian-Holkerian) carbonate

ramps in the Shannon Trough (Ireland) and the southern Lake District (UK) show a lateral uniformity of thickness without any corresponding changes in lithofacies (Adams *et al*., 1990; Somerville and Strogen, 1992).

These basins were originated as grabens and half grabens that initially received locally-derived red bed sediments deposited as alluvial fans and playa lakes within in a terrestrial or marginal marine setting. The local occurrence of evaporites and evaporite collapse breccias suggest that some basins may have been partly isolated during the initial Dinantian marine transgression (e.g. Dunham, 1973; Jacobs *et al*., 1982; Poty, 1982; Vogel *et al*., 1990; Ward, 1997). Jacobs *et al*. (1982) concluded that evaporites of V1a age (Chadian) in the Campine Basin were deposited in marginal marine conditions and were dissolved during exposure to form the Ourthe Breccia before the V2a (Arundian-Holkerian) zone implying a semi-arid, rather than arid, palaeoclimate condition.

Tournaisian to early Visean (Molinacian) systems: Distal ramp carbonates of Tournaisian to early Visean (Molinacian/Chadian) are known from the Bowland Basin and the western part of the Widmerpool Gulf in northern England where they consist of distal storm deposits, carbonate turbidites and basinal shale. Waulsortian carbonate buildups are also present (e.g. Figure 4-12), with their microfacies assemblages suggesting that they were deposited in the depth range of 130-280 m (Lees and Miller, 1985; Gawthorpe, 1987; Bridges and Chapman 1988). Equivalent shallow carbonate ramp facies are not exposed.
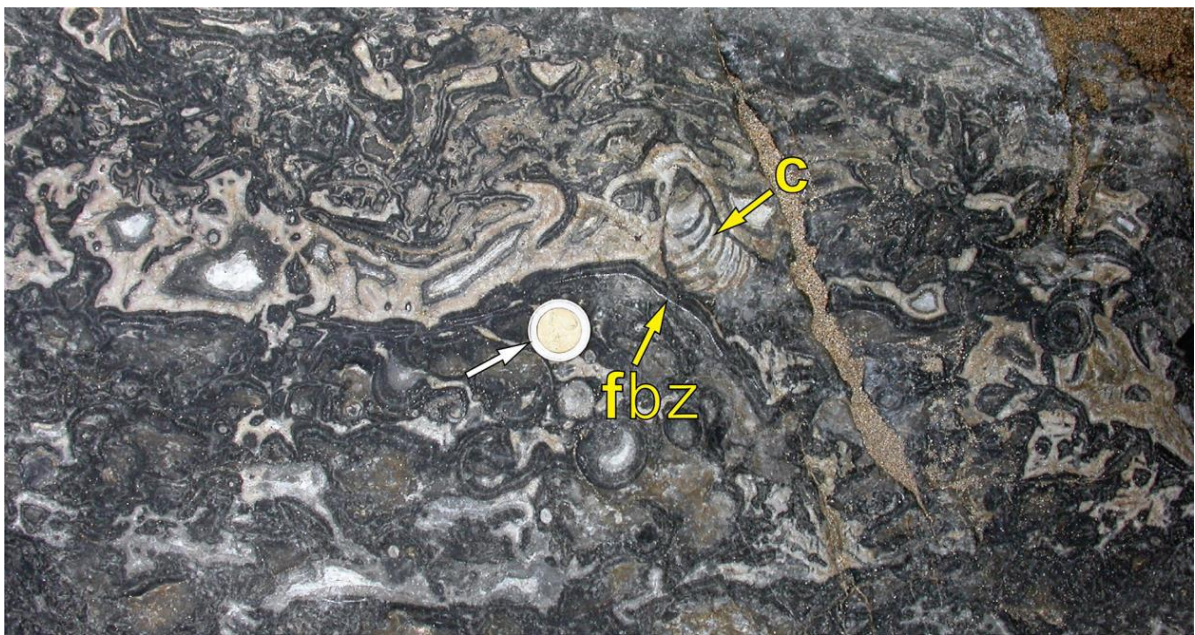
Figure 4-12: Field photograph from north County Kerry (SW Ireland), showing the close view of a Tournaisian Waulsortian limestone with complex and cemented cavities. fbz and c stand for fenestrate bryozoan and cephalopod shell, respectively. Scale is shown by a 2-euro coin (Murray and Henry, 2018).

Late Molinacian (Arundian) carbonate ramp systems are represented by the Red Hill Oolite of the Southern Lake District UK (Adams, 1984; Adams *et al*., 1990) and along the margins of the Shannon Trough in central Ireland (Somerville and Strogen, 1992). In both cases, these are oolitic carbonate systems with an inner ramp facies association of carbonate tidal flats and islands sheltered behind inner ramp ooid and peloidal grainstone shoals with cross bedding (Figure 4-13; late Molinacian). Mid carbonate ramp facies include bioturbated bioclastic and peloidal packstone and wackestone with occasional patch reefs formed by carbonate mud

mounds and encrusters (Adams 1984; Somerville and Stroen, 1992). The distal ramp facies association is represented by argillaceous wackestone and shale with rare burrows; in the case of the Southern Lake District, this facies also represents the subsequent drowning of the carbonate ramp.
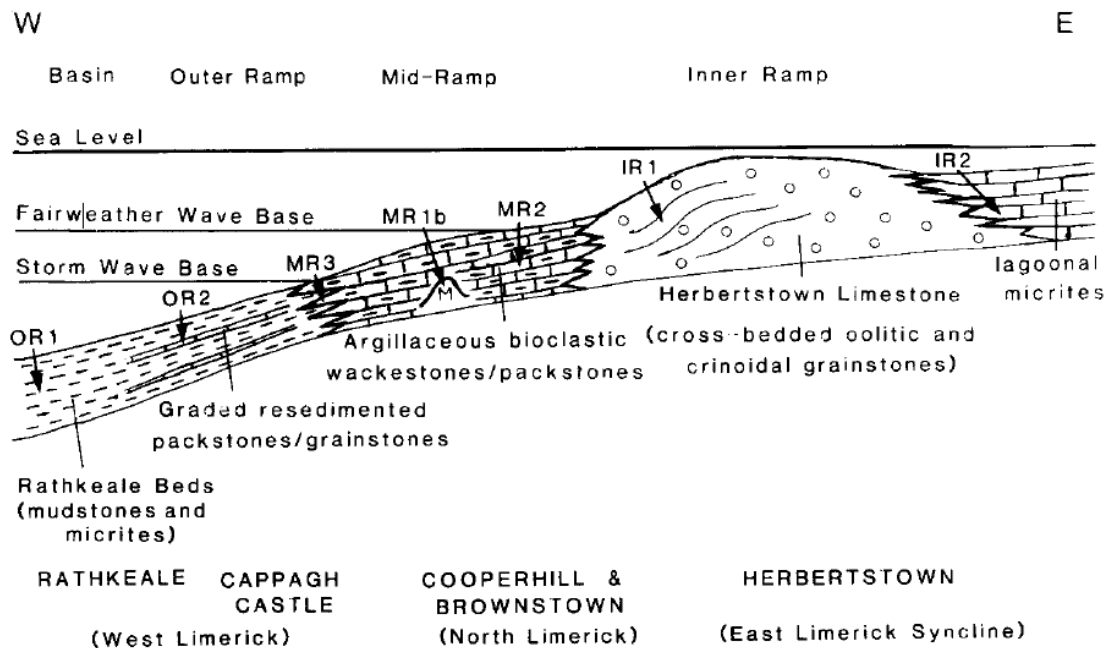
Figure 4-13: Late Molinacian (Arundian) carbonate ramp from the Shannon Trough in central Ireland (Somerville and Strogen, 1992).

Livian (Holkerian) carbonate ramp systems are better exposed than older carbonate systems and occur at outcrop in the Shannon Trough (Somerville and Strogen, 1992), southern Lake District (Adams *et al.*, 1990) and the Derbyshire carbonate platform (Schofield and Adams, 1990). Accordingely, distal- to mid carbonate ramp facies are represented by the Durinish Formation (Figure 4-14; Shannon Trough, Ireland) and the Park Limestone (Southern Lake District, UK), comprise bioturbated argillaceous packstone and unbedded bioclastic and peloidal packstone/grainstone. Based on Schofield and Adams (1985), inner carbonate ramp facies of the Livian Woo Dale Limestone are well-exposed over the Derbyshire carbonate platform. These comprise open marine fine grainstone and packstone with the local development of cross-bedding deposited in a subtidal inner ramp setting as bioclastic grainstone sheets with some carbonate sand bodies and barriers. Peritidal facies including intertidal fenestral carbonate mudstones organic-rich lagoonal facies were sheltered behind the carbonate barriers.

30

Figure 4-14: Thick- and thin-bedded limestones of the Durnish Formation near Foynes (Shannon Trough, Ireland). Height of road is around 12 m (from Best and Wignall, 2016).

4.2.4 Late Visean carbonate shelf and shelf margin depositional systems

The prevailing mode of carbonate deposition during Warnantian (Asbian to mid-Brigantian) was on flat-topped carbonate platforms (e.g. Sierra del Cuera, Spain; Tengiz and Kashagan, Kazakhstan) with steep-sided margins that pass down dip into slope and basinal depositional systems. The transition from carbonate ramp to shelf systems may be attributed to a number of factors. The Livian to early Warnantian (Holkerian/Asbian) boundary is associated with an extensional event that resulted in re-activation of basement faults and around structurally-controlled depositional highs with rapid subsidence controlled by basin-bounding faults creating a sharp demarcation between carbonate platforms growing around structural highs and basinal sediments deposited in surrounding areas (Gawthorpe *et al*., 1989; Ebdon *et al*., 1990; Fraser and Gawthorpe, 1990; Fraser *et al*., 1990; Somerville and Strogen, 1992). The onset of high frequency, high amplitude glacio-eustatic sea level changes caused by accretion of the southern hemisphere ice cap during the early Warnantian (Asbian) could be a further factor resulting in a highly episodic on/off style of carbonate production over carbonate platforms concentrating the carbonate production to platform tops (Horbury, 1989) or upper slopes (Kenter *et al*., 2005).

Shelf interior carbonates are cyclic comprising repeated shallowing upward cycles capped by emergent surfaces (e.g. Somerville, 1979; Walkden, 1987; Horbury, 1989; Adams *et al*., 1990; Davies, 1991; Van der Kooij *et al*., 2007, 2009, 2010). The basal part of these cycles comprises grainstone and packstone suggesting that the water depth immediately following transgression was not more than 10-15 m. These carbonate cycles generally lack peritidal facies with

emergence surfaces superimposed on subtidal facies. The shelf margins were associated with high energy conditions and a high energy facies belt of platform-margin grainstone shoals often occur at the shelf margin (e.g. Broadhurst and Simpson, 1967; Broadhurst and Simpson, 1973; Gawthorpe and Gutteridge, 1990; Adams *et al.*, 1990). Re-activation of basement faults associated with carbonate platform margins resulted in two types of platform margins with contrasting facies types and architecture:

> **Footwall carbonate platform margins:** These are controlled by an underlying basement fault that is episodically active during sedimentation. This limits the potential for basinward progradation of the carbonate platform leading to the development of accretionary platform margins and condensed or by-pass sedimentation on the slope. Owing to repeated footwall uplift, shelf edge facies are relatively thin with common erosion surfaces. Stacked carbonate mud mounds are present at the shelf break and often form part of the upper slope facies; other slope facies include bioclastic sediment reworked from the shelf and higher up the slope. The shelf break tends to be abrupt and facies belts associated with footwall margins tend to be narrow (few hundred m). Marginal slopes also tend to be relatively high angle (45+°).

> **Hangingwall carbonate platform margins:** These are not associated with underlying basement faults but are located over the gently-dipping surface of the underlying basement fault block. In these settings carbonate platforms are able to prograde down dip. The carbonate facies tend to be dominated by fine grained peri-platform wackestone and carbonate mudstone, often with slump structures. Scattered carbonate mud mounds may occur at the shelf break or upper slope facies. Isolated carbonate sand bodies enclosed by peri-platform wackestone and carbonate mudstone may be present in the upper part of the carbonate margin, passing down dip into storm beds (Gawthorpe, 1987; Gawthorpe *et al.*, 1989; Gutteridge, 2003). The shelf break and facies belts associated with hangingwall margins tend to be broad (few km). Marginal slopes also tend to be relatively low angle (5-10°).

These shelf carbonate systems can additionally be classified as:

Isolated carbonate platforms: These are carbonate platforms that developed on structural highs surrounded on all sides by basinal facies, examples include the Holme carbonate platform in the subsurface of northern England (e.g. Gutteridge, 1991; Evans and Kirkby, 1999), Uithuizermeeden and Luttelgeest carbonate platforms in the northern Netherlands (Van Hulten, 2012; Hoornveld, 2013; Boots, 2014; Boxem *et al.*, 2016). These carbonate platforms are generally free of siliciclastic sedimentation apart from possible sources within the exposed structural high.

Attached carbonate platforms: These are carbonate platforms that are attached to the flanks of structural highs within the Dinantian megabasin fringing the northern margin of the London-Brabant Massif. Despite the fact that these carbonate platforms are attached to basement highs, they contain minimal coarse-grained siliciclastic sediments. This suggests that the basement highs were either completely covered, were very small or were low relief. The other possibility is that the siliciclastic sediments were funneled to the basin at distinct points. Other attached carbonate platforms, such as the Derbyshire carbonate platform, were remote from areas of exposed basement and so behaved as clastic-free systems. Interbedded coarse clastics are only found where there is a local source of coarse clastics such as on the western part of the North Wales shelf on Anglesey (Walkden and Davies, 1983; Davies, 1991).

4.2.5 Carbonate slope and basinal depositional systems

There was no pelagic carbonate production during the Dinantian (Scholle et al., 1983) and thus, deposition of carbonates in basinal settings relied on reworking of peri-platform carbonates produced on surrounding carbonate platforms. Although, in microbial dominated carbonate systems slope shedding carbonates play an important role in sediment transportation and angle of repose (Keim and Schlager, 1999, 2001; Kenter *et al.*, 2005; Chensel *et al.*, 2017), as the height and angle of the slope increase, the slope evolves from depositional, to by-pass and erosional (Schlager and Ginsburg, 1981). In the latter case, general distal carbonate ramp and basinal facies include argillaceous carbonate mudstone with distal finely comminuted bioclastic calcarenites and calcisiltites deposited as distal turbidites and storm beds interbedded with deep water shales. These represent fine grained peri-platform carbonates reworked from surrounding carbonate platforms during high stands and hemi-pelagic mudstone settling from suspension. These facies are often cherty with occasional *Zoophycos* and *Chondrites* burrows. Based on Bábek *et al.* (2010, 2013), the shallow carbonate ramp progrades into the deep ramp facies of Tournaisian-Visean age during low stands with increased deposition of reworked bioclasts and intraclasts in the form of graded, sometimes amalgamated coarse-grained calcarenite to calcirudites as turbidites or tempestites on the distal part of the carbonate ramp. Gawthorpe and Clemmy (1985) and Gawthorpe (1987) proposed that major shedding of shallow water carbonate sediment in the form of debris flows, slumps and associated coarse carbonate turbidites into Dinantian basins, as a result of extensional events that caused re-activation of intra-basinal structures during enhanced tectonic activity. Wherese, the same feaures are considered by Reijmer *et al.* (2015) to be as normal slope destabilisation processes occurring typically in the microbial-dominated systems. Based on the available data non of the above mentioned scenarios can be excluded.

4.2.6 Late Warnantian (Brigantian) depositional systems

Many Brigantian depositional systems are either mixed carbonate-clastic systems or represent a transition from carbonate-dominated to clastic-dominated systems. The transition from carbonate- to clastic- sedimentation takes place as a result of southward progradation of large clastic systems sourced from outside the Dinantian megabasin. Generally, the transition is diachronous from north to south taking place in the Livian to early Warnantian (Holkerian/Asbian) in the central North Sea and parts of northern part of Northern England and during the Late Warnantian (Brigantian) further to the south in the UK and the North Sea basin (Waters *et al.,* 2007). However, carbonate sedimentation depends on the local path of the clastic systems through the basins and carbonate sedimentation may locally survive into the Late Warnantian (Brigantian). For example, on the southern Lake District carbonate platform, the Brigantian is dominated by thinly-bedded dark coloured argillaceous limestone with chert and interbedded mudstone passing southwards into cyclic grainstone with palaeokarst (Adams *et al*. 1990). This may represent a carbonate shelf poisoned by the progradation of fluvio-deltaic systems sourced from the north.

The Asbian/Brigantian boundary is also associated with a number of tectonic and stratigraphic events recognised across the Dinantian megabasin north of the London-Brabant Massif. An episode of crustal extension resulting in the reactivation of basement faults occurs around the margins of some carbonate platforms in northern England (Gutteridge, 1987; Gawthorpe *et al.*, 1989), the consequences of which were:

  o A change in the nature of cyclicity in shelf carbonates. The late Warnantian (Brigantian) shelf interior carbonates show a similar shallowing-upward cyclicity to that of early Warnantian (Asbian) shelf carbonates; however, the transgressive phase of Brigantian

cycles often show a deeper-water more argillaceous facies suggesting an increase in rate of subsidence.

- o Fault reactivation causes differential subsidence within carbonate platforms and formation of intrashelf basins.
- o Tilting of carbonate platform margins causing lateral facies differentiation along strike, uplift and local karstic incision and collapse with the local formation of boulder beds along some carbonate platform margins (Simpson and Broadhurst, 1967). The late Warnantian (Brigantian) carbonate systems often back-step relative to underlying early Warnantian (Asbian) carbonate systems.

4.3   Dinantian lithostratigraphy in the Netherlands

4.3.1 Introduction

The term Dinantian is used as a regional series for Lower Carboniferous in the Netherlands, Belgium and neighbouring countries (Groessens, 1989, 2006). The Dinantian successions are defined as Farne and Carboniferous Limestone Groups in offshore and onshore Netherlands (Kombrink, 2008 and references there in), respectively.

In the Dutch subsurface, the top of the Dinantian is quite clear in the onshore areas and roughly corresponds to the top of the Zeeland Formation (Visean), while sometimes in the upper Warnantian some clastics are present. The *Kolenkalk Group* is used as a synonym for the Lower Carboniferous carbonates in the region. The base of the Dinantian, however, is not properly defined and often is assigned to the base of the Zeeland Formation, while some other units have the same age (i.e. Bosscheveld and Pont d'Arcole Formations; Figure 4-15). Additionally, it is not clear how lithostratigraphic units were formalised, as often the descriptions are conflicting with the actual core data. Hence a proper lithostratigraphic revision for the Dinantian of the Dutch subsurface is required.

4.3.2 Bosscheveld Formation (OBBS; early Tournaisian/Hastarian)

The Bosscheveld Formation (code OBBS) is an informal unit defined by Van Adrichem Boogaert and Kouwe (1994), after the name of the Bosscheveld Quarter of the town of Maastricht, where the stratotype is located.

The type section of this unit is in the KSL-02 well, the interval 382 to 500.5 m (Van Adrichem Boogaert and Kouwe, 1994) and consists of interbedded dark grey, partly calcareous mudstones, fine-grained sandstones and limestones, often nodular and locally red in colour. This definition, however, conflicts with the clear presence of the Pont d'Arcole Formation between 382 and 400 m as proposed by Laenen (2003) to disply a very clear gamma ray log signature. In this study, we use an amended definition for the Bosscheveld Formation, excluding the Pont d'Arcole Formation, explained in Laenen (2003), referred to the 400 to 483.5 m interval in the well KSL-02. The lower boundary is poorly defined and, based on the literature, should be placed at the contact with the underlying, more monotonous siliciclastics of the Bollen Claystone/Evieux Formation (Condroz Group). The top of the unit is put at the disappearance of the carbonates at the top of the Bosscheveld Formation, equivalent of the Hastière Formation of Belgium, and the base of the shales of the Pont d'Arcole Formation. The age of this unit is late Famennian to early Tournaisian (Hastarian/early Courceyan). The Bosscheveld Formation was deposited in a shallow marine setting, probably as a condensed sequence.

4.3.3 Pont d'Arcole Formation (PDA; early Tournaisian/Hastarian)

The Pont d'Arcole Formation is an historical stratigraphic unit outcropping in Belgium, in the same type section of the Hastière Limestone, northwest of Hastière-Lavaux (Paproth *et al.*, 1983). The parastratotypes for the subsurface are represented by the Dutch well KSL-02 the

interval between 382 and 400 m, and by the Belgian wells 125E298 (Vieux-Leuze, SW Belgium) between 573 m and 589 m, 097E817 (Bossuit, SW Belgium) between 81.58 m and 107.95 m (Laenen, 2003). This unit is part of the Kolenkalk Group occurring in Belgium and NW Germany.

The formation comprises dark greenish, very fissile to black shales, which become progressively more calcareous and fossiliferous in the upper half of the section with rare sandstone intercalations. Carbonate intercalations increase towards the top of the unit, with few crinoidal limestones, bryozoans, brachiopods (including *Spiriferina peracuta*) and rare corals. This facies is fairly consistent over broad distances from the SW England to the Aachen region. These shales overlie the Bosscheveld Formation or the Hastière Limestone with a sharp contact. The upper boundary with the overlying Zeeland Formation or with the equivalent Landelies Limestone in Belgium is gradual. This unit is relatively thin: in the type section of Hastière-Lavaux it is 20 m, varying in other areas from 3 to 25 m (Poty *et al*., 2001; Laenen, 2003). The age is early Tournaisian (Hastarian/early Courceyan; Paproth *et al*., 1983). The biostratigraphic attribution is Cf1α foraminifera zone, base RC2 to RC1γ coral zones and Cc1 conodont zone (Figure 4-16; Poty *et al*., 2001; Laenen, 2003).

4.3.4 Zeeland Formation (CLZL; Tournaisian to Visean/Hastarian-Warnantian)

The Zeeland Formation (code CLZL), also known as Carboniferous Limestone, was defined by Cameron (1993) and Van Adrichem Boogaert and Kouwe (1994) for the shallow water carbonate facies. However, this unit has also been used in the literature for wells located in a proximal basinal environment, generating some confusion. In this study, we use the term "Zeeland Formation" as more generic for carbonate units of Lower Carboniferous age of both platform and proximal basin environments. This unit is present in the Dutch onshore and offshore subsurface along the northeastern flank of the London-Brabant Massif, continuing into the onshore outcrops of UK.

The type section is represented by the well S02-02 (Figure 4-17 and 4-18), drilled in the Dutch offshore, on the flank of the London-Brabant Massif. This unit has coverd the interval from 1883 to 2836 m of depth, with a total length of 953 m along hole. According to Van Adrichem Boogaert and Kouwe (1994) the Zeeland Formation is defined as a "*Formation of mainly light-grey to brownish and black limestones, and medium-grey to dark-brown dolomites. Intercalations of thin to medium-thickness fissile claystone and chert beds are common. The claystones occur mainly in the upper- and lowermost parts of the group. Towards the east, the number of these claystones increases gradually. The thickness of the formation in the southern Netherlands varies from 900 to 1400 m. In areas where the Zeeland Formation was truncated by later erosion, the upper part of the formation may be strongly leached and subsequently silicified. An enrichment in organic carbon is frequently observed under these circumstances*".

The top of the unit is placed at the transition from carbonate sediments to the clastics of the Epen Formation of the Limburg Group. The boundary either is represented by an unconformity with associated karst (e.g. O18-01), or by a gradual transition to the oil shales of the Geverik Member of the Epen Formation (GVK-01 and WSK-01 wells). The contact is sometimes difficult to define using the gamma ray log, due to the similar values recorded in the upper portion of the Zeeland and the Epen Formations. In some cases, where the younger unconformities erode deeply into the Carboniferous, the Zeeland Formation is also truncated (e.g. Saalian unconformity at CAL-GT-02 or the Cretaceous unconformity on the flank of the London-Brabant Massif). The definition of the boundary is also complicated by the presence of karst collapse and doline fills at the Dinantian/Namurian boundary along the northern margin of the London-Brabant Massif.

The base of this unit varies from sharp or transitional according to its location. The contact with the Pont d'Arcole Formation may be transitional showing a gradual upward increase of the carbonate content, for example, in the wells KSL-02 and WSK-01. Often the Tournaisian part of this unit may also be missing and the Visean carbonates are in unconformable contact with Devonian sandstones (e.g. UHM-02, LTG-01). This unit is found along the northeastern flank of the London-Brabant Massif in the Netherlands, UK and Belgium, as well as the NW part of Germany close to the Aachen area. The same unit has been found in the isolated platforms in the central and northern Netherlands, for example, in wells UHM-02 and LTG-01. In Belgium and Germany, this unit is usually subdivided into several formations. In the Netherlands, the Zeeland Formation is subdivided into Beveland, Schouwen and Goeree Members. The correlative basinal unit of the Zeeland shallow water carbonates is represented by the condensed Kulm facies encountered in Germany (Bless *et al.*, 1977) and by proximal basin deposits found in KSL-02, HEU-01 and WSK-01. In the North Sea, although unclear, there is a transition towards the clastic units of the British offshore, as found in well E06-01.

The age of the Zeeland Formation is Tournaisian to Visean. Depending on the location, the base of the formation is diachronous. In the isolated platforms of the central and northern Netherlands, the Tournaisian is missing and the Zeeland Formation is only Visean in age. Based on the available biostratigraphic data, on the flank of the London-Brabant Massif, where the contact is more transitional, the base is usually late Hastarian-Tn2 (early Courceyan). The top of the unit, when not eroded, is late Warnantian (Brigantian, V3c).

NETHERLANDS	CAMPINE	VESDER AACHEN	NAMUR	CONDROZ	DINANT NORTH	DINANT SOUTH	SOUTH AVESNOIS	Sub-Stages	Stages
Goeree	Loenhout			Anhée				Warnantian	Viséan
				Poilvache			St-Hilaire / St-Remy Chaussée		
				Thon-Samson			Limont Lmst		
				Bay-Bonnet					
				Seilles/Maizeret			Limont Lmst	Livian	
	Velp			Lives					
Schouwen	Visé		Neffe					Molinacian	
		Bernards-hammer	Terwagne	Hem.	Salet	Hem.	Terwagne		
		Barenstein			Braibant	Molignée			
		Hastenrath			Sovet				
Beveland	Vesder	Vesder	Avins		Leffe	Leffe / Waulsort	Godin	Ivorian	Tournaisian
			Flémalle				Grives Dolostone		
			Engihoul	Martinrive	Leffe	Leffe / Waulsort	Grives Dolostone		
			Engihoul	Ourthe		Bayard / Waulsort	Grives Lmst		
				Yvoir					
				Maurenne				Hastarian	
		Landelies Lmst	Engihoul	Landelies					
Pont d'Arcole			Pont d'Arcole						
			Hastière upper member						
Bosscheveld		Hastière (dol.)	Hastière lower-middle members				Avesnelles		
		Dolhain	Comblain-au-Pont				Etroeungt	Str.	Fa.

Figure 4-15: The Zeeland Formation and its members and equivalent formations of the surrounding areas (from Poty, 2016 integrated with Amler and Herbig, 2006).
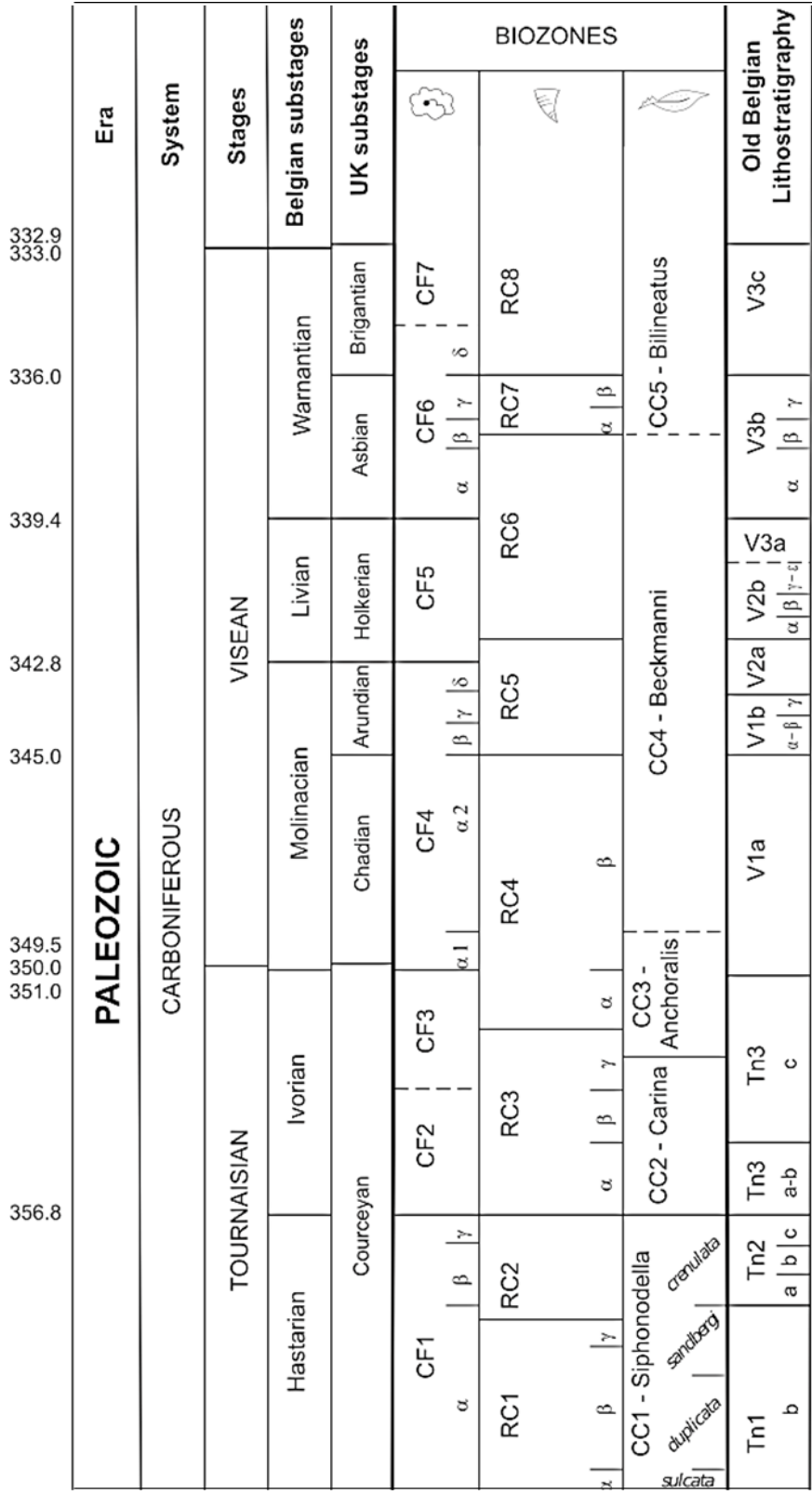
Figure 4-16: Biostratigraphic chart for the Dinantian developed for the north and northeastern Belgium (modified from Laenen, 2003). Note that the classification of biozones might be slightly different from the ones presented in the current study.
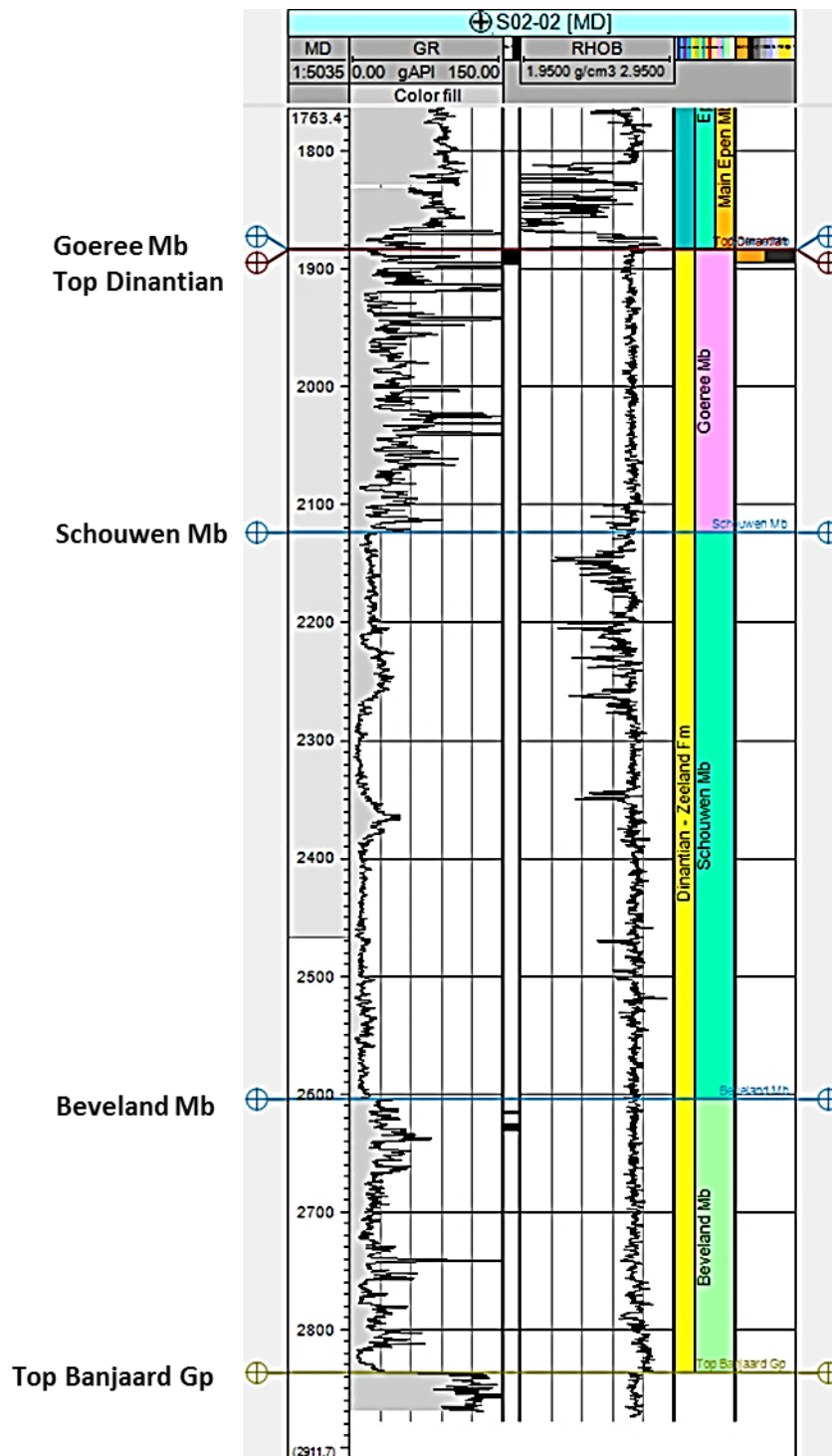
Figure 4-17: Type section for the Zeeland Formation in well S02-02.

Beveland Member (CLZLB; Hastarian-Chadian)

The lowermost subdivision of the Zeeland Formation is represented by the Beveland Member (CLZLB) and was defined by Van Adrichem Boogaert and Kouwe (1994) and was named after the island of Noord-Beveland in the province of Zeeland.

The type section is defined in well S02-02, the interval between 2604 and 2836 m, with a total thickness of 232 m along hole (Figure 4-18). Van Adrichem Boogaert and Kouwe (1994) also considered the KSL-02 well as an additional section (interval 338-382 m) but based on the current study the KSL-02 well is not representative of the Beveland Member, as it is very shaley

and represents a proximal basin environment. According to Van Adrichem Boogaert and Kouwe (1994), the Beveland Member is defined as "*A sequence of medium-grey or brown grey to dark-brown or brown-black, coarse-crystalline dolomites, often containing black organic intergrain residues. The dolomites are generally of secondary origin. In places minor grey to dark-grey limestone intercalations occur, as well as minor quantities of dark-brown to blackish siltstone and shaly claystone. In addition, dark beds of silicified dolomite are occasionally present.*" The onset and end of carbonate deposition appear to take place at different times in different parts of the basin. Thus, the base and top of the Beveland Member are likely to be diachronous, and their ages are a matter of debate and needs to be re-examined. In this study the top of Beveland Member may cover a range of Hastarian to early Livian (Chadian) (e.g. UHM-02).
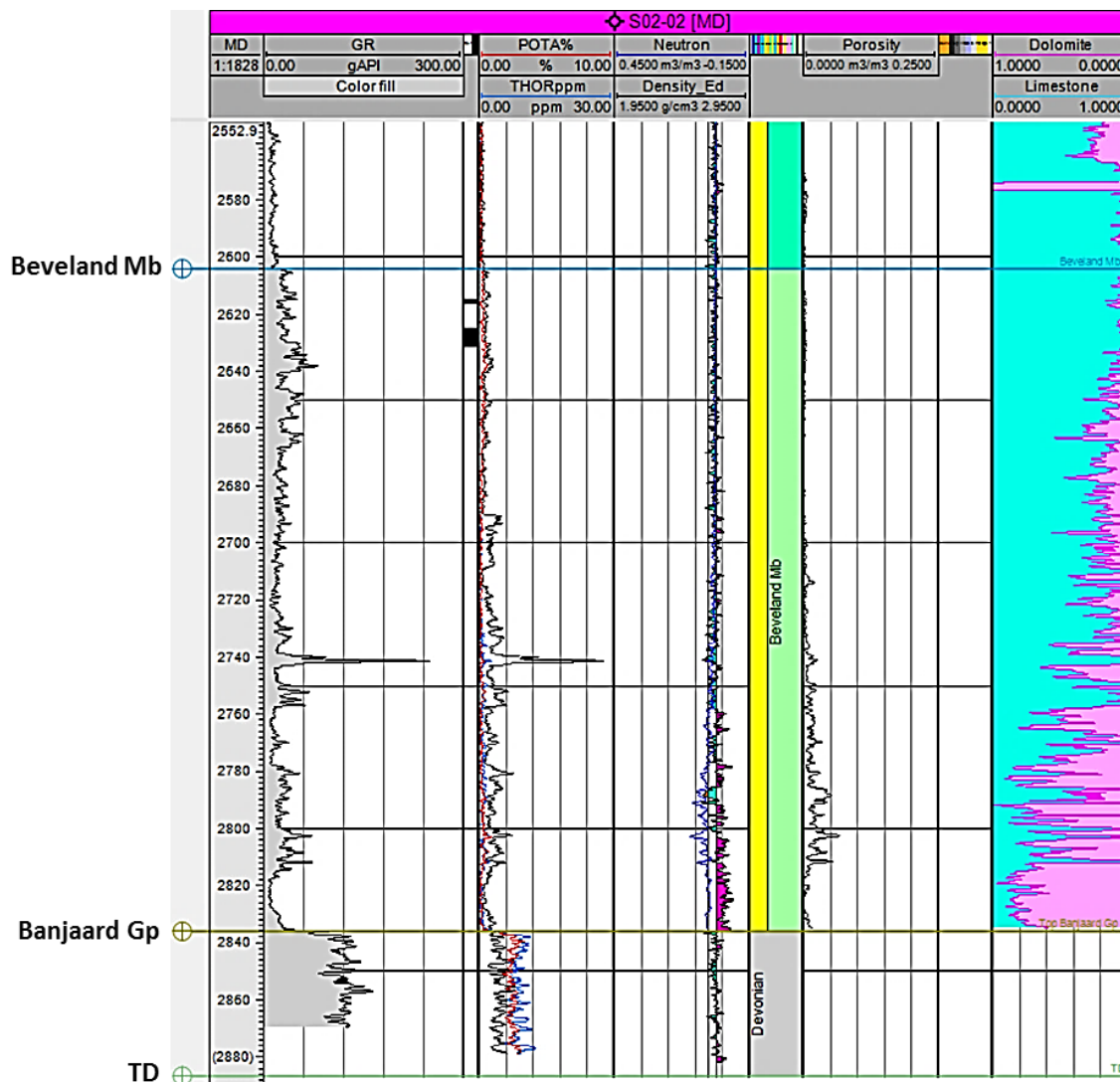
Figure 4-18: The Beveland Member in the S02-02 well. The pink colour stands for dolomitised proportions.

Schouwen Member (CLZLS; Molinacian-Livian)

The Schouwen Member (CLZLS) is defined by Van Adrichem Boogaert and Kouwe (1994) in the well S02-02 in the interval 2123 to 2604 m (thickness along hole 481 m). It is named after the western part of the island of Schouwen-Duiveland in the province of Zeeland. The latter

authors also considered the HEU-01 well as a parastratotype in the interval 114 to 502.7 m (Figure 4-19), but the current study assigned a rather different sedimentary environment in this well.

According to Van Adrichem Boogaert and Kouwe (1994), this member is defined as "*A thick sequence of light to dark-grey, dark- to yellowish-brown and brownish-black, and light yellowish-brown to dusty yellow-brown limestones. The dense limestones are micritic, biosparitic to biomicritic, locally oolitic and abundantly fossiliferous. In places coarsely crystalline calcite veins occur. Intergranular bituminous, organic material is often present. Locally, the limestones are dolomitised, especially near fault zones, or silicified in the leached zone in areas where later erosion truncated the Zeeland Formation.*"

The age is most likely early to middle late Visean. The boundaries of this member are not clearly defined in the original description, leaving a lot of uncertainty about the usage of this lithostratigraphic unit.
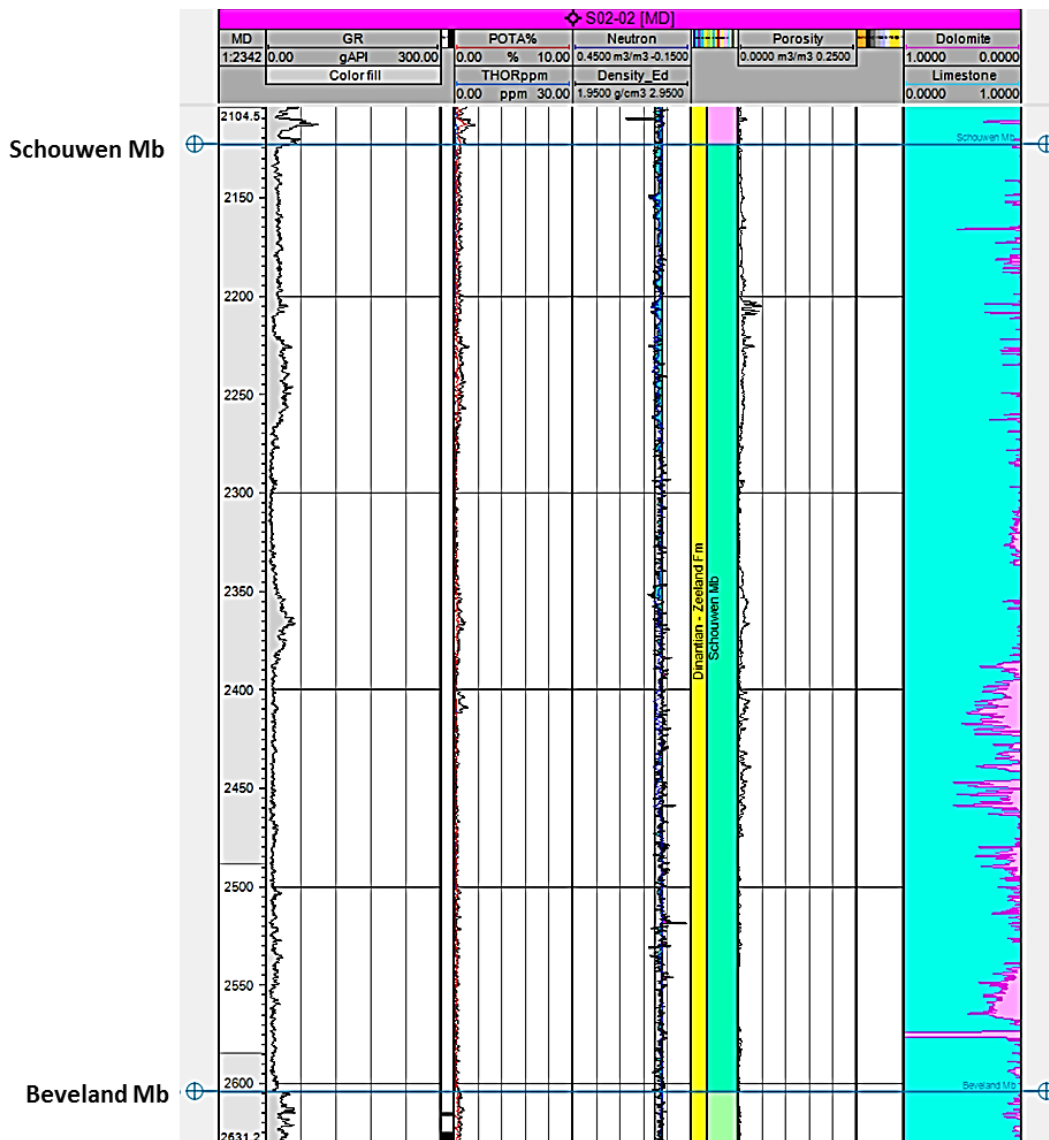
Figure 4-19: Reference section of the Schouwen Member in well S02-02. The pink colour stands for dolomitised proportions.

Goeree member (CLZLG; Warnantian)

The Goeree Member (CLZLG) was defined by Van Adrichem Boogaert and Kouwe (1994) and named after the western part of the island of Goeree-Overflakkee in the province of Zuid-Holland. The type section is in the well S02-02 between 1883 to 2123 m (thickness 240 m along hole) (Figure 4-20). An additional parastratotype is proposed in the well GVK-01 between 992 to 1492 m (Figure 4-21).

Based on the latter authors, this member is defined as "*A sequence of grey to dark-grey and black limestones, thin- to thick-bedded and often partly silicified. The limestone beds often grade into calcareous and/or silicified black shales or black cherts toward the top. Very thin beds of tuffaceous rock occur, predominantly in the upper part of the member.*"

The lower boundary is usually pinpointed by the gamma ray increase in respect to the previous member due to an increase of shales and/or volcanic tuffs in the upper part of the Zeeland Formation. However, these gamma ray spikes may be related to karst fills in wells along the northern margin of the London-Brabant Massif. The age of this member is mostly late Visean, Livian to late Visean, Warnantian (late Holkerian to Brigantian/V3a-v3c). This member corresponds to the Goeree Formation of Belgium (Laenen, 2003).
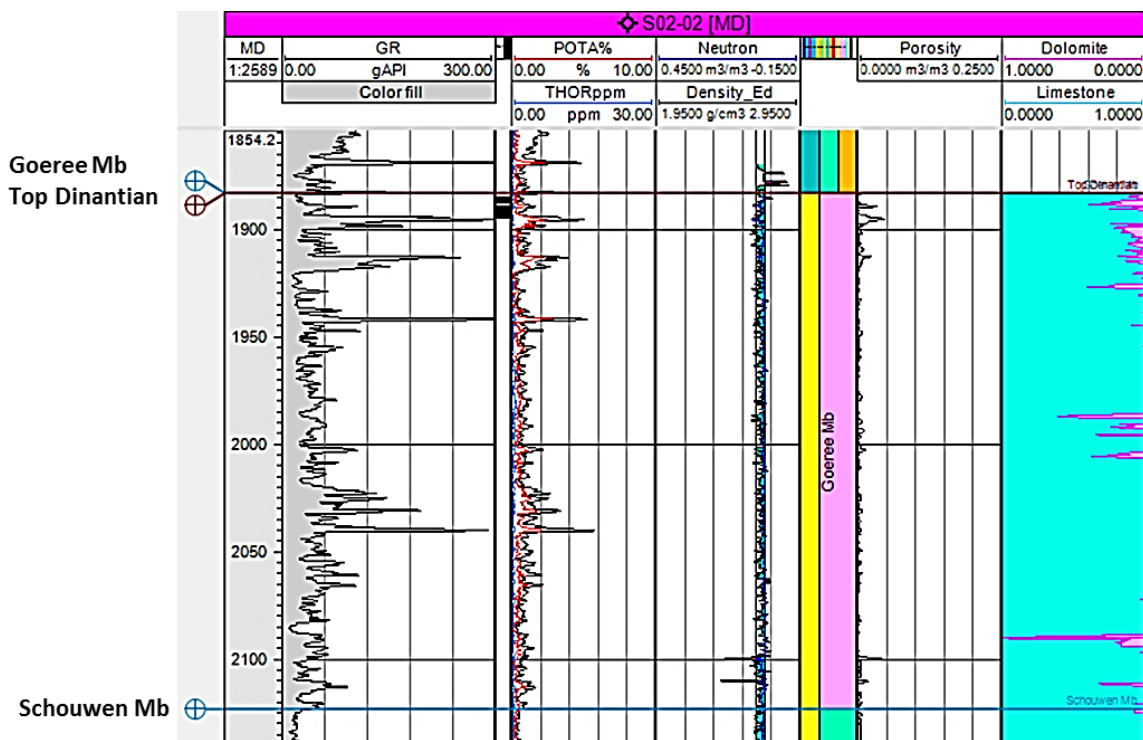
Figure 4-20: Type sections of the Goeree Member in well S02-02. The pink colour stands for dolomitised proportions.
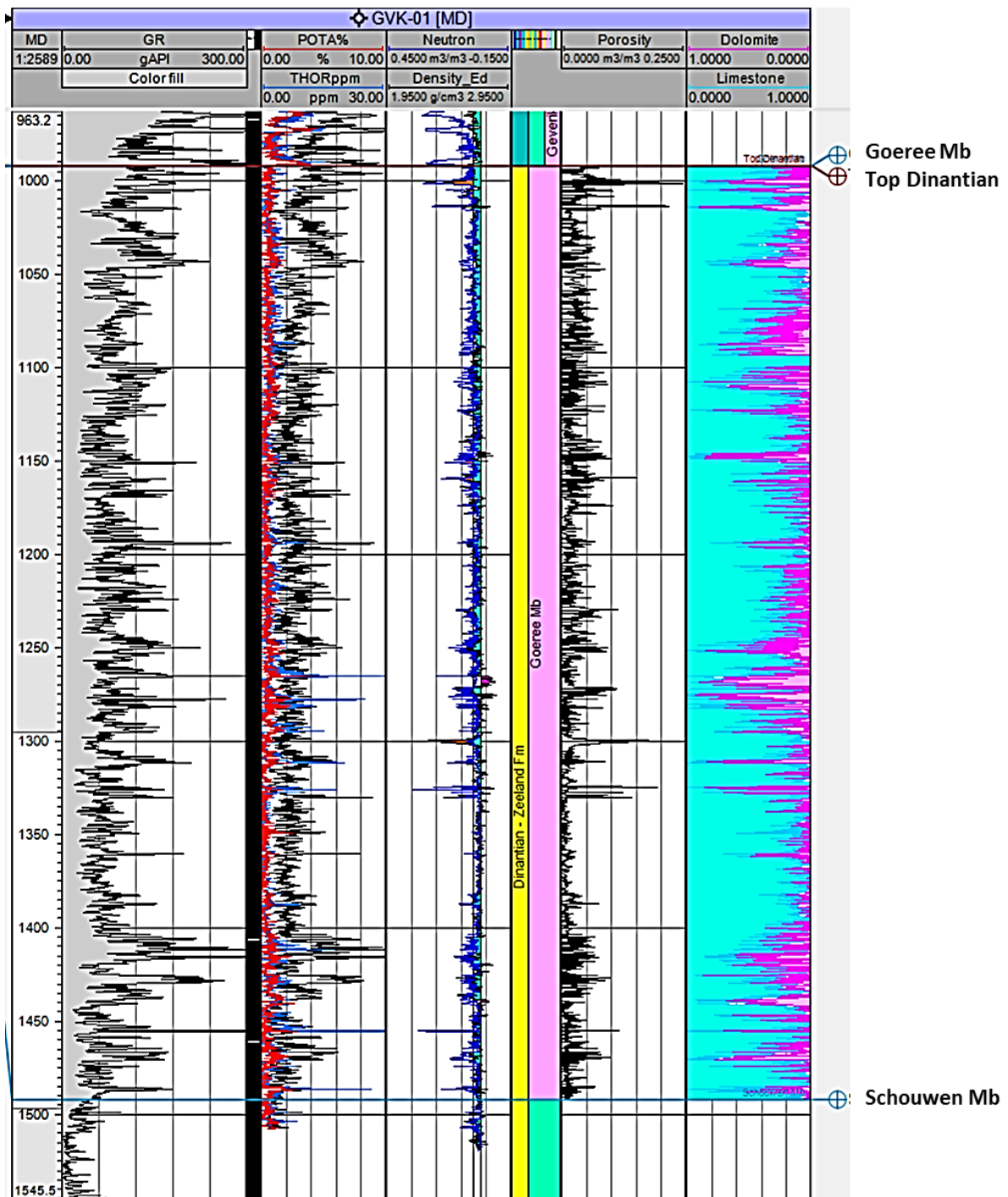
Figure 4-21: Parastratotype of the Goeree member in well Geverik-01. The pink colour stands for dolomitised proportions.

5. Methodologies and workflows applied in the project

5.1 Sequence stratigraphy

Two regional sequence stratigraphic frameworks have been developed by Pickard and Gutteridge (1997) and Reijmer *et al*. (2017) (Figures 5-1 and 5-3, Table 6-1). These frameworks are in agreement with each other and both show an evolution from a carbonate ramp to carbonate shoal and to a broad carbonate shelf, and eventually drowing of the shelf. The Dinantian carbonates observed in the UK part of the London-Brabant massif was considered as anologues in both frameworks. These frameworks do not incorporate the carbonate successions of the isolated carbonate platforms penetrated by LTG-01 and UHM-02 wells. Therefore, in the current study efforts have been made to place them within the regional sequence stratigraphic framework.

According to Pickard and Gutteridge (1997), Sequence 1 is late Tournaisian to early Visean (Chadian) in age and is speculated to represent a low relief carbonate ramp setting (Figure 5-2). This sequence corresponds to the D1 depositional unit introduced by Reijmer *et al*. (2017) (Figures 5-1 and 5-3). The onset of carbonate-dominated Dinantian succession in this sequence is marked on the wireline logs by a rapid shift to lower gamma ray activity. In the cores studied, Sequence 1 consists of cyclic shallow subtidal to intertidal rocks. Subtidal sediments typically possess grainstone or packstone textures indicating deposition in moderate to high-energy settings. Dolomitised intervals are common. It is possible that Sequence 1 will continue to thicken offshore where large Waulsortian buildups can be expected basinward of the studied wells. Sedimentary sequences basinward of the Waulsortian complexes are dominated by condensed deep-water shales and periplatform micritic sediments (WSK-01).

Sequence 2 is of Moliniacian to Livian age (Table 6-1) and corresponds to the D2 depositional unit introduced by Reijmer *et al*. (2017) (Figures 5-1 and 5-3). Cores presenting this interval consist of successions of grain-supported algal packstone and grainstone lithologies. Gama ray log is frequently uniform, but some variations suggest large-scale transgressive and regressive sequences. Correlation of gamma ray logs to the cored intervals shows that increased and decreased gamma ray activities correspond with slightly argillaceous algal packstones and thin calcareous shale intervals, and with 'cleaner' algal grainstone and packstones. The thick cycles of shallow water grainstones and packstones that characterise Sequence 2 developed on an aggrading carbonate platform: sedimentation kept pace with subsidence, cycles are thick and exposure surfaces uncommon. Offshore, sedimentation-rates were lower and condensed intervals developed.

Sequence 3 is of Warnantian age and corresponds to D3 depositional unit introduced by Reijmer *et al*. (2017) (Figures 5-1 and 5-3). This sequence developed as a flat-topped shelf fringed by a slope (Figure 5-2). Cyclic shallow subtidal sediments dominate shelf-top. Carbonate buildups are likely to have been present near the shelf break, either as isolated features associated with grainstone inter-buildup sediments or as a more-or-less continuous facies belt at the shelf break. The gamma ray log is generally moderate with some spikes in the slope sequences which are considered to result from the presence of uranium-rich sediments.

In the current study the recognised depositional sequences include ten depositional cycles. These cycles are defined by the biostratigraphic dating and their correlation with the distinct gamma ray log signatures. Sequence boundaries in carbonates were picked at gamma ray lows, above which an increase to a gamma ray high, generally indicated a maximum flooding surface with the upper part of the cycle represented by a generally cleaning-upwards gamma ray signature. Lateral variations in depositional setting, produce variations in cycle thickness and gamma ray signature. For example, basinal successions tend to be condensed with high gamma

43

ray readings, while shallower water carbonate ramp systems show cleaner gamma ray signature with a clearer distinction between transgressive, maximum flooding and high stand intervals. In contrast carbonate shelf cycles tend to have a very clean gamma ray response with any spikes mainly caused by high uranium-rich karst fills or soil. All available biostratigraphic and lithostratigraphic information was loaded into the Petrel project to constrain the range of stratigraphic ages of the Dinantian intervals in each borehole; this information was also incorporated for the overlying- and underlying parts of the succession so that any unconformities or stratigraphic breaks above and below the Dinantian could be identified. Since these high-resolution sequence stratigraphic correlations were based mainly on gamma ray log character, intervals with high gamma readings were checked in wells with a spectral gamma ray log to ensure that this response was caused by potassium content and not the presence of uranium or thorium. The depositional sequences and associated depositional cycles were recognised based on correlations of wells including O18-01, BHG-01, S02-02, KTG-01 and S05-01 in the SW Netherlands. Using the same approach, depositional sequences were regionally extrapolated and developed for other wells (UHM-02, LTG-01, WSK-01 and KSL-02). In some areas, the upper cycles are missing as a result of karstic erosion at the base of the overlying Limburg Group or the sub-Cretaceous unconformity. The depositional cycles have been arbitrarily labelled by codes. All depositional cycles except 3a are represented by at least one core. These cycles may represent 3rd order sedimentary sequences and their relationship with the three depositional sequences recognised by Pickard and Gutteridge (1997) are summarised by the following table:

Table 5-1: Depositional sequences identified in this study in integration with Pickard and Gutteridge (1997).

Depositional cycles (this study)	Depositional sequences Pickard and Gutteridge (1997)	Age	Depositional events
3b	Sequence 3	RC7β-RC8 (Warnantian)	Carbonate shelf-margin-basin systems
3a			
2d	Sequence 2	V1b-V2a (mid- to late Molinacian) to V2bß middle Visean age (Livian)	
2c			Carbonate ramp to shelf transition
2b			
2a			
1d	Sequence 1	Late Tournaisian (V1 or older) to *Eoparastaffella* Cf4α subzone of V1a (earliest Molinacian)	Carbonate ramp systems
1c			
1b			
1a			Initial flooding of basin
Clastics		Tournaisian	

44

Name	Depositional trend	Age	Lithofacies	Log characteristics	Seismic expression
D3	Drowning carbonate margin. Landward migration of deposition. Formation of extensive carbonate slope. Conformably overlying older formations.	Asbian and Brigantian	Open marine carbonate slope sediments. Welded carbonate breccia, boulder beds, bioclastic mass flow deposits, algal mounds and siliciclastic muds. Crinoids, algal laminations, bryozoans.	Moderate gamma-ray with abundant high gamma-ray spikes. Exceptionally high gamma-ray associated with mineralisations.	Formation of staircase geometry in landward direction, onlapped by overlying strata. Strong through at top, formed by down- and onlapping overlying Namurian strata.	
D2	Development of broad, rimmed carbonate shelf. Progressive onlap, overstepping older formations.	Chadian to Holkerian	Open marine shelf carbonate shoals with restricted lagoonal platform carbonates. Light brown, clean grainstone and packstone. Ooids, thick-walled shells, crinoids.	Uniform, blocky low gamma-ray.	Uniform transparent seismic facies, little to no internal structure. If visible, onlapping and downlapping reflectors (clinoform geometry). Platform rim and seaward mound structures are often discernible.	
D1	Extensive low relief carbonate ramp, onlapping basement.	Tournaisian to Chadian	Cyclic development of peritidal, marginal marine to shallow marine carbonates and extensive mudflats with evaporites. Often dolomitised. Dark-coloured, bioturbation, algal laminations, pedogenic structures.	Irregular alternation of intervals with low and moderate gamma-ray.	High-energy reflectors at base of carbonate sequence. Local infill of fault-bounded depression.	

Figure 5-1: Main depositional, lithofacies, log and seismic characteristics of depositional units D1-D3 recognised by Reijmer *et al*. (2017).
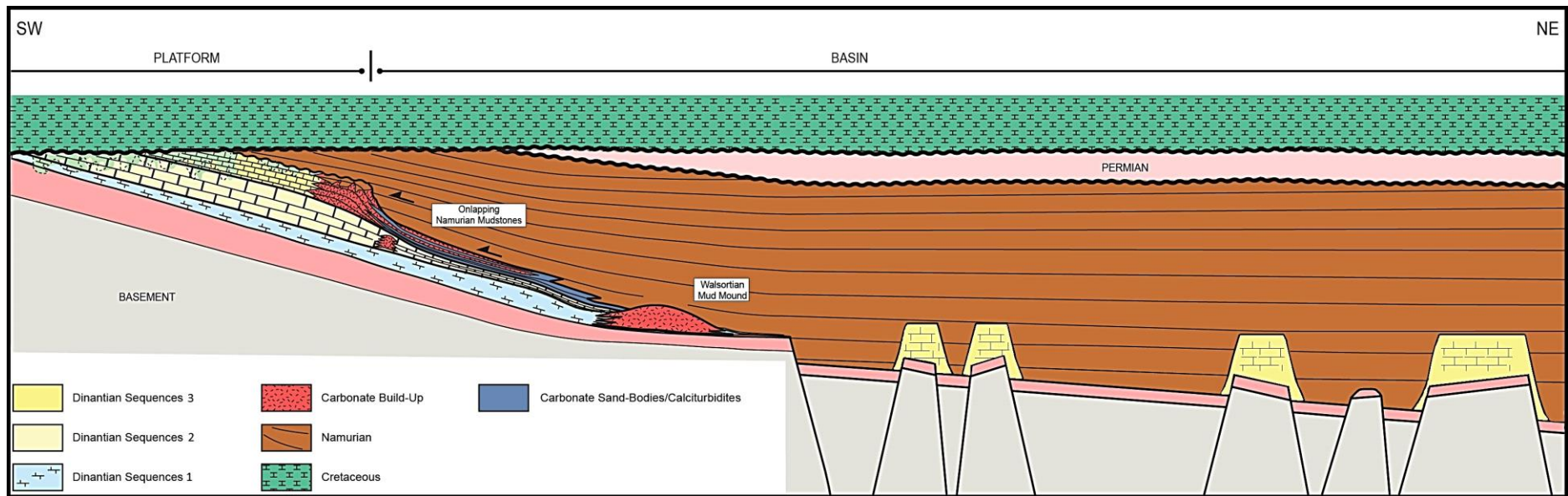
Figure 5-2: Schematic figure (not scaled) showing the general platform evolution model, modified from Total UK (1997). Note that in this figure the sequences are not delineated for the isolated platforms.

46
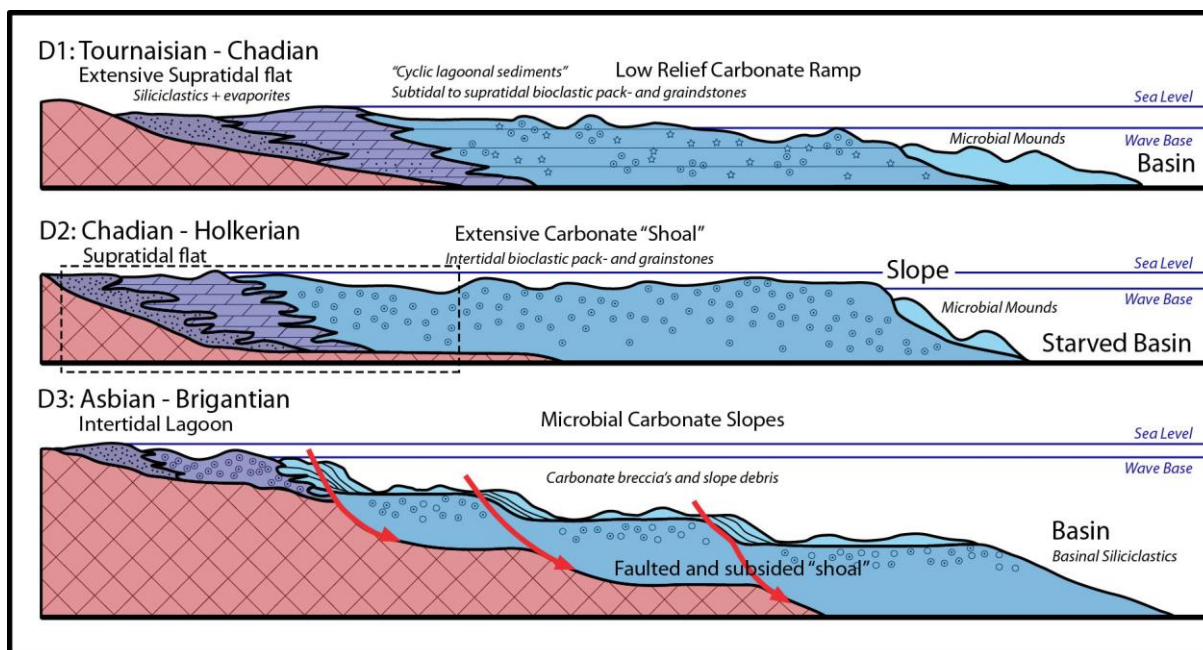
Figure 5-3: Schematic figure (not scaled) showing the facies model of D1, D2 and D3 (Reijmer *et al*., 2017) occurring north of the London-Brabant Massif.

The well control outside the southwestern Netherlands is very widely-spaced with short cored intervals and low resolution biostratigraphic data. Although the northern Netherlands has good quality 3D seismic data, it is difficult to link this to the southern Netherlands because the area is covered by a number of separate 2D surveys of varying vintage.

Biostratigraphic information from UHM-02 and LTG-01 were added to the Petrel project and matched with the ages of the groups of sedimentary sequences identified in the southern Netherlands.

5.2   Core logging

Cores were stored in two main locations in the Netherlands (Table 5-2):

Table 5-2: Cores evaluated for this study.

Assen NAM corestore	Zeist TNO corestore
BHG-01	GVK-01
KTG-01	HEU-01
S02-02	HEU-01-S1
S05-01	KSL-02
UHM-02	LTG-01
WSK-01	O18-01

Hand-drawn core logs were initially created, and these were later transferred into CoreCad software, where digital core logs and pdfs could be output. For some of the wells, basic core logs were already available-these were utilized and improved upon for this phase of work (Table 5-3).

GVK-01 was not logged, as a CoreCad log was already available on NLOG. Only specific intervals of HEU-01 and HEU-01-S1 were logged.

All cores were logged at either 1:50 or 1:100 scales. The following elements were captured: lithology, sedimentary structures, carbonate texture, grain size, bioturbation, allochems, fossils,

47

porosity and pore types, hydrocarbon shows, diagenetic features, karst features, fractures, depositional environments, and important surfaces (Figure 5-4). Core photography of important diagenetic features, facies, sequences, oil stains and allochems was also undertaken.

Core from the following wells were depth corrected to match the log response. The depth shifts of other cores were not determined because there were no distinctive features to match with log response and were therefore imported in Petrel according to the drillers' depth.

Table 5-3: Available core to wireline log shifts.

Well and core	Core depth	Equivalent log depth	Core shift
BHG-01, Core 2	2375.0 m	2382.0 m	Core 7.0 m shallower than log
KSL-02	357.4 m	354.4 m	Core 3.0 m shallower than log
KTG-01	974.0 m	979.0 m	Core 5.0 m shallower than log
UHM-02, Core 1	4751.2 m	4758.0 m	Core 6.8 m shallower than log
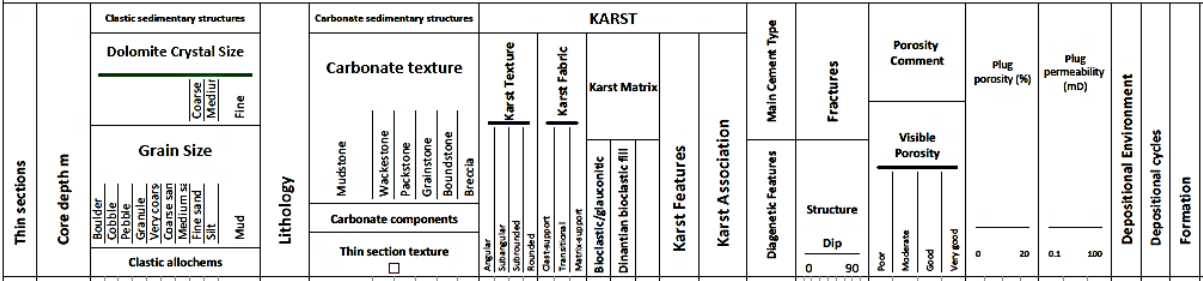
Figure 5-4: Example of a header of sedimentological core log with data tracks.

5.3   Petrography

Thin sections were made available to EBN through TNO at the NAM corestore at Assen. The number of studied thin sections is given in Table 3-2.

Petrographic descriptions were already available for the thin sections stored at NAM in the Pickard and Gutteridge (1997) report. However, the thin sections were re-visited and photomicrographs were re-taken in order to have a comprehensive set of digital data available. Photomicrographs were taken using an iPhone camera and a microscope adaptor due to absence of microscope camera facilities at the NAM corestore. Both PPL (plane polarised light) and XPL (cross polarised light) images were taken. It was not allowed to remove the NAM thin sections from the Assen corestore – all analyses had to be undertaken in-house.

Microscope facilities at Delft University were used to analyze the thin sections made available through TNO. Photomicrographs were taken using an integrated camera and basic petrographic descriptions were completed.

Thin sections were prepared from samples selected from cores to characterise the cement generations, to distinguish different diagenetic features and to gain more information on the cross-cutting relationships on a microscopic scale. Samples that were acquired at NAM core store in Assen were cut by NAM staff using an in-house rock saw. Samples that were acquired at the Zeist core store were hand selected from the core.

A total number of 22 new polished thin sections were prepared. In order to discriminate dolomite from calcite also taking their iron content into account, polished thin sections were stained using Alizarine Red S and Potassium Ferricyanide (Dickson, 1966). The classification

scheme used in petrography is based on Dunham (1962) for carbonate sedimentary rocks. The photomicrographs will be available at TNO.

5.4   Thin section scans

A total of 619 existing thin sections from core and side wall cores (SWCs) were scanned using an Epson Perfection V600 scanner, at 6400 dpi and 4000 dpi resolutions. The scanned thin sections will be available at TNO.

5.5   Cold Cathodoluminescence (CL)

CL is a qualitative diagenetic technique which, along with traditional microscopy, can allow a diagenetic description of the sample. CL colour and brightness are dependent on several factors. Luminescence in carbonate minerals is excited by Mn^{2+}, whilst Fe^{2+} typically quenches the CL response. The ratio of Mn/Fe and their associated emission colours are commonly related to geochemical environments, particularly to redox potential changes during cementation (Machel, 2000). CL is also useful in highlighting sometimes less obvious phases such as fluorite, kaolinite and also feldspar as well as minerals masked by hydrocarbons.

CL analyses was performed on 22 polished thin sections at Cambridge Carbonates (UK) using a Nikon Eclipse LV100 microscope with Q imaging Retiga EXi camera attached to a Technosyn CITL 8200 Mk5-1 cold cathodoluminescence system. The CL equipment uses a standard x-y stage vacuum chamber, with general beam settings ranging from 12 to 21 kV, which is sample dependent. The gun current was between 150-450 μA. The photomicrographs will be available at TNO.

5.6   Sulfur Isotopes

Three samples of pyrite were measured for their Sulphur isotopes ($\delta^{34}S$) to determine the possible organic or inorganic source of sulfates involved in mineralisation. The analysis was performed at PanTerra Geoconsultants B.V. (the Netherlands) using EA-IRMS. Tin capsules containing reference or sample material plus vanadium pentoxide catalyst were loaded into an automatic sampler from which they were dropped, in sequence, into a furnace held at 1080°C and combusted in the presence of oxygen. Tin capsules flash combust, raising the temperature in the region of the sample to ~ 1700° C. The combusted gases are then swept in a helium stream over combustion catalysts (tungstic oxide/zirconium oxide) and through a reduction stage of high purity copper wires to produce SO_2, N_2, CO_2, and water. Water is removed using a Nafion™ membrane. Sulphur dioxide is resolved from N2 and CO_2 on a packed GC column at a temperature of 32 °C. The resultant SO_2 peak enters the ion source of the IRMS where upon it is ionized and accelerated. Gas species of different mass are separated in a magnetic field then simultaneously measured on a Faraday cup universal collector array. Analysis was based on monitoring of mass/charge (m/z) 48, 49 and 50 of SO^+ produced from SO_2 in the ion source.

The reference material used for analysis was IA-R061 (Iso-Analytical working standard barium sulphate, $\delta^{34}S_{CDT} = +20.33$ ‰). IA-R025 (Iso-Analytical working standard barium sulphate, $\delta^{34}S_{V-CDT} = +8.53$ ‰), IA-R026 (Iso-Analytical working standard silver sulphide, $\delta^{34}S_{V-CDT} = +3.96$ ‰) and IA-R061 were used for calibration and correction of the ^{18}O contribution to the SO^+ ion beam.

Working standards are traceable to NBS-127 (barium sulphate, $\delta^{34}S_{CDT} = +20.3$ ‰), IAEA-SO-5 (barium sulphate, $\delta^{34}S_{CDT} = +0.5$ ‰) and IAEA-S-1 (silver sulphide, $\delta^{34}S_{CDT} = -0.3$ ‰).

Test samples of IA-R061 and IAEA-SO-5 were also measured as quality control check samples during analysis of your samples. The $\delta^{34}S$ values obtained for the quality control check samples are given in the table of results.

NBS-127, IAEA-S-1 and IAEA-SO-5 are distributed as isotope reference standards, by the International Atomic Energy Agency (IAEA), Vienna.

5.7 C and O stable isotopes

$\delta^{13}C$ and $\delta^{18}O$ values of 52 carbonate samples from matrix and cements were measured to determine fluid sources (e.g. marine, meteoric or diagenetic) and to infer the possible precipitation temperatures. This analysis was performed at Friedrich-Alexander-Universität (Erlangen-Nürnberg, Germany). Powder samples of at least 200 µg were obtained using a dental drill.

Carbonate powders were reacted with 100% phosphoric acid at 70 °C using a Gasbench II connected to a ThermoFisher Delta V Plus mass spectrometer. All values are reported in per mil relative to V-PDB. Reproducibility and accuracy was monitored by replicate analysis of laboratory standards calibrated by assigning $\delta^{13}C$ values of +1.95‰ to NBS19 and -47.3‰ to IAEA-CO9 and $\delta^{18}O$ values of -2.20‰ to NBS19 and -23.2‰ to NBS18. Reproducibility for $\delta^{13}C$ and $\delta^{18}O$ was ±0.0x and ±0.0y (1 std.dev.), respectively.

Oxygen isotope values of dolomite, siderite, aragonite etc. were corrected using the phosphoric acid fractionation factors given by Kim *et al*. (2007) and Rosenbaum and Sheppard (1986).

5.8 Fluid inclusion analysis/Microthermometry

Fluid inclusion microthermometry provides important information about temperature of mineral precipitation, fluid composition and salinity. A total number of 6 doubly polished sections (wafers) with a thickness of 150 µm were prepared. The analysis was performed at H-Expertise Services S.A.S. (Nancy, France). The samples generally contain aqueous inclusions. One dolomitic sample from KTG-01 also contains oil inclusions.

Epi-UV fluorescence observations were also conducted using a Zeiss AxioImager A1m microscope with an excitation filter centered at 365 ± 5 nm and an emission filter long pass around 400 nm. These planes are interpreted as the result of fluid entrapment along surfaces showing preferential crystallographic orientation (Van Den Kerkhof and Hein, 2001). They can be considered as primary fluids. Transgranular planes are the fluid inclusions planes intersect the grain boundaries. They represent the healing fractures, and thus are secondary fluids.

Phase transitions of aqueous fluid inclusions were measured at temperatures between -170 °C and +400 °C using a LINKAM MDS 600 heating-freezing stage equipped with a Sony Exwave HAD3 color video camera mounted on an Olympus BX 51 microscope at GeoRessources, Vandoeuvre-lès-Nancy summarises the observed phase transitions and their abbreviations. The microthermometric stage was thermally calibrated using CO_2 synthetic fluid inclusions standards for Tm (CO_2), H_2O synthetic fluid inclusions standards for the final ice melting (Tm ice) and cross-calibrated natural alpine fluid inclusions ("home" standard) for Th. The accuracy of measurements is estimated at ±0.2 °C for the final ice melting (Tm ice) (heating at 0.5-1 °C/min) and ±0.5 °C for the homogenization temperatures (Th) (heating at 1-5 °C/min).

Heating two-phases (oil-gas) inclusions to homogenisation provides a minimum trapping temperature. In the case of the petroleum and aqueous inclusions, Th establishes a minimal temperature of trapping of the inclusion. Nevertheless, considering the shallow slope of the isochores of the petroleum systems, Th can be very different and below the true temperature of trapping, up to tens of degrees, and this varies according to the composition of the petroleum fluid and the pressure.

5.9 X-ray diffraction (XRD) measurements

XRD analysis was used to obtain the detailed information on quality and quantity of minerals with special focus on the clays regarding their important role in provenance of sediments. This

analysis was performed on a total number of three samples at EMR RWTH Aachen (Germany). Rock samples were crushed manually in a mortar and milled subsequently with a McCrone Micronising mill for 20 minutes to ensure uniform crystallite sizes. Milling was done in ethanol to avoid dissolution of water-soluble components and strain damage to the samples. An internal standard (Corundum, 20 wt. %) was added to improve the accuracy of the analysis.

Bulk mineralogical compositions were derived from X-ray diffraction patterns measured on randomly oriented powders. The measurement was done on a Bruker AXS D8 Advance diffractometer using CuKa-radiation produced at 40 kV and 40 mA. The divergence slit is fixed at 1 mm, with a secondary Soller slit behind the sample. The detector is a scintillation counter with graphite monochromator. Diffractograms were recorded from 2° to 92° 2θ in 0.02° steps and a counting time of 5s.

Quantitative phase analysis was performed by Rietveld refinement using BGMN software, with customised clay mineral structure models (Ufer *et al.*, 2008). The precision of these measurements, from repetitions, is better than 0.1 wt. % for phases of which the content is above 2%. The accuracy is difficult to determine because of the lack of high purity clay mineral reference materials but is estimated to be better than 10% (relative).

5.10 Vitrinite reflectance

The study of vitrinite reflectance (VRr) is a key method for identifying the maximum temperature history of sediments in sedimentary basins. This method can be applied on samples with organic carbon (Corg) > 0.5%. The temperature can be determined using the equation of Barker and Pawlewicz (1994) for burial temperatures, as follows:

$T_{burial} = (\ln(VRr) + 1.68)/0.0124$

This analysis was performed on a total number of three samples at EMR RWTH Aachen (Germany). The petrographic analyses and vitrinite reflectance were performed on polished sections. The preparation of polished sections is described in detail by Littke *et al.* (2012). Vitrinite reflectance measurement was performed using a Zeiss Axioplan microscope equipped with a 50× Epiplan-NEOFLUAR oil immersion objective. Random vitrinite reflectance (VRr) measurements were conducted according to the standard procedure described in Taylor *et al.* (1998) and more details on the microscopic device are stated in Sachse *et al.* (2011). Each measurement was calibrated with a Cubic Zirconia standard (3.125%).

The preparation of the polished thin section was complicated due to the presence of water-soluble and swelling minerals. This was most pronounced for the BHG samples. The samples were thus doubly impregnated to ensure an even surface of the section. The quality of the polished BHG samples is not good for petrographic imaging but was sufficient for the vitrinite reflectance measurements.

5.11 Biostratigraphy

Palynological, microfaunal and thermal maturity (spore colouration) analyses were undertaken on 5 samples at Network Stratigraphic (UK). The aim of these analyses was to determine the age of karst filling sediments and the maximum temperature experienced by them. Digital photomicrographs of sub-Cretaceous karst fills were also provided for dating.

5.12 Map building

A Petrel project was compiled by Ten Veen *et al.* (2019). This master Petrel Project includes all the 3D seismic data available, most of the pre-existing interpretation and grids from TNO/NLOG, all public domain wells with composite logs and cultural data. Ten Veen *et al.* (2019) used publicly available Dutch gravity and magnetic datasets as well as German and Belgian data. Seismic horizons (time and depth grids) from Ten Veen *et al.* (2019), calibrated

by the wells and outcrop data, were used to delineate the key horizons of the Dinantian carbonates and construct the paleogeographic maps. The seismic interpretations were used to pinpoint the internal geometries of the Dinantian carbonates. Locally, the interpretation of Base Dinantian (?Top Devonian) and Base Cretaceous were added: this was particularly important for defining the subcrops of the Base Cretaceous unconformity and the extent of related karstification. The interpretation, obviously, is reliant on the quality of seismic data coverage and quality as shown in Figure 5-5. In this figure, good data quality means that the Dinantian package is well visible and well defined by sharp reflectors at top and occasionally bottom. Average data quality is referred when the Dinantian is visible, but the bottom and top reflectors are not sharp and tend to be discontinuous.

Poor data quality could be applied in several cases:

- o Top Dinantian is barely visible and the base is not visible at all in possible platform areas;
- o Top Dinantian is too deep, so is not possible to interpret it;
- o Top Dinantian interpretation is extremely uncertain due to poor seismic quality. This occurs especially in basinal areas.

When seismic quality is poor, the interpretation relies on well data, if available, and on the interpretation from the gravimetric/magnetic data.

The distinction between carbonate platform and basinal environment can be done on seismic only when the base Dinantian is visible: the shallow water carbonates are showing a clear separation between top and bottom Dinantian (about 200 ms), while in the basinal areas these two reflectors are joining together. This approach, however, could only be applied for the Brabant Platform and the isolated platforms of the Central-Northern Netherlands.

The shape of Uithuizermeeden and Fryslân platforms could be defined geometrically by the time contour at -2860 ms, showing that in that area the subsequent deformation did not cause any major tilting. In the Luttelgeest and Nagele platforms the same time contour is marking the base of the platform, rather than the margin edge, so a shallower time contour was used. Slope deposits were defined by their seismic character until the depth of about -3500 ms, where the seismic character changes, probably due to the lack of the carbonates.

Towards the east, the Californië area is defined only by the wells and partly by outcrops towards the southeast: in this case the base Dinantian is visible but the top Dinantian gets thinner eastwards.

The Winterswijk area and its transition towards the Kulm Basin are not covered by seismic. The Winterswijk Platform could only be postulated due to the presence of resedimented shallow water carbonates (from a nearby unknown platform) occurring in the WSK-01 well.

On the flank of the London-Brabant Massif, the margin of the platform is well imaged only in the offshore, while the seismic quality is quite poor in the onshore, often not allowing a proper imaging of the Dinantian carbonates, especially in Belgium. In this case we used also the wells for defining the facies distribution across the area. The boundary between the basinal facies identified in the Maastricht area (KSL-02, HEU-01, GVK-01) and the platform is highly speculative, as seismic data are not available. The connection between these basinal facies and the deeper Kempen Basin is postulated due to absence of evaporites, which are expected in intraplatform basins but not in open basins. The final facies interpretation was summarised in two maps, where a degree of confidence was assigned to each polygon by different colours.
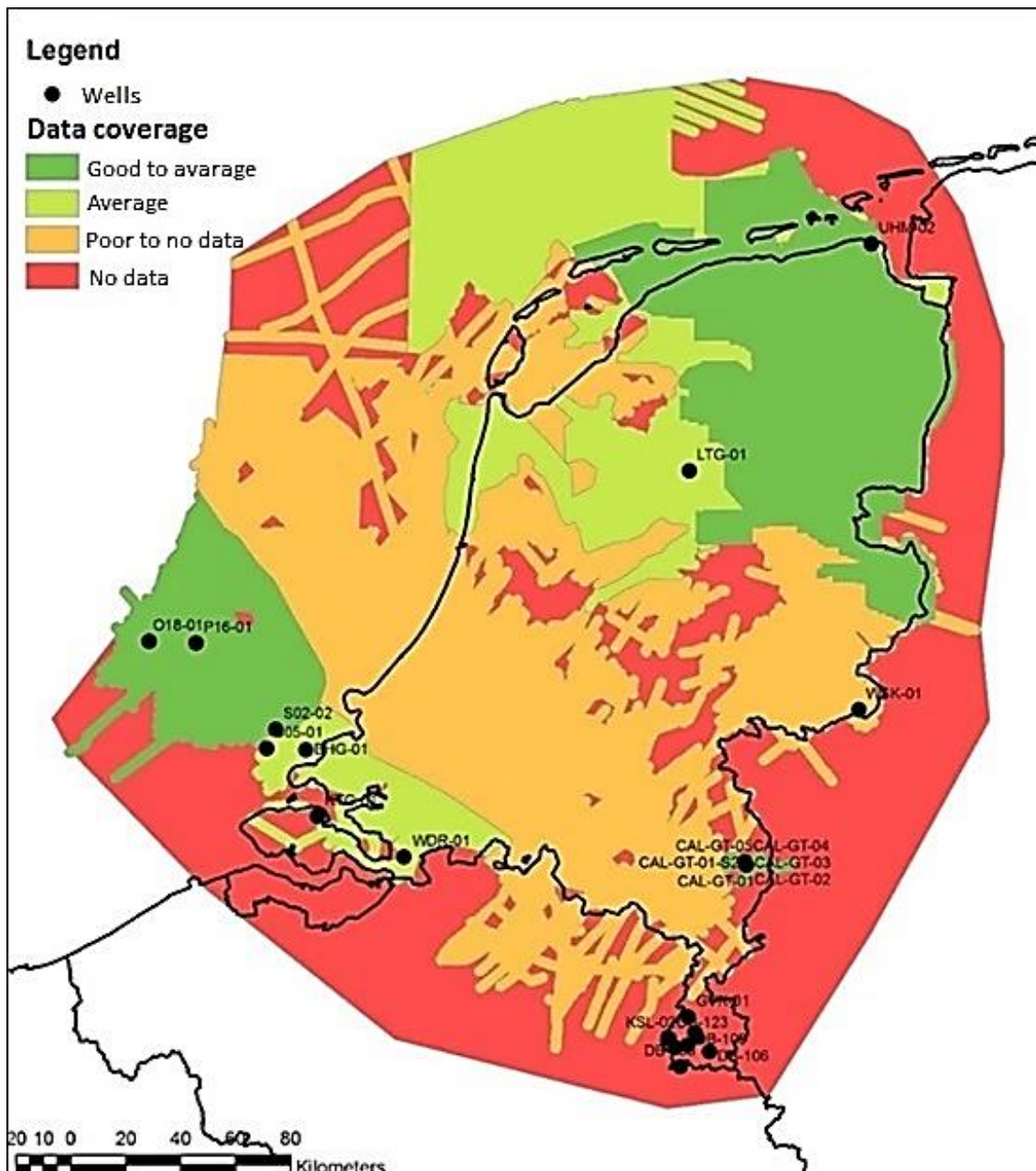
Figure 5-5: Map showing the seismic coverage for the Dinantian carbonates of the Netherlands.

5.13 1D Basin Modeling

Preliminary 1D basin models were developed for several wells, in order to understand their thermal evolution. These models were developed in Petromod 1D Express 2014.1 developed by Schlumberger. For each well, borehole temperatures and vitrinite reflectance data were imported for calibrating the 1D models.

The burial histories were developed starting from the detailed stratigraphy of the different wells, applying the Geological Timescale 2016 (Ogg *et al*., 2016). For each well, the paleobathymetric correction has been mostly ignored, as its impact is minor for preliminary models like these ones. The present-day surface temperature was computed automatically within the Petromod 1D software by applying the present-day latitude.

The choice of a detailed heat flow model was quite complex, as very few studies in the Netherlands address issues of the Lower Carboniferous/Devonian maturity (Figure 5-6). Two major heat flow events are reported in the literature during Late Carboniferous-Early Permian and the Upper Jurassic (Wygrala, 1991; Van Balen *et al.*; 2000, Kus *et al.*, 2005; Abdul Fattah *et al.*, 2012, 2014). A third Upper Cretaceous event is sometimes inferred, but its effects are unclear in the studied wells. The best matching model is derived from Abdul Fattah *et al.* (2014) and Bonté *et al.* (2014) who applied a strong and short-lived heat flow event during latest Carboniferous-Early Permian yielding a recomputed maximum heat flow of up to 150 mW/m^2.

The maturity was modeled within Petromod by using the Easy%RO algorithm (Sweeney and Burnham 1990), with the limitations of the algorithm itself: maturities higher than 4.71 %Ro, such as observed in KSL-02 or HEU-01, were impossible to model. Higher maturities might be more effectively modeled by using the alternative basin%Ro algorithm (Nielsen *et al.*, 2017). A temperature model was then computed for each well for the Beveland Formation, in order to compare the paleotemperatures with the actual data measured from microthermometry. A limitation of the approach is that possible heat flow events occurring after Permian are not properly recorded by vitrinite reflectance measurements as they may be obscured by the Permian heat flow event.
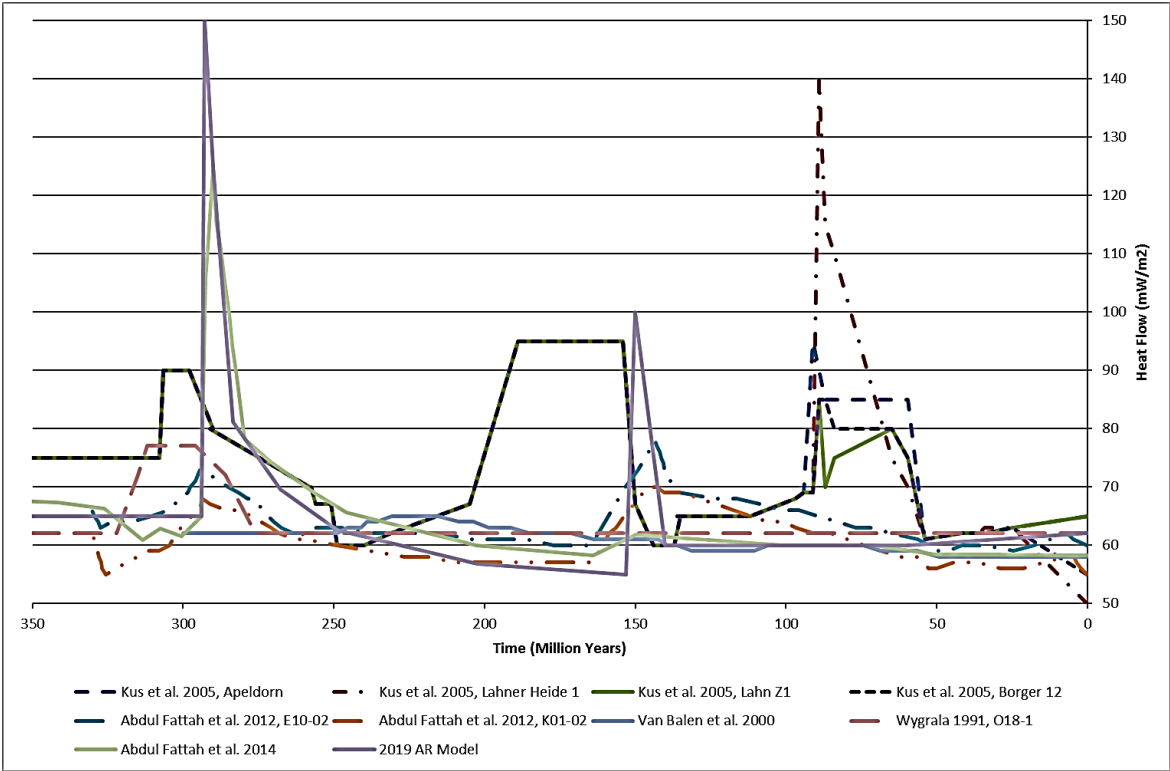
Figure 5-6: Heat flow models available for the Dutch regions. The model used in this study is the 2019 AR model.

54

6. Synthesis/Results

6.1 Sequence stratigraphy

The sequence stratigraphic framework developed for the entire region including ten depositional cycles is presented in Table 6-1.

Table 6-1: Sequence stratigraphic framework for the Dinantian carbonates in the Netherlands.

Depositional cycles (this study)	Colour	Depositional sequences (Pickard and Gutteridge, 1997)	Age	Depositional events
3b	Deep purple	Sequence 3	RC7β-RC8 (Warnantian)	Carbonate shelf-margin-basin systems
3a	Light orange			
2d	Yellow	Sequence 2	V1b-V2a (mid- to late Molinacian) to V2bß middle Visean age (Livian)	Carbonate ramp to shelf transition
2c	Dark Blue			
2b	Light blue			
2a	Purple			Carbonate ramp systems
1d	Light green	Sequence 1	Late Tournaisian (V1 or older) to *Eoparastaffella* Cf4α subzone of V1a (earliest Molinacian)	
1c	Orange			
1b	Pink			
1a	Cyan			Initial flooding of basin
Clastics			Tournaisian	

Cycle 1a occurs in all wells in the SW Netherlands apart from 53/12-02 and was cored across the 1a/1b cycle boundary in well KTG-01 (Figure 6-1). The foraminiferal assemblage indicates V1 or older, i.e. Tournaisian/Molinacian. The absence of archaediscids indicates the core is older than the Cf4β foraminiferal biozone (Figure 4-16). The presence of *Koninckopora* above 951.4 m shows that the uppermost part of the core is part of the Eoparastaffella Cf4α subzone of V1a, earliest Molinacian age. This sequence is missing in LTG-01 and UHM-02 wells. This represents the initial flooding of the basin; the TST varies in thickness and is characterised by a clean gamma ray interval above the thick high gamma ray fine clastics at the top of the Tournaisian. This is interpreted as deposition of clean carbonates in shallow water (Figure 6-2). This is followed by increasing gamma ray interpreted as deposition of more muddy carbonates in deeper water or perhaps resulted from continental influx. The HST of this cycle was cored in KTG-01 where it consists of thinly-bedded cyclic inner ramp carbonates with cycle boundaries marked by horizons with calcrete, rhizocretions or peritidal carbonates.

Cycle 1b occurs in all wells in the SW Netherlands apart from 53/12-02 and was cored across the 1a/1b cycle boundary in well KTG-01 (Figure 6-1). The foraminiferal assemblage indicates V1 or older, i.e. Tournaisian/Molinacian. The absence of archaediscids indicates the core is older than the Cf4β foraminiferal biozone (Figure 4-16). The presence of *Koninckopora* above 951.4 m shows that the uppermost part of the core is part of the *Eoparastaffella* Cf4α subzone of V1a, earliest Molinacian age. The 1b depositional cycle was also cored in S05-01 but no diagnostic age could be determined. The TST, maximum flooding interval and part of the HST was cored in well KTG-01; this shows an upward transition from thinly bedded wackestone deposited in a deep subtidal setting to thickly bedded cyclic grainstone and packstone with cycle top marked by peritidal facies and rhizocretions. Core in S05-01 shows that HST consists of thickly bedded high to moderate energy inner- to mid-carbonate ramp deposits (Figure 6-2).

The basal cycle boundary of the 1b depositional cycle represents an upward change to thicker, deeper ramp cycles.

Cycle 1c occurs in all wells in the SW Netherlands apart from 53/12-02 and was cored in wells S02-02 and S05-01 (Figure 6-1). In well S02-02, a V1a, Cf4α earliest Molinacian age is suggested by the microfauna including *Pachysphaerina pachysphaerica* (Bless, 1978). However, the presence of probable alga *Globochaetes* is indicative of the late Tournaisian Cf3 age (Figure 4-16). There was no definitive fauna in either wells. The presence of *Pachysphaerina pachysphaerica* and an absence of archaediscids and *Koninckopora* suggest a lower V1a Molinacian age. This cycle comprises a thick TST (not represented in core) with an HST that has a moderately high gamma ray signature. Core from the HST in wells S05-01 and S02-02 consist of cyclic shallow subtidal to peritidal shallow ramp carbonates with cycle tops marked by peritidal facies. The subtidal facies are dominated by oncoids, other coated and highly micritised grains suggesting deposition that took place in a relatively restricted shallow carbonate ramp setting (Figure 6-2).

Cycle 1d occurs in all wells in the SW Netherlands apart from 53/12-02 and was cored in wells BHG-01, O18-01 and S05-01 (Figure 6-1). In S05-01 the presence of *Koninckopora* and the absence of archaediscids suggests that this is part of the *Eoparastaffella* Cf4α subzone (Figure 4-16) of the V1a (earliest Molinacian) age. This comprises a thin TST; core from the HST indicates deposition in a high energy carbonate platform setting. This has been eroded and is overlain by karst collapse or fills in well BHG-01. In O18-01, early Carboniferous: Tournaisian/early Visean age of Tn1b/V1a is shown on the composite log. Cycle 1d shows a relatively thin low gamma ray TST passing up into a high gamma ray interval interpreted as a maximum flooding interval (not represented in core). Cores were taken in the early to late HST parts of the 1d cycle; BHG-01 consists of very fine, well sorted grainstone/packstone deposited in a high energy setting above normal wave base; S05-01 consists of thickly bedded bioclast grainstone/packstone with intraclasts, bioclasts and coated grains deposited in an inner to mid ramp depositional setting (Figure 6-2); O18-01 comprise dolomitised wackestone and packstone that represent redeposited storm beds sedimented in a more distal carbonate ramp setting compared with wells BHG-01 and S05-01.

Cycle 2a occurs in all wells in the SW Netherlands (Figure 6-1) apart from 53/12-02. It was cored in well S05-01. In S05-01, Bless (1982) attributed the core to a V1a-V2a, Molinacian age. However, the presence of archaediscids requires a slightly younger V1b-V2a (mid- to late Molinacian) age. This cycle consists of a moderate gamma ray TST passing up into a high gamma interval interpreted as a maximum flooding interval (not represented in core). In well S05-01 a low gamma ray HST was cored that consists of medium- to thickly-bedded bioclast packstone/grainstone (Figure 6-3) with some coated grains deposited in an inner carbonate ramp setting.

Cycle 2b occurs in all wells in the SW Netherlands (Figure 6-1) apart from 53/12-02 and BHG-01. It was cored in well S05-01. Core 6 the macrofaunal assemblage suggests a V2a-V2b age corresponding to late Molinacian or early Livian age (Bless, 1982); however, the fauna does not preclude a mid-Molinacian age. The macrofaunal assemblage in Core 5 suggests a V2b-V3a mid-Livian age (Bless, 1982). This cycle consists of a thin TST with increasing-upward gamma towards a high gamma maximum flooding interval with an overlying decreasing-upwards gamma HST. The 2b depositional cycle was cored in S05-01 in the uppermost part of the HST where it consists of medium-bedded bioclastic grainstone/packstone with some coated and micritised grains (Figure 6-3). This was deposited in a high energy setting above normal wave base, in an inner carbonate ramp or carbonate shelf interior.

Cycle 2c occurs in all wells in the SW Netherlands (Figure 6-1) apart from 53/12-02 and BHG-01. It was cored in well S05-01. A diverse suite of foraminifera is present; the rare occurrence of archaediscids at the angulatus stage indicates the *Neoarchaediscus* Cf6 foraminiferal assemblage. The age is therefore V3b or earliest Warnantian age (Bless, 1982). The base of core 4 contains a foraminiferal assemblage indicating a V2b-V3a or Livian age. This cycle has a thin TST with increasing gamma towards a high gamma maximum flooding interval with a thickly bedded low gamma HST. The 2c depositional cycle was cored in S05-01 in the HST where it consists of medium-bedded bioclastic grainstone/packstone with some coated and micritised grains (Figure 6-3). There is no indication of emergence within the core. This suggests this cycle was deposited in a moderate to high energy setting above or near normal wave base in an inner platform setting.

Cycle 2d occurs in all wells in the SW Netherlands apart (Figure 6-1) from 53/12-02, KTG-01 and BHG-01. It was cored in well S05-01 where the upper part was dated as the Cf6 foraminiferal zone indicating a V3b or early Warnantian age; the base of the core was dated as V2b-V3a age. The gamma signature of this cycle is flat with a thin TST to slightly increased gamma maximum flooding interval with a higher gamma HST. Core 1 to 4 in S05-01 consists of medium- to thickly-bedded bioclast coated grain peloid packstone/grainstone (Figure 6-3) with no indication of emergence. The presence of oncolitically coated grains suggests a slightly restricted environment in a high energy, carbonate platform interior setting.

Cycle 3a occurs in wells LTG-01, UHM-02, 53/12-02 and O18-01 (Figure 6-1). In O18-01 core from the TST to maximum flooding interval encountered bioturbated carbonate mudstone and wackestone with some interbedded packstone (Figure 6-4) interpreted as storm deposits. The generally low gamma signature in the HST suggests deposition in generally shallow water carbonate shelf setting. However, common gamma spikes are interpreted as common karst cavities infilled by mudstone, similar to that seen in the O18-01 core obtained from the overlying depositional sequence described below. In LTG-01, cores from the TST and HST comprise high energy carbonate platform interior facies.

Cycle 3b occurs in wells UHM-02, 53/12-02 and O18-01 (Figure 6-1); it was cored in UHM-02 and O18-01. A RC7β-RC8 (Warnantian) age, equivalent to the Late Asbian and Brigantian, was obtained from O18-01. Dark grey mudstone infills of karst cavities are present in the core but no miospores were recovered and so the age could not be determined. The overall stratigraphic relationships in well O18-01 suggest that this karst was sub-Limburg and probably Namurian or Westphalian in timing. In UHM-02, a short core comprising high energy carbonate platform interior facies with a thin shale interpreted as a soil was found. The core in O18-01 consists mainly of bioclast wackestone/carbonate mudstone with whole fenestrate bryozoan sheets, articulated brachiopods, gastropods, bivalves and a goniatite (Figure 6-4). The micritic matrix generally has a micropeloidal texture. Common irregular cm- to dm-sized cavities lined by fibrous calcite cement that are also partly infilled by peloidal geopetal and bioclastic sediment. These cavities may represent stromatactoid cavities that formed as modified shelter cavities in a micrite matrix around fenestrate bryozoan sheets. The depositional setting is interpreted as carbonate mud mounds that were associated with a carbonate shelf margin. The 3b depositional sequence is interpreted as a carbonate platform margin in O18-01 and equivalent shelf interior, slope or basinal facies elsewhere. The gamma signature is generally erratic, with gamma spikes are interpreted as mudstone-filled karst cavities or organic rich intercalations.
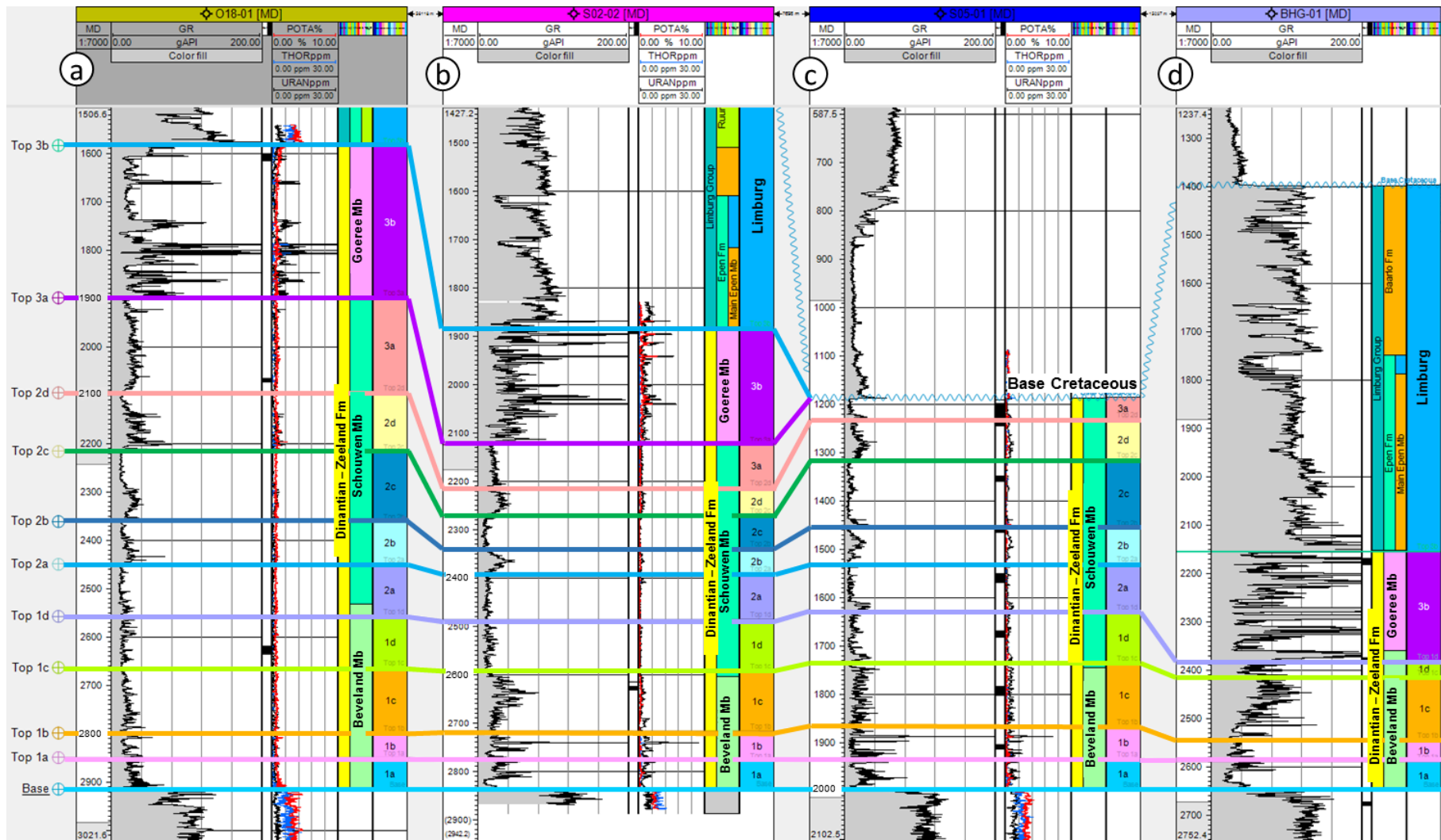
Figure 6-1: Correlation of key wells in SW Netherlands: a) O18-01. b) S02-02. c) S05-01. d) BHG-01. The KTG-01 well is not included here since it contains only the 1a and 1b depositional cycles.
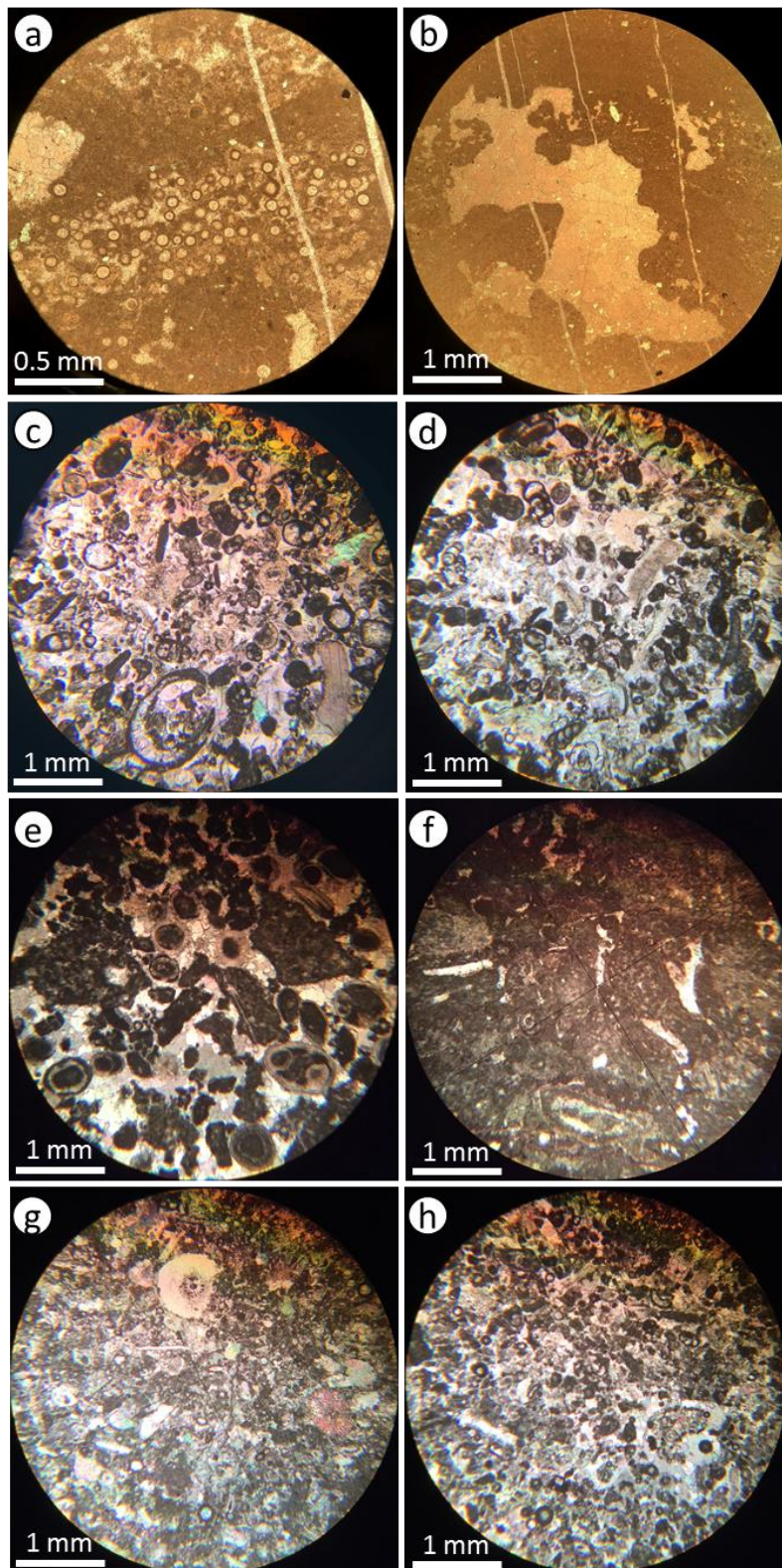
Figure 6-2: Photomicrographs showing examples of microfacies represented in the depositional cycles of Sequence 1 in KTG-01 and S05-01 wells: a, b) Depositional cycle 1a, 995.20 m, fenestral mudstones and wackestones and bioclastic-peloidal grainstone (KTG-01). c, d) Depositional cycle 1b, 1911.20 m, bioclastic-peloidal grainstone. e) Depositional cycle 1c, 1786.90 m, (algal boundstone-) coated grain grainstone. f) Depositional cycle 1c, 1790.80 m, coated grain-bioclastic grainstone. g, h) Depositional cycle 1d, 1670.70 m and 1673.40 m, fine bioclastic (-peloid) pack-grainstone.

59
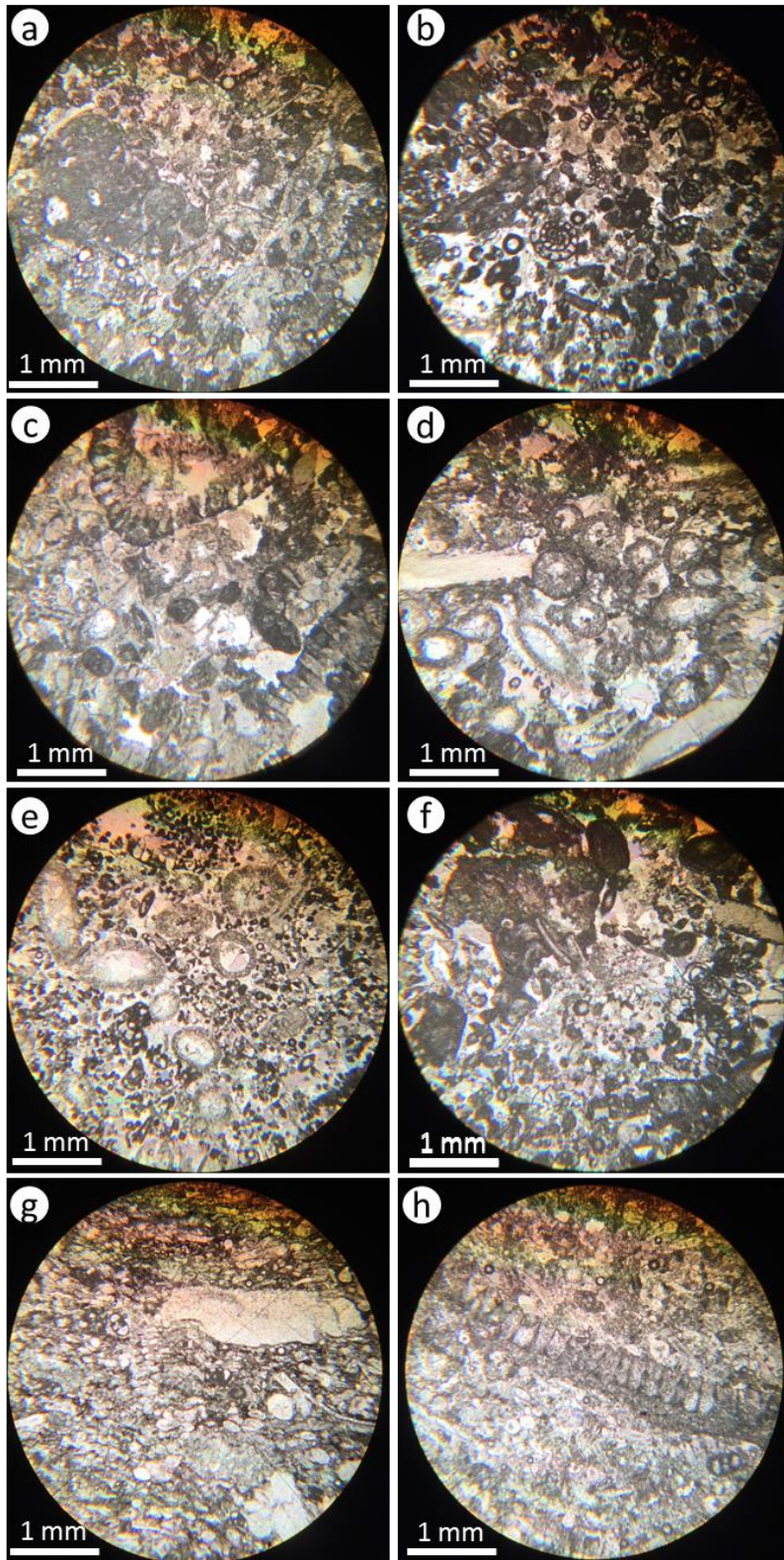
Figure 6-3: Photomicrographs showing examples of microfacies represented in the depositional cycles of Sequence 2 in S05-01 well: a) Depositional cycle 2a, 1564.50 m, bioclastic-coated grain-peloid grainstone. b) Depositional cycle 2a, 1560.80 m, fine bioclastic grainstone. c, d) Depositional cycle 2b, 1456.50 m and 1463.70 m, bioclastic-peloid grainstone. e, f) Depositional cycle 2c, 1350 m and 1456.50 m, bioclastic-coated grain-peloid grainstone. g, h) Depositional cycle 2d, 1238.80 m and 1239.80 m, bioturbated bioclastic pack- to grainstone.
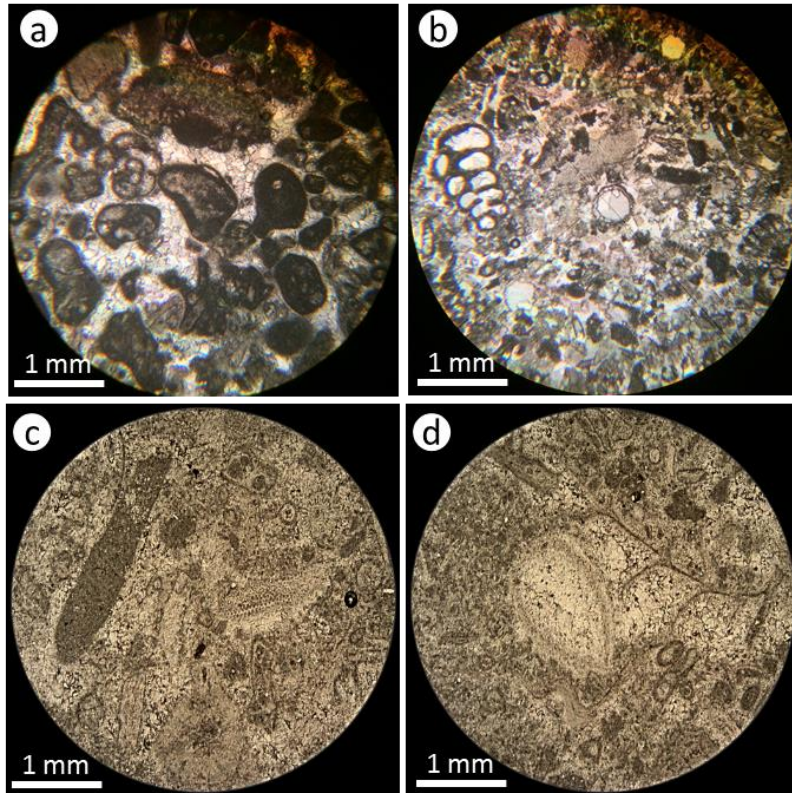
Figure 6-4: Photomicrographs showing examples of microfacies represented in the depositional cycles of Sequence 3 in S05-01 and O18-01 wells: a, b) Depositional cycle 3a, 1190 m and 1204.70 m, bioclastic-peloid pack- and grainstones (S05-01). c, d) Depositional cycle 3b, 1605 m, bioclast wackestone (O18-01).

6.1.1 High resolution sequence stratigraphic sub-division of wells WSK-01 and KSL-02

Ten depositional cycles have been recognised in the Dinantian successions of WSK-01 and KSL-02 that are tentatively correlated with the ten depositional cycles recognised in the SW Netherlands (Figure 6-5).

Table 6-2: Log character of the recognised depositional sequences.

Depositional cycles	Gamma ray log character	Depositional setting
3b	Gamma ray increases upwards to very high followed by low gamma ray HST	Condensed deposition in basin during LST and TST; high stand shedding of carbonates into basin
3a		
2d	Moderate to high gamma ray, with progressive increase through interval. Generally high gamma ray in KSL-02	Mid-to distal carbonate ramp or carbonate slope in WSK-01; distal basin in KSL-02
2c		
2b		
2a		
1d	Moderate to low with moderate to high peaks interpreted as max. flooding followed by low gamma ray HST	Distal carbonate ramp with increasing carbonate input as ramp progrades during HST. Maximum flooding events marked by high gamma intervals
1c		
1b	Very high gamma ray by low gamma ray top	Deep water (dolomitised in KSL-02)
1a	Low to moderate gamma ray HST	Initial transgression of basin

The cycles have been grouped as follows according to the gamma ray log character using the same approach for the wells in the SW Netherlands. The overall depositional setting of the WSK-01 well is interpreted as proximal to distal slope in which the carbonate intervals were

61

introduced in the form of redeposited platform sediment. The depositional cycles are interpreted in terms of the expected evolution of surrounding carbonate platforms.

1a and 1b depositional cycles: These cycles are interpreted as the initial deposits in the basin following the late Tournaisian/early Visean transgression. The 1a depositional cycle is interpreted as shallow-water carbonates deposited during the initial transgression of the basin. Core in KSL-02 shows the high gamma ray interval of the 1b depositional cycle (equivalent to the Pont d'Arcole Formation) represents deep water argillaceous limestone and shale. The upper, low gamma ray part of the 1b cycle consists of dolomitised wackestone and carbonate mudstone deposited in a basinal or deep ramp setting.

1c and 1d depositional cycles: The 1c depositional cycle is cored in KSL-01 and consists of dolomitised bioclastic wackestone and carbonate mudstone interpreted as distal carbonate ramp facies; the initial low gamma ray reflects the deposition of redeposited carbonates sourced from shallow to mid-ramp settings during the TST. The higher gamma ray interval represents the drowning of the source of redeposited carbonates during the maximum flood. The higher gamma ray intervals at the top of the cycle are interpreted as increased supply of redeposited carbonates as the carbonate ramp progrades during the HST. The 1d depositional cycle is cored in KSL-01 and consists of deep-water argillaceous limestone and shale.

2a to 2c depositional cycles: These cycles have higher, more uniform gamma ray signatures. they are interpreted as distal ramp or carbonate slope facies, possibly associated with a transition from carbonate ramp- to flat-topped carbonate shelves in surrounding carbonate platforms. The low gamma ray intervals interpreted as influx of resedimented carbonates during high stands. The overall high gamma ray signature in KSL-02 suggests that this was deposited in a more distal setting than WSK-01.

2d to 3b depositional cycles: These cycles show an increasing-upward gamma ray signature that is interpreted as distal carbonate slope or basinal facies. The high gamma ray intervals are interpreted LST to TST intervals when there was no carbonate production on the exposed carbonate platforms and no export of peri-platform carbonates to the surrounding basin. The low gamma ray intervals are interpreted as HSTs when carbonate production was taking place on flooded carbonate platforms with some high stand shedding of carbonates to the basin.
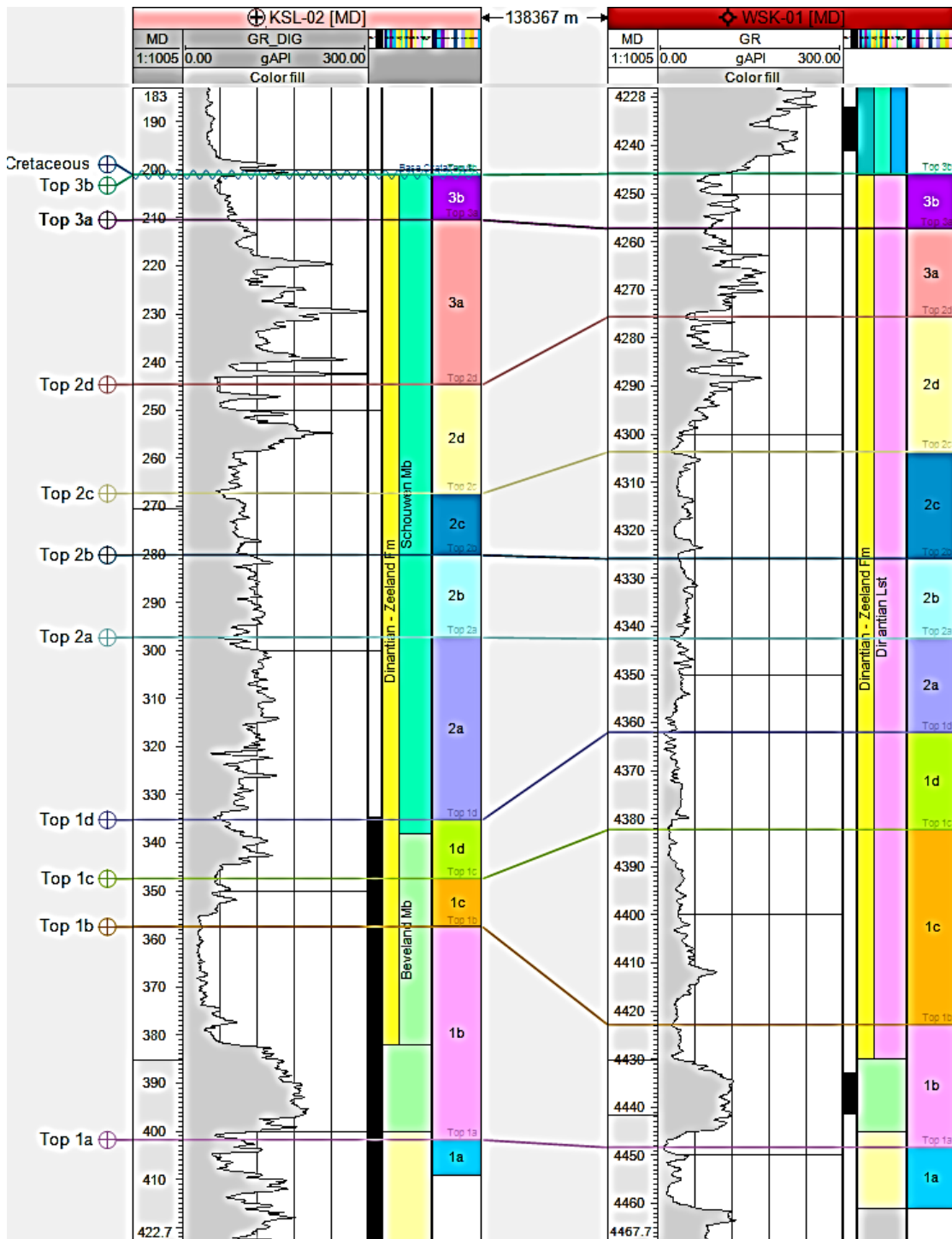
Figure 6-5: Correlation between the KSL-02 and WSK-01 wells.

6.1.2 High resolution sequence stratigraphic correlation with the north Netherlands

The well control outside the southwestern Netherlands is very widely-spaced with short cored intervals and low resolution biostratigraphic data. Although the northern Netherlands has good quality 3D seismic data it is difficult to link this to the southern Netherlands because the area is covered by a number of separate 2D surveys of varying vintage.

Biostratigraphic information from UHM-02 and LTG-01 were added to the Petrel project and matched with the ages of the groups of sedimentary sequences identified in the southern Netherlands (Table 6-1and Figure 6-6) as follows:

63

Sequence 1, 1c and 1d cycles: These cycles are part of a depositional sequence that is ?late Tournaisian to earliest Molinacian age. The basal 1c depositional cycle represents the initial transgression of the structural high and the establishment of the high energy carbonates platform interior sedimentation.
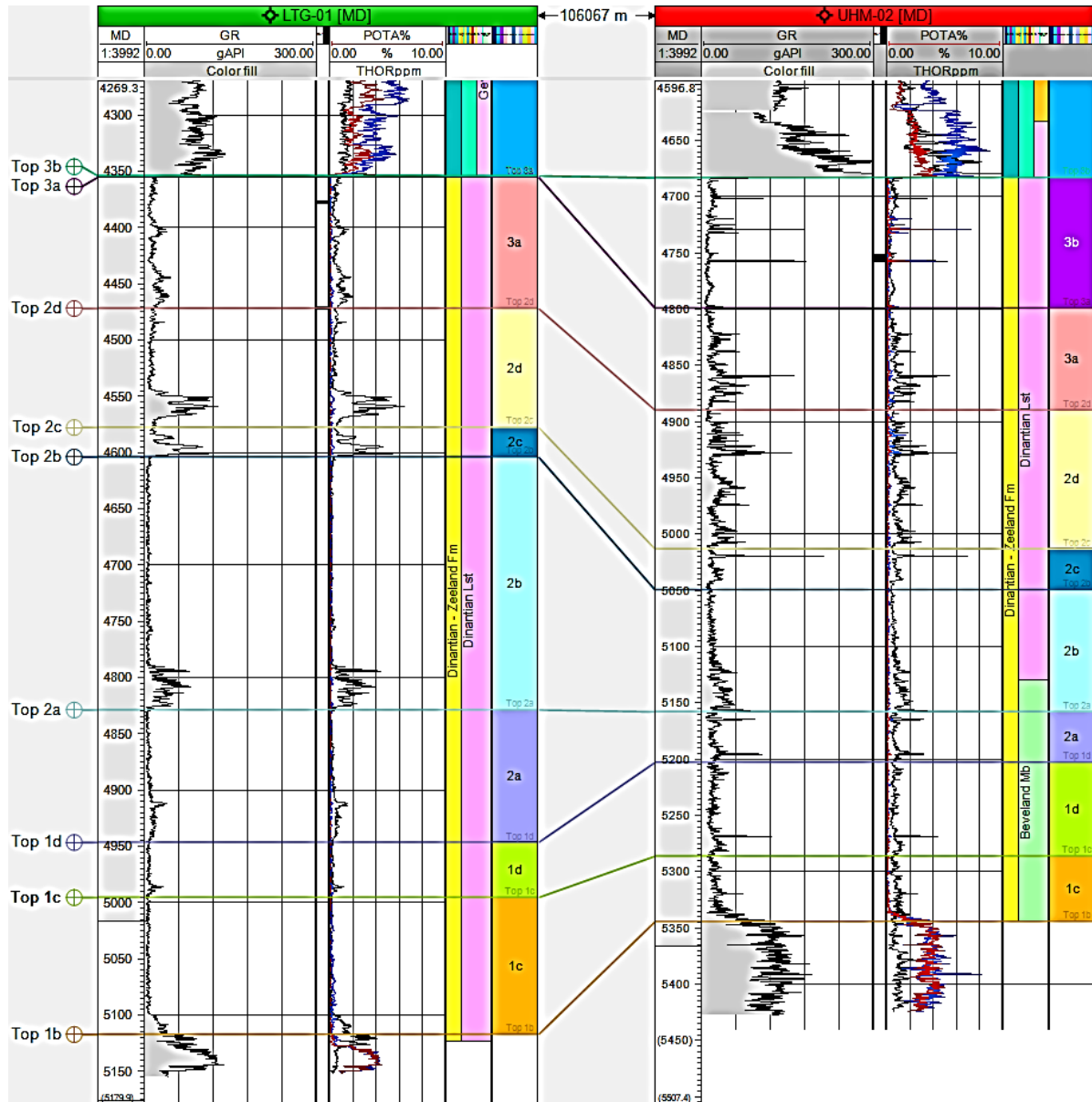
Figure 6-6: Correlation between the LTG-01 and UHM-02 wells in the Central-Northern Netherlands.

Sequence 2, 2a to 2d cycles: These cycles are part of a depositional sequence that is mid- to late Molinacian to middle Visean age. These depositional cycles represent high energy carbonate platform interior sedimentation with higher gamma ray transgressive or maximum flooding shales deposited across the carbonate platform.

Sequence 3, 3a and 3b cycles: These cycles are part of a depositional sequence that is Warnantian in age. The 3a depositional cycle in UHM-02 and LTG-01 is interpreted as high energy carbonate platform interior facies. Seismic stratigraphic studies indicate that the LTG-01 well was drilled down flank of the carbonate platform and the later Dinantian cycles may be present. The 3b depositional cycle in UHM-02 is interpreted as high energy carbonate platform

interior sedimentation. Gamma ray spikes within it may represent wind-blown volcanic soils or organic material deposited on the exposed carbonate platform.

6.2 Sedimentology

6.2.1 Depositional facies recognised in cores

Karst collapse or fill: This depositional facies consists of pebble- to-boulder sized breccio-conglomerates with clasts derived from carbonate shelf margin and shelf interior settings. The matrix comprises dark siliciclastic mudstone and layered bioclastic grainstone. This is interpreted as a cave fill or cave collapse breccia with the clasts sourced from the surrounding host limestone and the host matrix represent marine and terrestrial infills. Examples are BHG-01 Core 1, S02-02 Cores 1 and 2. This facies is typical of the 3a and 3b sequences.

Subaerial mudstone: This depositional facies is a dark grey fissile mudstone with no bioclasts. It contains illite-chlorite-smectite mixed layer clays with quartz and K feldspar; the latter are interpreted as detrital components and are silt-sized or smaller. This is interpreted as a windblown soil, possibly of volcanic origin. An example is in UHM-02 Core 1, in sequence 3b.

Emergent facies (non-karst): Calcrete nodules and rhizocretions are sometimes present in bioclast wackestone or packstone deposited in a subtidal setting. Occasional vadose cement may also be present. These were deposited at the top of cycles in a supratidal setting and are associated with soil development or the colonisation by plants. Examples are in KTG-01, S05-01 Core 9, sequences from 1a to 1c.

Peritidal facies: These depositional facies consists of carbonate mudstone or wackestone with desiccation features including fenestrae or mud cracks. They occasionally contain interbedded ornate hardgrounds that may represent intertidal microkarst. This depositional setting underwent episodic wetting and drying between high and low tide. Example is in KTG-01, sequence 1b.

Subtidal above normal wave base (bioclastic): Thickly bedded fine bioclast peloid packstone/grainstone with micritisation of allochems. Occasional concentrations of large bioclasts including crinoids, brachiopod shells, *in situ* corals and occasional intraclasts are present. This was deposited on the inner part of a carbonate ramp or shelf interior close to the margin of a carbonate platform. Examples are in UHM-02 Core 1, BHG-01 Core 2, KTG-01, LTG-01 Cores 1 and 2, S02-02 Cores 3 and 4, S05-01 Cores 5, 7, 8, 10 and 11, covering all the Dinantian sequences from 1a to 3b.

Subtidal above normal wave base (coated grain): Thickly bedded fine bioclast peloid coated grain packstone/grainstone with micritisation of allochems. Coated grains include both oncoids and ooids; occasional intraclasts may also be present. This was deposited on the inner part of a carbonate ramp or shelf interior close to the margin of a carbonate platform. The occurrence of coated grains and abundant micritisation may suggest a restricted environment, where it is associated with peritidal facies, this facies may represent a carbonate barrier. Examples are in UHM-02 Core 1, BHG-01 Core 2, KTG-01, S02-02 Cores 3 and 4, S05-01 Cores 1 to 5, 8 and 9, covering all the Dinantian sequences from 1a to 3b.

Subtidal low energy, below normal wave base: This depositional facies consists predominantly of bioclast wackestone and packstone that is generally well-bioturbated. The bioclast assemblage includes crinoids, brachiopods, corals, bivalves, benthic foraminifera and algae. Bioclasts are often micritised. The open marine bioclast assemblage suggests that this was deposited on the mid- to shallow part of a carbonate ramp. Examples are in KTG-01 and S05-01 Core 6, from sequence 1a to 2b.

Subtidal below storm wave base: This depositional facies consists predominantly of argillaceous bioclast carbonate mudstone and wackestone that shows varying degrees of bioturbation. Bedding is picked out by microstylolitic partings. Interbedded layers and lenses and graded beds with scoured bases of bioclast wackestone/packstone with reworked bioclasts including crinoids, brachiopods and bivalves are also present. The open marine bioclast assemblage suggests that this was deposited on the mid- to distal part of a carbonate ramp. This is typical of sequence 1a.

Carbonate build-up: This depositional facies is a bioclast wackestone with whole fenestrate bryozoans and large stromatactoid cavities lined by radial fibrous marine cement and geopetal infills of peloids and micrite. The matrix is a micropeloidal bioclast peloid carbonate mudstone/wackestone occasionally with articulated brachiopods, benthic foraminifera, molluscs and calcareous algae. This is interpreted here as a microbial carbonate mud mound; the occurrence in the late Visean of O18-01 suggests that this may be part of a carbonate shelf margin or upper slope facies. Examples are in O18-01 Cores 3 and 4, sequence 3b.

Resedimented and slumped carbonates: This depositional facies consists of thinly bedded argillaceous carbonate mudstone, wackestone or fine packstone with broken up bioclasts including crinoid ossicles and short stems, disarticulated brachiopods. Occasional whole brachiopod shells are present. Some slumped intervals are present. Examples are in WSK-01, HEU-01 and HEU-01-S1, covering the entire Dinantian interval.

Basinal mudstone: This depositional facies consists of bioclastic shale rich in crinoids. Examples are in KSL-02 (lower part) and WSK-01, in the interval relative to 1a to 1d sequences.

Altered basinal mudstone: This depositional facies comprises black powdery siliceous mud rock that was probably originally argillaceous basinal facies that has been highly altered. Examples are in KSL-02 (upper part), HEU-01 and HEU-01-S1, mostly from sequences 2d to 3b.

6.3 Carbonate Platform Evolution

6.3.1 Brabant Platform

In the southern Netherlands, the evolution of the Brabant carbonate platform has been inferred by well and seismic data. The Brabant platform carbonates developed on the London-Brabant Massif, from the Tournaisian, overlying Devonian clastics. The nucleation of the carbonate platform appears to have taken place around small carbonate mud mounds, which coalesced into a larger carbonate platform. This behaviour is very clear on Figure 6-7, where a drowned carbonate mound is onlapped by the slope carbonates of the younger Brabant platform. Waulsortian mounds are not really evident in seismic and often synsedimentary features could be confused with mound geometries.

The northern carbonate platform margin appears to be flat-topped, with a slope angle of about 9° (Figures 6-8 and 6-9), and controlled by either active synsedimentary tectonics (Pickard and Gutteridge, 1997) or slope processes such as slumping, gravity-driven debris or shelf margin erosion as a result of over-steepening (Reijmer *et al*., 2015) (Figure 6-10). The structure of the southern margin towards the Maastricht area is not clear, as there are no seismic lines available. In particular, the fault movements appear to be synchronous across the basin during Tournaisian and the Visean, with vertical displacements decreasing from northern to southern Netherlands. In particular, in the southern Netherlands, these were probably transtensional movements forming structural highs over which condensed or eroded successions developed. The structural template also controlled the overall thickness of the carbonate platform. In the structural lows, however, there was the possibility of evaporite precipitation, as exemplified by the St Ghislain well in which Ivorian to Warnantian evaporites are reported (Groessen *et al*., 1979). In the

nearby Belgian Campine basin, the dissolution of evaporites was postulated to explain several karst collapse features in this area (Dreesen *et al*., 1985, 1987).

The entire carbonate platform started to backstep progressively at the end of Visean, with the deposition of the Goeree Member. A buildup related to the last phase of the platform is recorded in the Poederlee well in Belgium. At the very end of the life of this platform, the internal sector of the platform part was exposed with the development of karst, which was enhanced by the increasing amplitude of sea-level changes. The external sector of the platform started to tilt towards the Kempen Basin and was intensely dissected by faulting.

The carbonate factory stopped its activity due to the exposure and the increased input of clastics during latest Visean, early Namurian: the Namurian succession onlaps the external part of the Brabant carbonate platform, while is paraconformable with the inner part.

The total thickness of this platform is up to 953 meters in well S02-02.

6.3.2 Winterswijk area

The presence of a carbonate platform has been postulated close to the WSK-01 well, as the well succession was interpreted as a distal ramp. Seismic imaging is very poor in the area, so it is not possible to define the extent of this carbonate platform.

6.3.3 Venlo area Platform

The term "Venlo Platform" is here used to define the extensive Dinantian carbonate platform that was drilled by the Californië, Wachtendonk-1 and Schwalmtal-1001 wells and is also outcropping extensively in Germany. The potential connection with the Brabant platform has been widely discussed during this project, but to this point has not been demonstrated. The maximum thickness of this platform is about 500 m and is not properly characterised in the subsurface due to limited data. The depositional environment appears to be a carbonate ramp, but its boundary is not clear as this platform is poorly imaged in seismic. The lower part of the carbonate succession is strongly dolomitised, especially in well Wachtendonk-1 (Bless *et al*., 1976).
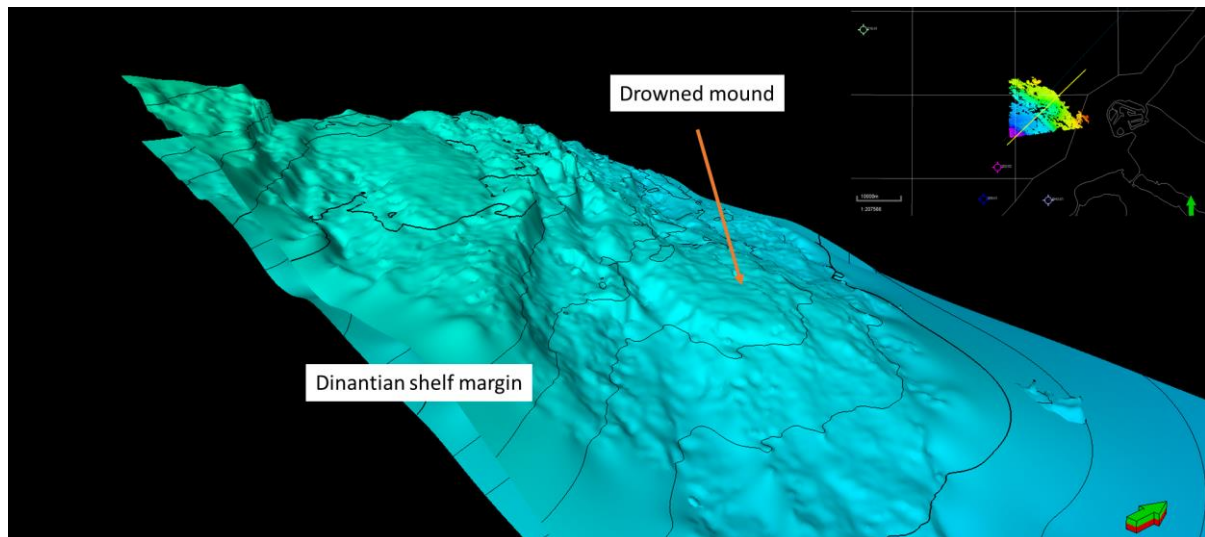
Figure 6-7: Top Dinantian surface showing the Dinantian carbonate platform margin, with the slope deposits covering a drowned mud mound.
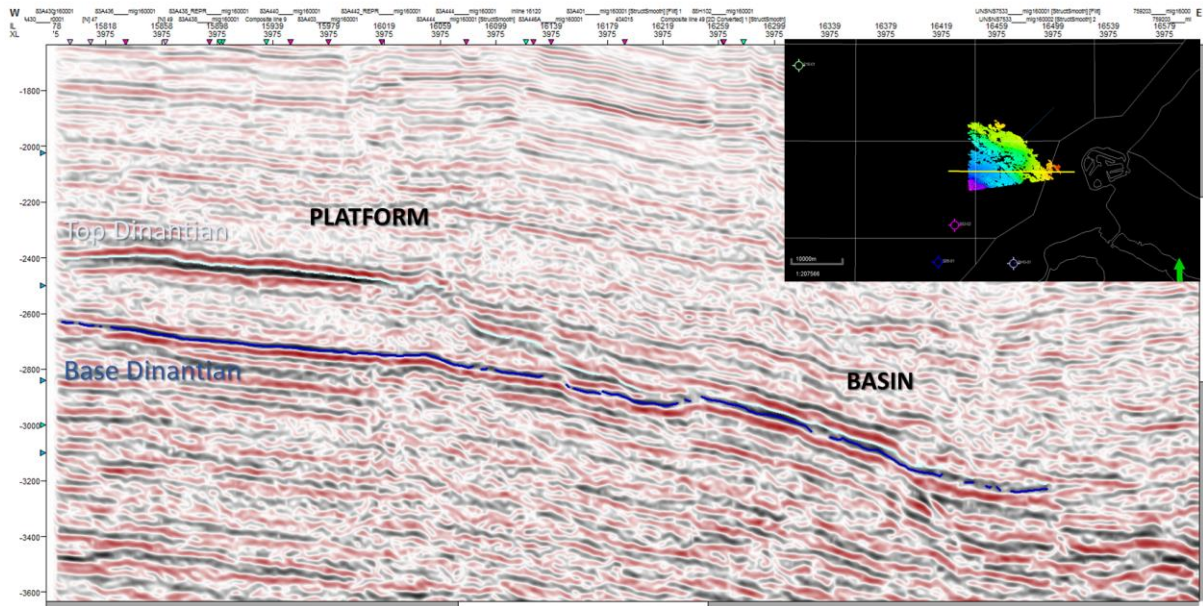
Figure 6-8: Example of platform margin NE of S02-2 well. Note the sharp topographic margin and the thickness variation from the platform to the basin.
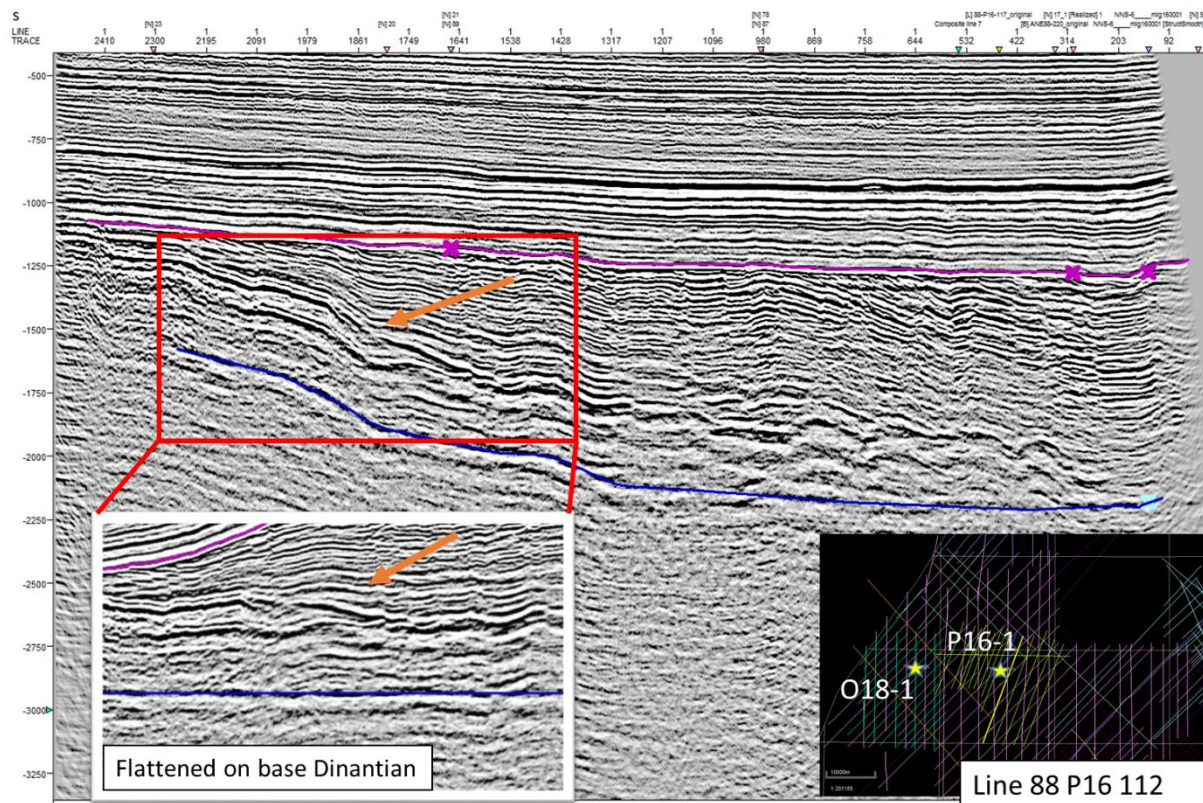
Figure 6-9: Carbonate platform margin (orange arrow) during Warnantian in the offshore area close to P16-01.
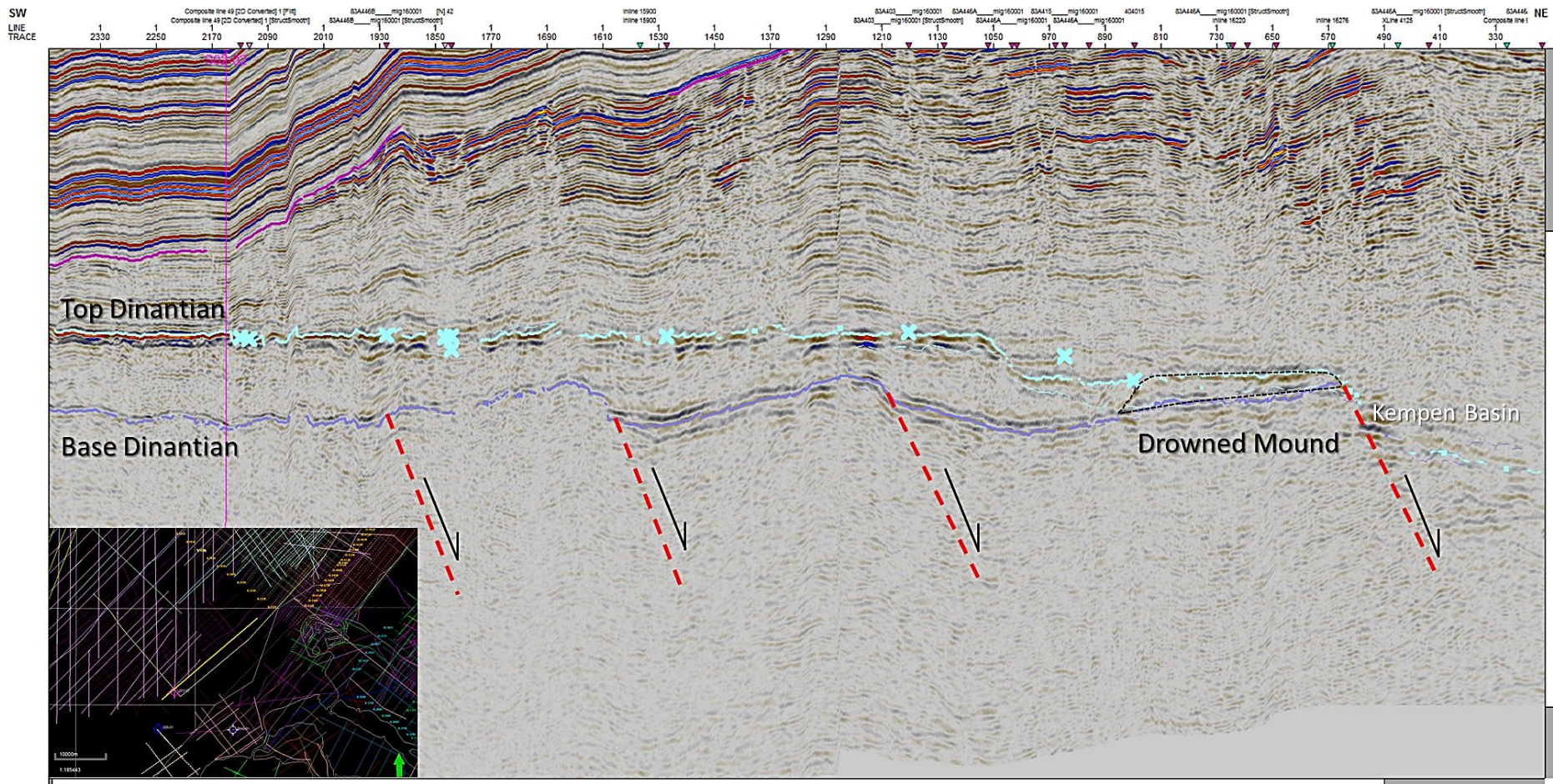
Figure 6-10: Interpreted line 83a446, crossing well S02-02 flattened on top Dinantian sea level, showing possible tectonic control on the development of the Brabant carbonate platform.

6.3.4 Central-Northern Netherlands

In the central and northern Netherlands, several highs with possible carbonate buildups were recognised (Figure 6-11; Ten Veen *et al.*, 2019). In the central-northern Netherlands, two of these highs have proven carbonate platforms, Uithuizermeeden and Luttelgeest, identified by well penetrations.
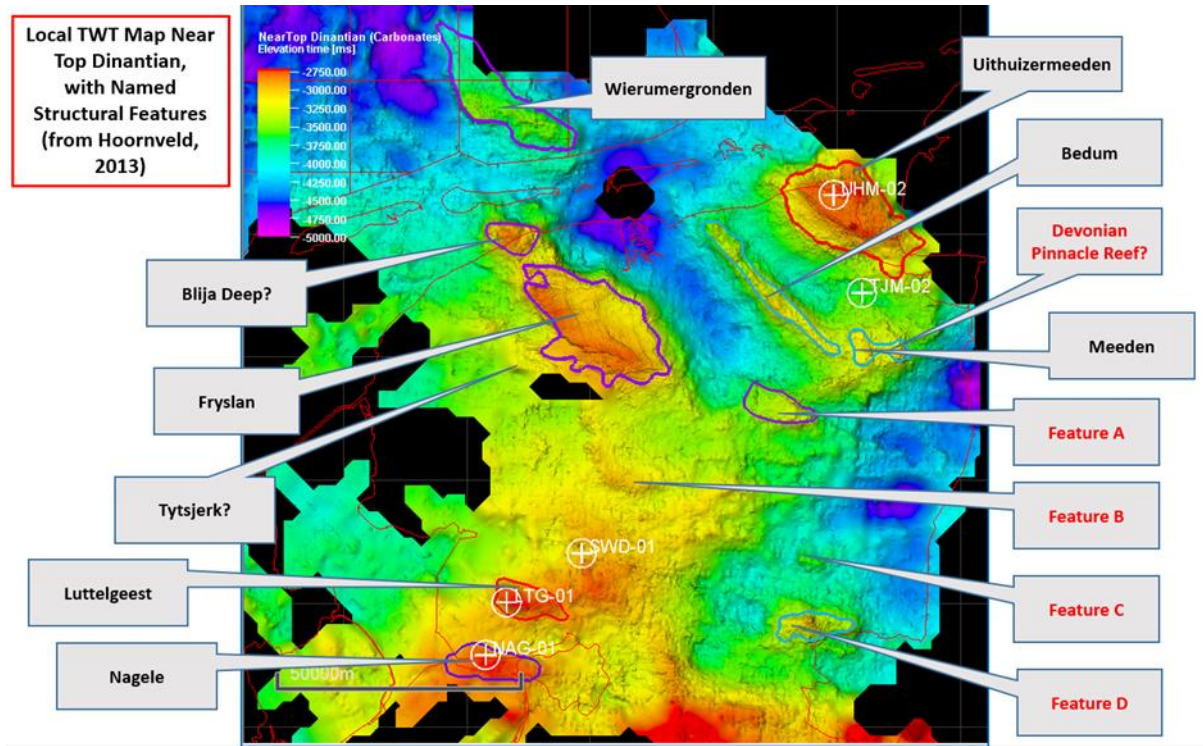
Figure 6-11: Overview of potential carbonate buildups recognised on seismic images (modified from Ten Veen *et al.*, 2019). Uithuizermeeden and Luttelgeest are proven isolated carbonate platforms. Fryslân and Nagele are unproven but possible isolated carbonate platforms because they are not drilled but their seismic images show carbonate geometries. Wierumergronden and other highs are inconclusive since they were either too high or deep to develop any carbonate buildup during Dinantian. Note that the NAG-01, SWD-01 and TJM-02 wells do not penetrate the Dinantian carbonates.

Uithuizermeeden (UHM) Platform

The Uithuizermeeden platform is the most prominent carbonate feature visible in the northern Netherlands and has been drilled by the well UHM-02. It sits directly below the Groningen Gas Field.

The measured thickness of the shallow water carbonates in UHM-02 well is 662 m and was drilled roughly in the center of the platform. The edges of the platform are slightly elevated (shown in Ten Veen *et al.*, 2019), and the surrounding slopes have a dip of about 12° (Figure 6-12), with an increase in the upper slope up to 30°. The area of the platform-top (the projected area) is more than 130 km^2 (Figure 6-13).
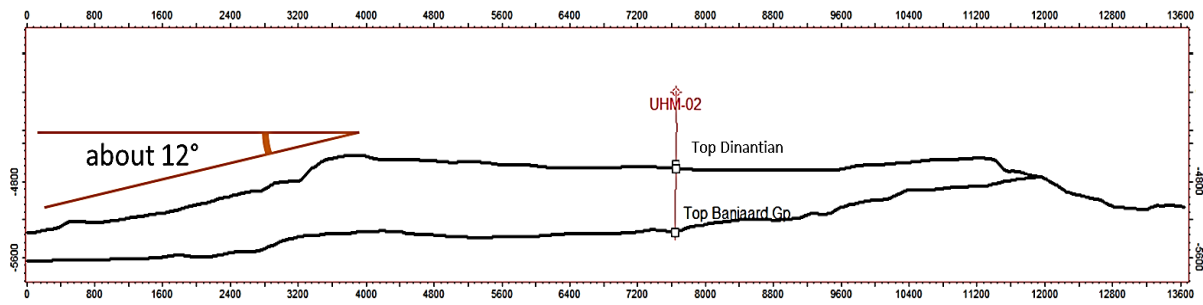
Figure 6-12: E-W profile crossing the UHM-02 well, showing the geometry of the Uithuizermeeden platform without vertical exaggeration.
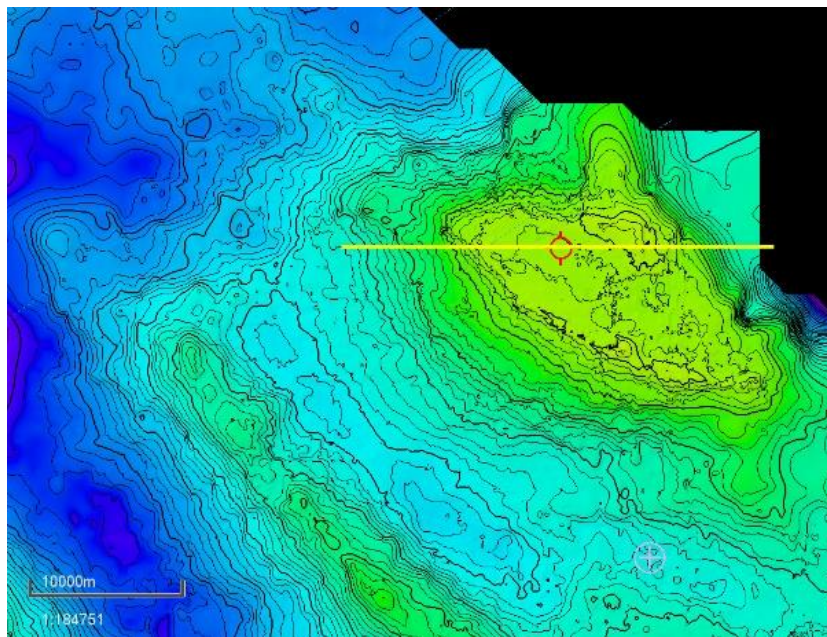
Figure 6-13: Map of the top of Dinantian with the visible feature of the UHM Platform. The yellow line indicates the seismic section shown in Figure 6-14.

The evolution of this platform is shown in Figure 6-14 and can be summarised as follows:

1. Tilted Devonian fault block during Early Carboniferous (earliest Tournaisian). This may have had as much as 1 km vertical height with respect to surrounding sea floor. Strong erosion is expected from this structural high, with the development of a thick wedge of clastics in Tournaisian basins; in the North Sea, well E06-1 encountered 700m of Tournaisian clastics that could be related to this erosional phase in the region. Well Munsterland-1 shows an extreme condensation of the coeval basins, explained with the temporary shutdown of carbonate production.

2. Carbonate deposition onlapped the structural high from the west. This early phase of deposition may be latest Tournaisian in age but was not necessarily encountered in the well. The eastern part of the high may have been exposed and could have shed clastics onto the high and into the basin. Mounded seismic geometries may represent isolated buildups that later coalesced into a more widespread carbonate platform.

3. Early Visean carbonate deposition is well established, but considerably thicker to the west compared to the east. The fault-block high may still have been exposed (i.e. not covered by carbonates) at this stage, so the high may have still been shedding clastics.

71

Sidewall cores suggest that the base of the UHM-02 carbonate interval was a mixed carbonate clastic interval. It is possible at this stage that a rimmed margin is established, although reflectors in the platform "interior" still remain chaotic, perhaps due to the patchy development of these carbonates or karstification related to high order depostional cycles.

4. Expansion of carbonate platform and deposition on top of structural highs. Development of more parallel reflectors suggests the platform interior setting is better established.

5. At the end of the Visean, the carbonate platform developed a thickness of more than 600 m and a topographic relief of some 2 km above the surrounding basin. The isolated platform may have developed a rimmed margin with parallel reflectors in the platform interior.

6. Onlap of the Namurian onto the slope of the older carbonate isolated platform and death of the carbonate platform as it is suffocated by clastics drived from the north.
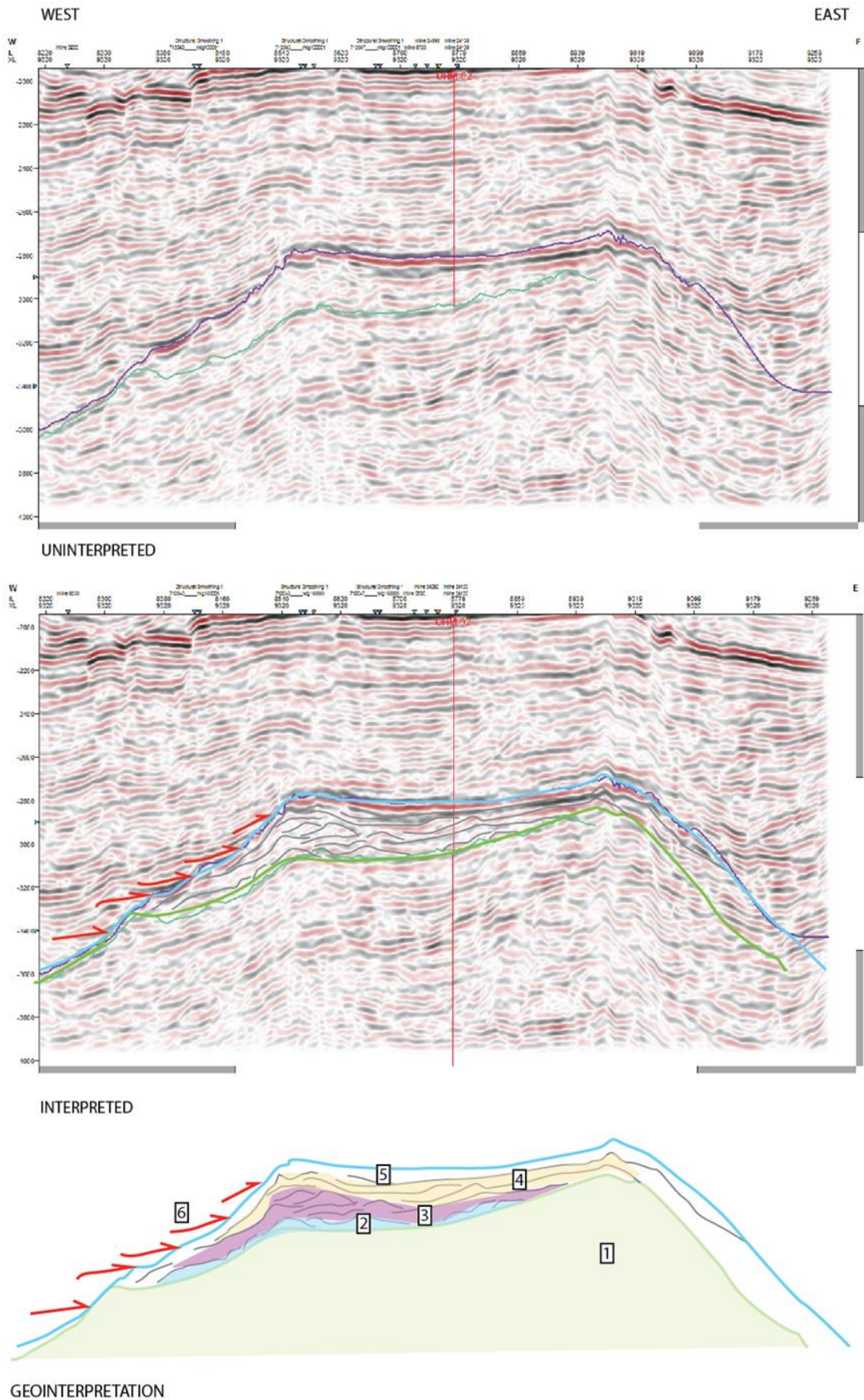
Figure 6-14: Uninterpreted, interpreted and geointerpreted west-east section through UHM platform.

73

It is not always clear how the eastern margin of the platform has developed. A relatively localized "apron" (Figures 6-13 and 6-14) is developed at the base of the platform, which could be explained by a number of scenarios:

a. A depositional apron composed of reworked probable clastic material derived from the tilted fault block.
b. A carbonate apron derived from reefal material deposited on the high, but no longer present there.
c. No clear features indicating moat or channels (shown by Faugères *et al*., 1999) can be pinpointed but the geometry could tentatively indicate a possible contourite deposit.
d. A shallow-water carbonate platform nucleated around the northern margin of the UHM high, deposited during the early stages of shallow water carbonate production around the southern margin of the high. The carbonate platform around the northern margin may not have developed subsequently as a result of steep depositional topography of the northern margin of the exposed basement.

A strong reflector is present within the tilted fault block. This has been mapped as Base Devonian, but it was noted that there was possibility some of the reflectivity was caused by multiples from the overlying salt.

Luttelgeest (LTG) Platform

The Luttelgeest isolated platform has been proven by drilling but is only covered by 2D seismic lines, only two of which properly define the structure (Figures 6-15 and 6-16). The total thickness of the shallow water carbonates encountered by the LTG-01 well is 768 m with a platform-top (the projected area) of 20 km^2. Initial observations are that Luttelgeest differs from Uithuizermeeden platform as it is not founded on a narrow topographic high and the published lines show a relatively flat base with horizontal reflectors below. The broader structural high where the Luttelgeest buildup is growing is also forming the basement for the unproven Nagele platform. However, other 2D lines suggest that there is indeed some structural character below, and it is likely that a fault-block high is the seeding point for the carbonates. It is difficult to map internal structures within the carbonate package as the quality of the data are too poor. The lowermost part of the carbonate package has not been dated, so it cannot be confirmed if the Tournaisian is present. The vast majority of the platform is Molinacian to Livian in age. The age of Livian near the top of the carbonate interval suggests that the entire Warnantian (Asbian-Brigantian) is missing in the well. However, seismic data show that the well penetrates the margins of the isolated platform (Figure 6-17), thus it is possible that either the well did not encounter the younger part of the stratigraphy seen in the centre of the Uithuizermeeden platform or was already drowned before or during Brigantian. In that case, this interval is represented instead by a more condensed platform slope facies during this time interval.
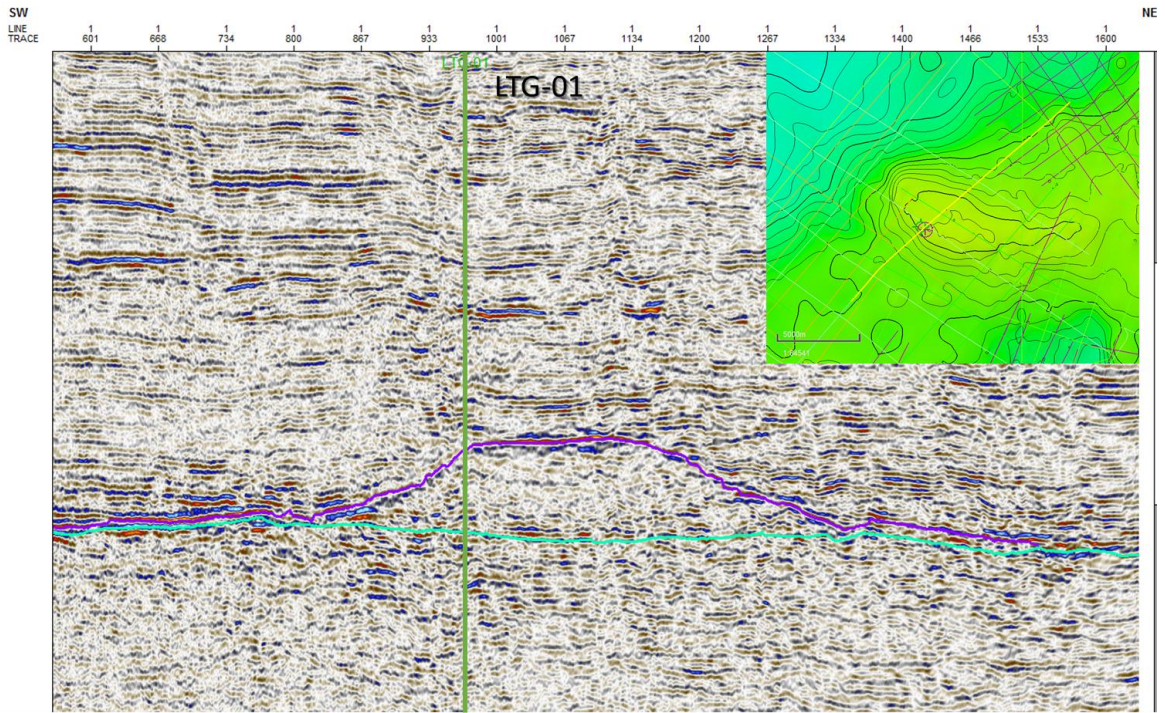
Figure 6-15: SW-NE 2D line through Luttelgeest platform. The green and purple lines indicate the base and top of the Diantian carbonates, respectively.
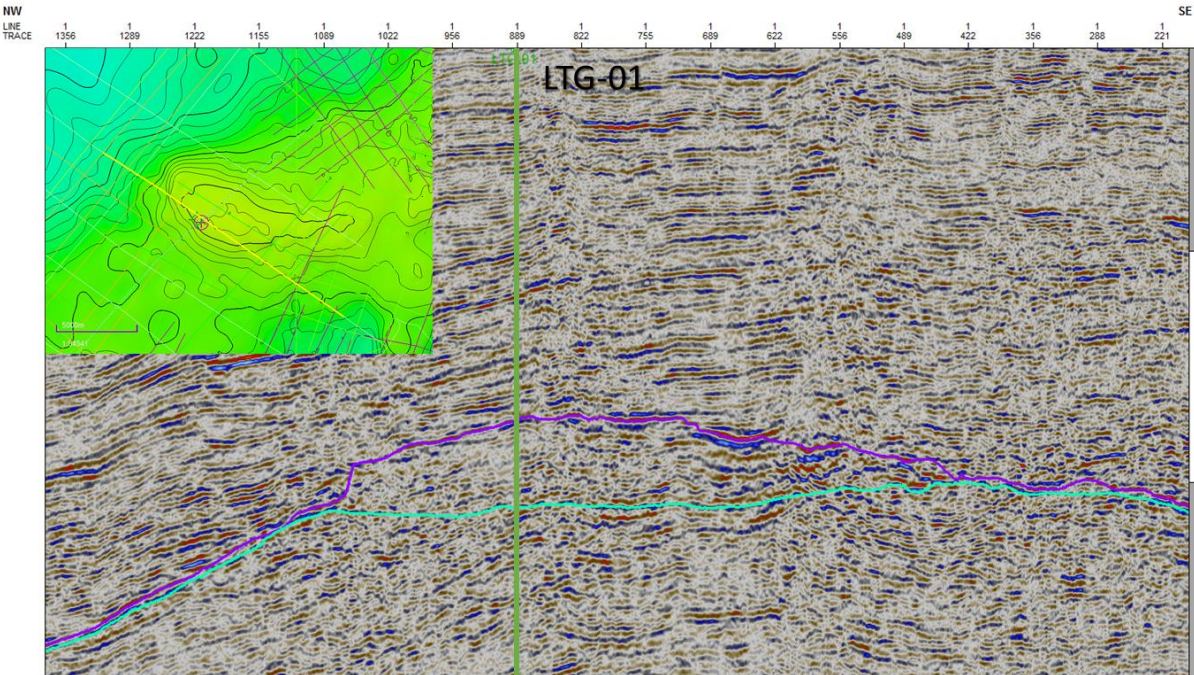
Figure 6-16: NW-SE 2D seismic lines through Luttelgeest platform. The green and purple lines indicate the base and top of the Diantian carbonates, respectively.
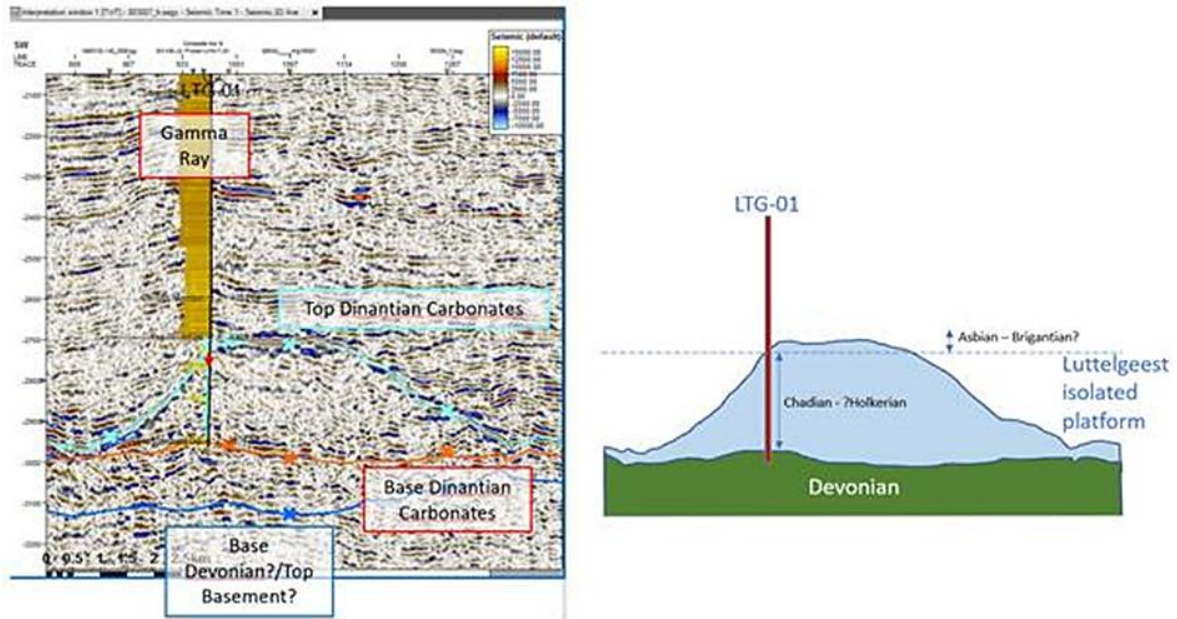
Figure 6-17: Geo-interpreted line through Luttelgeest showing the well situation at the margin of platform.

Bedum High

The Bedum structure is an NW-SE elongate structure to the SW of the Uithuizermeeden platform (Figures 6-18 and 6-19). It is clear that a structural high exists, as the Namurian sediments onlap onto the high. However, it would appear that any carbonates on top are either thin or even non-existent. Comparison on a flattened line below with Uithuizermeeden platform (Figure 6-19) indicates that whilst the top carbonate is picked at a reflector with strong acoustic impedance in Uithuizermeeden, this character is not present in Bedum.
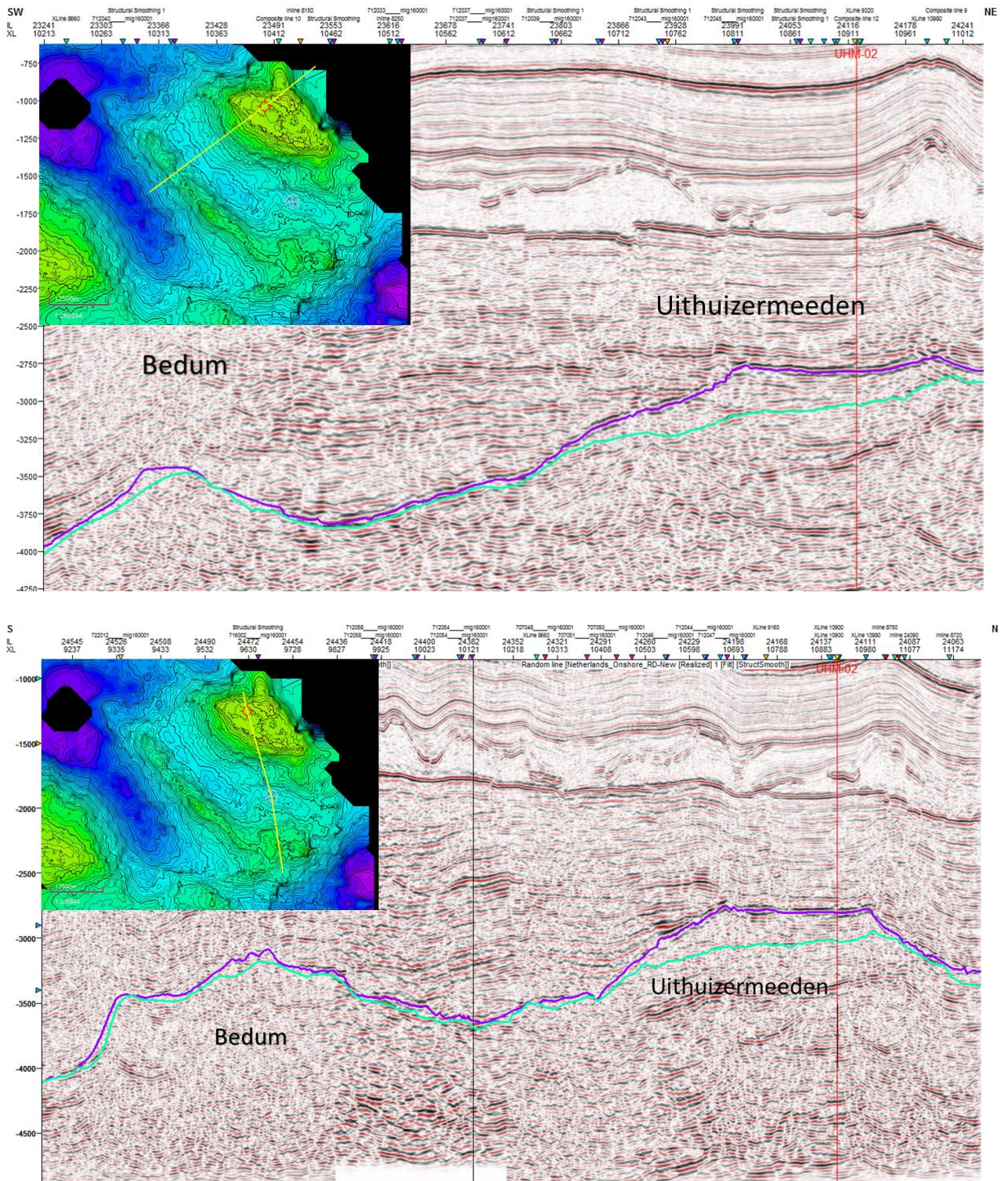
Figure 6-18: SW-NE and S-N lines through the Bedum High. The green and purple lines indicate the base and top of the Diantian carbonates, respectively.
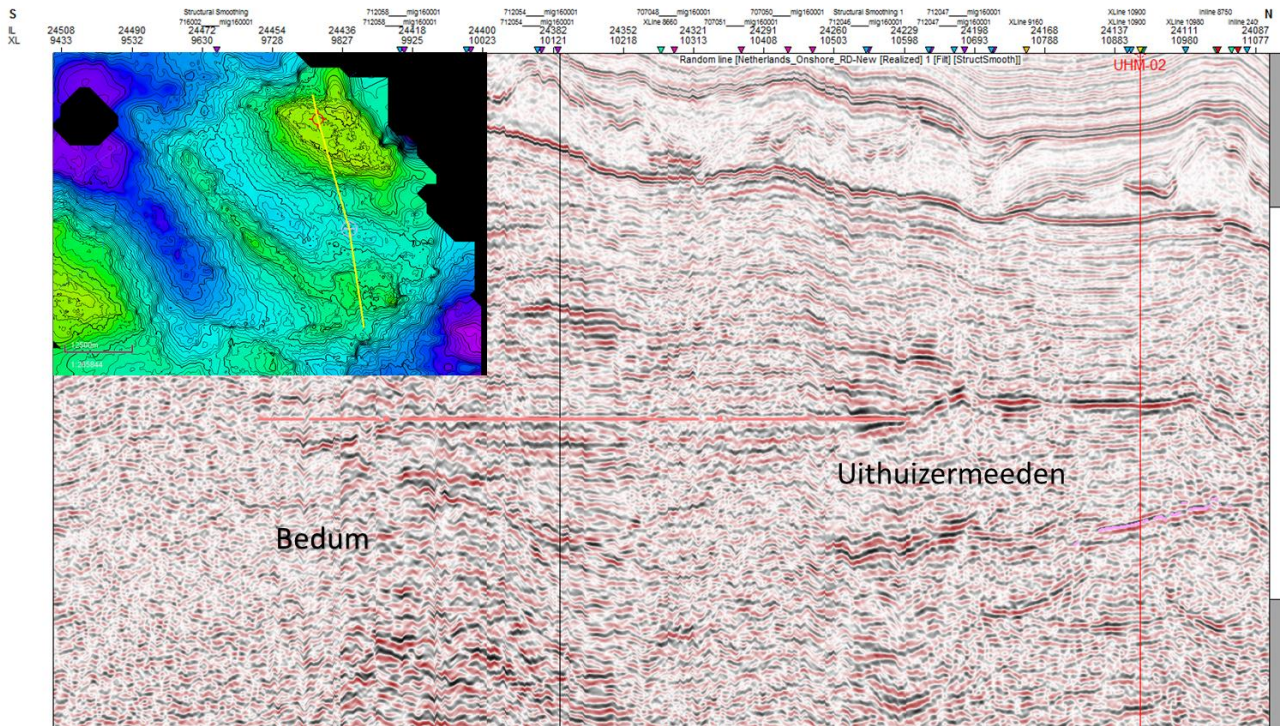
Figure 6-19: Flattened line from Bedum to Uithuizermeeden platform.

Fryslân High and Blija

The Fryslân structure is located towards the north of the Netherlands, and again is a NW-SE oriented high with a potential for carbonates. The potential carbonate package on the Fryslân Platform is around 150-200 ms, and fault control on geometry of the high is very clear to the north.
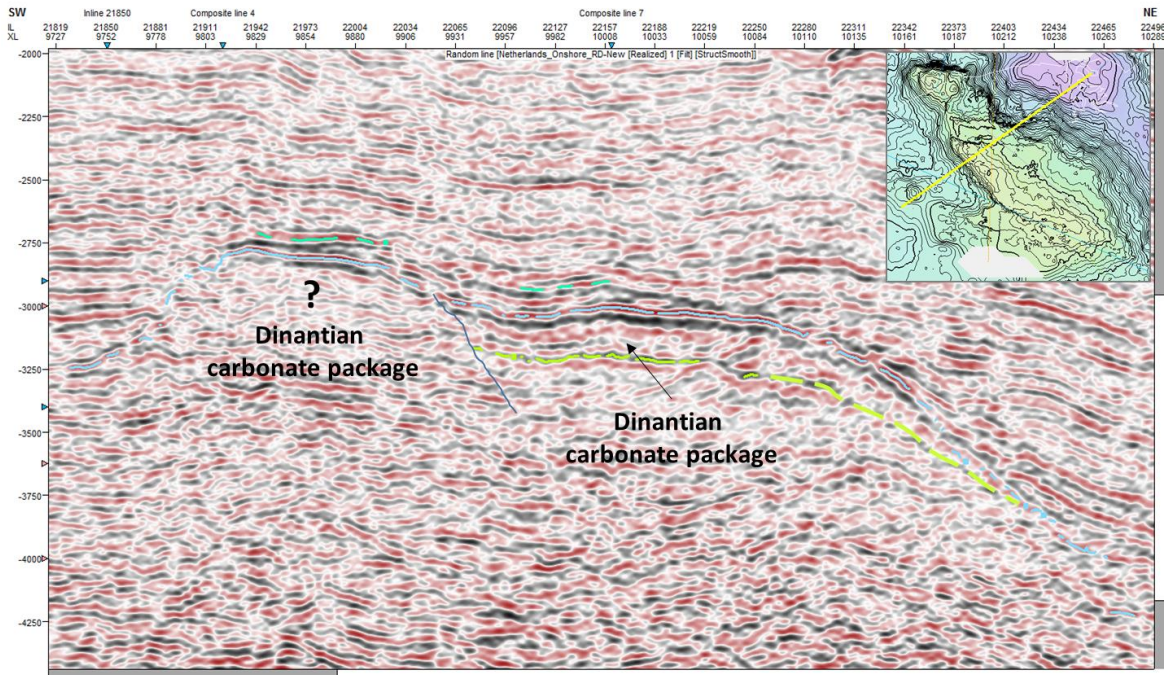
Figure 6-20: SW-NE interpreted 3D line through Fryslân High. The green and blue lines indicate the base and top of the Diantian carbonates, respectively.

Variance attribute shows clear cross-cutting faults in the platform that post-dates the carbonate package. The platform has less internal structure compared to the UHM platform. Internal reflectors mainly appear flat. However, it is noted that the platform onlaps a high to the northeast (Figure 6-21). The map below shows the extent of the potential carbonate package as it onlaps the high. If the seismic is flattened on an intra-Namurian pick, it is possible to see the carbonate package onlapping a high. Whether the carbonate package onlaps another structural high in the southwest of the Fryslan Platform (Figure 6-20) cannot be fully determind. A confident interpretation of the available siesmics images is limited by their inadequate quality.

The interpreted seismic below shows the NW margin of the Fryslân platform (Figure 6-21), the Blija Deep, which is interpreted as a tilted fault block contains no carbonate platforms.
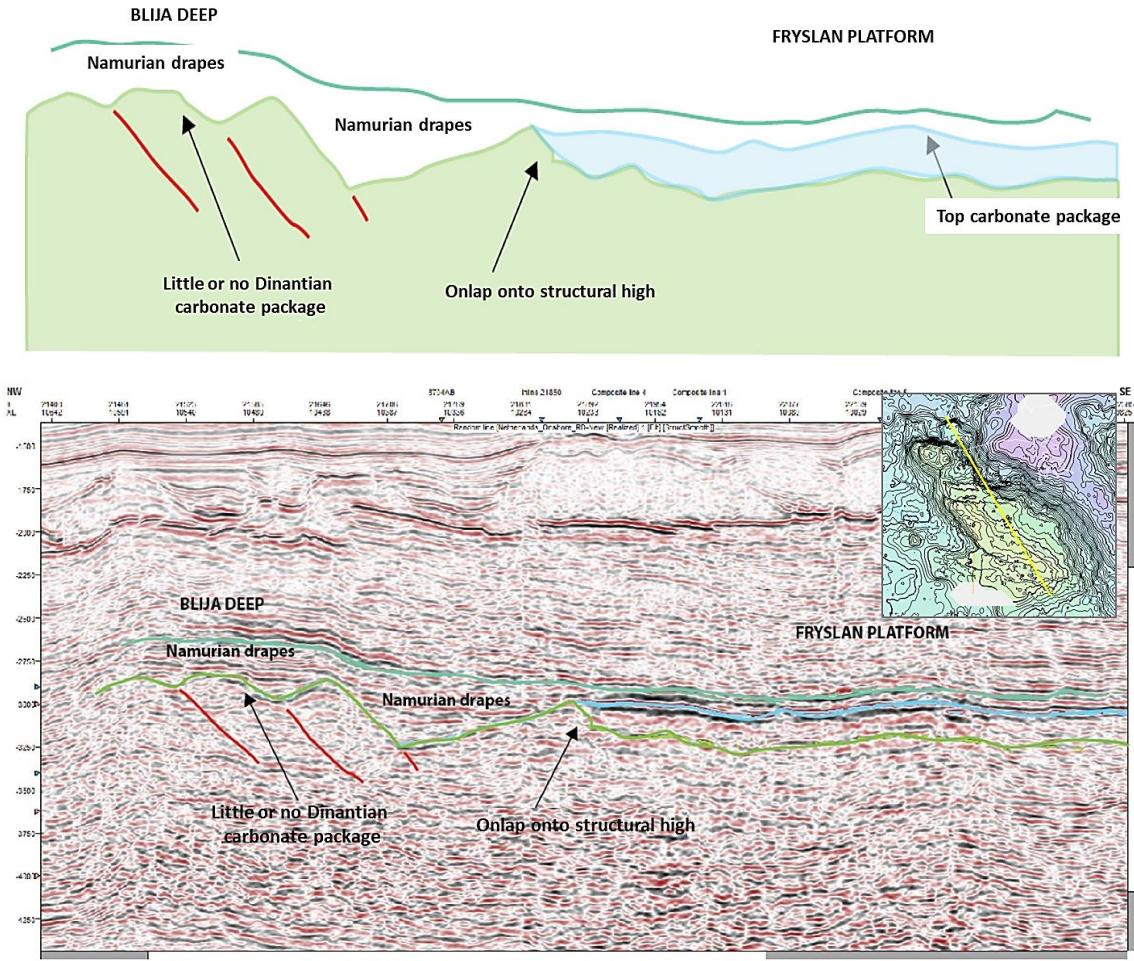
Figure 6-21: NW-SE Geoseismic interpretation, seismic interpretation and uninterpreted line through Fryslân Platform and Blija (NW-SE line). The lower green and the blue lines indicate the base and top of the Diantian carbonates, respectively. The dark green line indicates the top of Namurian deposits.

Wierumergronden High

The Wierumergronden High is located in the north of the 3D dataset and has limited coverage to the North. The structure is NW-SE trending. A Dinantian package may be present in the southeastern part of the structure, but is probably not related to the presence of carbonates (Figures 6-22 and 6-23). The strong acoustic impedance contrast of the top Dinantian reflector diminishes to the north, but any basal Dinantian reflector is uncertain.
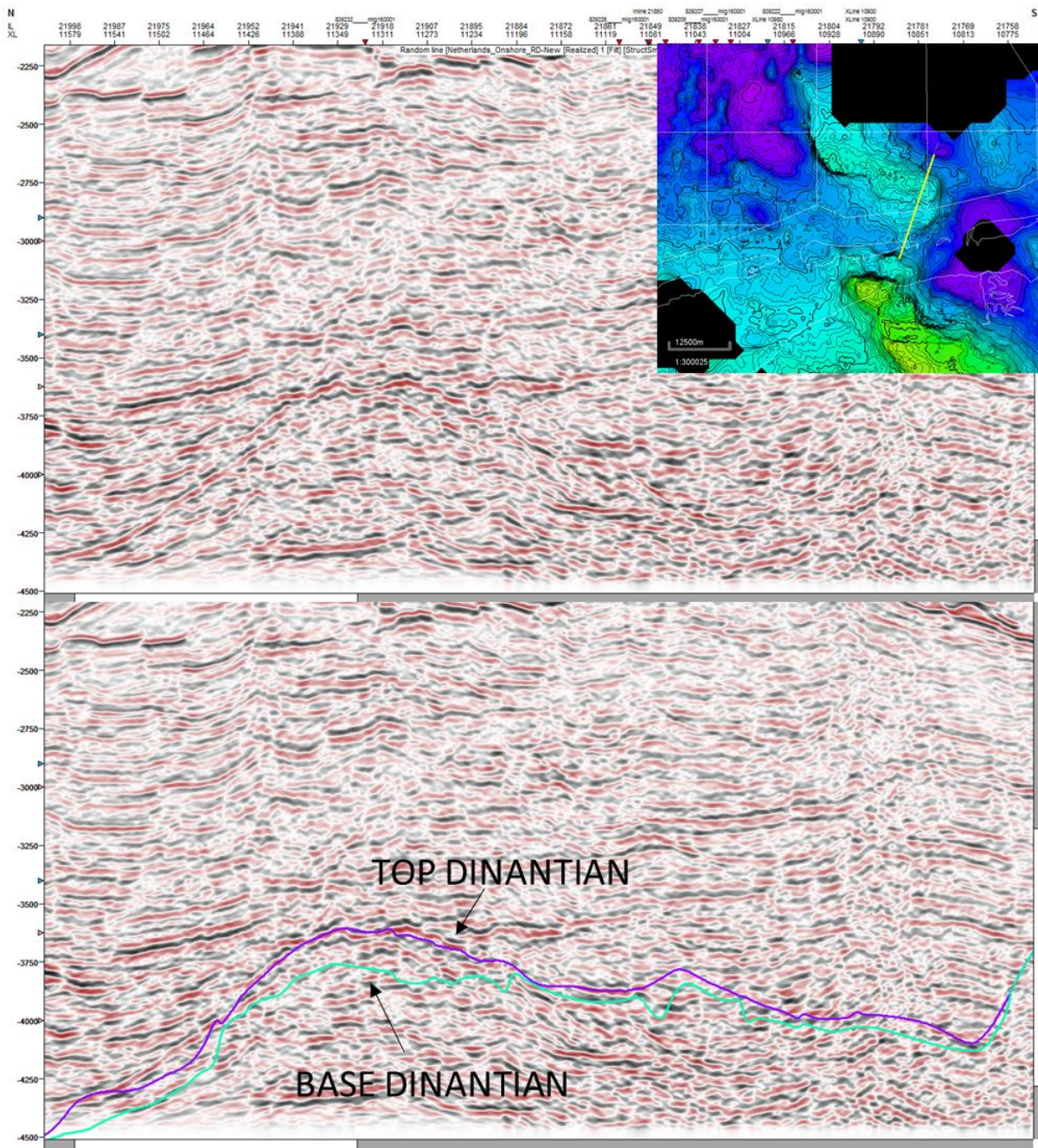
Figure 6-22: N-S uninterpreted and interpreted line through Wierumergronden High.
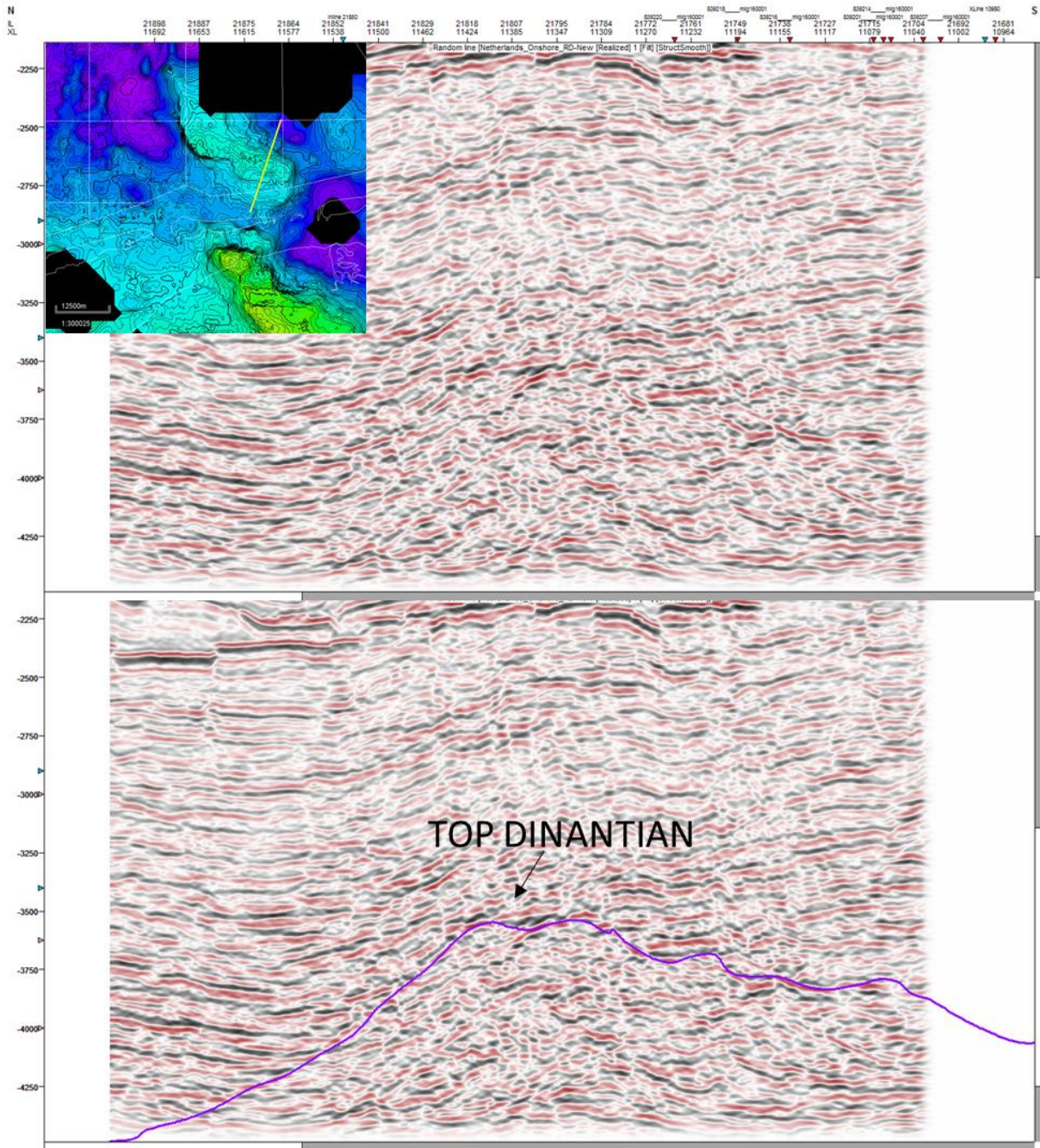
Figure 6-23: N-S uninterpreted and interpreted line through Wierumergronden High, located further north of the line shown in Figure 6-22.

Nagele

The Nagele well was drilled near Luttelgeest platform, but the well did not drill as far as the Dinantian, so it remains untested. The high is covered by poor quality 2D seismic. It is possible that a carbonate buildup has also onlapped onto a structural high that can only be imaged in one or two lines (Figure 6-24).
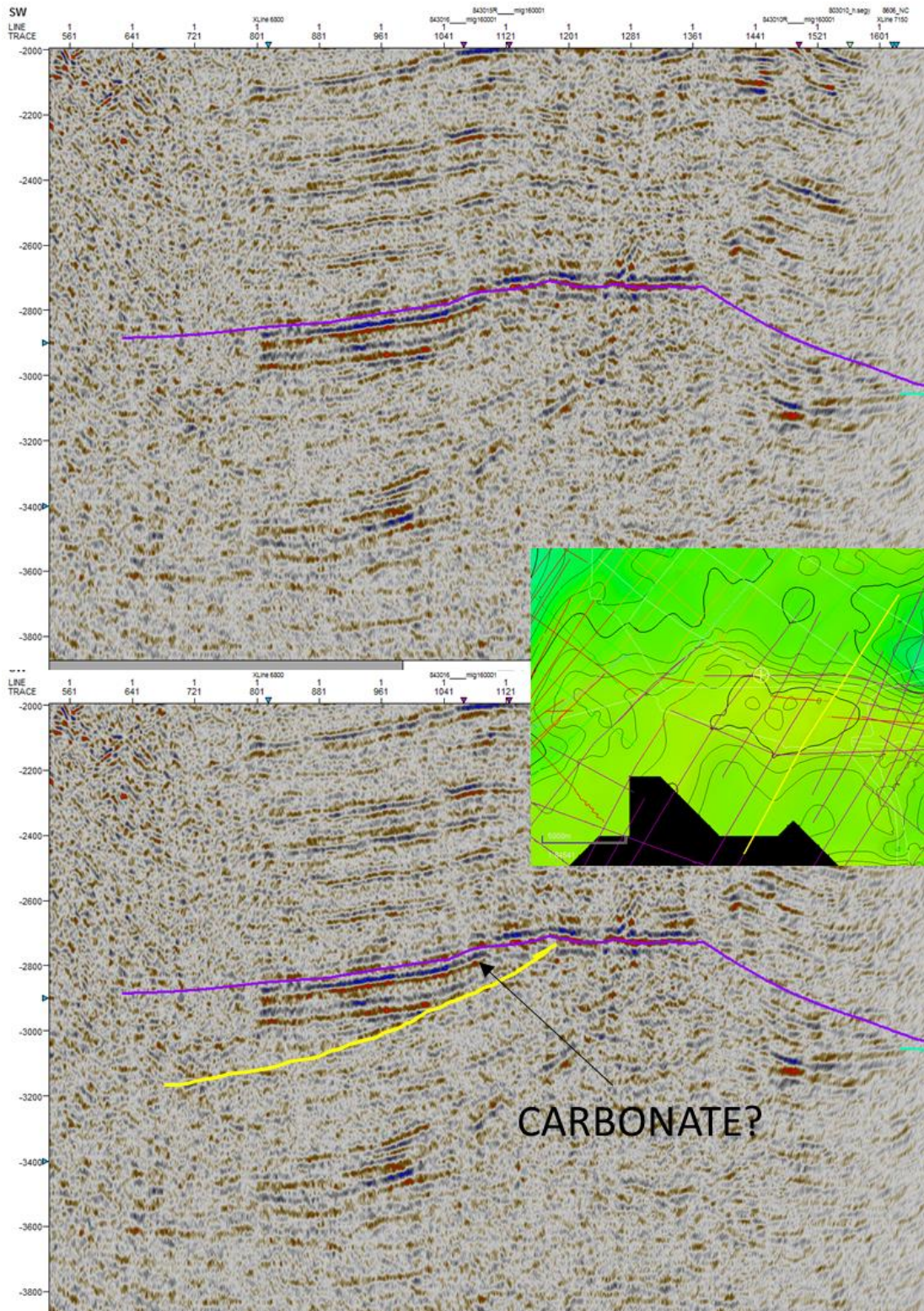
Figure 6-24: Uninterpreted and interpreted SW-NE 2D seismic line through Nagele. The yellow and purple lines indicate the base and top of the Diantian carbonates, respectively.

### 6.3.4 Comparison between global Dinantian depositional models and The Netherlands

In the subsurface of SW Netherlands, Dinantian carbonate depositional systems strongly resemble those of the UK, with Tournaisian carbonate ramps evolving towards Visean rimmed carbonate platforms similar to Kashagan platform (Ronchi *et al.*, 2010), less elevated (as shown in Ten Veen *et al.*, 2019) with gentle slopes of about 8-9°. Waulsortian mounds potentially can be present in the onshore and offshore areas though have been not properly identified in seismic images. During the late Warnantian, the depositional system switched to a more mixed clastic-carbonate system, with organic rich carbonates intercalated with fine clastics. In the northern Netherlands, the depositional systems are quite peculiar in respect of typical Dinantian platforms outcropping in UK and Belgium, as the former represent isolated platforms in a rapidly subsiding basin. In this case, the carbonate platform evolved directly into a rimmed shelf, without evidence of carbonate ramps or Waulsortian mounds. In terms of analogues, these platforms resemble those of the Precaspian Basin, such as Tengiz (Weber *et al.*, 2003; Kenter *et al.*, 2006; Harris, 2008; Collins *et al.*, 2013) or Kashagan (Ronchi *et al.*, 2010). However, the Dutch platforms drown during Late Visean while carbonate production in the Precaspian Basin continues into the Upper Carboniferous and Lower Permian. These platforms are microbially-produced but their facies are relatively more grain-supported and represent much larger depositional systems compared with the northern Netherlands examples. Furthermore, the Precaspian platforms have distinctly steeper margins (20-35°; Kenter *et al.*, 2005; Ronchi *et al.*, 2010) in comparison to the ones in the Netherlands and UK.

6.4 Facies maps

Two different conservative facies maps have been created for the Tournaisian, Molinacian to Livian and Warnantian (Asbian to Brigantian) time intervals (Figures 6-25 and 6-26). All facies maps are presented in the GIS project associated with this report. Because the input data quality is extremely variable, each polygon was given a degree of confidence to. The outlines of the southern basin, where KSL-02 and HEU-01 were drilled, are still uncertain and was defined as an open basin because of the absence of evaporites. The presence of a thick succession of evaporites in the St Ghislain well in Belgium, suggests that some areas around the London-Brabant Massif could be interpreted as a closed hypersaline intrashelf basin that was completely surrounded by platform facies. The Warnantian map was built mostly using seismic data. In the offshore portion of the Brabant Platform we infer a partial retrogradation of the margin, documented by a thin package of slope deposits downlapping on the older platform top. The reconstructed maps are partly comparable with the palaeogeography map presented by Boxem et al. (2016). The main differences are in details of the platform outlines, and the absence of carbonate platform at Bedum High and Maastricht region. Moreover, Nagele and part of the Winterswijk area is considered as a plausible carbonate platform. The outlines of the Winterswijk platform are not yet clear.
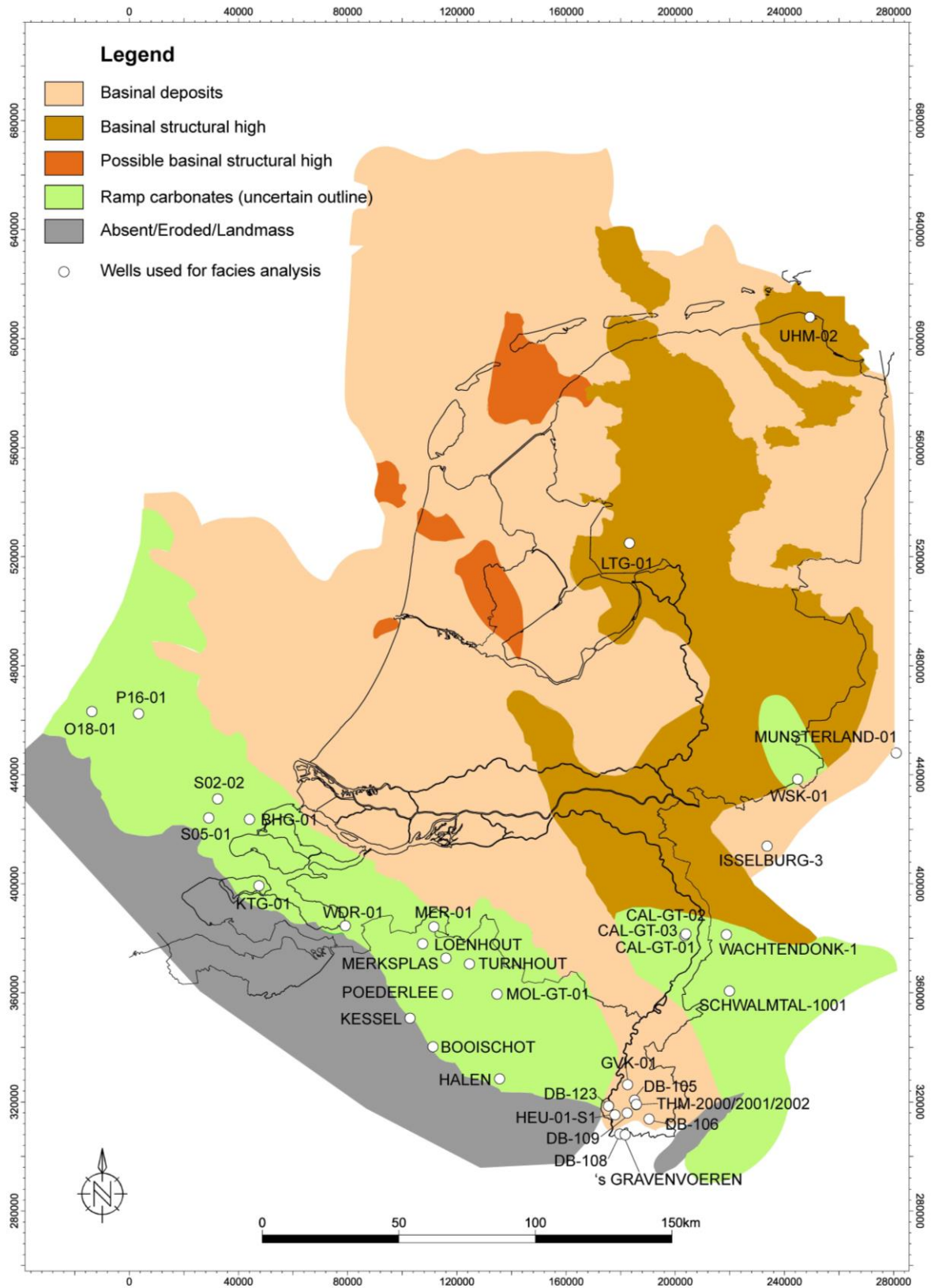
Figure 6-25: Reconstructed facies map showing the conservative distribution of the carbonate platforms during Tournaisian.
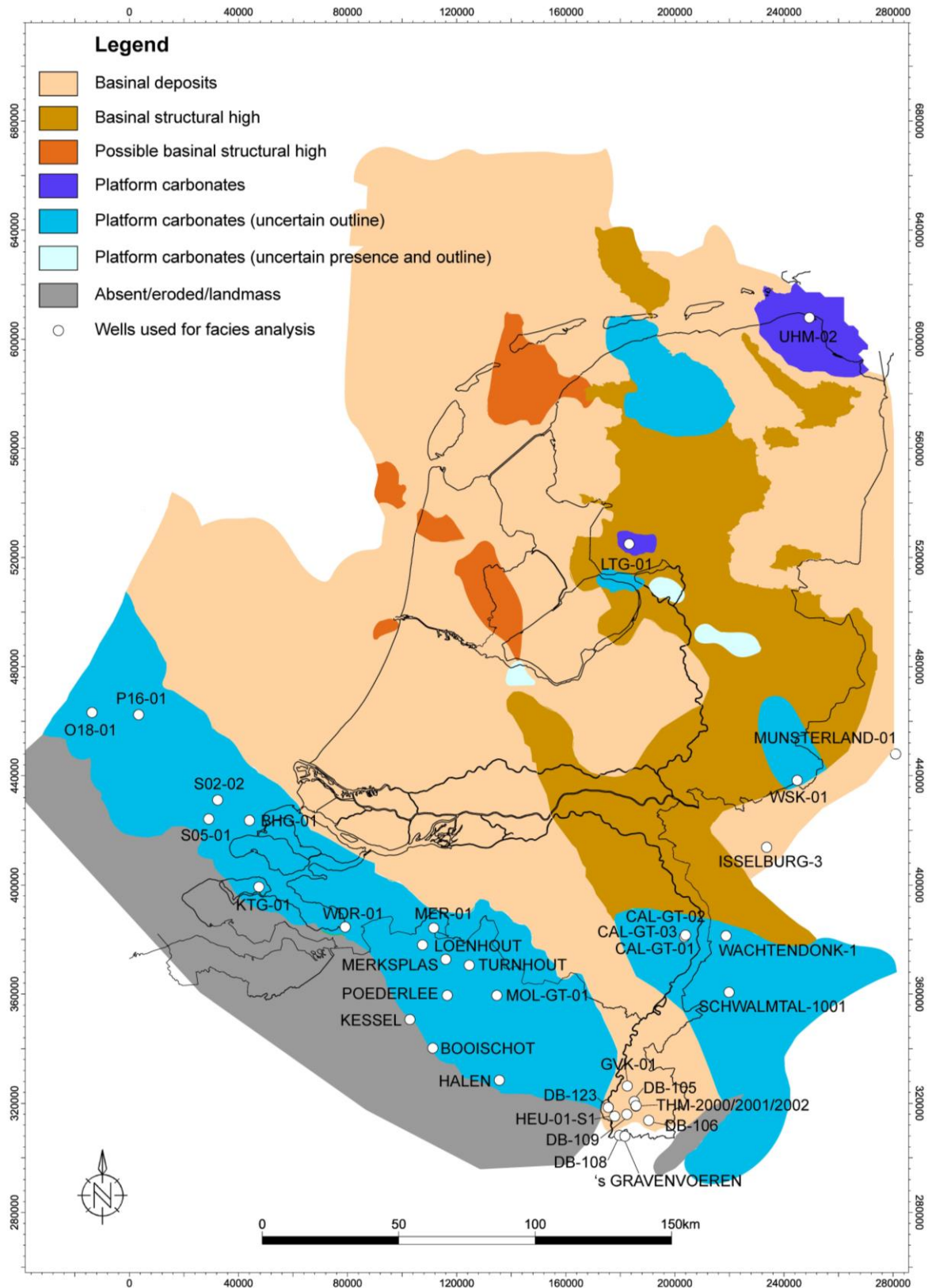
Figure 6-26: Reconstructed facies map showing the conservative distribution of the carbonate platforms during Visean (Molinacian to Livian interval, and Warnantian).

6.5 Karst systems and exposure of the Dinantian carbonates

Up to three phases of karstification affected the Dinantian carbonates. The distribution of the latest two phases of karstification is indicated in Figure 6-27, while the intra-Dinantian one is not clearly mappable.
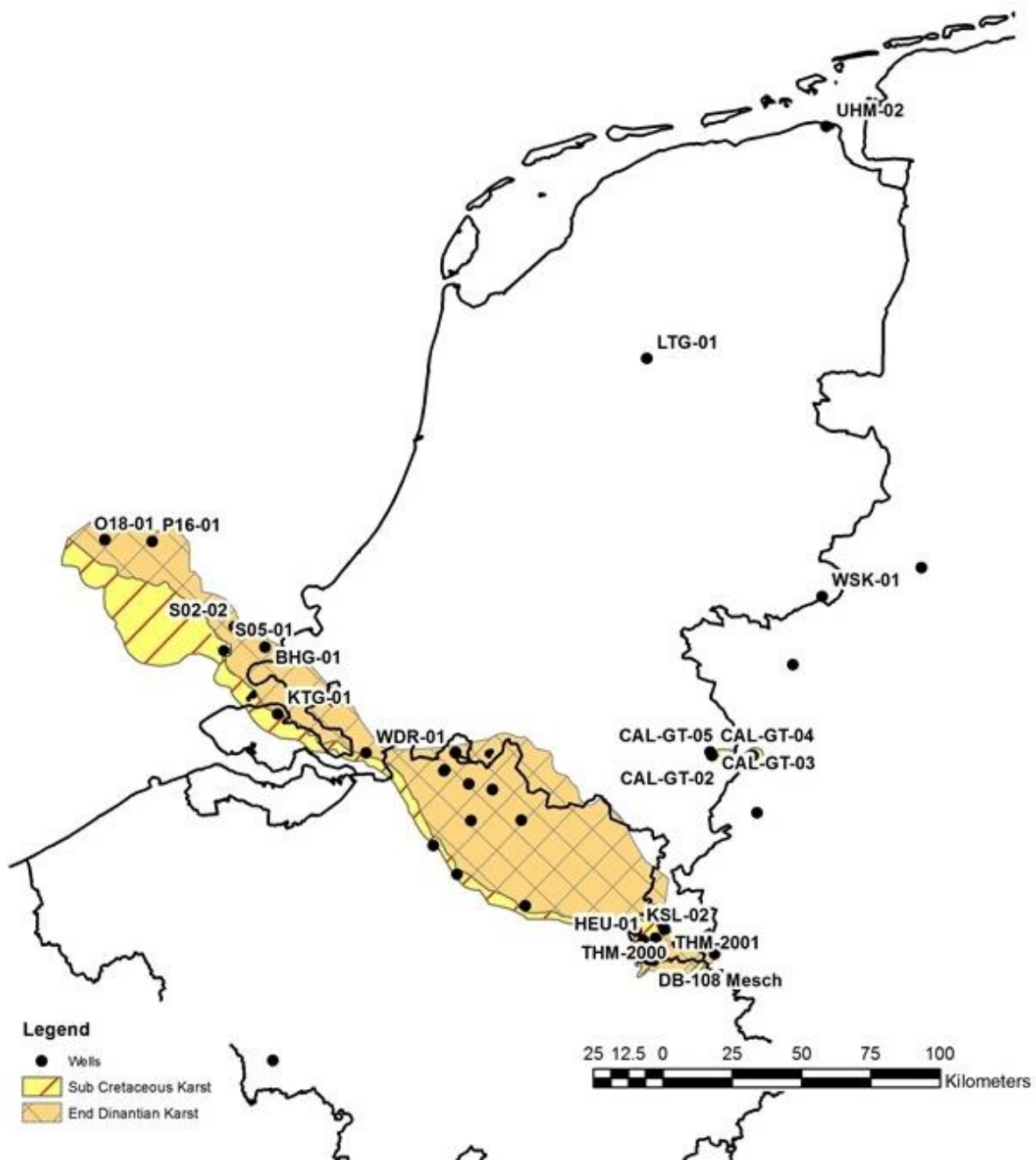
Figure 6-27: Map showing the distribution of end Dinantian (sub-Namurian) and sub-Cretaceous karsts.

6.5.1 Intra-Dinantian karst in the SW Netherlands

Occasional spar-fill cavities and enlarged fractures within the Dinantian carbonates of wells S05-01 and KTG-01 contain geopetal infills of peloids and Dinantian benthic foraminifera (Figure 6-28). This indicates a Dinantian age for the karst infill and is interpreted as exposure events associated with cycle boundaries. These are likely to form layer parallel karst systems within the Dinantian. Petrography analysis did not indicate significant porosity development

within these karstic features. These features are not associated with high variations in the petrophysical analyses perhaps due to the limitations of the latter analysis in detecting such small-scale components.
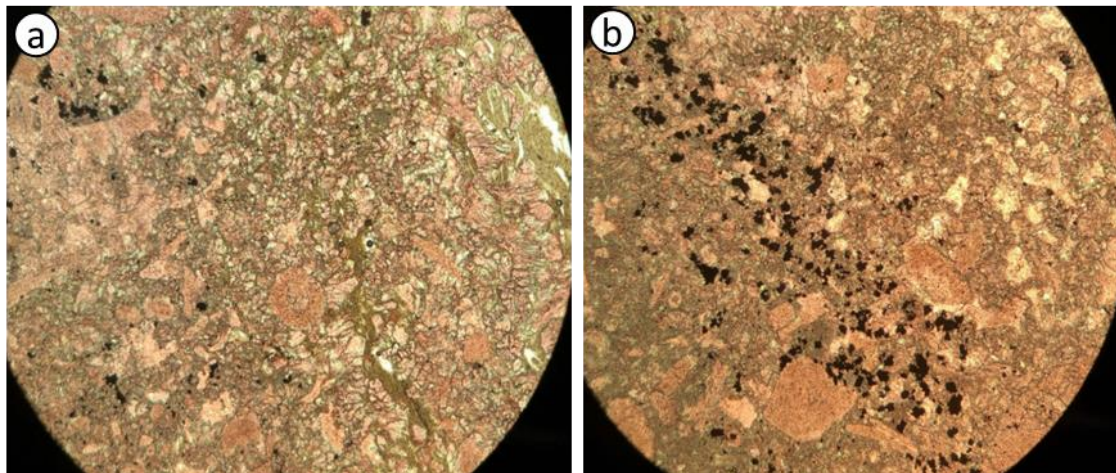
Figure 6-28: a) Dinantian karst fill with crinoids and beresellid algae with greenish mudstone matrix. KTG-01 962.25 m; fov 4 mm. b) Pyritic layer (dark spots) in Dinantian karst fill with crinoids and beresellid algae (KTG-01 962.25 m; fov 4 mm).

6.5.2 Sub-Limburg (Namuran) karst in the SW Netherlands

A phase of karstic exposure of Dinantian carbonates occurred at the top of Dinantian platform carbonates at their boundary with the overlying Limburg Group. Cores 3 and 4 in well O18-01 contain enlarged fractures, fossils and depositional stromatactoid cavities in in-place platform margin carbonate facies that have been totally or partly infilled by dark grey mudstone (Figure 6-29). Miospores in this mudstone in well BHG-01 indicate a maximum (oldest) Namurian age for this karst fill; O18-01 was also sampled for biostratigraphic dating but the results were not conclusive pointing to a post-Dinantian pre-Limburg age of exposure and infill.

Figure 6-29: a) Mudstone infill of enlarged fractures cross-cut by spar-filled fractures (punctuated) O18-01, 5297.0 ft. b) Mudstone infill (white arrows) of stromatactoid cavities in platform margin carbonates, O18-01, 5295.5 ft. c) Geopetal infill (white arrow) of Goniatite by mudstone, O18-01, 5250.5 ft.

87

The sub-Limburg Group karst was cored in wells BHG-01 and S02-02 that consist mainly of pebble- to boulder-sized clast- and matrix-supported limestone breccio-conglomerates. Clasts include bioclast wackestone with whole fenestrate bryozoans and stromatactoid cavities and bioclast wackestone. The matrix of the breccio-conglomerates comprises dark siliciclastic mudstone, layered bioclastic grainstone and pale grey carbonate mudstone. Intervals of matrix-supported breccias are also present with angular, to sub-rounded clasts of pale brown and greenish friable mudstone (Figure 6-30). The carbonate clasts were derived from shelf margin and interior carbonate facies while the brown and green mudstone clasts may have been derived from a soil or terrestrial setting. An interval of *in situ* brecciation occurs with fitted fractures infilled by calcite cement (Figure 6-30). This is interpreted as a crackle-mosaic breccia indicating incipient failure of in place limestone above a cavity. Some clasts in S02-02 contain rounded cavities that cross-cut depositional fabrics. There is an initial phase of pendant vadose cement in these cavities in which the pendant cement is no longer vertical indicating the limestone breccia was exposed prior to reworking (Figure 6-30). The brecciated intervals at the tops of BHG-01 and S02-02 are interpreted as a series of cave fill or cave collapse breccia with some intervals of crackle brecciated host rock. The clasts were sourced from the surrounding host limestone and the matrix represents marine and terrestrial infills.
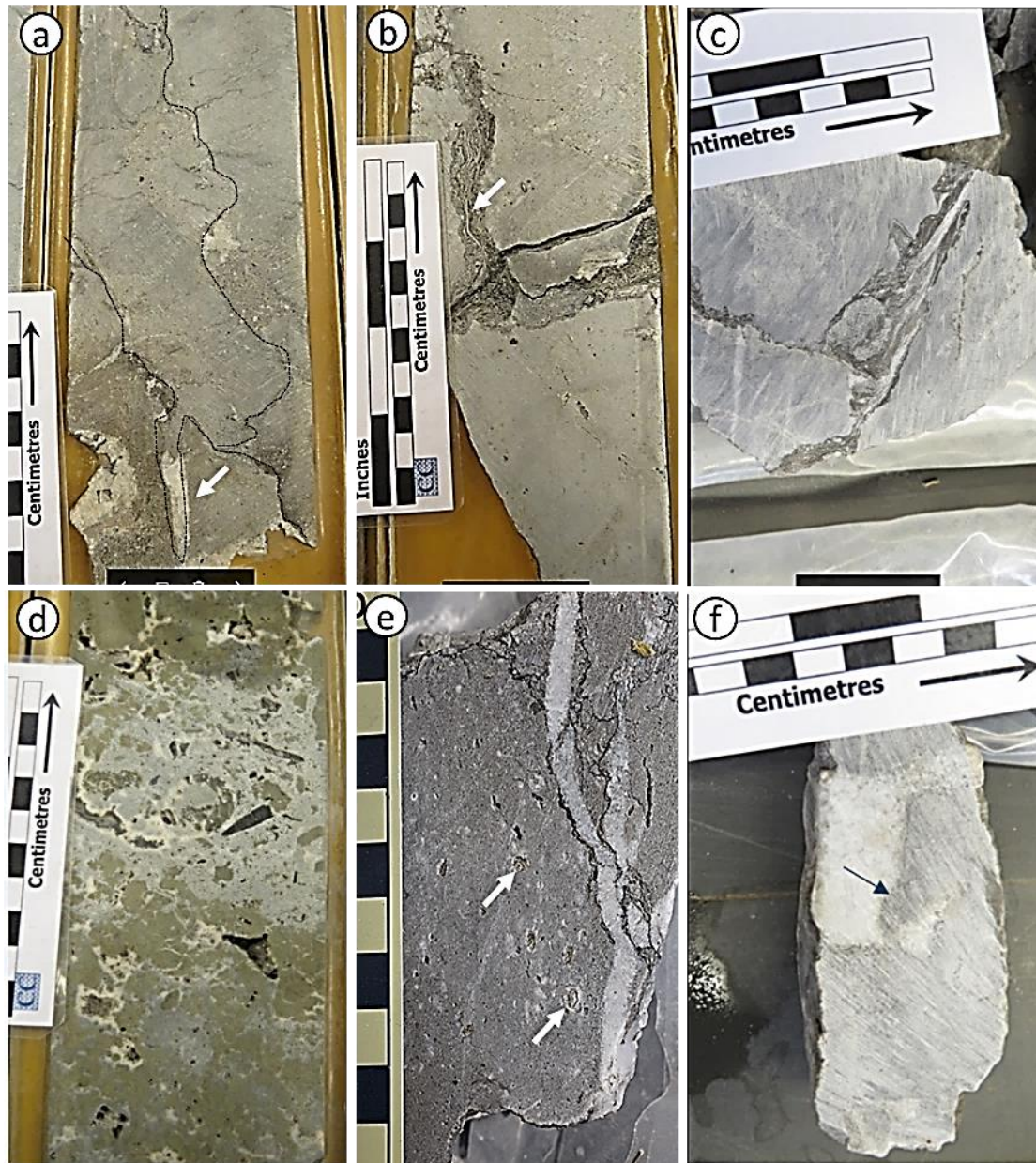
Figure 6-30: a) Crackle-mosaic breccia (punctuated) cemented by calcite (white arrow) above karst cavity, BHG-01, 2175.4 m. b) Dark mudstone (white arrows) between cobble-sized limestone clasts, BHG-01, 2171.8 m. c) Dark mudstone between cobble-sized limestone clasts, S02-02, 1890.1 m. d) Mudstone clasts in pyritised matrix-supported breccia BHG-01, 2176.2 m. e) Matrix-supported breccia with brown and green mudstone clasts (white arrows) cemented by calcite; S02-02, 2176.2 m. f) Pendant cement in cavity in clast (arrow), indicates that the clast was rotated S02-02, 2175.4 m.

Correlation of depositional cycles in the basal part of BHG-01 (Figure 6-1), together with biostratigraphic dating from Core 1 shows that majority of the Dinantian successions are present in BHG-01. However, BHG-01 contains the thinnest Dinantian successions of these wells (Figure 6-1), thinner even than S05-01 in which an estimated 20-25% of the Dinantian is missing as a result of sub-Cretaceous erosion. It is not possible to extend the high-resolution sequence stratigraphic correlation of BHG-01 above the 1d cycle (Figure 6-1); since it consists of gamma ray peaks that are interpreted as mudstone infills of a karst body.

The upper part of the Dinantian in S02-02 shows a similar signature with frequent gamma ray peaks (Figure 6-1), also interpreted as a karst body. In S02-02, the karst body cuts down to the 2d depositional cycle. An isopach map (Figure 6-31) of the Limburg Group indicates a thickening from 450 m to 750 m near the well BHG-01 that can possibly be interpreted as the effect of karst collapse. Moreover, the palaeogeological map of the sub-Limburg unconformity shows overstep down to the 1d and 2d depositional cycles in wells BHG-01 and S02-02, respectively. In well O18-01, the Limburg Group is either conformable or sub-Limburg erosion is limited to the topmost Dinantian depositional cycle.
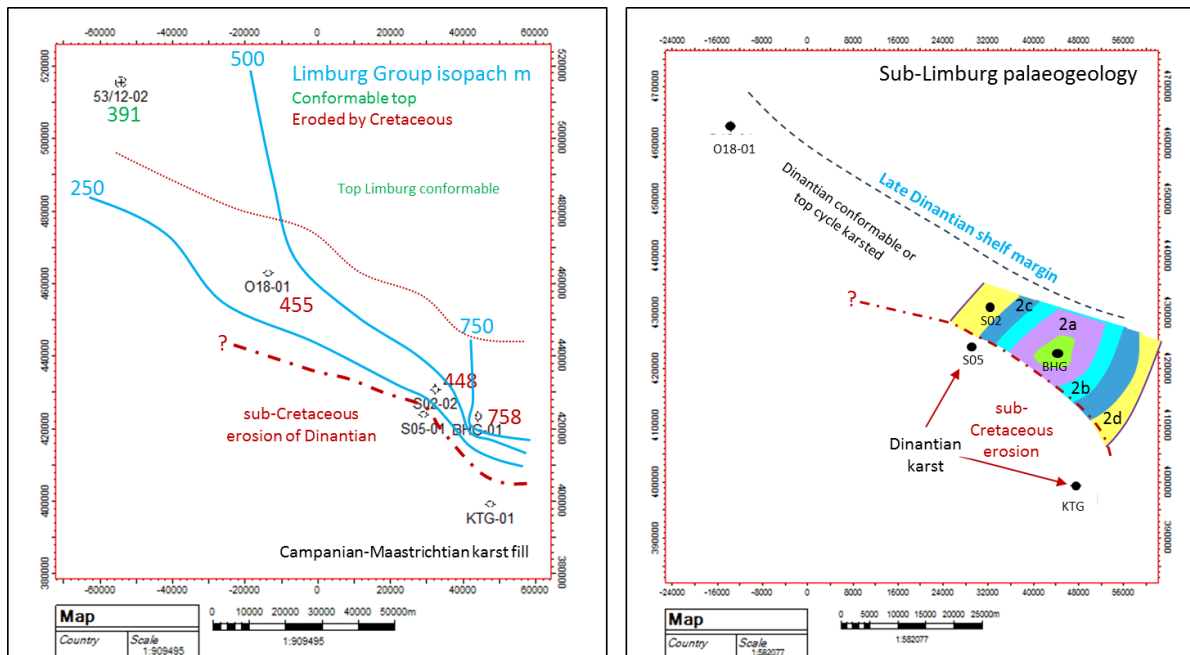
Figure 6-31: Left: Limburg Group isopach in SW Netherlands. The red dotted line indicates the late Dinantian shelf margin; the blue numbers indicate the contourd thickness of the Limburg Group; the green numbers are actual thickness of the Limburg Group in well (complete sequence); the red numbers are actual thickness in well (incomplete sequence due to Cretaceous erosion). Right: Sub-Limburg Group palaeogeological map in SW Netherlands. Colours represent subcrop of units 1d (green), 2a (purple), 2b (light blue), 2c (dark blue) and 2d (yellow).

The karst collapse and fill encountered in cores in BHG-01 and S02-02 are interpreted as the products of doline collapse of the top Dinantian carbonates during a period of exposure at the end Dinantian. Evidence of dolines and other karst features can also be observed on seismic lines across the carbonate platform in the SW Netherlands (Figures 6-32 to 6-34). The top Dinantian reflector varies from rugose and discontinuous in up dip areas to a more uniform high amplitude reflector down dip that is interpreted as a transition from karst influenced in up dip areas to a conformable boundary with no emergence in down-dip areas. This is also associated with the chaotic seismic character within the Dinantian interpreted as collapse features associated with depressions in the top Dinantian reflector interpreted as doline collapses (Figures 6-32 to 6-34).
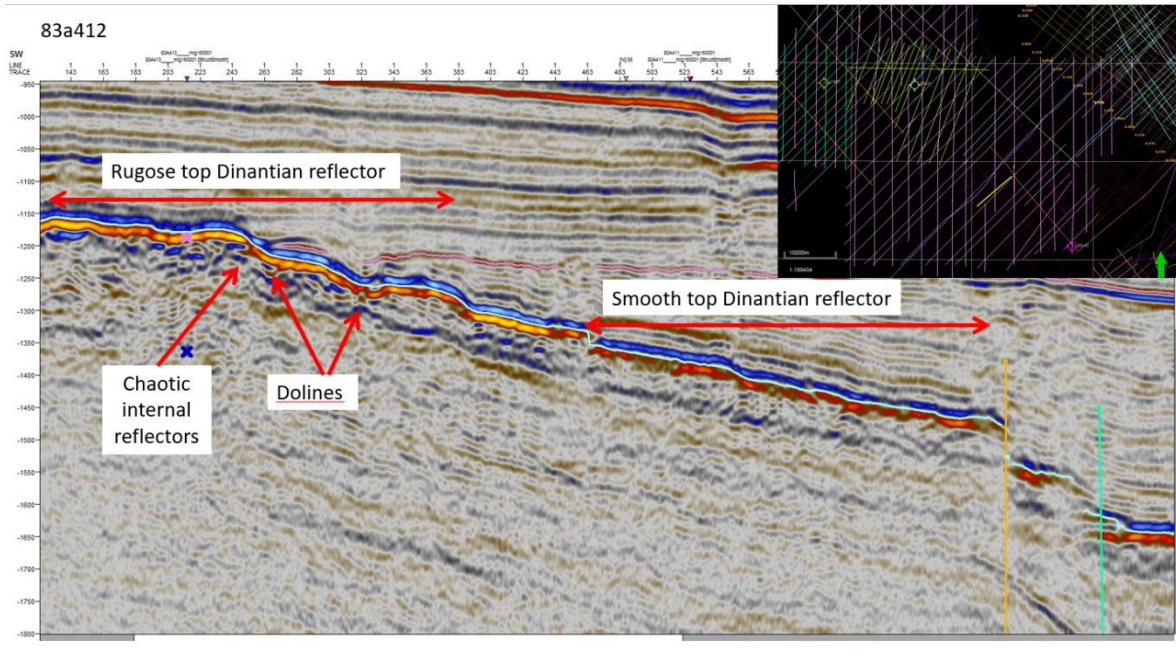
Figure 6-32: Dip line showing lateral variation in character of top Dinantian reflector and possible seismic expression of karst features in Dinantian.
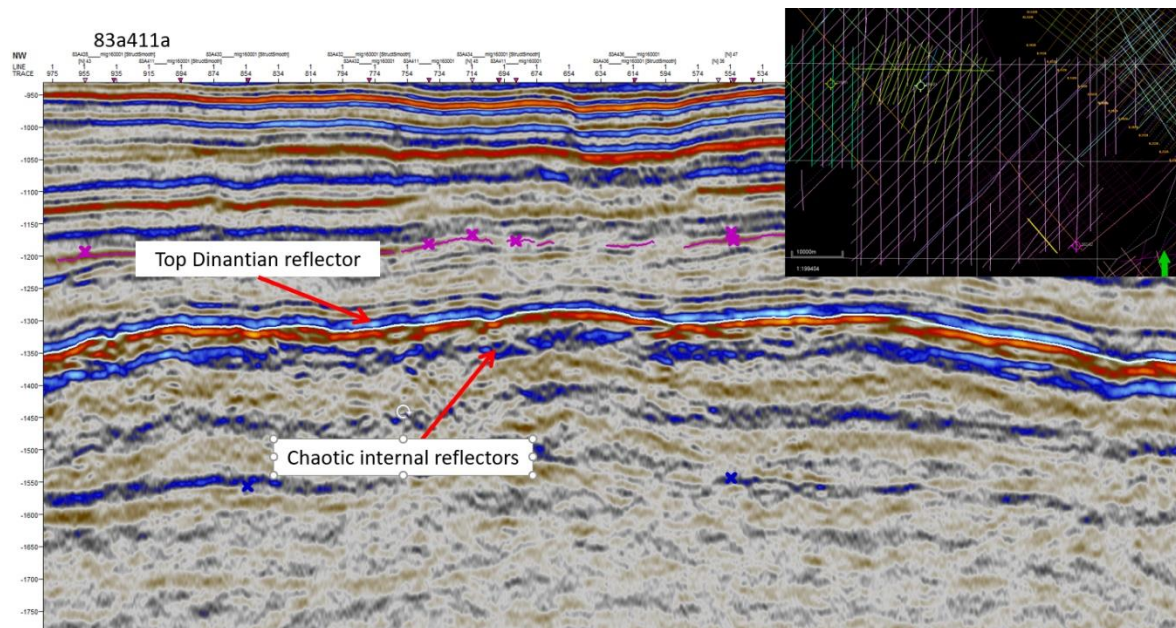
Figure 6-33: Strike line along up-dip part of Dinantian margin showing rugose nature of top Dinantian reflector and chaotic internal seismic character.
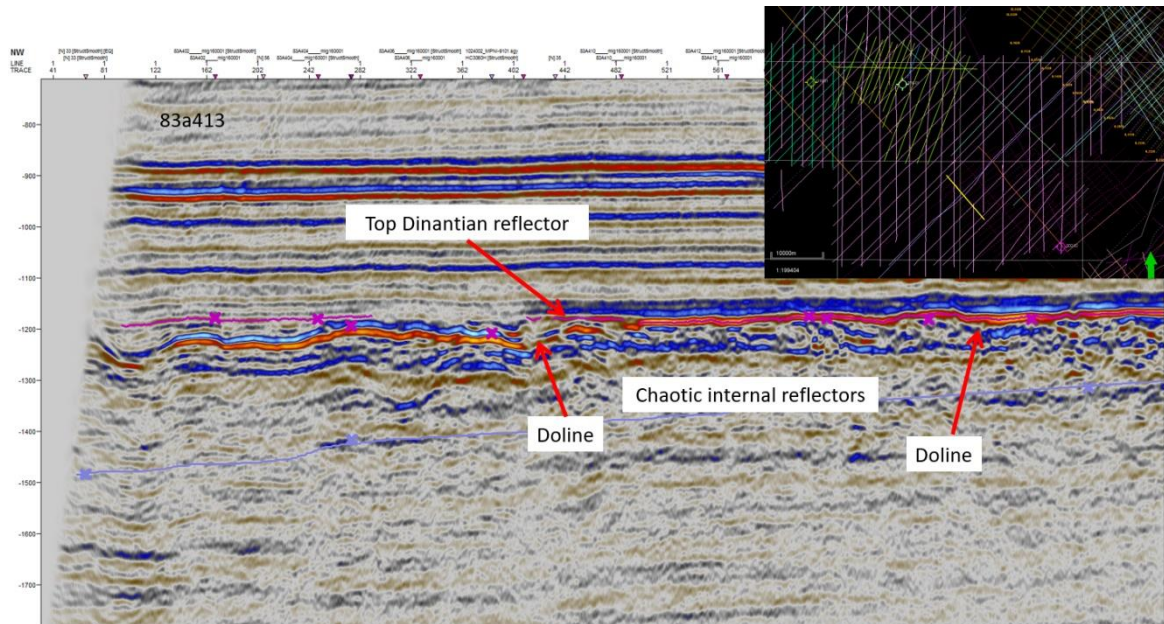
Figure 6-34: Strike line along up-dip part of Dinantian margin showing rugose nature of top Dinantian reflector with possible doline collapses and chaotic internal seismic character.

6.5.3 Karstic exposure of isolated carbonate platforms in the northern Netherlands

The Fryslân, Uithuizermeeden and Luttelgeest isolated carbonate platforms in the northern Netherlands have the potential to contain karst systems within the Dinantian succession, related to high-frequency sea-level fluctuations as shown by Ronchi *et al*. (2010) in the Kashagan platform. However, the Dinantian-Namurian boundary at the top of these platforms may be represented by a drowning unconformity and so the occurrence of karst is less probable. Cores from wells LTG-01 and UHM-02 do not contain any clear evidence of karst pore systems. However, since both of these wells only contain short cores it is possible that any karst system was petrographically missed. The presence of an organic and clay-rich centimeter sized horizon at the top of UHM-02 may point to temporal exposure periods. Seismic data across the Uithuizermeeden and Luttelgeest platforms show good reflector continuity across the platforms with a consistent high amplitude top carbonate reflector, without any significant evidence of karst geometry (Figure 6-35). There is also no apparent disruption, dimming or chaotic seismic facies associated with karst systems. Similarly, seismic attributes including variance, dip deviation or amplitude show no character attributable to karst. It is likely that the carbonate platforms became drowned rather than karstified. However, it should be noted that the resolution of the interpreted seismic images allows detecting large and moderate-sized (meter-sized) karstification but not adequately revealing the small-sized karstic features as comprehensively shown in Ten Veen *et al*. (2019). The latter features are usually centimeter-sized vugs.
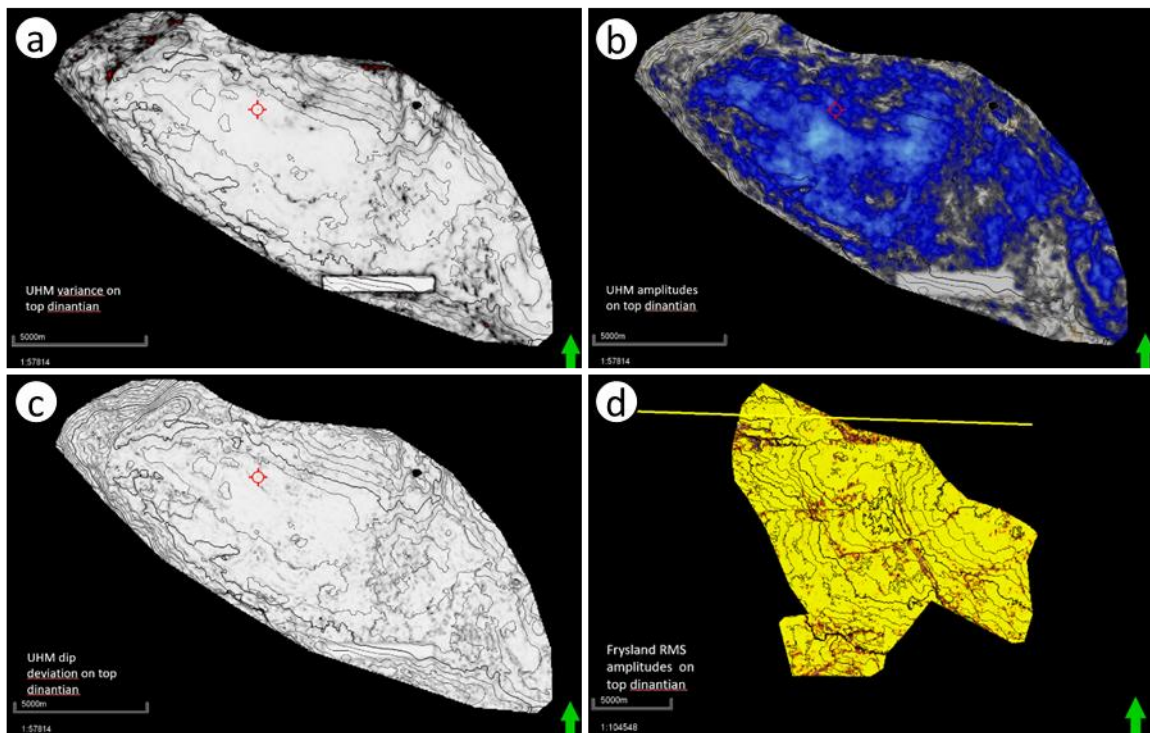
Figure 6-35: a) Variance on the top Dinantian, UHM carbonate platform. b) Amplitude on the top Dinantian, UHM carbonate platform. c) Dip deviation on the top Dinantian, UHM carbonate platform. d) RMS amplitude on the top Dinantian, Fryslân carbonate platform.

6.5.4 Sub-Cretaceous karst in the SW Netherlands

A phase of karstic exposure of Dinantian carbonates occurred beneath the sub-Cretaceous unconformity in the SW Netherlands. Some sediment fills of karst cavities in KTG-01 contain planktonic foraminifera that gave Campanian-Maastrichtian ages indicating the date of transgression and infill of the karst system. Karst cavities are also present in core from S05-01, but these cannot be conclusively demonstrated to be sub-Cretaceous karst fills because they lack any characteristic sediment fill. Sub-Cretaceous karst features include:

Fractures and cavities: KTG-01 and S05-01 cored contains a pervasive system of sub-vertical to oblique fractures that often connect to sub-horizontal or oblique larger cavities (Figure 6-36; Vandenberghe *et al.*, 1986). The fractures have rounded irregular, poorly-fitted margins and are often sinuous to curvilinear. The fractures often show abrupt changes in width with the aperture changing from hairline- to several cm- over a few mm along the length of the fracture. Some cavities and fractures cross-cut or exploit pre-existing denticular stylolites. The cavities and fractures often contain internal geopetal sediment (Figure 6-37). A characteristic key hole passage is present in the KTG-01 which formed initially as a phreatic passage that formed by dissolution along a denticular stylolite, that evolved in a vadose environment.
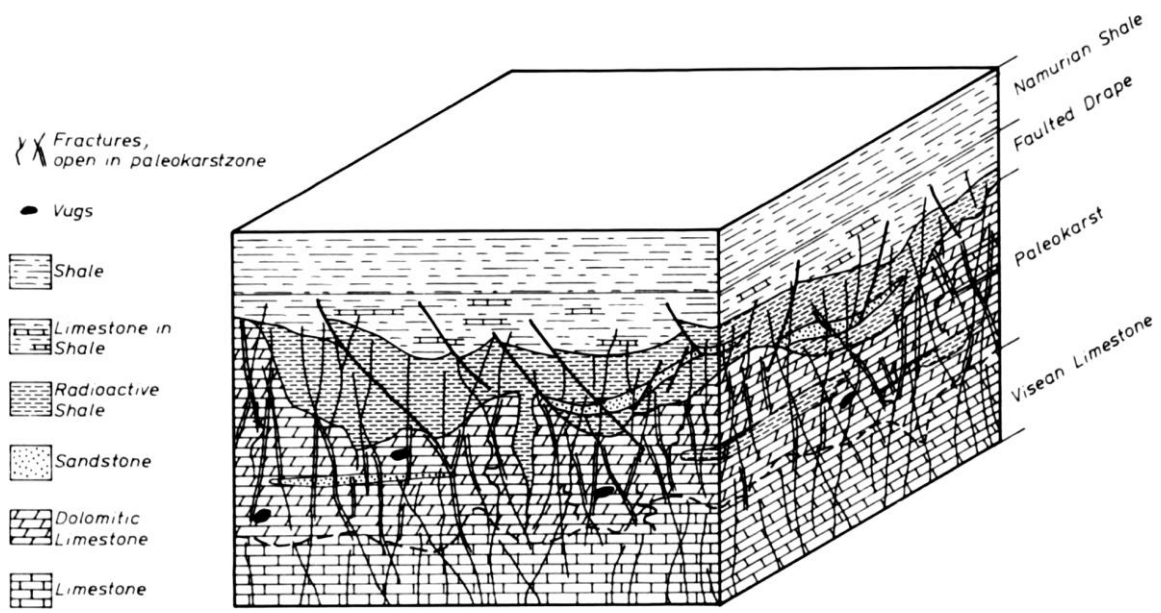
Figure 6-36: Model for the Namurian karst developed by Vandenberghe *et al.* (1986).
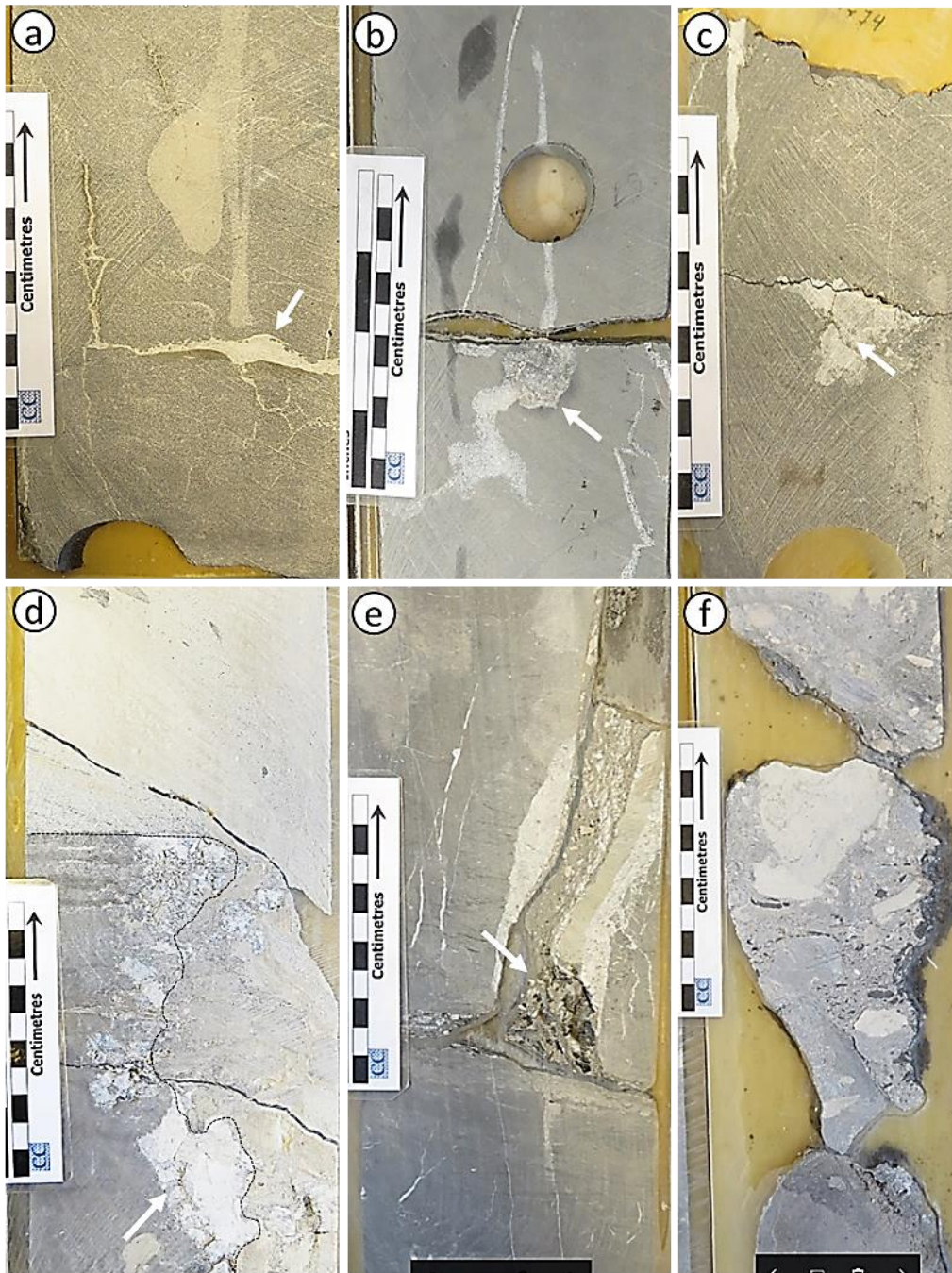
Figure 6-37: a) Sub-horizontal cavity with geopetal infill (white arrow), KTG-01, 966.0 m. b) Enlarged fracture infilled by calcite spar (white arrow), KTG-01, 954.0 m. c) Key hole passage (white arrow) cemented by calcite; KTG-01, 968.0 m. d) Cavity with vertical margin infilled by layered geopetal sediment (punctuated) and cemented at the margins (white arrow), KTG-01, 977.0 m. e) Fracture infilled by carbonate mudstone, grey mudstone and chalk breccia KTG-01, 954.0 m. f) Cavity infilled with clasts of chalk and organic-rich mudstone; KTG-01, 968.0 m**.

Sediment-filled cavities: Irregular cavities including enlarged fractures and caves up to 0.5 m in size are present in the Dinantian carbonates; these tend to exploit dolomitised intervals owing to the presence of matrix porosity that allows access of meteoric water for dissolution. These cavities often have multiple sediment fills that include sorted glauconitic grainstone and packstone with inoceramids and planktonic foraminifera; layered carbonate mudstone,

95

calcisiltite and calcarenite; clay-rich sediment and breccia of organic-rich mudstone and chalk. Sedimentary structures in the cave-fill sediment include lamination indicating detrital reworking by water flowing through the cave system and some cave fills contain fenestrae that indicate desiccation and deposition in the vadose zone. Some clay-rich cave fills contain replacive calcite crystals that show split crystal growth suggesting that the fine carbonate component has been neomorphosed (Figure 6-38).
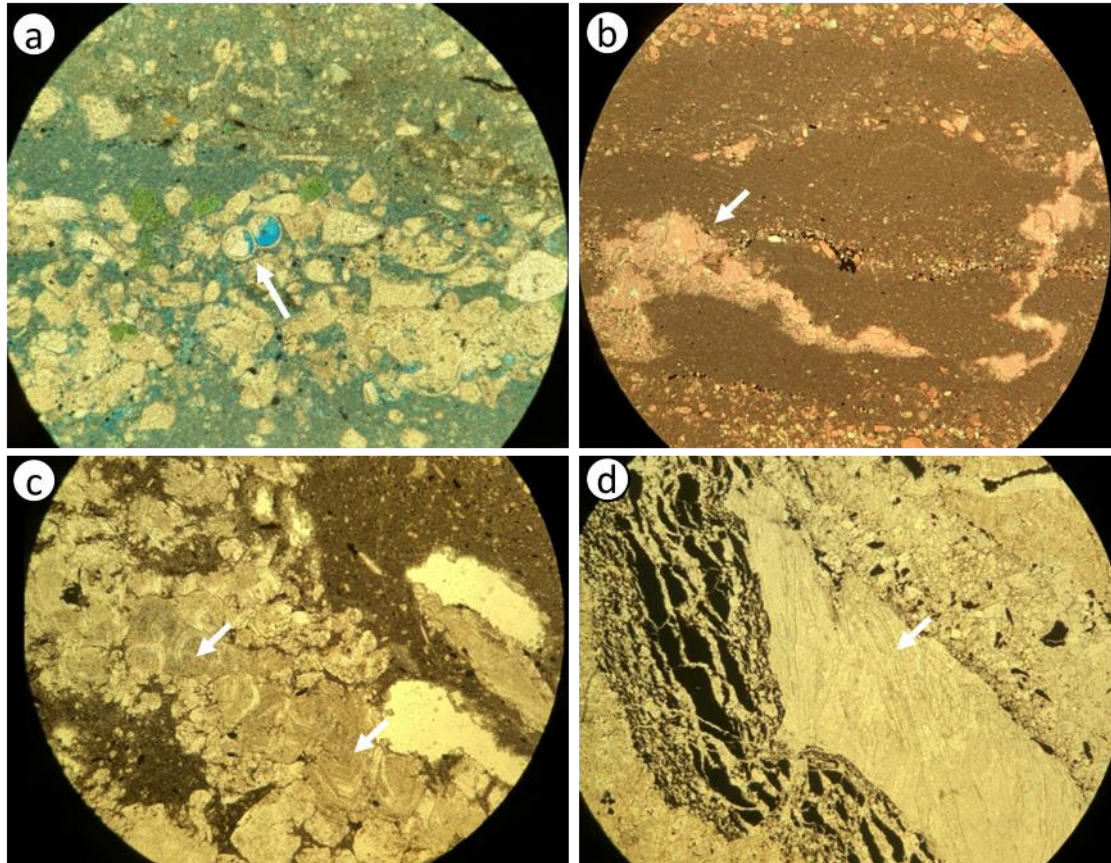
Figure 6-38: a) Karst infill with inoceramids and globigerinids. KTG-01, 967.0 m; fov 4 mm. b) Karst infill by layered carbonate mudstone with fenestrae. KTG-01, 967.0 m; fov 4 mm. c) Infill of karst cavity by partly neomorphosed carbonate mudstone. KTG-01, 992.75 m; fov 4 mm. d) Neomorphic calcite replacing clay-rich infill of karst cavity. KTG-01, 985.0 m; fov 4 mm.

There is therefore evidence of deep vadose penetration of the Dinantian carbonates during sub-Cretaceous exposure; the deepest karst features observed in core occur 77 m below the sub-Cretaceous unconformity in KTG-01 and 161 m below the sub-Cretaceous unconformity in S05-01. In addition, there are several zones in the cored interval of KTG-01 that show enlargement of fractures and cavities by dissolution; these may represent different positions of the water table within the karst that may reflect a geomorphological evolution of the palaeosurface.

6.5.5 Sub-Cretaceous exposure in the southern Netherlands

The uppermost 170 m of the Dinantian in HEU-01 consists of a highly microporous, siliceous, powdery mudstone at least 170 m thick, the uppermost 50 m of which is white where it has undergone severe bleaching; the base of the white zone is marked by two reddish horizons a few centimeter thick. The rest of the interval is very dark grey to black with occasional white patches in the upper most 50 m of the dark zone. It is an organic-rich mudstone with up to 5% TOC that consists of types 1 and 2 organic matter of possible algal and lacustrine origin. The clay mineral assemblage is dominated by kaolinite and illite. In core, the mudstone is

completely uniform with no sedimentary structures or bedding. Microfacies include organic-rich, argillaceous and slightly calcareous mudstone with peloids and sponge spicules (Figure 6-39).

Figure 6-39: a) Dark grey powdery mudstone, HEU-01, 225 m. b) Fractures in basinal Dinantian carbonate mudstone infilled by the dark grey powdery mud, HEU-01, 343 m.

The lower part of the Dinantian in HEU-01 and most of the cored sections of HEU-01-S1 consists of argillaceous carbonate mudstone and thin, graded beds of bioclastic packstone with very finely comminuted bioclasts; with some intervals that are also slumped. Microfacies includes very fine grained bioclastic peloid packstone with common beresellid algae (Figure 6-40). These facies are interpreted as distal resedimented carbonate turbidites and hemi-pelagic organic-rich mudstones deposited in a basinal or slope setting.
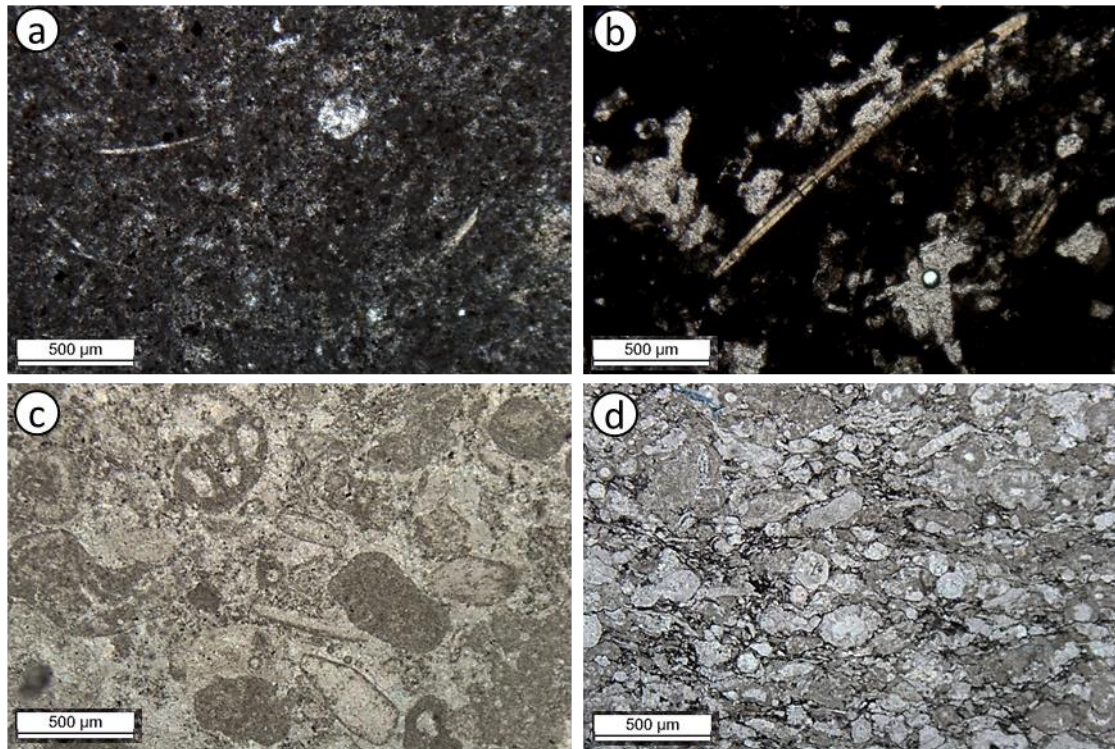
Figure 6-40: a) Argillaceous peloid packstone, HEU-01, 177 m. b) Mudstone with sponges, 270 m. c) Peloid-bioclastic grainstone, 315.90 m. d) Bioclastic packstone, HEU-01, 344.50 m.

In HEU-01-S1, the very dark grey to black powdery mudstone occurs as infills in fractures. It also occurs as intervals interbedded with the basinal facies; some of these intervals contain layers of clast/matrix-supported breccio-conglomerate with pebble-sized clasts of the surrounding argillaceous carbonates. The very dark grey to black powdery mudstone is interpreted as a deep penetrative weathering product of Dinantian argillaceous basinal carbonates and mudstone (Figure 6-41; Bless, 1976, 1982). It was probably associated with the sub-Cretaceous unconformity. The interbedded mudstone with breccia layers and infill of fractures observed in HEU-01-S1 have been interpreted as infills of fractures and cavities in the host limestone that formed beneath the weathering blanket as shown by Figures 6-42 and 6-43. The lacustrine and algal organic matter may have originated from lakes on the palaeosurface (Figure 6-42). The very dark grey powdery mudstone is also recorded from wells GVK-01 and Thermae-2000 suggesting that the Dinantian also underwent deep weathering in these areas (Figure 6-43). Namurian mudstone is present in GVK-01 and the presence of the weathered mudstone in the Dinantian succession suggests that the weathering was sufficiently intense to penetrate beneath the Namurian cover.
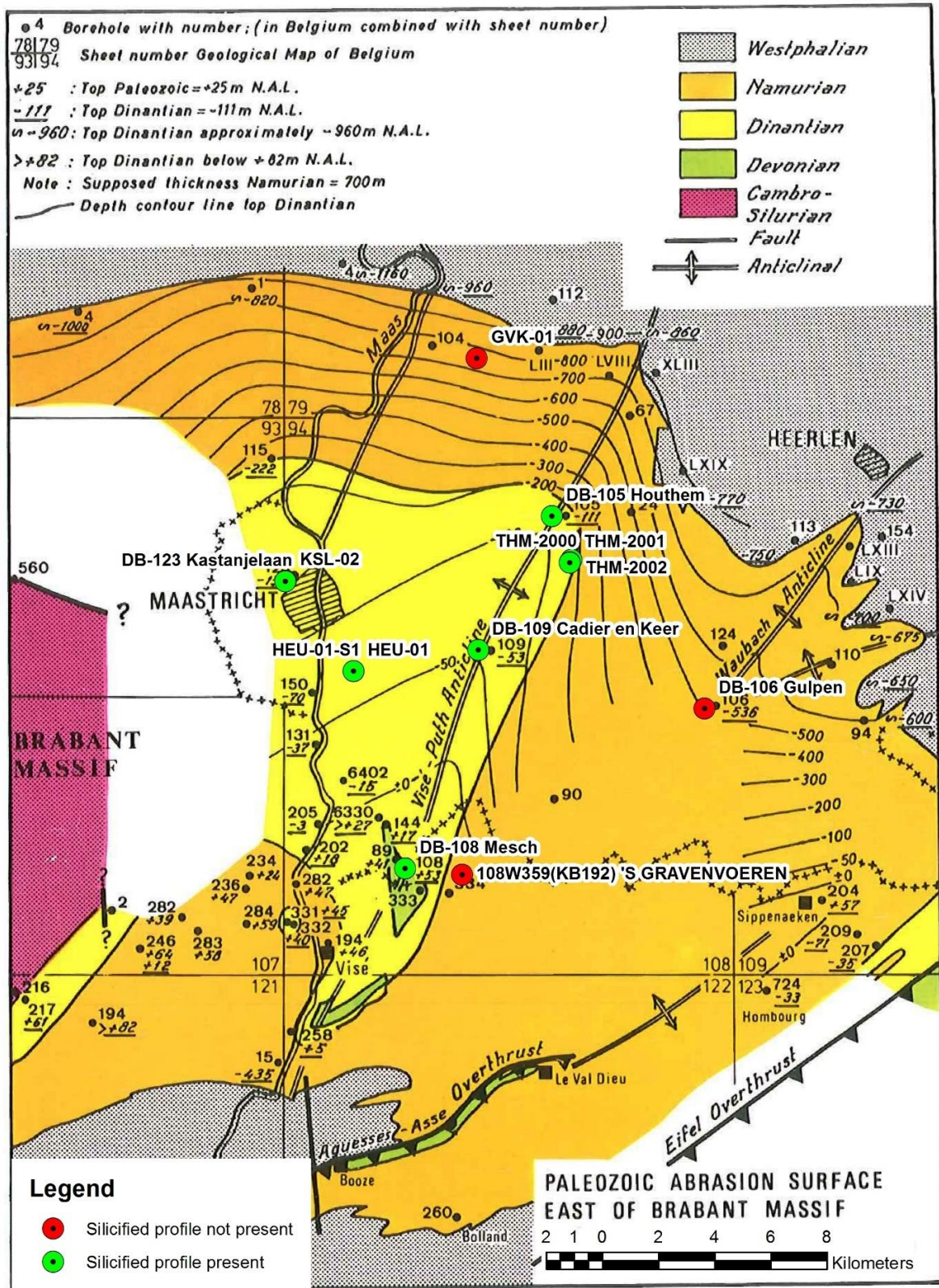
Figure 6-41: Cretaceous subcrop map in the Limburg province from Bless *et al*. (1976), with the indication of the wells with a silicified/kaolinitic weathering profile.
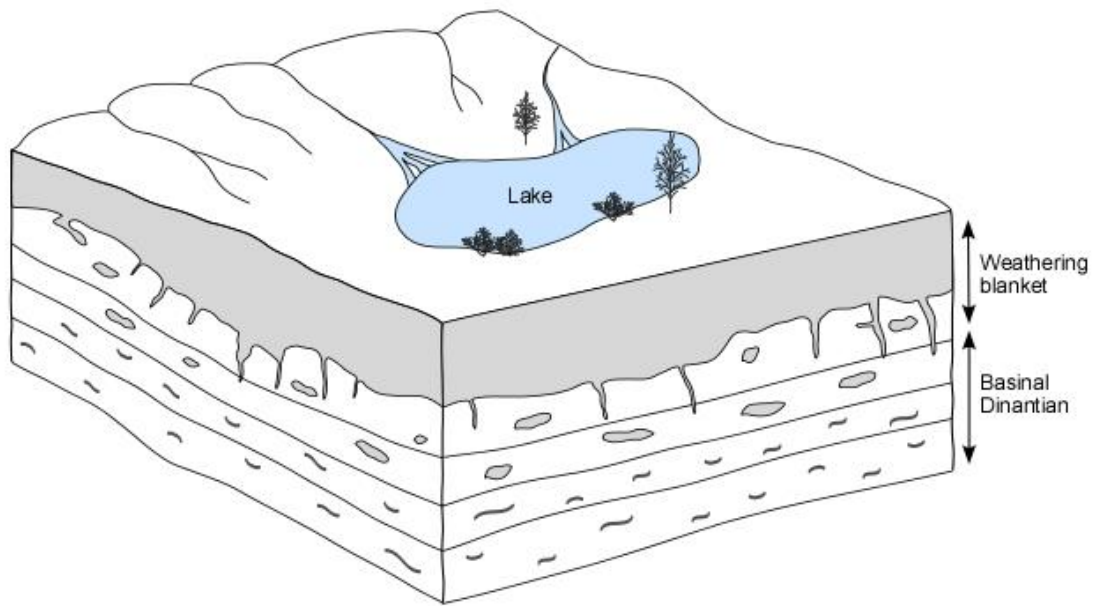
Figure 6-42: Model of superficial weathering profile of dark powdery mudstone in Heugem wells. The grey colour shows the extent of meteoric weathering and development of a weathering blanket (not scaled).
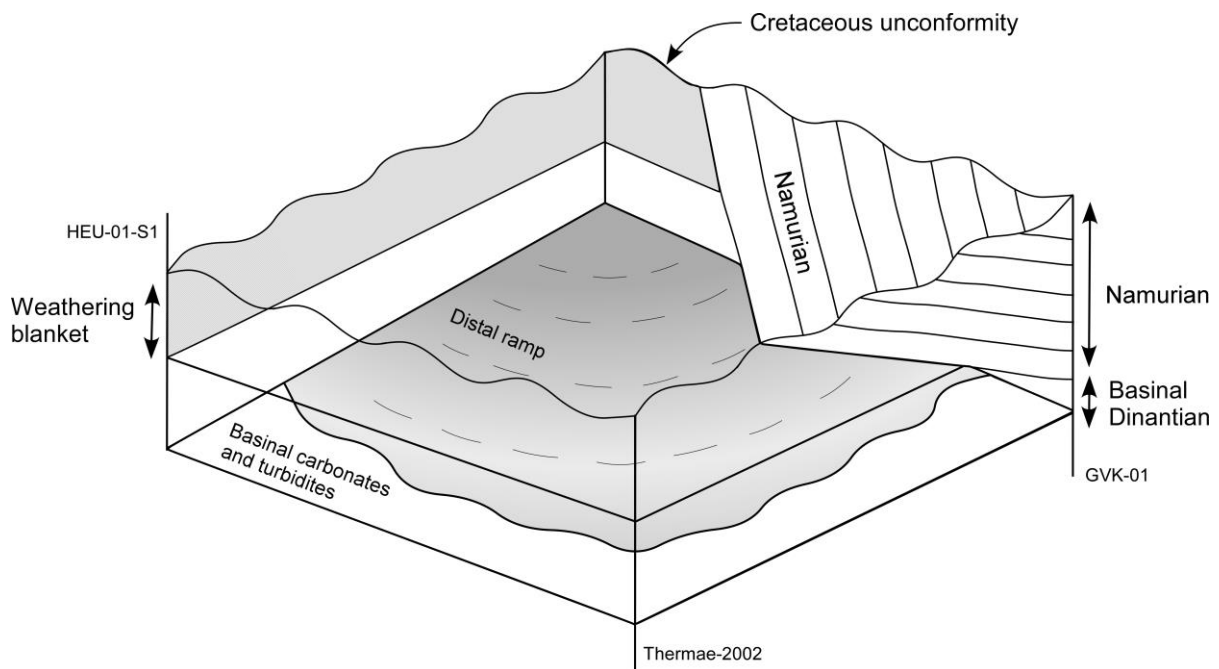
Figure 6-43: Stratigraphic and lateral distribution of sub-Cretaceous weathering profile in the SE Netherlands.

6.5.6 Karst in the Californië wells

High permeability zones in the Dinantian in well CAL-GT-01 have been attributed to a combination of a high density of open fractures in the Bosscheveld Formation associated with the Tegelen Fault zone, and karstification and/or hydrothermal dissolution within the Zeeland Formation. There is no core or petrographic information to constrain the age of this dissolution

episode. Since the karst interval occurs near the top of the Zeeland Formation where it is overlain by a thick Limburg Group, assuming a karstification of meteoric origin, the most likely age is pre-Limburg Group. However, if the karstification is of hydrothermal origin associated with dolomitisation or (de)dolomitisation, as suggested by Poty (2014), it is post-Limburg Group because the Namurian siliciclastics are also partially dolomitised. Other possible phases of karstification are likely over the eastern flanks of the structure where there is increasing erosion leading to complete laying of the Limburg Group beneath the sub-Rotliegendes and sub-Cretaceous unconformity (Figure 6-44).
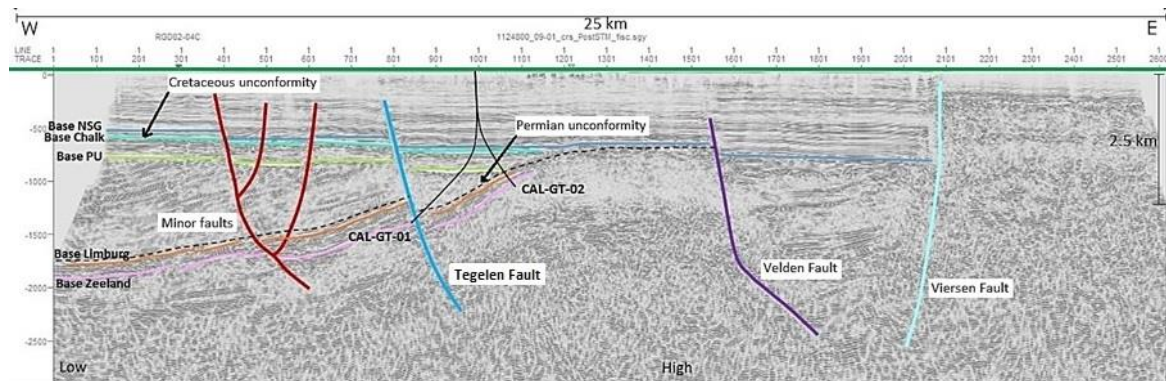
Figure 6-44: Seismic setting of Californië wells (Reith, 2018).

6.6 Diagenesis

The study area has been subdivided into four geographical areas to better understand the diagenesis and its impact on reservoir quality. These areas are based on the distribution of the studied wells. Note that detailed diagenetic evaluations are presented in the well descriptions in Appendix A of this report, and thus this section serves as a summary.

6.6.1 Northern Netherlands (UHM-02 and LTG-01)

The data supporting the diagenetic studies of the northern platforms have been contributed from the pre-existing reports (Gutteridge *et al.,* 2002b; Goldberg *et al*., 2017). Additional analyses have not been undertaken in the northern Netherland wells, except for vitrinite reflectance and XRD analysis of claystones in the core of UHM-02. Fluid inclusion evaluations were undertaken previously by Gutteridge *et al.* (2002b), and have been incorporated into the analyses. Clumped isotope data were also provided by Goldberg *et al*. (2017) for LTG-01, but due to uncertainties regarding the quality of the measured samples (e.g. recrystallisation and/or physical mixing) these data have been used with caution. Stable isotope data (O and C) were undertaken by Gutteridge *et al.* (2002b), and have been combined with isotope data acquired for this project for other wells. Both LTG-01 and UHM-02 have similar diagenetic histories.

Early diagenesis (eogenesis and early burial)

Early diagenetic events include a phase of marine cementation (calcite cements, termed C1), and what appears to be relatively minor phases of meteoric dissolution and subsequent cementation by meteoric calcite cements (C2 cement). Evidence for karstification of the UHM-02 and LTG-01 platforms is very limited, with only minor (cemented) vugs present. Although minor, some fractures may be dissolution-enhanced in UHM-02, and possibly have a karstic origin. A phase of early equant calcite cement occludes primary porosity.

Stable isotope analysis of the bulk limestone (i.e. calcite matrix samples) yielded $\delta^{18}O$ values which are depleted compared to the Dinantian marine reference values, while the $\delta^{13}C$ values fall within the marine reference range (Figure 6-45). The low $\delta^{18}O$ values for UHM-02 are most

likely the result of temperature fractionation and this is supported by very high vitrinite reflectance values (4.683±0.312%) and limited evidence of karst in the studied core.

Figure 6-45: Stable isotope signatures of the Dinantian carbonates (limestone matrix) sampled in BHG-01, KSL-02, KTG-01, O18-01, S05-01 and UHM-02.

Burial diagenesis

The formation of stylolites and at least two generations of cemented fractures are the key aspects of burial diagenesis in UHM-02 and LTG-01. Stylolites are pervasive particularly in UHM-02, and calcite-cemented fracture sets are seen to pre- and post-date these stylolites.

Pre-stylolite fractures commonly have an anastomosing and complex shape. Whilst it is possible that these have a karst origin (for example in UHM-02), the cementation phase is certainly high temperature (fluid inclusion analysis yields average temperatures of 190-200 °C) from hypersaline pore fluids (24-25 wt. % eq. NaCl). These are cogenetic with nearly pure CO_2 and CO_2-H_2O (+salts) inclusions.

Fractures that post-date stylolites are typically sub-vertical and cemented by calcite cements, and in LTG-01 these fractures were reactivated, and two late saddle dolomite cements occur within the veins (SD1, which is ferroan in nature and SD2 which is non-ferroan). In LTG-01, these veins locally have a sub-horizontal aspect to them. Fluid inclusion analyses from UHM-02 (Gutteridge *et al*., 2002b) indicate the calcite cements have homogenisation temperature in the range 166-269 °C (mode 180 °C), with salinities ranging from 25-28 wt. % eq. NaCl (however, hydrates are present that introduce errors into the salinity measurement).

Data are not available for the conditions of precipitation for the late saddle dolomites seen in fractures in LTG-01. The nature of the crystals (saddle morphology) indicate they precipitated from hot pore fluids (>60 °C). Dolomitisation occur in both UHM-02 and LTG-01, but not in the cored intervals. Cuttings and log-based petrophysical analysis suggest dolomites are more prevalent towards the base of the Visean intervals. The dolomites are generally meso to coarse crystalline. Coarse dolomite crystals and saddle dolomite crystals are also present in cuttings in both wells, and are likely to represent fracture or vug cements. The dolomites have a dull luminescent core surrounded by non-luminescent dolomite. Locally, a finer-crystalline replacement dolomite occurs which has a bright CL character (Gutteridge *et al*., 2002b).

102

It is not possible to establish the cross-cutting relationships of the dolomites as they are only present in cuttings. The coarse nature, and presence of saddle dolomite cements suggests that they are highly unlikely to be early diagenetic in origin. The association with fractures in cuttings may indicate that these are fracture fed dolomites, and it is feasible that the replacement dolomites are a similar phase to those dolomite cements seen in fractures in the core of LTG-01. Further geochemical (e.g. stable C and O isotopes) and fluid inclusion analysis (e.g. microthermometry and crush leach) would help place the timing of the dolomitisation.

Diagenesis in the context of burial/thermal history

Petrographic observations, and similar microthermometry and geochemical characteristics (Figure 6-45) suggest that both LTG-01 and UHM-02 have similar burial/thermal histories that can be explained by short-lived heat flow events relating to uplift and erosion occurred in the Early Permian and Late Jurassic. Fluid inclusion data for the pre- and post-stylolite fractures in UHM-02 suggest precipitation from pore waters of 190-200 °C and 180 °C, respectively. From the temperature history plot for UHM-02, it is feasible that the cements are associated with Late Carboniferous burial, or most likely associated with the early phase of uplift (heat flow peak) and structuration in the Late Carboniferous to Early Permian (Figure 6-46). Considering the hyper-saline fluids indicated in fluid inclusion microthermometry, it is (also) possible that they relate to a Late Jurassic higher heat flow, again related to an uplift or structuration event. The salinity of the pore fluids is generally high, indicating cements precipitated from basinal brines. If the dolomites at the base of both UHM-02 and LTG-01 are genetically related to the saddle dolomites in the fractures in the core of LTG-01, it is probable that dolomitisation post-dated the calcite cementation phases within the veins indicating the syn-tectonic nature of these dolomites. More work is required to quantify/confirm this hypothesis.
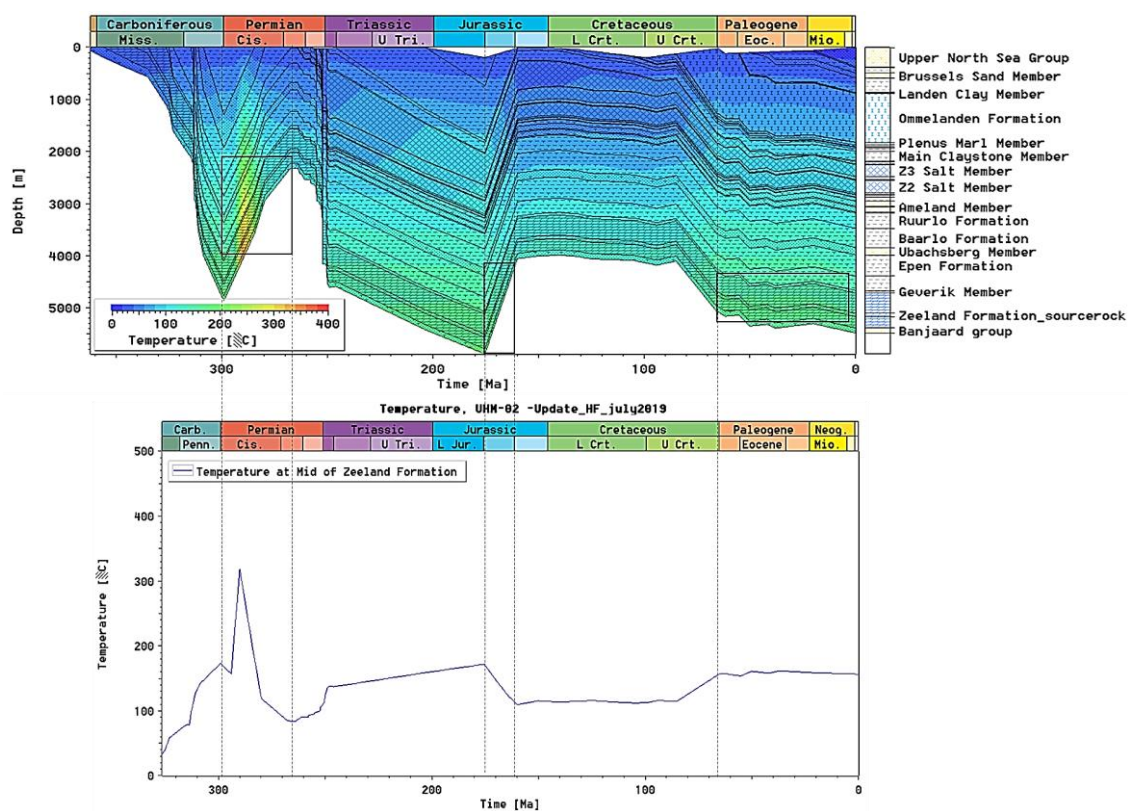
Figure 6-46: Burial curve and modeled temperature history (modified from Bouroullec *et al*., 2019) showing the possible timing of the burial diagenetic phases in UHM-02 (166 to 269 °C).

6.6.2 SW Netherlands (O18-01, S05-01, BHG-01, KTG-01)

Additional diagenetic data were acquired for several wells in the SW Netherlands. Stable C and O isotope data was obtained for all wells except S02-02, and fluid inclusion data were sampled in O18-01, BHG-01 and KTG-01. Sulphur isotope analysis was undertaken in BHG-01. No diagenetic data were available for well S02-02. The southwestern wells have variably experienced a complex diagenetic history which is summarised in Figure 6-47.
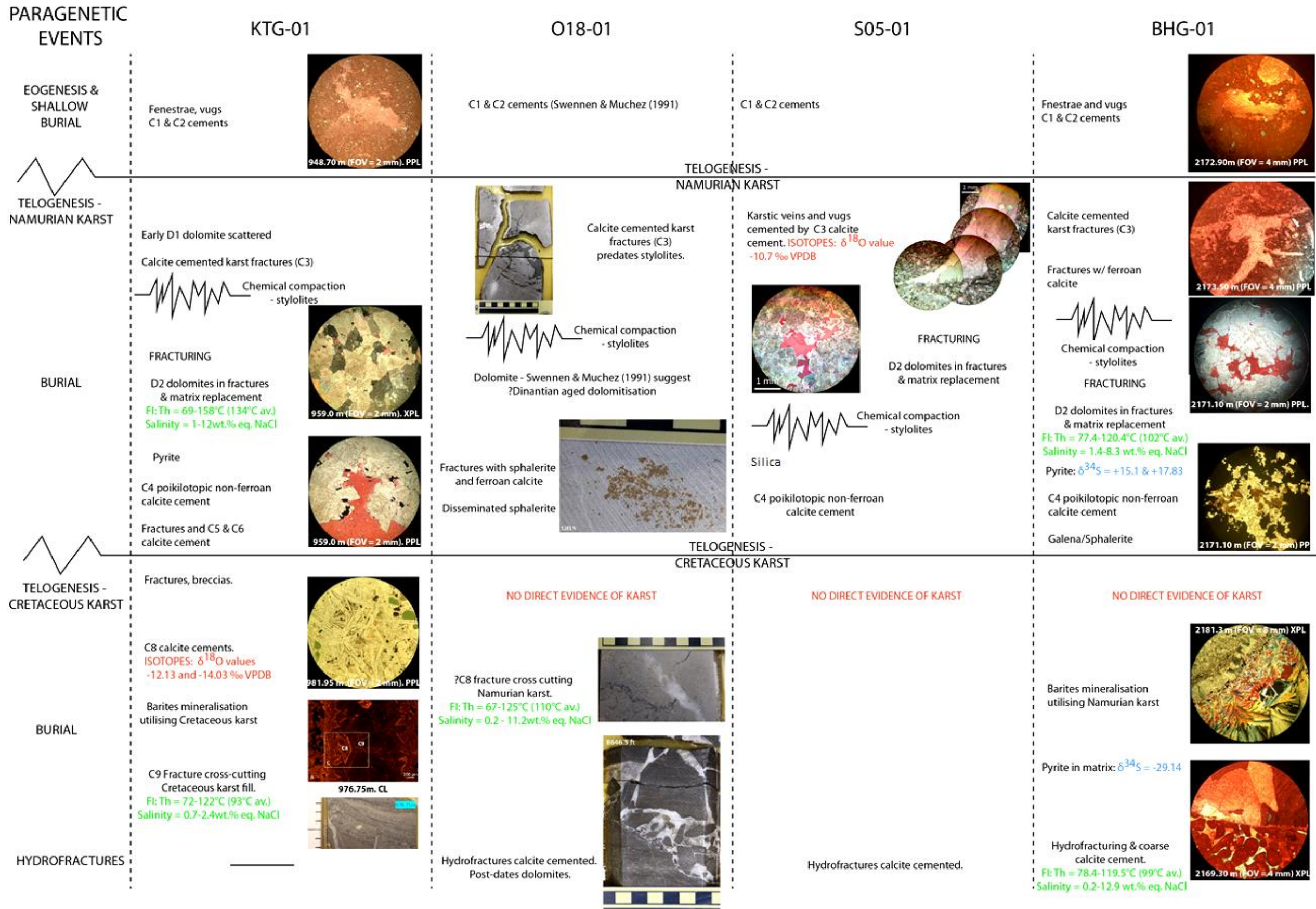
Figure 6-47: Summary of diagenetic events in the SW wells.

Early diagenesis (eogenesis and early burial)

Fine crystalline columnar and fibrous calcite cements fringing components and cementing shelter porosity and early veins in the Dinantian limestones are most likely of marine, meteoric or very shallow burial origin. These early calcite cements (referred to as C1 and C2 in the well description reports; Figure 6-47) were observed in all of the studied wells. In some cases (where new thin section petrography allowed CL to be performed such as in O18-01) fibrous and equant calcite cements with fine non-, bright and dull cathodoluminescence zones can be interpreted as meteoric cements. Pre-burial dolomite precipitation (referred to as D1 in the well description reports) has been observed locally in the KTG-01 well (Figure 6-47).

Stable isotope analysis of the bulk limestone (i.e. calcite matrix samples) yielded $\delta^{18}O$ values which are depleted compared to the Dinantian marine reference values, while the $\delta^{13}C$ values fall within the marine reference range (Figure 6-45). The large range of $\delta^{18}O$ values (i.e.-10.2 to -4.4 ‰ VPDB) of the limestone host rocks indicate that multiple step recrystallisations took place. The associated fractionation of the oxygen isotopes resulted most likely from recrystallisation under high temperatures and/or due to interaction with meteoric fluids. Both processes are supported by the occurrence of high temperature diagenetic phases on one hand and karst processes on the other hand.

Telogenesis – Sub-Limburg (Namurian) karst

As discussed in Section 6.5, an important phase of uplift occurred at the end Visean/Early Namurian, and resulted in the formation of localised karst. This affected most wells in the SW Netherlands. Veins, with irregular margins which appear to be dissolution-enhanced, are cemented by calcite cements (C3) (Figure 6-47). The cements have isotopic signatures which are depleted ($\delta^{18}O$ values of -10.7 and -11.5 ‰ VPDB; from S05-01 well) suggesting they are either sourced from meteoric or hot fluids (or a mixture). Fluid inclusion analyses were not performed on these cements.

Burial diagenesis

Post-dating the telogenesis of the Namurian karst, is a complex suite of burial diagenetic phases, the most important of which is chemical compaction, continued burial cementation, fracturing and dolomitisation (Figure 6-47).

Chemical compaction manifests itself as stylolites, and these are frequently represented in the cores (particularly in S05-01). Dolomitisation is an extremely important diagenetic phase regionally. When looking at the well-logs (see correlation panels in Appendix C), dolomite is particularly dominant in the lower parts of the Dinantian stratigraphy, especially in the Beveland Member. All wells exhibit dolomitisation to varying extent in this interval. Both core and petrographic analyses indicates that the dolomites are commonly fracture related. D2 dolomites occur both as matrix replacive dolomites, and as dolomite cements within fractures and enlarged pore spaces. Cross-cutting relationships of the dolomites most likely indicate that they occurred at, or around the time when stylolites were formed – in some examples, dolomites appear to pre-date stylolites, and in other examples the dolomites appear to post-date stylolite formation.

Stable isotope analyses indicate that the dolomite is characterised by depleted $\delta^{18}O$ values ranging between -14.9 and -3.7 ‰ VPDB with $\delta^{13}C$ values falling within the marine range. In general, the matrix dolomite has less depleted $\delta^{18}O$ values than the dolomite cement. The isotope signature of the matrix dolomites roughly overlaps with the isotope signature of the limestone host rocks (Figure 6-48). Therefore, the isotope signature of the matrix dolomite can be interpreted as rock buffered, whereas the isotope signature of dolomite cement is more representative of the diagenetic phase.

Two dolomite samples were selected for fluid inclusion microthermometry, i.e. KTG-01 591.10 m and BHG-01 2178.37 m. The analysis of these two dolomite samples showed a good overlap in precipitation temperature and salinity range for dolomite of the southwestern (KTG-01 591.10 m and BHG-01 2178.37 m) and also southern (KSL-02 366.55 m) Netherlands (Figure 6-49). A clear salinity trend shows that the parent fluids of the dolomites consisted of a warm basinal brine (3.5 X sea water salinity) and a low salinity (fresh water) end member. The fairly narrow temperature range indicated that the fluids had similar temperatures at the time of dolomite precipitation (100-140 °C). Hence, a meteoric freshwater end member must have circulated to significant depths in the basin to warm up and reach similar temperatures as the basinal brines. The dolomite sample from KTG-01 contains two sets of cross-cutting dolomite cemented fractures, the youngest of which contains oil inclusions with yellow-green to blue-green fluorescence corresponding to 40-45 API. The occurrence of the hydrocarbons indicates dolomitising fluids were circulating along faults and fractures when source rocks reached the oil window.
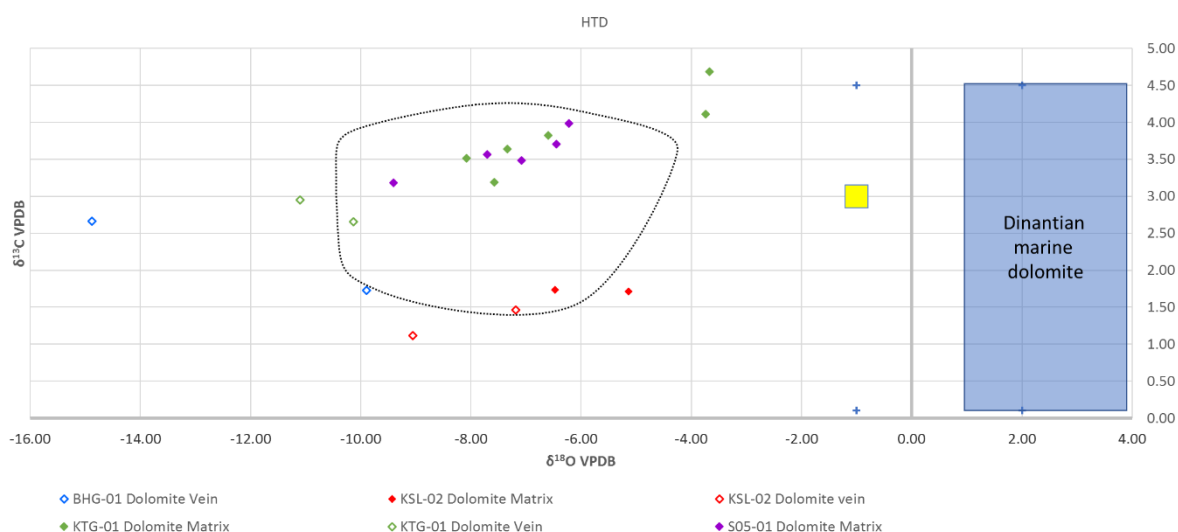
Figure 6-48: Stable isotope cross plot of the dolomite samples of the BHG-01, KSL-02, KTG-01 and S05-01 cores. An average of 2.5 ‰ VPDB is added to the reference values of Dinantian marine calcites; yellow area after Muchez *et al.* (1991) and blue area after Nielsen *et al.* (1994) to estimate the reference values of Dinantian marine dolomites.
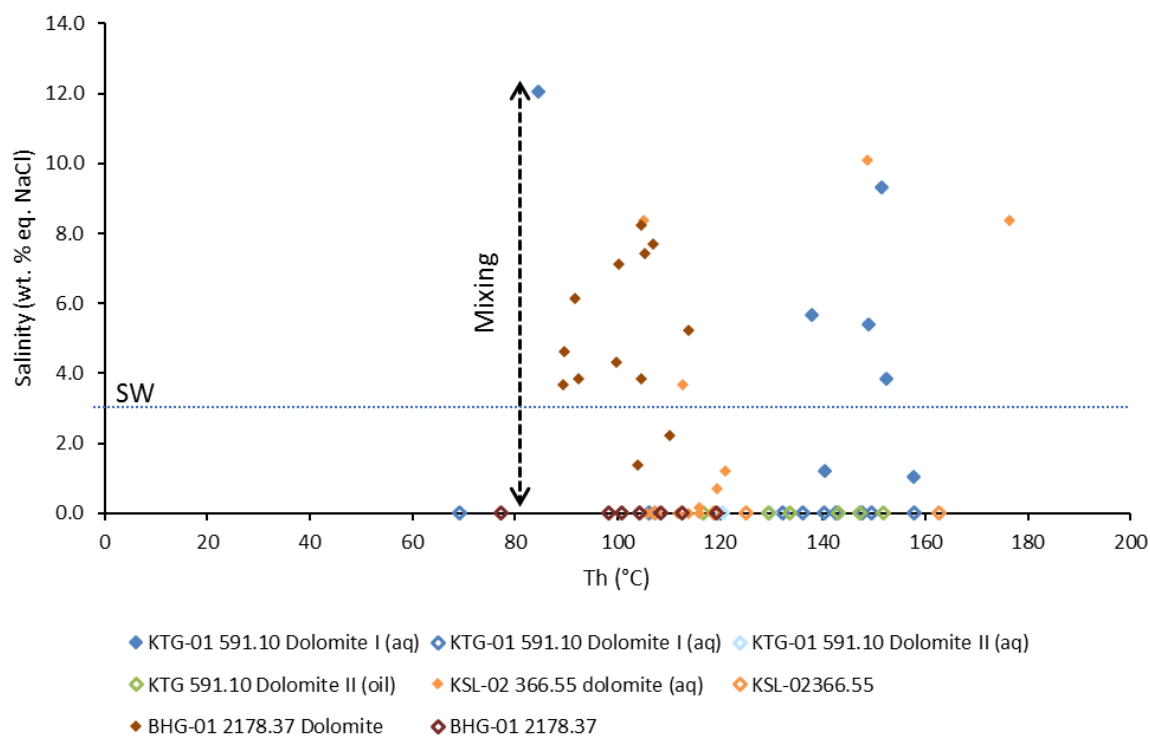
Figure 6-49: Fluid inclusion microthermometry results of the selected dolomite samples. One outlier of KSL-02 366.55 m (Th 128.9 °C and Salinity 27.7 wt. % eq. NaCl) is not displayed. Inclusions for which Tm ice could not be observed an arbitrary salinity of 0 wt. % eq. NaCl has been considered (marked by hallow symbols). These data points should only be considered as temperature indicators. The dotted line indicates sea water salinity.

A phase of mineralisation is often seen in association with or post-dating the dolomitisation. In a number of examples, pyrite is noted to post-date dolomite fractures, and in extreme examples (such as BHG-01) significant pyrite is present in the dolomites. Coarse, non-ferroan, calcite cement (C4) commonly cements remaining pore space in fractures, vugs or intercrystalline porosity (Figure 6-47); however, this is not pervasive, and some pores do remain open. Galena and sphalerite are also a late phase of mineralisation associated with the dolomitisation events. Sphalerite occurs in dolomite- and calcite cemented fractures in BHG-01, and also as disseminated phases and in fractures in O18-01.

In KTG-01 and O18-01 a number of additional generations of calcite fracture cements are recognised (C5, C6) (Figure 6-47). These may be comparable to the fractures documented by Swennen and Muchez (1991) where ferroan calcite was documented. No geochemical or CL analyses of these cements have been made.

Telogenesis – Cretaceous karst

A further phase of uplift and karstification occurred in the southwest area, affecting in particular the KTG-01 well. This is documented in detail in Section 6.5. The uplift is variably reflected in the wells, but undoubtedly initiated circulation of meteoric fluids through the successions.

Calcite cementation and associated barites is present in both the Cretaceous karst in KTG-01 and the Namurian karst in BHG-01. It is unclear at this stage what the source of the barite's mineralisation is, but it is possible that it took advantage of fluid pathways associated with the karst (Figure 6-50).

108
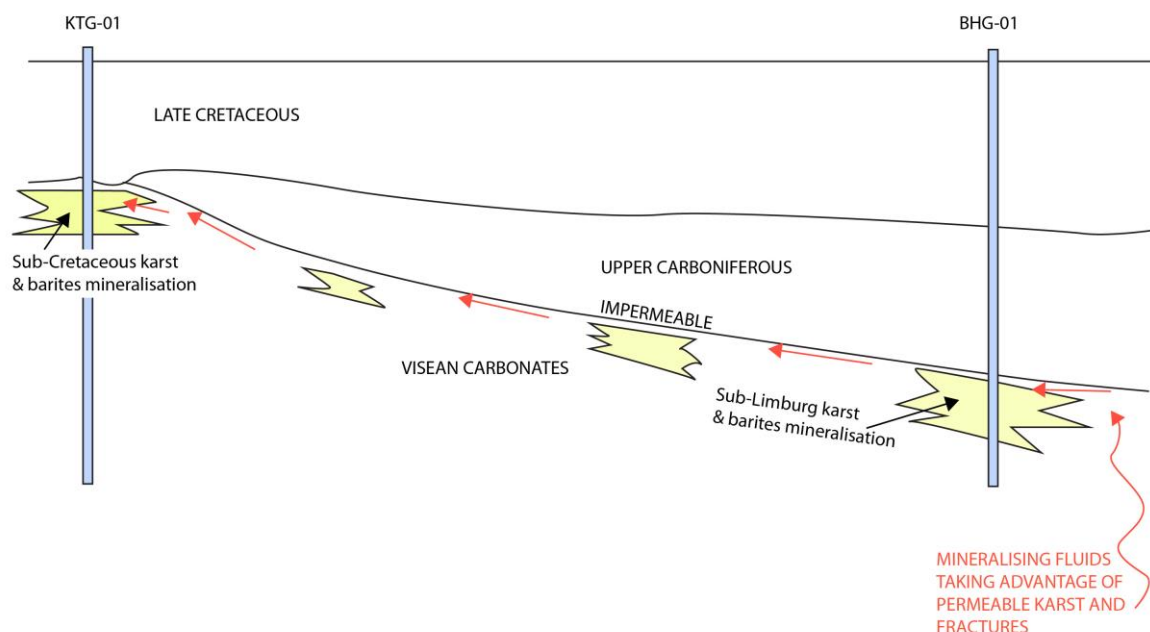
Figure 6-50: Schematic diagram for barites precipitation.

Fractures are also noted to cross-cut karst. In the O18-01 core a sample was collected of a calcite vein (?C8) post-dating the Namurian karst infill (Figure 6-47). No other indications regarding the timing of this diagenetic phase are available. The cathodoluminescence pattern of this calcite consists of a non-luminescent core and finely zoned dull to bright rim. The succession of non- to bright and dull luminescence may reflect a change in redox conditions, i.e. from oxic to sub-oxic and reducing. The stable isotope signature of this sample is: $\delta^{18}O$ values of -11.4 ‰ VPDB and $\delta^{13}C$ values of 3.1 ‰ VPDB. Fluid inclusion microthermometry revealed precipitation temperatures of 92.7 °C to 125.0 °C (average 110 °C and one outlier of 67.0 °C). The salinity of the parent fluid shows a clear mixing trend of a high (11.2 wt. % eq. NaCl) and low (0 wt. % eq. NaCl) salinity endmember. Both fluids had similar temperatures as indicated by the fairly narrow Th range (92.7 °C to 125.0 °C).

The calcite vein cross-cutting the mineralised Cretaceous karst infill in KTG-01 (C9 calcite) was also studied, and is characterised by non- and bright luminescence which may reflect pore waters becoming progressively anaerobic and reducing. The C9 calcite is known to have precipitated from a fluid with a salinity lower than sea water and temperatures ranging from 72.9 to 122.4 °C. The very small salinity range is interpreted as the result of the interaction of a meteoric fluid with the country rock or minor mixing with marine pore waters.

Burial-Hydrofracturing

Hydrofracturing is seen in core in O18-01 and BHG-01 (Figure 6-47). Hydrofracturing results in shards of angular host rock, with oblique breccia fabrics; both features occur in the 1d sedimentary sequence. The breccia comprises angular clasts that often show a fitted fabric with adjacent clasts and adjacent fracture walls. Sometimes a geopetal accumulation of angular granule- to pebble-sized clasts between coarser clasts can be found at the base of brecciated zone. These brecciated zones are cemented by late pyrite and calcite, and in O18-01 a later dolomite cement is present. In O18-01, the fractures clearly post-date dolomitisation, whilst in BHG-01, there is evidence that they post-date the dolomites. Petrography analysis shows that in BHG-01 the fractures cut stylolites with dolomite rhombs concentrated along them.

In BHG-01 the calcite phase cementing the breccia is characterised by high precipitation temperatures and variable salinity. The BHG-01 2379.10 m calcite shows alternating ferroan

and non-ferroan growth zones, depleted $\delta^{18}O$ values of -10.6 ‰ VPDB and $\delta^{13}C$ values of 0.2 ‰ VPDB. Fluid inclusion microthermometry yielded precipitation temperatures and parent fluid salinities very similar to the O18-01 5266 ft calcite post-dating the Namurian karst with homogenisation temperatures ranging between 78.4 and 119.5 °C and salinity between 0.2 and 12.9 wt. % eq. NaCl.

Based on the similar temperature and salinity ranges of the O18-01 5266 ft and BHG-01 2379.10 m calcites it can be speculated that these calcites precipitated from fluids with similar sources at similar times.

Diagenesis in the context of burial/thermal history

The D2 dolomites show a good overlap in precipitation temperature and salinity range for dolomite of the southwestern (KTG-01 591.10 m and BHG-01 2178.37 m) and southern (KSL-02 366.55 m) Netherlands (Figure 6-50). A clear salinity trend shows that the parent fluids of the dolomites consisted of a warm basinal brine (3.5 X sea water salinity) and a low salinity (fresh water) end member. The fairly narrow temperature range indicated the fluids had similar temperatures at the time of dolomite precipitation. Hence, a meteoric freshwater end member must therefore have circulated to significant depths in the basin to warm up and reach similar temperatures as basinal brines (Figure 6-51). This restricts dolomite precipitation to periods with considerable basin inversion and exposure of lifted blocks such as the Lower Permian (Saalian phase) and Middle-Late Jurassic to Upper Cretaceous. Since the dolomitisation pre-dates a Cretaceous phase of karstification, it is more likely that the Late Jurassic is an optimum period for dolomitisation. If the dolomitisation occurred during the Late Jurassic it can be classified as a hydrothermal event, i.e. the precipitation temperatures of the dolomite are significantly higher than the ambient temperature of its host rock (Figures 6-52 and 6-53). Igneous activity is recorded during the Saalian and Middle-Late Jurassic, which may have triggered hydrothermal fluid flow.

Dolomites in KTG-01 also contain oil. Two possible source rocks can be considered, i.e. Namurian continental deposits and Jurassic shales. The Namurian source rocks may have reached maturity during the Late Carboniferous- Early Permian. Jurassic Posidonia shales start generating hydrocarbons in the adjacent Western Netherlands Basin during the Upper Jurassic. Based on the homogenisation temperatures of around 150 °C none of those source rocks can be excluded. The dolomites were therefore most likely precipitated prior to the Cretaceous karstification.
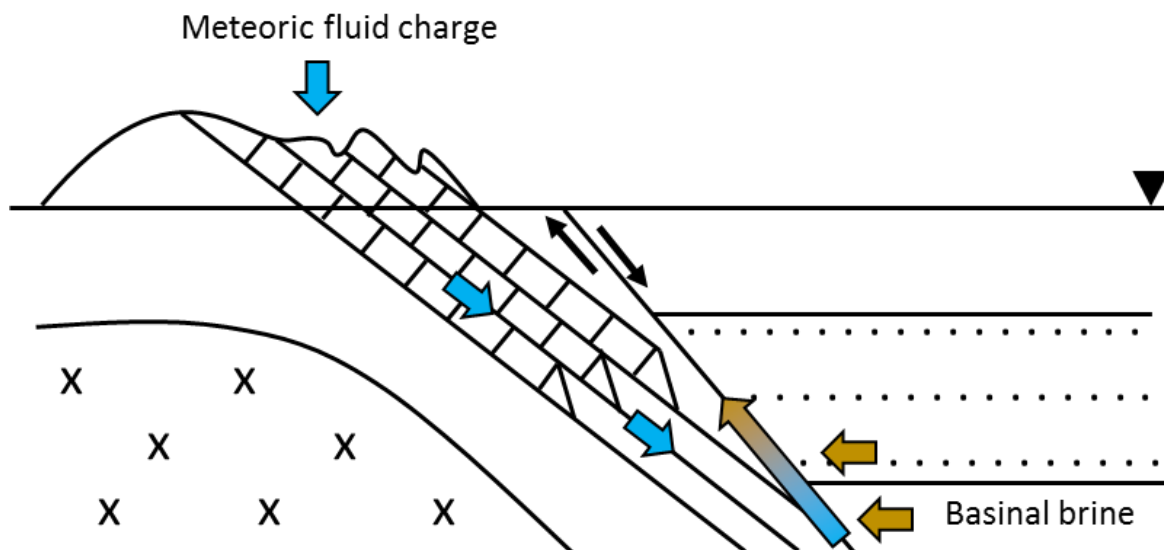
Figure 6-51: Simplified sketch for the origin and setting of the low saline fluids during Variscan orogeny or the Upper Jurassic- Lower Cretaceous rifting.

There are two calcite cement phases that post-date the karst periods. The post-Namurian fracture-fill in O18-01 (calcite C8; Figure 6-47) could have precipitated under increasing reducing (burial) conditions from a meteoric fluid mixed with a basinal brine. A considerable hydraulic head must have allowed the meteoric fluid to flow to great depth into the basin where it could have warmed up to 92.7-125.0 °C. There are two periods during which inversion tectonics could have allowed the percolation of meteoric fluids, i.e. during the Lower Permian Saalian phase (1) and Middle-Late Jurassic to Upper Cretaceous (2). The former event, though cannot be entirely excluded, is less likely since the climatic conditions being arid were not allowing a dominant fresh water system to persist and infiltrate into burial settings. During these two periods the Dinantian carbonates did not reach high burial temperatures and the precipitation of the calcite post-dating the Namurian karst can be interpreted as a hydrothermal event. Igneous activity is recorded during the Saalian and Middle-Late Jurassic. These igneous events may have triggered hydrothermal fluid flow.

The C9 calcite, present in fractures in KTG-01 (Figure 6-47), is interpreted to be younger than the Santonian since it cross-cuts the Santonian sediments filling the Cretaceous karst cavities. The parent fluid of the C9 calcite was considerably warmer than the Beveland Member and can be interpreted as a hydrothermal event. The influx of meteoric waters post-dating the Santonian implies continued exposure of the hinterland.
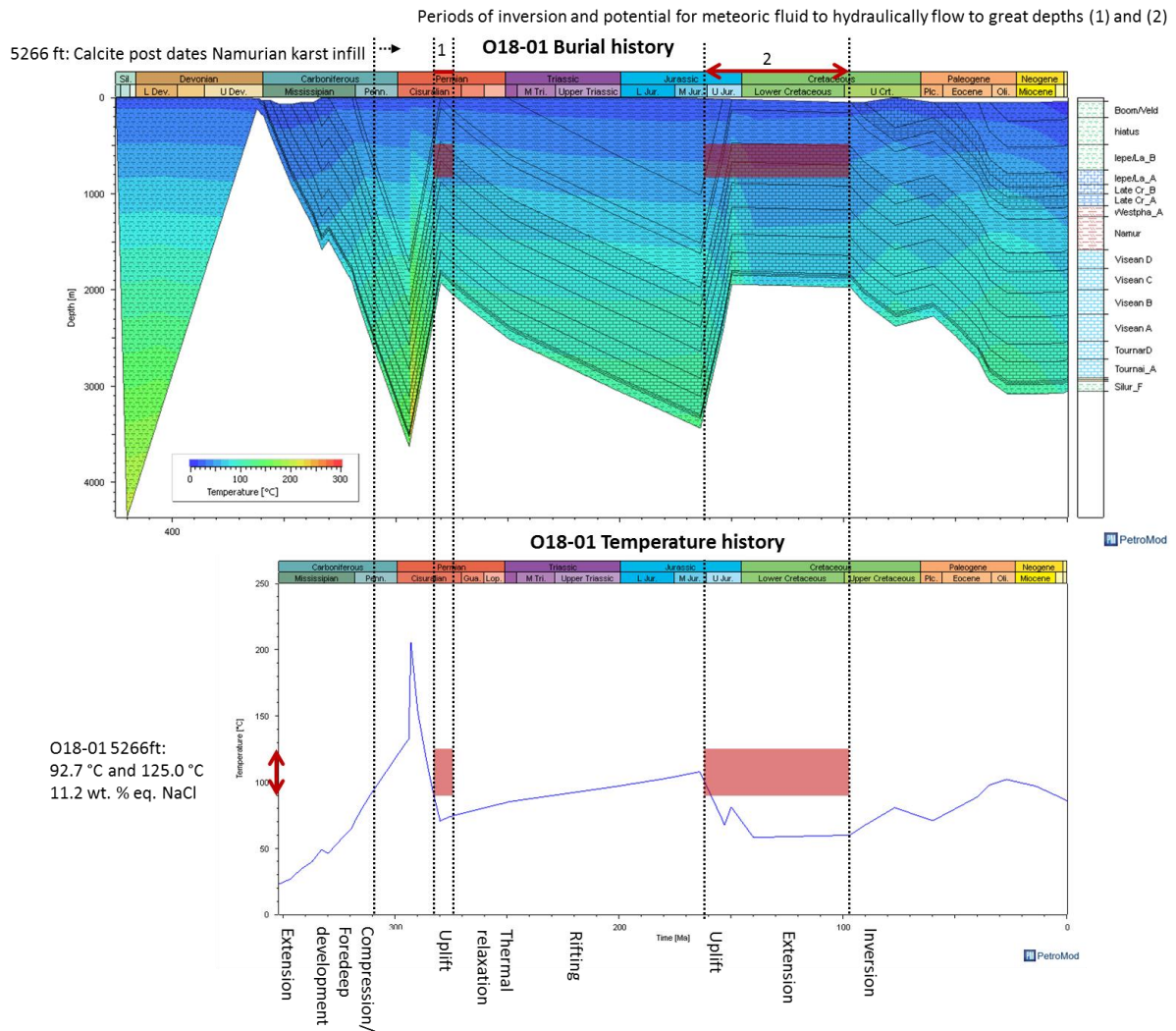
Figure 6-52: Interpretation of the timing and structural setting of the O18-01 (5266 feet) calcite post-dating the Namurian karst.

The hydrofracturing in O18-01 and sampled in BHG-01 is characterised by high precipitation temperatures and variable salinity (Figure 6-49). The hydrofracturing post-dates the D2 dolomitisation. Based on the similar temperature and salinity ranges of the O18-01 5266 ft and BHG-01 2379.10 m calcites it could be speculated that these calcites formed out of fluids with similar sources at similar times. It is possible that the Cretaceous inversion was a period where overpressure and hydrofracturing could have taken place.
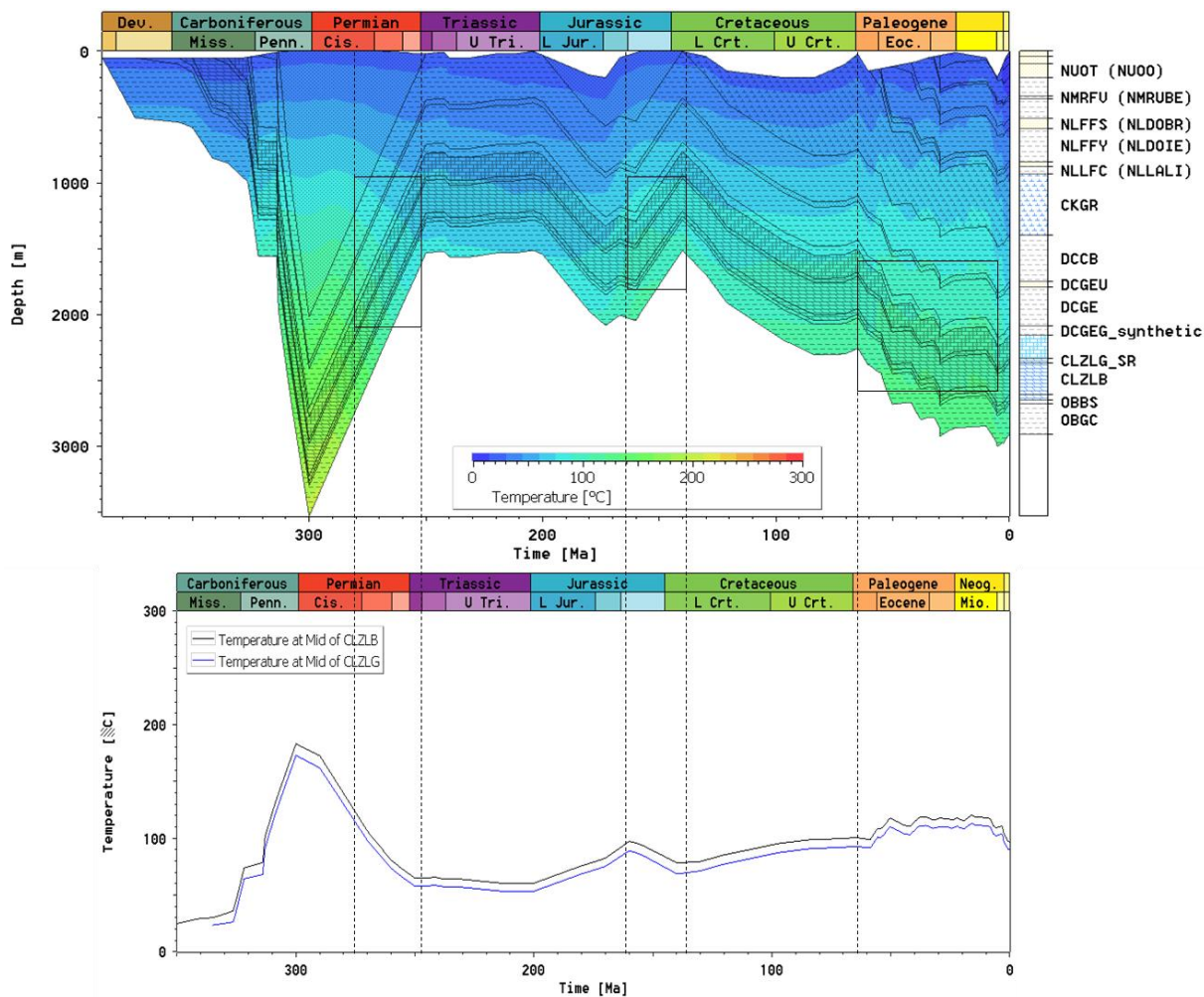
Figure 6-53: Possible timing for the precipitation of the BHG-01 (2379.10 m) calcite cements (78.4 to 119.5 °C).

6.6.3 East and SE Netherlands (WSK-01, KSL-02, GVK-01, HUE-01)

The KSL-02 well was subjected to additional diagenetic studies, C and O stable isotope work and fluid inclusion analysis of fracture cements. The diagenetic evaluations of GVK-01 were not part of this new study. However, a comprehensive report by Mathes-Schmidt (2000) frames the diagenetic phases into the context of this well (Figure 6-54). No diagenetic data are available for WSK-01.

Early diagenesis (eogenesis and early burial)

Fine crystalline columnar and fibrous calcite cements fringing components and cementing shelter porosity and early veins in the Dinantian limestones are most likely of marine, meteoric or very shallow burial origin. These early calcite cements (referred to as C1 and C2 in the well description reports) were observed in HEU-01 and KSL-02 wells (Figure 6-54). For the KSL-02 well Mathes-Schmidt (2000) indicates micritisation, syntaxial calcite cements, neomorphosis and minor silicification (chalcedony seams and silica in radiolaria and spiculites) as early diagenetic phases. Minor dolomite precipitation, referred to as D1 in the well description reports (appendices), has been observed in HEU-01 and possibly in the GVK-01 and WSK-01 wells.

Stable isotope analysis of the calcite matrix samples yielded $\delta^{18}O$ values that are depleted compared to the Dinantian marine reference values, while the $\delta^{13}C$ values fall within the marine

113

reference range (Figure 6-55). The limestone matrix of KLS-02 reveals $\delta^{18}O$ values of -9.6 ‰ VPDB (Figure 6-55). The fractionation of the oxygen isotopes resulted most likely from recrystallisation under high temperatures and/or the interaction with meteoric fluids.

HEU-01	KSL-02	GVK	Diagenetic phase	Early	Post-chemical compaction
+	+	A?	C1		
+	-	MD?	D1		
+	+	B?	C2		
+	+	+	Stylolites		
+	+	-	Si		
+	+	-	C3		
+	+	+	D2		
+	+	-	Recrystallisation		
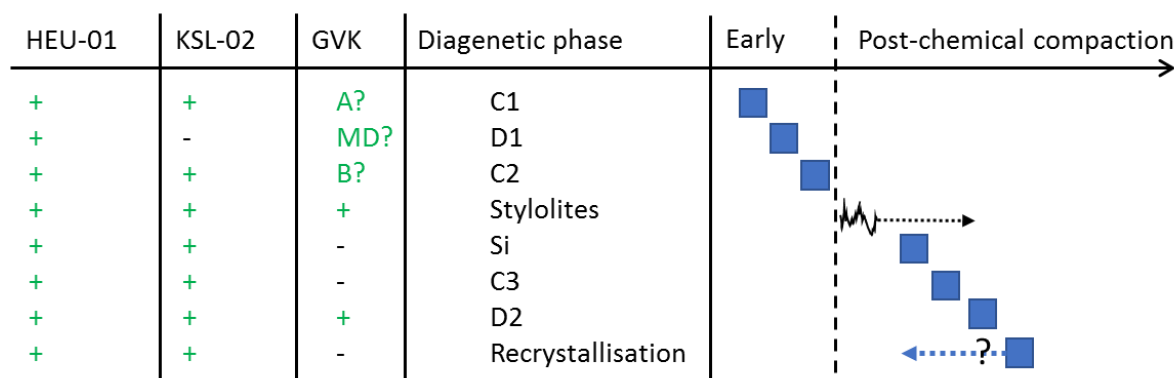
Figure 6-54: Overview of the diagenetic phases and their presence in the HEU-01-S1, KSL-02 and GVK-01. Note that in the GVK-01 column the letters refer to nomenclature used by Mathes-Schmidt (2000).

Burial diagenesis

Chemical compaction is often pervasive in these wells (WSK-01, KSL-02, GVK-01, HUE-01), with formation of stylolites. A phase of dolomitisation only affected the KSL-02 well (very minor amounts in HEU-01 and none in GVK-01), and is considered to occur at or around the time of stylolite formation as there is evidence of stylolites both pre- and post-dating dolomitisation. Similarly, it may indicate that dolomite post-dates the onset of chemical compaction and pre-dates the last phase of sylolites (post-Cretaceous burial). Replacement dolomitisation (D2) occurs in an interval at the base of the Beveland Formation in KSL-02. The replacement dolomite is fine to medium crystalline and consists of sub- to anhedral crystals. In CL the dolomite is generally dull luminescent. Stable isotopes for the dolomite matrix suggest these are less depleted that the limestone matrix. D2 dolomites also occur in fractures in KSL-02. The dolomites typically have saddle morphology. Fluid inclusion microthermometry of the D2 dolomite shows that it precipitated from a high temperature fluid: 105.1-176.3 °C, average 125.1 °C. The salinity of the fluid covers a wide range. Most Tm ice measurements indicate salinities of 0-10.1 wt. % eq. NaCl. One measurement indicates extremely high salinity of 27.7 wt. % eq. NaCl. Mixing of a high and a low salinity fluid may have occurred. The dolomite vein samples are characterised by more depleted $\delta^{18}O$ values than the equivalent matrix.
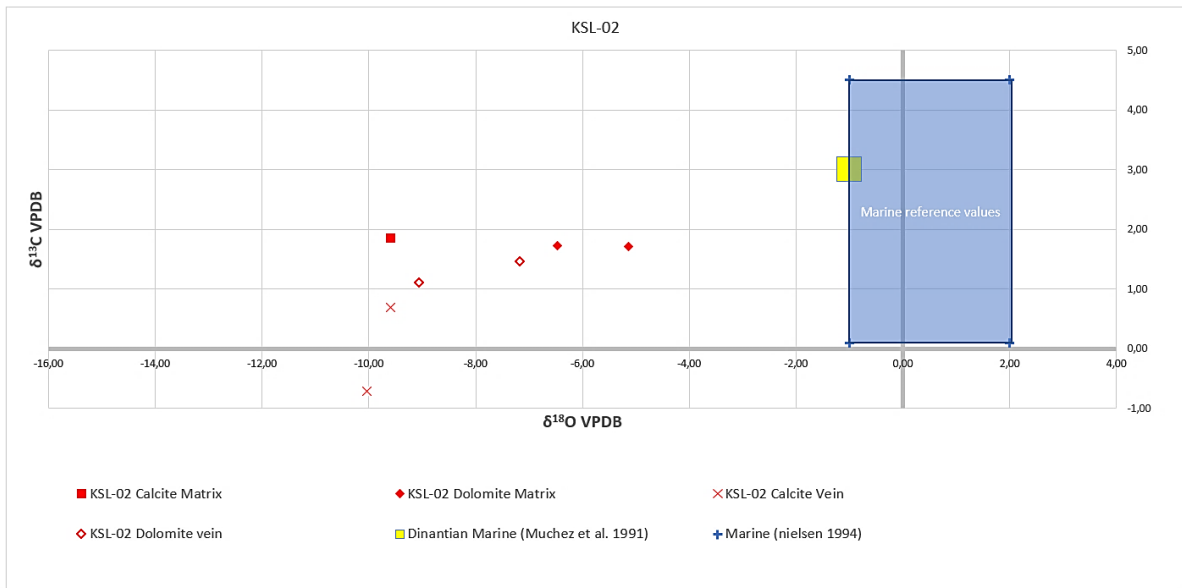
Figure 6-55: Stable isotope cross plot of the KSL-02 samples; yellow area shows the reference values of the Dinantian marine limestones after Muchez *et al*. (1991) and blue area after Nielsen *et al.* (1994).

A set of fractures cemented by equant calcite (C3) post-dates the dolomitisation (Figure 6-54). Calcite cements occurring in veins are characterised by depleted δ^{18}O values and δ^{13}C values. The C3 calcite is coarse crystalline and twinned. It is characterised by fairly wide, dull to non-luminescent bands.

A major diagenetic event, which is pervasive in the SE wells, is silicification of the matrix, as well as veins. This is especially pronounced in the HEU-01 and HEU-01-S1 wells, and appears as a microporous, black, powdery mudstone. Kaolinitisation also occurs, with a complete decolouration of the silicified shales in HEU-01. Silica cement is associated to a phase of fracturing and brecciation. The quartz can be both crystalline and amorphous, and post-dates dolomitisation. This pervasive silicification is not noted in other areas.

Nyhuis (2012) reports fluid inclusion microthermometry data obtained mostly from quartz cemented veins and rare calcite cemented veins in GVK-01 (Figure 6-56). The vast majority of the fluid inclusions are described as secondary in origin. The data do not allow differentiating between measurements from primary and secondary inclusions or the mineralogy of the host mineral, i.e. calcite or quartz. Plotting the data shows that two groups in the most likely secondary inclusions can be observed, i.e. a high and a low salinity group (Figure 6-56). Inclusions of both groups are characterised by fairly high homogenisation temperatures (Figure 6-56) and the occurrence of CO_2 and CH_4 gases.
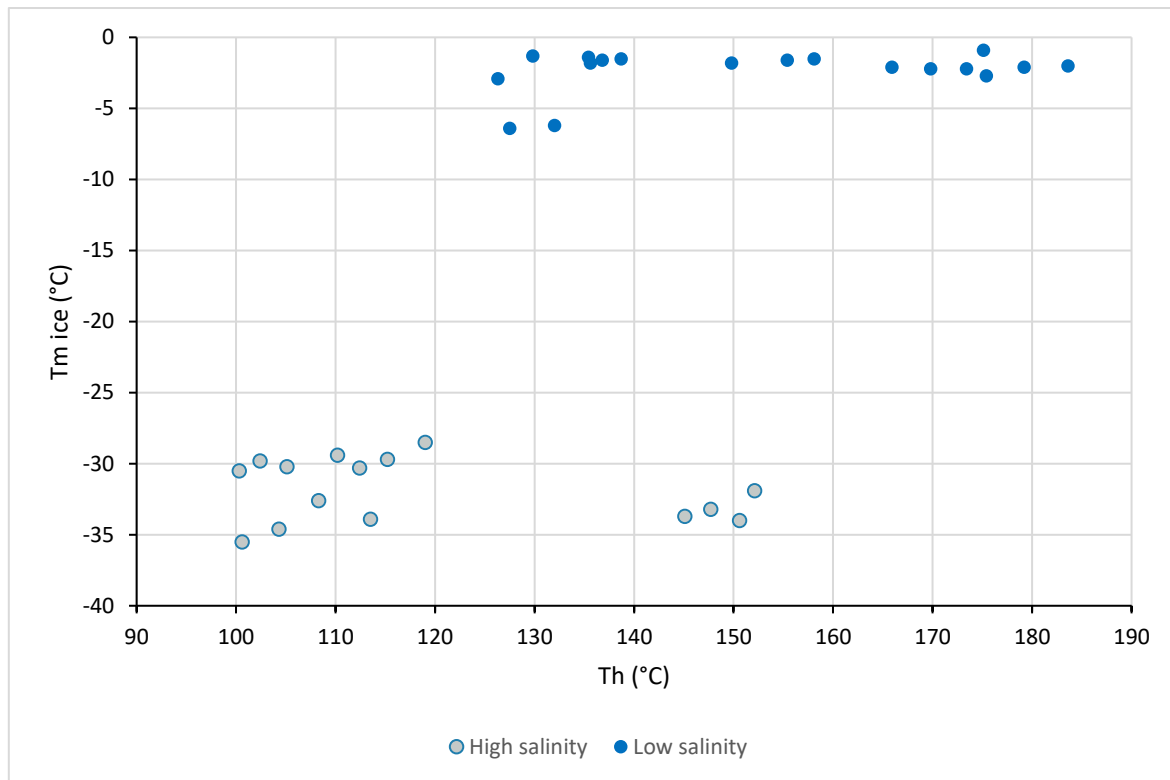
Figure 6-56: Cross plot of the fluid inclusion data reported by Nyhuis (2012). A high and a low salinity group can be observed in the data. Note that the majority of the measurements were most likely obtained from secondary inclusions in quartz.

Both Bless *et al*. (1981) and Friedrich *et al*. (1987) reported high concentrations of zinc within the Visean succession the SE Netherlands, up to 1467 ppm (Figure 6-57). The mineralisation does not seem to be associated with the presence of sulphides. Non sulphides could be associated with the prolongated exposure related to the base Cretaceous unconformity.
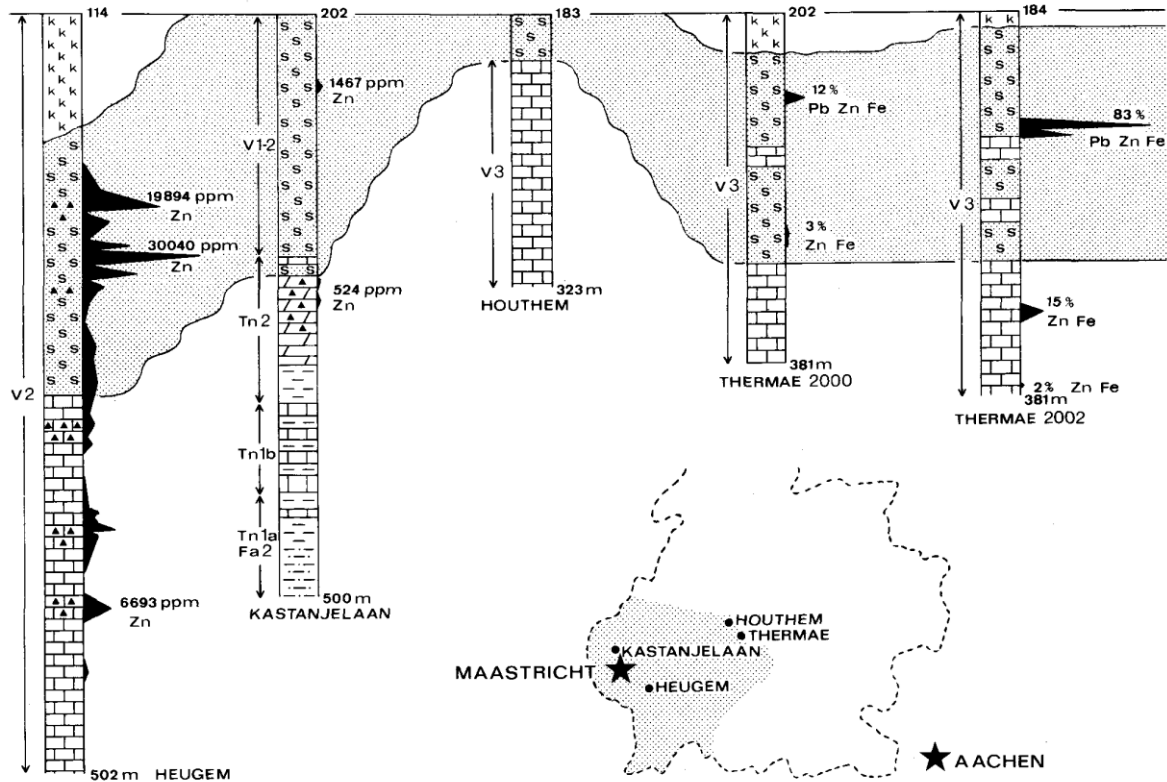
Figure 6-57: Distribution of Zn concentrations in different wells in the Maastricht area from Friedrich *et al*. (1987).

Diagenesis in the context of burial/thermal history

The studied sediments in the SE Netherlands wells have very high Vitrinite reflectance in comparison to other areas (Figure 6-58). The elevated degree of maturity can be explained by relatively deep burial and the probable presence of an intrusive body in the region of Maastricht, documented by an outstanding magnetic anomaly (Ten Veen *et al*., 2019). It is not possible to figure a burial history curve for KSL-02 or HEU-01 due to limitations of the EasyRo% algorithm.
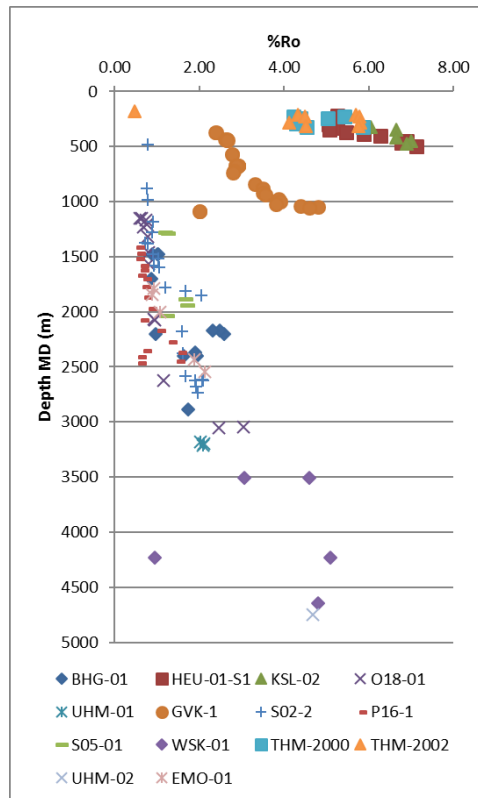
Figure 6-58: Vitrinite reflectance data. Note that the wells in the SE (HEU-01, GVK-01, and KSL-02) have very high %Ro values at a shallow depth.

The temperature history for GVK-01 can be modelled, and it is likely to be representative of KSL-02 and HEU-01, although GVK-01 is a cooler end-member (Figure 6-58). A strong thermal event occurred during Permian. The computed erosion is about 4500 m for the Permian Unconformity and 1250 m for the Cretaceous Unconformity.

The temperature and salinity range of the D2 dolomite observed in KSL-02 overlaps with the temperature and salinity range of the fracture-related, hydrothermal dolomites of the KTG-01 and BHG-01 wells. The parent fluid of the dolomites can be interpreted as the result of the mixing of warm fresh water and basinal brines. As discussed for the KTG-01 and BHG-01 dolomites, a considerable hydraulic head is required for fresh water to percolated to sufficient depth to be warmed up to 105.1-176.3 °C (average 125.1 °C). Therefore, the preferred timing of the dolomitisation in the SW Netherlands was interpreted as Middle-Late Jurassic (Figure 6-59). It is possible that the D2 dolomitisation in the East and SE Netherlands occurred at the same time as in the SW Netherlands. In that case the D2 dolomitisation can be classified as a hydrothermal event.

Two sets of fluid inclusion data can potentially be tied to the temperature curve, D2 dolomites and the silicification documented by Nyhuis (2012). Based on petrographic evaluation, we know that the D2 dolomitisation post-dates the silicification. It is perhaps possible to tie the dolomitisation event to the thermal spike during the Early Permian; however, given that the dolomites are likely fracture-fed, it is also possible that they may relate to a later hydrothermal event that isn't marked by the heat-flow model. These dolomites are likely hydrothermal in origin.

The fluid inclusion data of Nyhuis (2012) show two different temperature-salinity groups, i.e. a high salinity group (Tm: -6.4 to -0.9 °C and Th: 125 to 184 °C) and a low salinity group (Tm: -35.5 to -28.5 °C and Th: 100 to 152 °C). The low salinity group requires a model for fresh

118

water to be circulated at high temperatures possibly provided by the sub-Cretaceous exposure. It is possible that igneous activity played a role in the hydrothermal fluid flow.
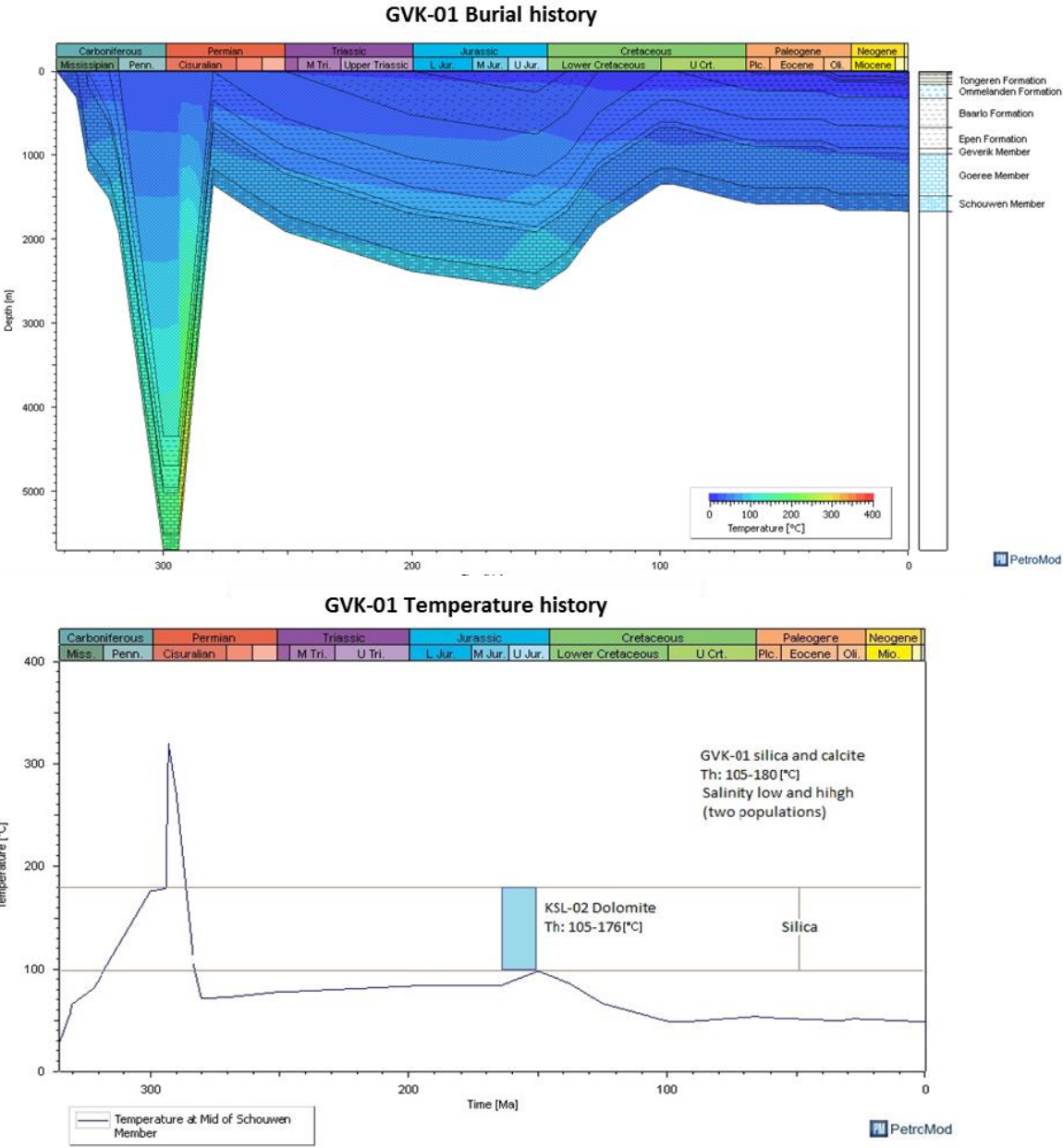
Figure 6-59: Burial curve and computed temperature evolution of the Schouwen member for GVK-01, based on the heat flow model.

6.6.4 East Netherlands (Californië wells)

Based on Poty (2014), reservoir quality enhancement is most likely related to dolomitization and (de)dolomitisation processes producing intercrystal pores in combination with fracture formation and brecciation that could be associated with faulting. Some indications of (de)dolomitisation were also observed in the current study, which agrees with the findings of Poty (2014) for the same wells. No detailed diagenetic work has been carried out on the sediments recovered from the Californië wells, however, a brief paragenetic sequence could be constructed from the cuttings of CAL-GT-02. The Mississippi Valley Type (MVT) mineralisation in the Californië wells is associated with dolomitisation. This shows that the main event responsible for the generation of matrix porosity is replacement of the limestone by dolomite. In grain-supported limestone, the dolomite initially replaces the matrix with the preservation of inherited intergranular and new intercrystal pores (Figure 6-60). The occurrence of dolomites within the Namurian siliciclastics overlaying the Dinantian carbonates suggests a burial origin for these dolomites rather than an early contemporaneous dolomitisation. A precise timing of the main diagenetic events and dolomitisation cannot be suggested due to the lack of appropriate samples and cross-cutting relationships. Based on Sr-Pb isotopic characteristics, Chatziliadou (2009) attributed the timing of the MVT and calamine mineralisation in the Stolberg-Aachen-Kelmis mining district (Germany) and Thermae 2002 (the SE Netherlands) to 134.3 ± 1.3 and 134.5 ± 4.1 Ma, respectively, which defines a period of formation from the Late Jurassic to Early Cretaceous. Note that the latter age can only be assigned to the east Netherlands (Californië wells) if the mineralisations arose from the same event, which is not neccessarily the case here.
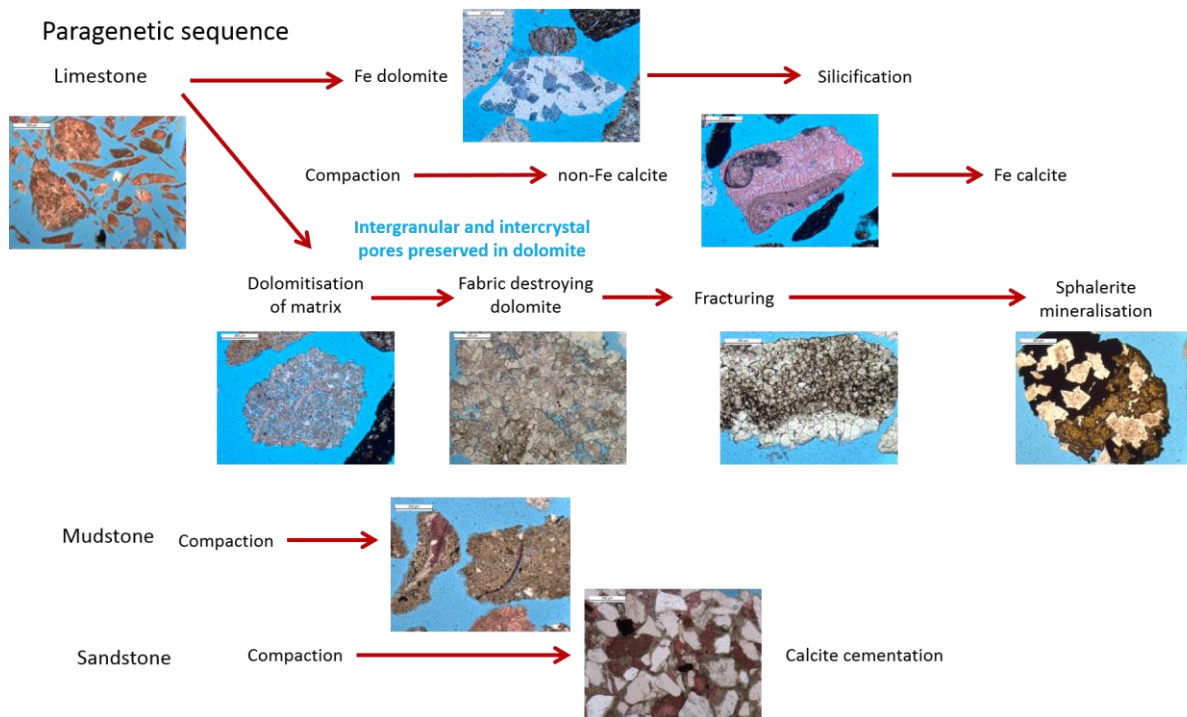
Figure 6-60: Paragenetic sequence based on cuttings from CAL-GT-02.

The fabric-replacive dolomite also locally contains intercrystal porosity. Further fracturing events have the potential to generate more porosity; however, fractures observed in cuttings were cemented by dolomite with euhedral fracture terminations suggesting that relict porosity may be present in some factures. The observed dolomitisation is associated with a subsequent phase of mineralisation.

120

6.6.5 Comparison between global Dinantian diagenesis models and the Netherlands

Hollis (1998), Walkden and Williams (1991) and Hollis and Walkden (2012) performed comprehensive diagenetic studies on the Visean carbonates of the Derbyshire platform (UK). Muchez *et al*. (1991a and b) undertook studies on the diagenesis of Visean carbonates in the Campine Basin (Belgium) based on the Heibaart, Poederlee and Turnhout boreholes. Ronchi *et al*. (2010), Collins *et al*. (2014) and Dickson and Kenter (2014) investigated the diagenesis of the Lower to Upper Carboniferous Precaspian platforms (Kashagan and Tengiz, Kazakhstan). Van der Kooij *et al*. (2007, 2009, and 2010) discussed the early diagenetic modifications of the Upper Carboniferous microbial carbonates exposed in Sierra del Cuera (northern Spain). They described similar near-surface diagenetic features including marine cement fringes, particularly fibrous calcite cements, followed by meteoric dissolution (karstification) and cementation. The karst collapse breccia filled with subaerial exposure condition deposits (clay minerals) can be pinpointed in all of the aforementioned platforms. The karstic dissolution has produced a significant early secondary moldic porosity which is well preserved particulary in the Kashagan platform, but also reported from the Heibaart well. In the Kashagan platform, dissolution vugs and channels, up to several centimeters in size, developed locally below the sequence boundaries. This porosity is partially cemented by burial cements but not completely blocked by them. The early diagenetic phases in all of these platforms are followed by several generations of late calcite cement and saddle dolomite appearing in the matrix and veins. In the Derbyshire and the Precaspian platforms these cements are associated with MVT mineralisation. The Precaspian platform margins have been the preferential sites for the development of fractures and subsequent mineralisation but this has not been exclusively noted for the Derbyshire and Campine Basins. In the Derbyshire platform, fluid inclusions are characterised by an overall temperature upturn from 57 to 200 °C with fluids of relatively low to high salinity (4.4-23 wt. % eq. NaCl). Muchez *et al*. (1991a and b) reported similarly fluids of increasing temperature from 50 to 150 °C for the calcites to 200 °C for the saddle dolomite. Ronchi *et al*. (2010) reported fluid inclusions of hot (70-120 °C) and low to moderately saline (0-11 wt. % eq. NaCl) in the Kashagan platform. Collins *et al*. (2014) described much higher burial fluid temperatures within the Tengiz platform reaching up to 226 °C. Hollis (1998) and Ronchi *et al*. (2010) suggested basin-derived formation waters as the main source of the burial fluids (e.g. clay dewatering). Muchez *et al*. (1991a and b) concluded that the pore fluids in the studied wells were related to an evolution from meteoric to an increasing component of basinal fluids.

The eodiagenetic evolution of the Netherlands Dinantian carbonates is comparable to the ones reported from UK, Belgium and the Precaspian Basin. The breccia texture observed within the early karsts (BHG-01) resembles the karstic collapse breccia reported from the Derbyshire, Heibart well and inner Kashagan platform but the porosity induced by the early karstification is rather less preserved in comparison with the Precaspian ones. Currently, the Kashagan and Tengiz platforms are buried at depths of 3700 and 4200 m, respectively, which can induce significant compaction. The preservation of early porosity within the Precaspian platforms can perhaps be related to occurrence of framework cements (e.g. circumgranular), circulation of organic acids and early emplacement of oil within the pore spaces, and the thermal conductivity effect of the overlaying salt deposits.

The mesodiagenesis modifications of the Netherlands Dinantian carbonates are also largely similar to the ones described above. In general, the cores studied from the Netherlands are fractured and affected by fault related hydrothermal dolomitisation everywhere and MVT mineralisation specifically in SW and SE Netherlands. The parental fluids originating such diagenetic products exploited the fractures and the pre-existing early karst features leaving some porosity unblocked and generated some more vuggy porosity. According to Collins *et al*.

(2014), the enlarged fracture vugs in the Tengiz platform resulted from circulation of corrosive H_2S bearing basinal fluids produced by thermochemical sulphate reduction (TSR). Based on evidences of (de)dolomitisation observed in the cuttings of CAL-GT-01, possible circulation of H_2S bearing fluids as a (de)dolomitising agent was hypothesised by Poty (2014). Enriched sulphur isotope ($\delta^{34}S$) values (+15.1 and +17.83‰) measured from the MVT associated pyrite crystals (BHG-01) although reflects the normal seawater sulphate and may also be interpreted as occurrence of TSR, which is considered as a process generating H_2S within the fluid system (Machel, 1989). The latter fluids migrated through faults and fractures which dominantly affected the Precaspian platform margins priming them to porosity enhancement. The wells penetrating the Dinantian carbonates in the Netherlands, except for LTG-01, are drilled within the inner platform area and thus the nature of diagenetic modifications affecting the reservoir quality of the platform margins cannot be fully assessed. Furthermore, understanding the level of their intensity could be biased by the sampling strategies. In LTG-01, although not enough samples are available for a comprehensive study, fault-related hydrothermal dolomitisation has enhanced the matrix porosity at the platform margins.

The burial fluids reported from the Derbyshire and the Precaspian platforms show similar temperature and salinity ranges to the ones in the Belgian Campine Basin and the Netherlands Dinantian carbonates. However, the low saline burial fluids that have been considered as basinal by Hollis (1998) and Ronchi *et al.* (2010) have been interpreted as topography-driven meteoric waters (after Heydari, 1997) in the Netherlands and Belgium Campine Basin. The influence of these meteoric waters, as expected, diminishes within the northern Netherlands isolated platforms (LTG-01 and UHM-02). The fluid system within the latter isolated platforms was dominated by basinal brines.

6.7 Petrophysical properties

In general, the reservoir quality of the Dinantian carbonates is relatively poor (Figures 6-62 and 6-63), with most of porosity values below 2% or even 1% (Carlson, 2019). There are some rare outliers, reaching up to 48%. These porous intervals resulted from preferential late leaching of the non-silicified carbonates of HEU-01 and KSL-02 wells. These wells show good porosity in the silicified interval, but permeability always tends to remain low (10 mD).

There is no clear difference in terms of depositional facies and the observed petrophysical properties: most the impact on porosity and permeability is linked to diagenetic effects. One of the main diagenetic modifications affecting the porosity is dolomitisation. Although this process is very heterogeneous, a clear relation can be pinpointed, e.g. in wells LTG-01 and UHM-02, porosity is influenced by the amount of dolomite, even doubling the poor porosities of the limestones (Figures 6-61, 6-65 and 6-66). It is also evident that dolomitisation increased the matrix porosity in the well O18-01 with the presence of intercrystal and mouldic pores in dolomitised limestone in Core 6. All wells have at least some short intervals with porosity exceeding 2 % but mostly range between 2 and 6 %. The maximum dolomitisation-related porosity is evident in wells KTG-01 and BHG-01. Among the wells drilled in the SW Netherlands, the latter wells were the only ones that have had flow to the surface, KTG-01 without lift and BHG-01 with N2 lift. Based on the wireline logs and core measurements, in the former well the porosity reaches 15% at the interval of 975 m, while the mode of porosity in the other intervals does not exceed 4-5%. In the BHG-01 well, the intervals affected by the double effect of Top-Namurian karstification and dolomitisation (2178 m), show a porosity maximum of 10%. The use of analogs is in this case extremely important, in order to create conceptual models for the most important diagenetic events, such as dolomitisation and to predict the reservoir quality.
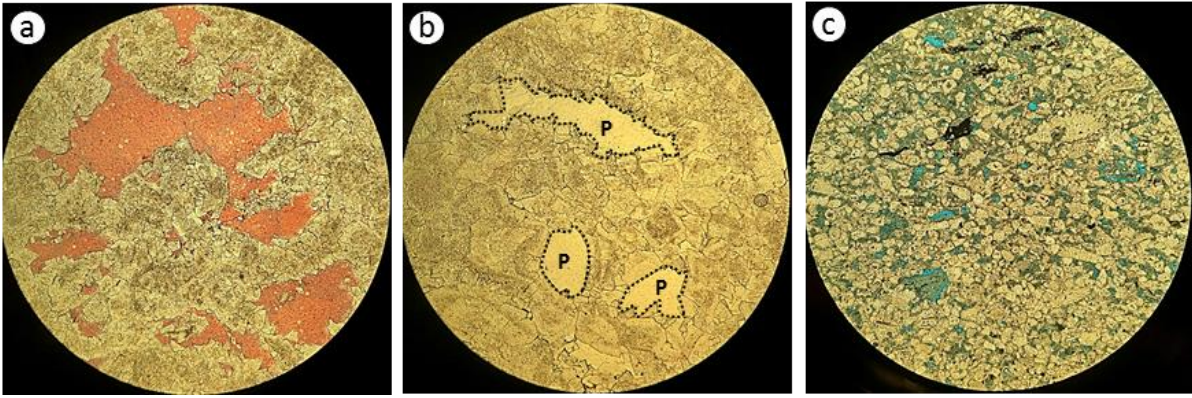
Figure 6-61: a) Dolomite with calcite cemented pores, KTG-01 987.30 m (fov 4 mm). b) Dolomite with mouldic to vuggy porosity, KTG-01 964.90 m (fov 4 mm). c) Cretaceous karst infill (blue impregnation), KTG-01 983.76 m (fov 8 mm).
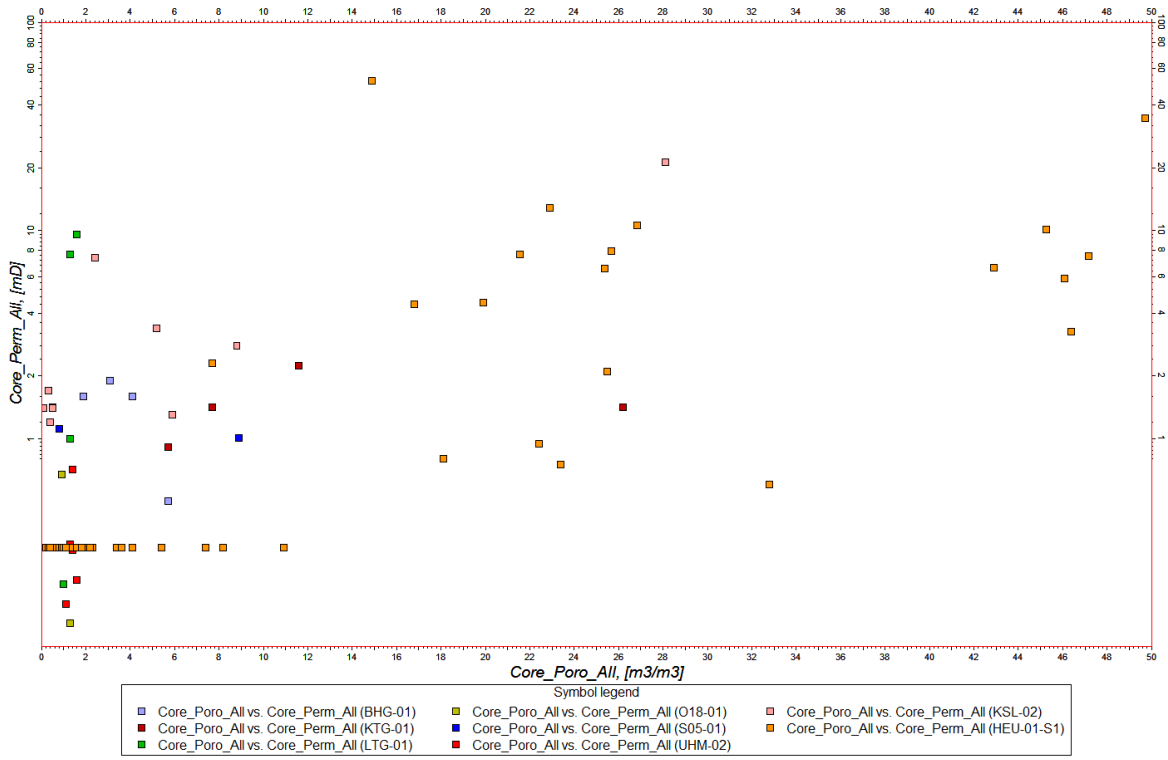
Figure 6-62: Core porosity vs core permeability in all the Dinantian wells.
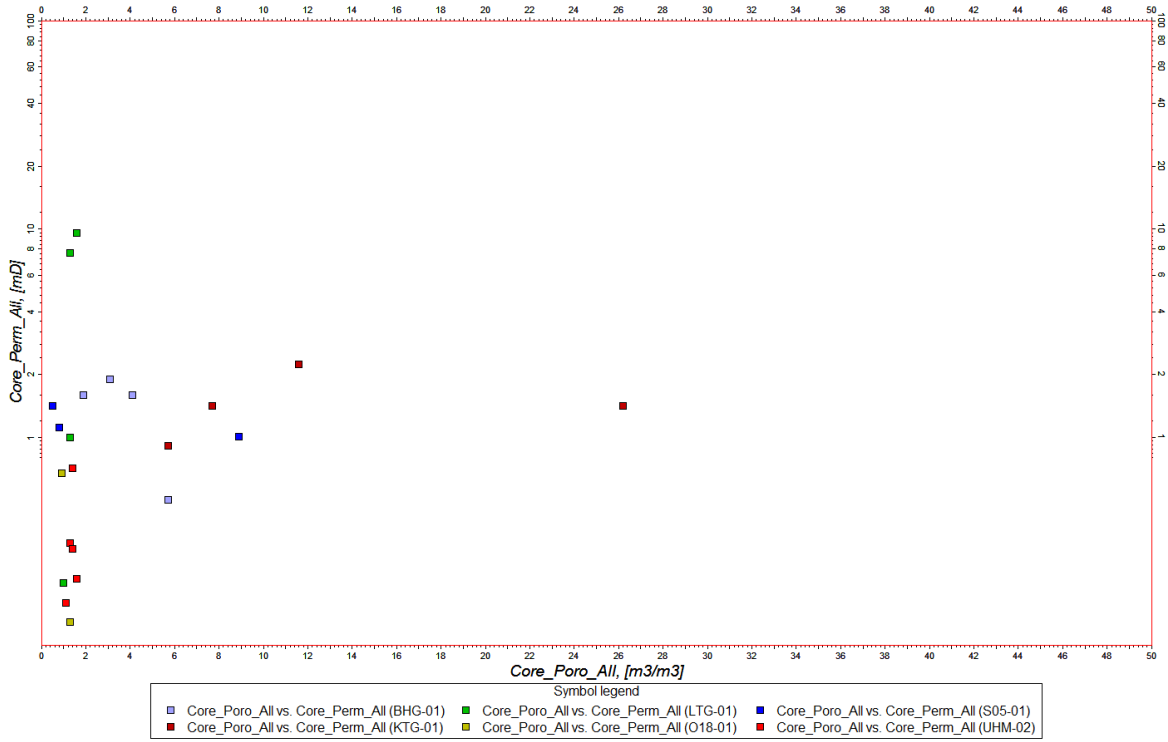
Figure 6-63: Core porosity vs core permeability without HEU-01 and KSL-02.
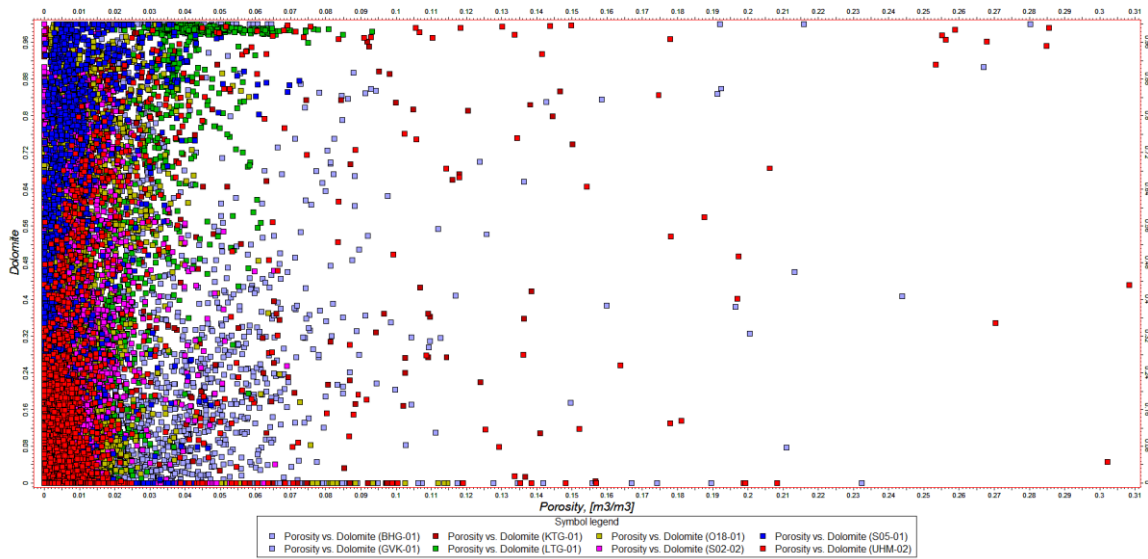
Figure 6-64: Well log porosity vs amount of dolomite in all the wells showing a relative porosity increase in function of dolomitisation.
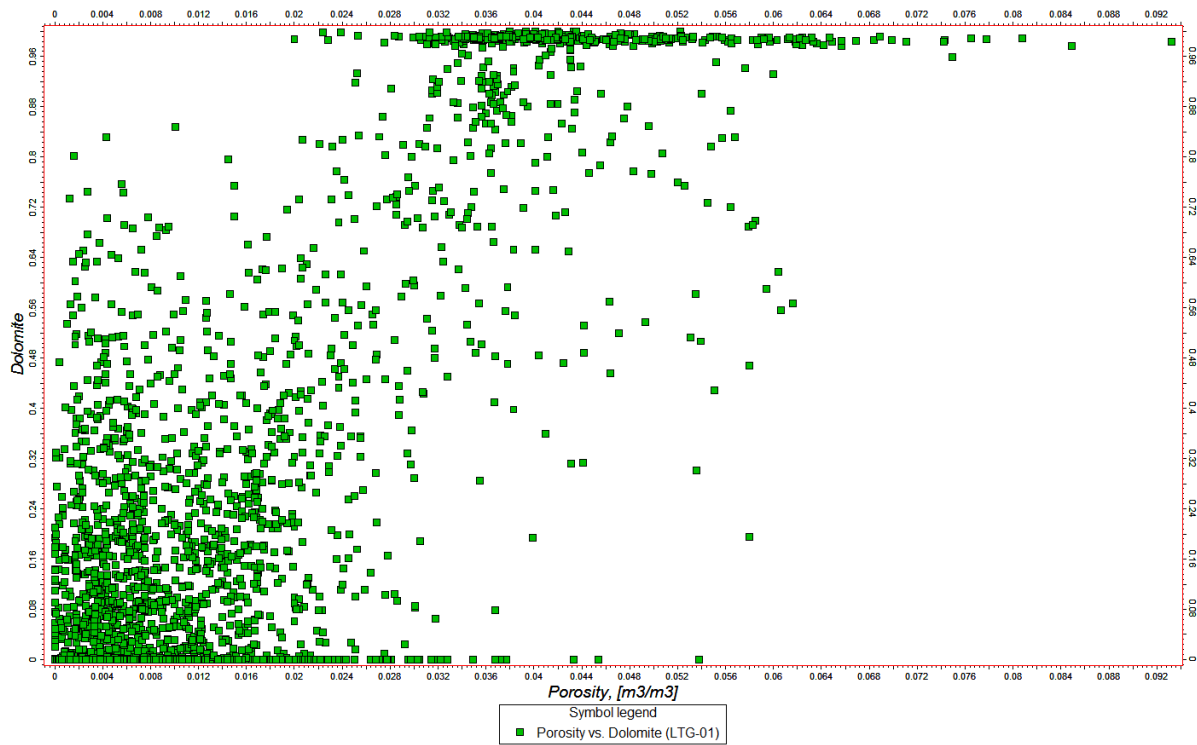
Figure 6-65: Dolomite fraction vs porosity in LTG-01 well.
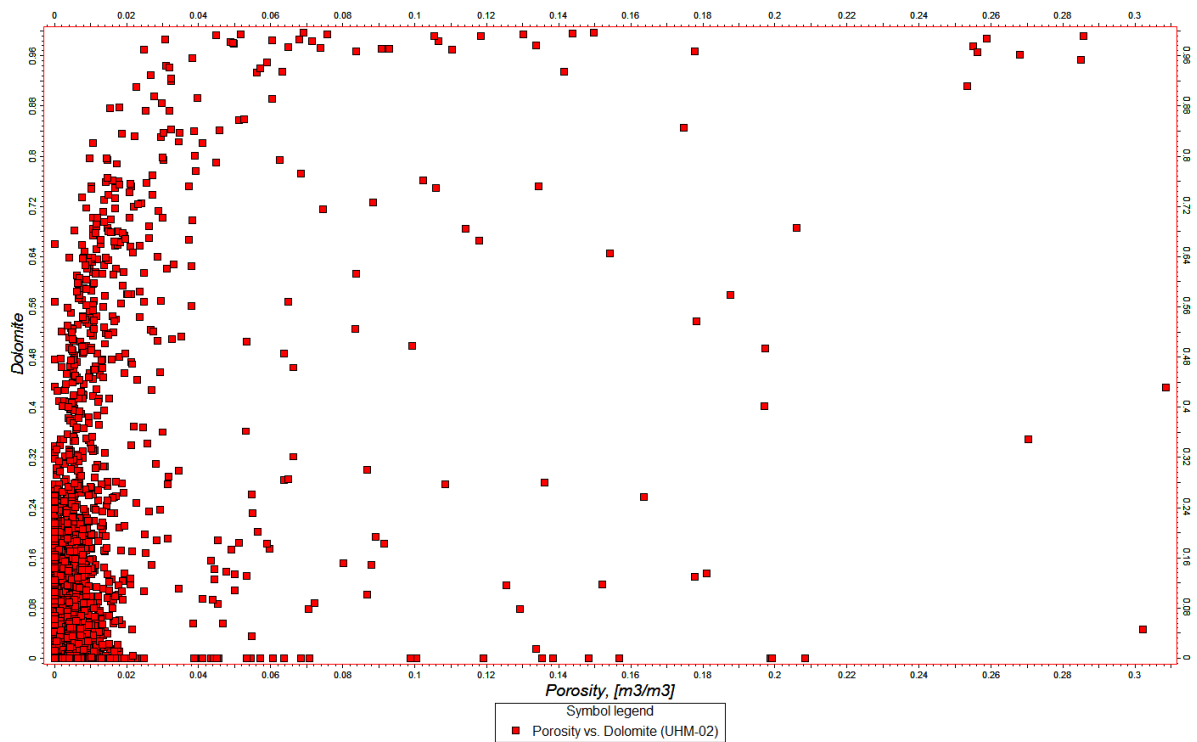
Figure 6-66: Dolomite fraction vs porosity in UHM-02 well.

7. Literature list/references

The literature list presented in this study is only a summary of the most important used ones.

Abbink, O. A., Devuyst, F. X., Grotsch, J., Hance, L., van Hoof, T. B., Kombrink, H., and van Ojik, K. (2009). The Lower Carboniferous of Key-well UHM-02, Onshore The Netherlands, and Implications for Regional Basin Development. 71st EAGE Conference and Exhibition-Amsterdam, The Netherlands.

Abdul Fattah, R., and Verweij, J. M. (2014). Maturity of Carboniferous Source Rocks in Central Onshore Netherlands. The Impact of the Permian Thermal Anomaly. In First EAGE Workshop on Basin and Petroleum Systems Modeling (p. 5). Dubai.

Abdul Fattah, R., Verweij, J. M., and Witmans, N. (2012). Reconstruction of burial history, temperature, source rock maturity and hydrocarbon generation for the NCP-2D area, Dutch Offshore. Utrecht, TNO-034-UT-2010-0223, .

Adams, A. E. (1984). Development of algal-foraminifera-coral reefs in the Lower Carboniferous of Furness, NW England. Lethaia, 17 233-249.

Adams, A. E., Horbury, A. D., and Abdel Aziz, A. A. (1984). Controls on Dinantian sedimentation in south Cumbria and surrounding areas of NW England. Proceedings of the Geologists Association, 101 19-30.

Amantini, E., Ricaud, Y., and Grégoire, N. (2009). Development of the performance of the Loenhout UGS (Antwerp - Belgium) Drilling through a highly karstified and fissured limestone reservoir under gas storage operation. In 24th World Gas Conference (p. 9).

Aretz, M., and Chevallier, E. (2007). In: Palaeozoic Reefs and bioaccumulations: climatic and evolutionary controls. Geological Society of London special Publication, 275, 163-188.

Aretz, M., and Herbig, H-G. (2003). Coral-rich bioconstructions in the Visean (late Mississippian) of South Wales (Gower Peninsula, UK). Facies, 49, 221-242.

Bábek, O., Kalvoda, J., Aretz, M., Cossey, P.J., Devuyst, F-X., Herbig, H-G., and Sevastopulo, G. (2010). The correlation potential of magnetic susceptibility and outcrop gamma ray logs at Tournaisian-Visean boundary sections in western Europe. Geologica Belgica, 13, 291-308.

Bábek, O., Kalvoda, J., Cossey, P. J., Šimíček, D., Devuyst, F-X., and Hargreaves, S. (2013). Facies and petrophysical signature of correlation potential of Tournaisian-Visean (Lower Carboniferous) sea-level cycle in ramp to basinal settings of the Wales-Brabant Massif, British Isles. Sedimentary Geology, 284-285, 197-213.

Bancroft, A. J., Somerville, I. D., and Strank, A.R.E. (1988). A bryozoan buildup from the Lower Carboniferous of North Wales. Lethaia, 21, 51-65.

Barker, C. E., and Pawlewicz, M. J. (1994). Calculation of vitrinite reflectance from thermal histories and peak temperature: A comparison of methods, in Mukhopadhyay, P. K., and Dow, W. G. (eds), Vitrinite Reflectance as a Maturity Parameter. ACS Symposium series, 570, 216-229.

Batten, D. J., Streel, M., Dusar, M., and Bless, M. J. M. (1987). Late Cretaceous palynomorphs from the boreholes Thermae 2002 (Valkenburg a/d Geul, The Netherlands) and 's-Gravenvoeren (Belgium). Annales de La Societe Geologique de Belgique, 110, 47-51.

Best, J., and Wignall, P. B. (2016). Introduction to the Field Guide. A Field Guide to the Carboniferous Sediments of the Shannon Basin, Western Ireland, 1-15.

Bless, M. J. M., Bouckaert, J., Bouzet, P., Conil, R., Cornet, P., Fairon-Demaret, M., Groessens, E., Longerstaey, P., Meesen, J. P. M. T., Paproth, E., Pirlet, H., Streel, M., Amerom, H. W. J. and Wolf, M. (1976). Dinantian rocks in the subsurface north of the Brabant and

Ardenno- Rhenish massifs in Belgium, the Netherlands and the Federal Republic of Germany. Mededelingen Rijks Geologische Dienst, nieuwe serie, 27, 81-195.

Bless, M. J. M., Bouckaert, J., Conil, R., Groessens, E., Kasig, W., Paproth, E., Poty, E., Van Steenwinkel, M., Streel, M., Walter, R. (1980). Pre-permian Permian depositional environments around the brabant Brabant massif in Belgium, The Netherlands and Germany. Sedimentary Geology, 27, 1-81. https://doi.org/10.1016/0037-0738(80)90031-7

Bless, M. J. M., Boonen, P., Dusar, M., and Soille, P. (1981). Microfossils and depositional environment of late Dinantian carbonates at Heibaart (northern Belgium). Annales de La Société Géologique de Belgique, 104, 135-165.

Bless, M. J. M. (1982). The Famennian and Dinantian in the boreholes Heugem-1/1a and Kastanjelaan-2 (Maastricht, the Netherlands): summary of results. Publicaties van het Natuurhistorisch Genootschap in Limburg, (1-4), 56-58.

Bonté, D., van Wees, J.-D., and Verweij, J. M. (2012). Subsurface temperature of the onshore Netherlands: new temperature dataset and modelling. Geol. Mijnbouw-N. J. G., 91, 491-515.

Bonté, D., Van Wees, J.-D., Fattah, R. A., Nelskamp, S., and Cloetingh, S. (2014). Permian Basin maturation: proof for pervasive magmatic heat flow in the Netherlands. General Assembly Conference Abstracts, 16(EGU2014-9225), 9225.

Bos, S. and Laenen, B. (2017). Development of the first deep geothermal doublet in the Campine Basin of Belgium. European Geologist Journal, 43, 16-20.

Boots, R. (2014). Regional context of a potential Dinantian play. TNO-2014-R11604, 129 pp.

Boulvain, F. (2001). Facies architecture and diagenesis of Belgian Late Frasnian carbonate mounds. Sedimentary Geology, 145, 269-294.

Bouroullec, R., Nelskamp, S., Kloppenburg, A., Abdul Fattah, R., Foeken, J. P. T., ten Veen, J. H., Geel, C. R., Debacker, T., Smit, J. (2019). Burial and Structural Analysis of the Dinantian Carbonates in the Dutch Subsurface (SCAN). Downloadable from www.nlog.nl.

Boxem, T. A. P., Veldkamp, J. G., and van Wees, J. D. A. M. (2016). Ultra-diepe geothermie: Overzicht, inzicht & to-do ondergrond. TNO report, R10803, 53 pp.

Bridges, P. H., and Chapman, A. J. (1988). The anatomy of a deep water mud-mound complex to the south west of the Dinantian platform in Derbyshire, UK. Sedimentology, 35, 139-162.

Bridges, P. H., Gutteridge, P., and Pickard, N. A. H. (1995). The environments setting of early Carboniferous mud-mounds. In: Special Publication of the International Association of Sedimentologists, 23, 171-190.

Broadhurst, F. M and Simpson, I. P. (1973). Bathymetry on a Carboniferous reef. Lethaia, 6, 367-381.

Broadhurst, F. M., and Simpson, I. P. (1967). Sedimentary infillings of fossils and cavities at Treak Cliff, Derbyshire. Geological Magazine, 104, 443-448.

Carlson, T. (2019). Petrophysical Report of the Dinantian Carbonates in the Dutch Subsurface (SCAN). Downloadable from: https://www.nlog.nl/sites/default/files/2019-08/scan_dinantien_petrophysics_report.pdf.

Chatziliadou, M. (2009). Rb-Sr Alter und Sr-Pb Isotopencharakteristik von Gangmineralisationen in paläozoischen Gesteinen am Nordrand des linksrheinischen Schiefergebirges (Raum Stolberg-Aachen-Kelmis) und Vergleich mit den rezenten Thermalwässern von Aachen-Burtscheid. Rheinisch-Westfälischen Technischen Hochschule Aachen.

Chesnel, V., Merino-Tomé, O., Fernández, L. P., Villa, E., and Samankassou, E. (2017). Spatial and temporal distribution of microbial carbonates, skeletal and non-skeletal grains in a Pennsylvanian carbonate platform (Valdorria, Northern Spain). Palaeogeography, Palaeoclimatology, Palaeoecology, 476, 106-139.

Collins, J., Narr, W., Harris, P. M. (Mitch), Playton, T., Jenkins, S., Tankersley, T., and Kenter, J. A. M. (2013). Lithofacies, Depositional Environments, Burial Diagenesis, and Dynamic Field Behavior in a Carboniferous Slope Reservoir, Tengiz Field (Republic of Kazakhstan), and Comparison with Outcrop Analogs. In SEPM Special Publication (Vol. 105, pp. 50–83). https://doi.org/10.2110/sepmsp.105.11

Davies, J. R. (1991). Karstification and pedogenesis on a late Dinantian carbonate platform, Anglesey, North Wales. Proceedings of the Yorkshire Geological Society, 48, 297-321.

De Putter, T., Rouchy, J. M., Herbosch, A., Keppens, E., Pierre, C., and Groessens, E. (1994). Sedimentology and palaeo-environment of the Upper Visean anhydrite of the Franco-Belgian Carboniferous basin (Saint-Ghislain borehole, southern Belgium). Sedimentary Geology, 90, 77–93. https://doi.org/10.1016/0037-0738(94)90018-3

Debout, L., and Denayer, J. (2018). Palaeoecology of the upper Tournaisian (Mississippian) crinoidal limestones from south Belgium. Geological Belgica, 21, 111-127.

De Jager, J. (2007). Geological development. In: Wong, T. E., Batjes, D. A. J., and de Jager, J. (eds), Geology of the Netherlands. Royal Netherlands Academy of Arts and Sciences, 197-221.

Dejonghe, L. (1983). Indice de mineralisation sulfuree (Fe, Zn, Sb, Cu, Ni, Co) liee aux strates du Frasnien (limite F2/F3) dans le sondage d'Heibaart (Loenhout, Province d'Anvers). Bulletin de La Société Belge de Géologie, 92, 165-175.

Dickson, J. A. D. (1966). Carbonate identification and genesis as revealed by staining. Journal of Sedimentary Petrology, 36, 491-505.

Dickson, J. A. D. and Kenter, J. A. M. (2014). Diagenetic evolution of selected parasequences across a carbonate platform: Late Paleozoic, Tengiz Reservoir, Kazakhstan. Journal of Sedimentary Research, 84, 664-693.

Dreesen, R., Bouckaert, J., Dusar, M., Soille, P., and Vandenberghe, N. (1985). Collapse structures at the Dinantian-Silesian contact in the subsurface of the Campine Basin, N of the Brabant Massif (N-Belgium). Congrès International de Stratigraphie et de Géologie Du Carbonifère, 7-14.

Dreesen, R., Bouckaert, J., Dusar, M., Soille, J., and Vandenberghe, N. (1987). Subsurface structural analysis of the late-Dinantian carbonate shelf at the northern flank of the Brabant Massif (Campine Basin, N-Belgium). Mémoires Pour Servir à l'explication Des Cartes Géologiques et Minières de La Belgique, 21, 1-37.

Dunham, R.J. (1962). Classification of carbonate rocks according to depositional texture. In: Ham., W. E. (eds), Classification of Carbonate Rocks. American Association of Petroleum Geologists Memoir, 1, 108-121.

Dunham, K. C. (1973). A recent deep boring near Eyam, Derbyshire. Nature Physical Sciences 241, 84-85.

Ebdon, C. C., Fraser, A. J., Higgins, A.C., Mitchener, B. C., and Strank, A. R. E. (1990). The Dinantian stratigraphy of the East Midlands: a seismo-stratigaphic approach. Journal of the Geological Society of London, 147, 519-536.

Evans, D. J., and Kirkby, G. A. (1999). The architecture of concealed Dinantian sedimentary sequences over the central Lancashire and Holme Highs, northern England. Proceedings of the Yorkshire Geological Society, 52, 297-312.

Faugères, J. C., Stow, D. A. V., Imbert, P. and Viana, A. (1999). Seismic features diagnostic of contourite drifts. Marine Geology, 162, 1-38.

Fraser, A. J., and Gawthorpe, R. L. (1990). Tectono-stratigraphic development and hydrocarbon habitat of the Carboniferous of northern England. In Hardman, R. F. P., and Brooks, J. (eds), Tectonic controls on British hydrocarbon reserves. Special Publication of the Geological Society, 55, 49-86.

Fraser, A. J., Nash, D. F., Steele, R. P., and Ebdon, C. C. (1990). A regional assessment of the intra-Carboniferous play of Northern England. In: Brooks, J. (eds), Classic Petroleum Provinces. Geological Society of London Special Publication, 50, 417-440.

Friedrich, G., Bless, M. J., Vogtmann, J., Wiechowski, A. (1987). Lead-zinc mineralization in Dinantian rocks of boreholes Thermae 2000 and Thermae 2002 (Valkenburg a/d Geul, the Netherlands). Annales de la Société géologique de Belgique, 110, 59-75.

Gawthorpe, R. L. (1987). Tectono-sedimentary evolution of the Bowland Basin, N England, during the Dinantian. Journal of the Geological Society of London, 144, 59-71.

Gawthorpe, R. L., and Clemmy, H. (1985). Geometry of submarine slides in the Bowland Basin (Dinantian) and their relation to debris flows. Journal of the Geological Society of London, 142, 555-565.

Gawthorpe, R. L., Gutteridge, P., and Leeder, M. R. (1989). Late Devonian and Dinantian basin evolution in Northern England and North Wales. In: Arthurton, R. S., Gutteridge, P. and Nolan, S. C. (eds), The role of tectonics in Devonian and Carboniferous sedimentation in the British Isles Occasional Publication of the Yorkshire Geological Society 6, 1-23.

Geluk, M. C. (2000). Late Permian (Zechstein) carbonate-facies maps, the Netherlands. Geologie En Mijnbouw/Netherlands Journal of Geosciences, 79, 17-27.

Geluk, M. C., Dusar, M., and De Vos, W. (2007). Pre-Silesian. In: Wong, T. E., Batjes, D. A. J., and de Jager, J. (eds), Geology of the Netherlands. Royal Netherlands Academy of Arts and Sciences, 27-42.

Groessens, E. (1989). A history of the subdivision of the Dinantian subsystem. Bulletin de La Société Belge de Géologie, 98, 183-195.

Groessens, E. (2006). Dinantian. Geologica Belgica, 9, 157-162.

Groessens, E., Conil, R., and Hennebert, M. (1979). Le Dinantien du sondage de Saint-Ghislain. Stratigraphie et Paléontologie. Memoires Pour Servir a l'explication Des Cartes Géologiques et Minières de La Belgique, 22, 137.

Gutteridge, P. (1990). The origin and significance of the distribution of shelly macrofauna in late Dinantian carbonate mud mounds of Derbyshire. Proceedings of the Yorkshire Geological Society, 48, 23-32.

Gutteridge, P. (1991). Aspects of Dinantian sedimentation in the Edale Basin, north Derbyshire. Geological Journal, 26, 245-269.

Gutteridge, P., (1995). Late Dinantian (Brigantian) carbonate mud-mounds of the Derbyshire carbonate platform. In: Monty, C. L. V., Bosence, D. W. J., Bridges, P.H., and Pratt, B.R. (eds), Carbonate Mud Mounds, their origin and evolution. Special publication of the International Association of Sedimentologists, 23, 289-307.

Gutteridge, P. (2003). A record of the Brigantian limestone succession in the partly infilled Dale Quarry, Wirksworth. Mercian Geologist, 15, 219-224.

Harris, P. M. (2008). Geologic framework for the Tengiz and Korolev isolated carbonate platforms, Kazakhstan. Search and Discovery, (20060), 60.

Heidary, E. (1997). Hydrotectonic models of burial diagenesis in platform carbonates based on formation water geochemistry in North American sedimentary basins, In: Montanez, J. P., Gregg, J. M., and Shelton, K. (eds), Basinwide diagenetic patterns: Integrated

petrologic, geochemical, and hydrologic considerations: SEPM Special Publication, 57, 54-79.

Herbig, H. G., and Mamet, B. (2014). A muddy to cleat carbonate ramp, Latest Devonian, Velbert Anticline (Rheinisches Schiefergebirge, Germany). Geologica et Palaeontologica, 40, 1-25.

Herzog, C. (2005). Die Geothermiebohrung "RWTH-1": technische, geologische und bergrechtliche Aspekte eines Geothermieprojektes in öffentlicher Trägerschaft, 186. http://134.130.184.8/opus/volltexte/2006/1318/

Higgs, K. T., Dreesen, R., Dusar, M., and Streel, M. (1992). Palynostratigraphy of the Tournaisian (Hastarian) rocks in the Namur Synclinorium, West Flanders, Belgium. Review of Palaeobotany and Palynology, 72, 149-158. https://doi.org/10.1016/0034-6667(92)90182-G

Hladil, J. (2005). The formation of stromatactis-type fenestral structures during the sedimentation of experimental slurries - a possible clue to a 120-year-old puzzle about stromatactis. Bulletin of Geosciences, 80, 193-211.

Hollis, C. (1998). Reconstructing fluid history: an integrated approach to timing fluid expulsion and migration on the Carboniferous Derbyshire Platform, England. Geological Society, London, Special Publications, 144, 153-159.

Hollis, C., and Walkden, G. M. (2012). Burial diagenetic evolution of Lower Carboniferous (Dinantian) of the southern margin of the Askrigg Platform and a comparison with the Derbyshire Platform. Petroleum Geoscience, 18, 83-95. https://doi.org/10.1144/1354-079311-049

Horbury, A. D. (1989). The relative roles of tectonism and eustacy in the deposition of the Urswick Limestone in south Cumbria and north Lancashire. In: Arthurton, R. S., Gutteridge, P., and Nolan, S. C. (eds), The role of tectonics in Devonian and Carboniferous sedimentation in the British Isles Occasional Publication of the Yorkshire Geological Society, 6, 153-169.

Hoornveld, N. (2013). Dinantian carbonate development and related prospectivity of the onshore. Master thesis, Vrije Universiteit Amsterdam (the Netherlands),142 pp.

Jacobs, L., Swennen, R., van Orsmael, J., Notebaert, L., and Viaene, W. (1982). Occurrences of pseudomorphs after evaporite minerals in the Dinantian carbonate rocks of the eastern part of Belgium. Bulletin van de Belgische Vereniging voor Geologie, 91, 105-123.

Keim, L., and Schlager, W. (1999). Automicrite facies on steep slopes (Triassic, Dolomites, Italy). Facies, 41, 15-26.

Keim, L., and Schlager, W. (2001). Quantitative compositional analysis of a Triassic carbonate platform (Southern Alps, Italy). Sedimentary Geology, 139, 261-283.

Kenter, J. A. M., Harris, P. M., and Della Porta, G. (2005). Steep microbial boundstone-dominated platform margins—examples and implications. Sedimentary Geology, 178, 5-30.

Kenter, J. A. M., Harris, P. M., Collins, J. F., Weber, L. J., Kuanysheva, G., and Fischer, D.J. (2006). Late Visean to Bashkirian platform cyclicity in the central Tengiz buildup, Precaspian Basin, Kazakhstan: Depositional evolution and reservoir development. In: Harris, P. M., and Weber, L. J. (eds), Giant hydrocarbon reservoirs of the world: From rocks to reservoir characterization and modeling. AAPG Memoir 88, SEPM Special Publication, 7-54.

Kim, S. T., Mucci, A., and Taylor, B. E. (2007): Phosphoric acid fractionation factors for calcite and aragonite between 25 and 75 °C: Revisited. Chemical Geology, 246, 135-146.

Kley, J. and Voigt, T. (2008). Late Cretaceous intraplate thrusting in central Europe: Effect of Africa-Iberia-Europe convergence, not Alpine collision. Geology, 36(11), 839–842. https://doi.org/10.1130/G24930A.1

Kombrink, H., (2008). The Carboniferous of the Netherlands and surrounding areas; a basin analysis, Geologica Ultraiectina. 294, Ph.D. thesis, University of Utrecht, 184 pp.

Kus, J., Cramer, B., and Kockel, F. (2005). Effects of a Cretaceous structural inversion and a postulated high heat flow event on petroleum system of the western Lower Saxony Basin and the charge history of the Apeldorn gas field. Netherlands Journal of Geosciences-Geologie en Mijnbouw, 84, 3-24.

Laenen, B. (2003). Lithostratigrafie van het pre-Tertiair in Vlaanderen. Deel II: Dinantiaan and Devoon. Vito Report.

Lagrou, D., and Coen-Aubert, M. (2017). Update of the Devonian lithostratigraphic subdivision in the subsurface of the Campine Basin (northern Belgium). Geologica Belgica, 20, 1-13. https://doi.org/10.20341/gb.2016.017

Lee, M., Aronson, J. L., and Savin, S. M. (1985). K/Ar dating of time of gas emplacement in Rotliegendes sandstone, Netherlands. American Association of Petroleum Geologists Bulletin, 69, 1381-1385.

Lees, A. (1997). Biostratigraphy, sedimentology and palaeobathymetry of Waulsortian and peri-Waulsortian rocks during the late Tournaisian regression, Dinant area, Belgium. Geological Journal, 32, 1-36.

Lees, A., Hallet, V., and Hibo, D. (1985). Facies variation in Waulsortian buildups, part 1; a model from Belgium. Geological Journal. 20, 133-158.

Lees, A., and Miller. J. (1985). Facies variation in Waulsortian buildups, part 2; mid-Dinantian buildups from Europe and North America. Geological Journal, 20, 159-180.

Lipsey, L., Pluymaekers, M., Goldberg, T., van Oversteeg, K., Ghazaryan, L., Cloetingh, S., and van Wees, J. D. (2016). Numerical modelling of thermal convection in the Luttelgeest carbonate platform, the Netherlands. Geothermics, 64, 135-151.

Littke, R., Urai, J. L., Uffmann, A. K., and Risvanis, F. (2012). Reflectance of dispersed vitrinite in Palaeozoic rocks with and without cleavage: Implications for burial and thermal history modeling in the Devonian of Rursee area, northern Rhenish Massif, Germany. International Journal of Coal Geology, 89, 41-50. https://doi.org/10.1016/j.coal.2011.07.006

Lögering, M. J., Kolb, J., Meyer, F. M., and Schwarzbauer, J. (2006). Paläofluide in störungskon- trollierten Bruchsystemen der Aachener Geothermie- Bohrung. TSK 11 Göttingen 2006, 1, 4.

Lundmark, A. M., Gabrielsen, R. H., Strand, T., and Ohm, S. E. (2018). Repeated post-Caledonian intra-cratonic rifting in the central North Sea: Evidence from the volcanic record in the Embla oil field. Marine and Petroleum Geology, 92, 505-518. https://doi.org/10.1016/j.marpetgeo.2017.11.018

MacCarthy, I. A. J., and Gardiner. P. R. R. (1987). Dinantian cyclicity: a case history from the Muster Basin of southern Ireland. In: Miller, J., Adams, A. E., and Wright, V. P. (eds), European Dinantian Environments, 199-232.

Machel, H. G. (1989). Relationships between sulphate reduction and oxidation of organic compounds to carbonate diagenesis, hydrocarbon accumulations, salt domes, and metal sulphide deposits. Carbonates and Evaporites, 4, 137.

Machel, H. G. (2000). Application of cathodoluminescence to carbonate diagenesis. In: Pagel M., Barbin V., Blanc P., Ohnenstetter, D. (eds), Cathodoluminescence in Geosciences Springer, Berlin, Heidelberg, 271-301. https://doi.org/10.1007/978-3-662-04086-7_11

Machel, H., and Lonnee, J. (2002). Hydrothermal dolomite - A product of poor definition and imagination, Sedimentary Geology, 152, 3 - 4, 163-171.

Mathes-Schmidt, M. E. (2000). Mikrofazies, Sedimentationsgeschehen und paläogeographische Entwicklung im Verlauf des oberen Viséums im Untergrund der Niederrheinischen Bucht und des Campine-Beckens. Ph.D. thesis, University of Aachen (Germany), 245 pp.

McGhee, G. R. (1996). The late Devonian mass extinction: the Frasnian/Famennian crisis. Columbia University Press, 302 pp.

Muchez, P., and Viaene, W. (1987). Sedimentological study of the Upper Visean Strata in the 'S Gravenvoeren borehole. Katholieke Universiteit Leuven.

Muchez, P., Conil, R., Viaene, W., Bouckaert, J., and Poty, E. (1987). Sedimentology and biostratigraphy of the Visean carbonates of the Heibaart (DzH1) borehole (northern Belgium). Annales de La Société Géologique de Belgique, 110, 199-208.

Muchez, P., Viaene, W.A., and Marshall, J. D. (1991a). Origin of shallow burial cements in the Late Visean of the Campine Basin, Belgium. Sedimentology Geology, 73, 257-271.

Muchez, P., Viaene, W. A., Keppens, E., Marshall, J. D., and Vandenberghe, N. (1991b). Vein cements and the geochemical evolution of subsurface fluids in the Campine Basin (Poderlee borehole, Belgium), Journal of the Geological Society of London, 148, 1005-1117.

Muchez, P., Viaene, W., Bouckaert, J., Conil, R., Dusar, M., Poty, E., Soille, P. and Vandenberghe, N. (1991). The occurrence of a microbial buildup at Poederlee (Campine Basin, Belgium); biostratigraphy, sedimentology, early diagenesis and significance for early Warnantian paleogeography. Annales de la Societe Geologique de Belgique, 113, 329-339.

Muchez, P., and Langenaeker, V. (1993). Middle Devonian to Dinantian Sedimentation in the Campine Basin (Northern Belgium): Its Relation to Variscan Tectonism. Special Publications of International Association of Sedimentologists, 20, 171-181. https://doi.org/10.1002/9781444304053.ch10

Muchez, P., Marshall, J. D., Touret, J. L. R., and Viaene, W. (1994). Origin and migration of palaeofluids in the Upper Visean of the Campine Basin, northern Belgium. Sedimentology, 41, 133-145. https://doi.org/http://dx.doi.org/10.1111/j.1365-3091.1994.tb01395.x

Murray, J., and Henry, T. (2018). Waulsortian limestone: Geology and Hydrogeology, Coference: Groundwater Matters: science and practice, Tullamore, Ireland.

Nielsen, P., Swennen, R., and Keppens, E. (1994). Multiple-step recrystallization within massive ancient dolomite units: an example from the Dinantian of Belgium. Sedimentology, 41, 567-584.

Nielsen, S. B., Clausen, O. R., and McGregor, E. (2017). basin%Ro: A vitrinite reflectance model derived from basin and laboratory data. Basin Research, 29, 515-536. https://doi.org/10.1111/bre.12160

Ogg, J. G., Ogg, G., and Gradstein, F. M. (2016). A Concise Geologic Time Scale. https://doi.org/10.1016/B978-0-444-59467-9.00001-7

Paproth, E., Conil, R., Bless, M. J. M., Boonen, P., Bouckaert, J., Carpentier, N., Coen, M., Delcambre, B., Deprijck, C., Deuzon, S., Dreesen, R., Groessens, E., Hance, L., Hennebert, M., Hibu, D., Hahn, G. and R., Hislaire, O., Kasig, W., Laloux, M., Lauwers, A., Lees, A., Lys, M., Op de Beek, K., Overlau, P., Pirlet, H., Poty, E., Ramsbottom, W., Streel, M., Swennen, R., Thorez, J., Vanguestaine, M., Van Steenwinkel, M. and Vieslet,

J. L. (1983). Bio-and Lithostratigraphic Subdivisions of the Dinantian in Belgium, a review. Annales de La Société Géologique de Belgique, 106, 185-239.

Pharaoh, T., England, R. and Lee, M. (1995). The concealed Caledonide basement of Eastern England and the Southern North Sea - a review. Studia geophysica et geodaetica, 39, 330-346.

Pickard, N. A. H. (1992). Depositional controls on Lower Carboniferous microbial carbonate buildups, eastern Midland Valley of Scotland. Sedimentology, 39, 1081-1100.

Pickard, N. A. H., and Gutteridge, P. (1997). Dinantian depositional systems and exploration potential: offshore and onshore, The Netherlands. Sedimentological study. Cambridge Carbonates report for NAM, 596 pp.

Pierre, C., and Rouchy, J. M. (1986). Oxygen and sulfur isotopes in anhydrites from Givetian and Visean evaporites of Northern France and Belgium. Chemical Geology, 58, 245-252. https://doi.org/10.1016/0168-9622(86)90013-8

Poty, E. (1982). Palaeokarsts et bréches d'effondrement dans le Frasnian moyen des environs de Visée leur influence dans la palaeogeographie Dinantienne. Annales de la Société Géologique de Belgique, 105, 315-337.

Poty, E. (2014). Report on cuttings from the CAL-GT-01S borehole. Unpublished report EBN BV.

Poty, E. (2016). The Dinantian (Mississippian) succession of southern Belgium and surrounding areas: stratigraphy improvement and inferred climate reconstruction. Geologica Belgica, 19, 177-200.

Poty, E., Hance, L., Lees, A., and Hennebert, M. (2001). Dinantian lithostratigraphic units (Belgium). Geologica Belgica, 4, 69-94. https://popups.uliege.be/1374-8505/index.php?id=1930.

Reijmer, J. J. G., Mulder, T., and Borgomano, J. (2015). Carbonate slopes and gravity deposits. Sedimentary Geology, 317, 1-8.

Reijmer, J. J. G., Palmieri, P., Groen, R., and Floquet, M. (2015). Calciturbidites and calcidebrites: Sea-level variations or tectonic processes?. Sedimentary Geology, 317, 53-70.

Reijmer, J. J., Johan, H., Jaarsma, B., and Boots, R. (2017). Seismic stratigraphy of Dinantian carbonates in the southern Netherlands and northern Belgium. Netherlands Journal of Geosciences, 96, 353-379.

Reith, D. F. H. (2018). Dynamic simulation of a geothermal reservoir, Case study of the Dinantian carbonates in the Californië geothermal wells, Limburg, NL. Master thesis, University of Delft (the Netherlands), 103 pp.

Ronchi, P., Ortenzi, A., Borromeo, O., Claps, M., and Zempolich, W. G. (2010). Depositional setting and diagenetic processes and their impact on the reservoir quality in the late Visean–Bashkirian Kashagan carbonate platform (Pre-Caspian Basin, Kazakhstan). AAPG Bulletin, 94, 1313-1348. https://doi.org/10.1306/01051009130

Rosenbaum, J., and Sheppard, S. M. (1986). An isotopic study of siderites, dolomites and ankerites at high temperatures. Geochimca Cosmochimca Acta, 50, 1147-1150.

Sachse, V. F., Littke, R., Heim, S., Kluth, O., Schober, J., Boutib, L., Jabour, H., Perssen, F., Sindern, S. (2011). Petroleum source rocks of the Tarfaya Basin and adjacent areas, Morocco. Organic Geochemistry, 42, 209-227. https://doi.org/10.1016/j.orggeochem.2010.12.004.

Schofield, K., and Adams, A. E. (1985). Stratigraphy and depositional environments of the Woo Dale Limestones formation (Dinantian), Derbyshire. Proceedings of the Yorkshire Geological Society, 49, 225-233.

Scholle, P. A., Bebout, D. G., and Moore, C. H. (1983). Carbonate Depositional Environments: Tulsa, Oklahoma, AAPG Memoir 33, 704 pp.

Schroot, B. M., Van Bergen, F., Abbink, O. A., David, P., Van Eijs, R., and Veld, H. (2006). Hydrocarbon potential of the Pre-Westphalian in the Netherlands on- and offshore. TNO report NITG 05-155-C, 421 pp.

Simpson, I. P., and Broadhurst, F. M. (1967). A boulder bed at Treak Cliff, North Derbyshire. Proceedings of the Yorkshire Geological Society, 37, 141-151.

Sissingh, W. (2004). Palaeozoic and Mesozoic igneous activity in the Netherlands: A tectonomagmatic review. Geologie En Mijnbouw/Netherlands Journal of Geosciences, 83, 113-134. https://doi.org/10.1017/S0016774600020084

Smit, J., van Wees, J. D., and Cloetingh, S. (2016). The Thor suture zone: From subduction to intraplate basin setting. Geology, 44, 707-710. https://doi.org/10.1130/G37958.1

Smit, J., van Wees, J.-D., and Cloetingh, S. (2018). Early Carboniferous extension in East Avalonia: 350 My record of lithospheric memory. Marine and Petroleum Geology, 92, 1010-1027. https://doi.org/10.1016/j.marpetgeo.2018.01.004

Somerville, I. D. (1979). Minor cyclicity in late Asbian (upper D1) limestone in the Llangollen district of North Wales. Proceedings of the Yorkshire Geological Society, 42, 317-337.

Somerville, I. D., and Strogen, P. (1992). Ramp sedimentation in the Dinantian limestones of the Shannon Trough, Co. Limerick, Ireland. Sedimentary Geology, 79, 59-75.

Sweeney, J. J. and Burnham, A. K. (1990). Evaluation of a Simple Model of Vitrinite Reflectance Based on Chemical Kinetics. AAPG Bulletin, 74, 1559-1570.

Taylor, G. H., Teichmüller, M., Davis, A., Diessel, C. F. K., Littke, R., and Robert, P. (1998). Organic Petrology. Gebr. Borntraeger, Berlin-Stuttgart, 704 pp.

TenVeen, J. H., de Haan, H. B., de Bruin, G., Holleman, N., Schöler, W. (2019). Seismic Interpretation and Depth Conversion of the Dinantian carbonates in the Dutch subsurface (SCAN). Downloadable from www.nlog.nl.

Ter Borgh, M. M., Jaarsma, B., and Rosendaal, E. A. (2019). Structural development of the northern Dutch offshore: Paleozoic to present. Geological Society, London, Special Publications, 471, 115-131.

Total UK. (2007). A Regional Review of the Dinantian Carbonate Play: Southern North Sea and Onshore UK. A report prepared for the UK DBERR, 64 pp.

Trautwein-Bruns, U., Hilgers, C., Becker, S., Urai, J. L., and Kukla, P. A. (2011). Fracture and fault systems characterising the intersection between the Lower Rhine Embayment and the Ardennes-Rhenish Massif – results from the RWTH-1 well, Aachen, Germany. Zeitschrift Der Deutschen Gesellschaft Für Geowissenschaften, 162, 251-275. https://doi.org/10.1127/1860-1804/2011/0162-0251

Ufer, K., Kleeberg, R., Bergmann, J., Curtius, H., and Dohrmann, R. (2008). Refining real structure parameters of disordered layer structures within the rietveld method. Zeitschrift Fur Kristallographie, Supplement, 27, 151-158. https://doi.org/10.1524/zksu.2008.0020

Uffmann, A. K., Littke, R., and Rippen, D. (2012). Mineralogy and geochemistry of Mississippian and lower Pennsylvanian Black Shales at the northern margin of the Variscan Mountain Belt (Germany and Belgium). International Journal of Coal Geology, 103, 92-108.

Vachard, D., Izart, A., and Cozar, P. (2017). Mississippian (middle Tournaisian-late Serpukhovian) lithostratigraphic and tectonosedimentary units of the southeastern Montagne Noire) (Hérault, France). Géologie de la France, N01, 47-88.

Van Adrichem Boogaert, H. A. and Kouwe, W. F. P. (1994). Stratigraphic nomenclature of the Netherlands; revision and update by RGD and NOGEPA, Section B, Devonian and Dinantian, Mededelingen Rijks Geologische Dienst, 50 pp.

Van Balen, R. T., Van Bergen, F., De Leeuw, C., Pagnier, H., Simmelink, E., Van Wees, J.-D., and Verweij, H. (2000). Modelling the evolution of hydrocarbon systems in the inverted West Netherlands Basin, the Netherlands. Journal of Geochemical Exploration, 69-70, 685-688. https://doi.org/10.1016/S0375-6742(00)00110-2

Van Bergen, M. J., and Sissingh, W. (2007). Magmatism in the Netherlands: expression of the north-west European rifting history. In: Wong, T. E., Batjes, D. A. J., and de Jager, J. (eds), Geology of the Netherlands. Royal Netherlands Academy of Arts and Sciences, 197-221.

Van den Haute, P., and Vercoutere, C. (1990). Apatite fission-track evidences for a Mesozoic uplift of the Brabant massif: preliminary results. Annales de La Société Géologique de Belgique, 112, 443-452.

Van den Kerkhof, A. M., and Hein, U. F. (2001). Fluid inclusion petrography. Lithos, 55, 27-47. https://doi.org/10.1016/S0024-4937(00)00037-2

Van der Kooij, B., Immenhauser, A., Steuber, T., Hagmaier, M., Bahamonde, J. R., Samankassou, E., and Merino Tomé, O. (2007). Marine Red Staining of a Pennsylvanian Carbonate Slope: Environmental and Oceanographic Significance. Journal of Sedimentary Research, 77, 1026-1045.

Van der Kooij, B., Immenhauser, A., Csoma, A., J., B., and Steuber, T. (2009). Spatial geochemistry of a Carboniferous platform-margin-to-basin transect: Balancing environmental and diagenetic factors: Sedimentary Geology, 219, 136-150.

Van der Kooij, B., Immenhauser, A., Steuber, T., Rionda, J. R. B., and Tome, O. M. (2010). Controlling factors of volumetrically important marine carbonate cementation in deep slope settings: Sedimentology, 57, 1491-1525.

Van Hulten, F. F. N. (2012). Devono-carboniferous carbonate platform systems of the Netherlands. Geologica Belgica, 15, 284-296.

Van Steenwinkel, M. (1990). Sequence stratigraphy from 'spot' outcrops – example from carbonate dominated setting: Devonian-Carboniferous transition, Dinant synclinorium (Belgium). Sedimentary Geology, 69, 259-280.

Vandenberghe, N., Poggiagliomi, E., and Watts, G. (1986). Offset-dependent seismic amplitudes from karst limestone in northern Belgium. First Break, 4, 9-27.

Vandenberghe, N., Dusar, M., Laga, P., and Bouckaert, J. (1988). The Meer well in North Belgium. Mémoires Pour Servir à l Explication des Cartes Géologiques et Minières de La Belgique, 25, 29.

Vandenberghe, N., Dusar, M., Boonen, P., Fan, L. S., Voets, R., and Bouckaert, J. (2000). The Merksplas-Beerse geothermal well (17W265) and the Dinantian reservoir. Geologica Belgica, 3, 349-367. https://doi.org/10.1146/annurev-lawsocsci-120814-121449

Vercoutere, C., and Van Den Haute, P. (1993). Post-Palaeozoic cooling and uplift of the Brabant Massif as revealed by apatite fission track analysis. Geological Magazine, 130, 639-646. https://doi.org/10.1017/S001675680002094X

Vogel, K., Muchez, P., and Viane, W. (1990). Collapse breccias and sedimentary conglomerates in the lower Visean of the Vesdre area (E Belgium). Annales de la Société Géologique de Belgique, 113, 359-371.

Walkden, G. M., and Davies, J. R. (1983). Polyphase erosion of subaerial omission surfaces in the late Diantian of Naglesey, North Wales. Sedimentology, 30, 861-878.

Walkden, G. M., and Williams, D. O. (1991). The diagenesis of the late Dinantian Derbyshire-East Midland carbonate shelf, central England: Sedimentology, 38, 643-670.

Ward, J. (1997). Early Dinantian evaporites of the Easton-1 well, Solway Basin, onshore Cumbrian, England. In: Meadows, N.S., Trueblood, S.P., Hardman, M., and Cowan, G. (eds), Petroleum Geology of the Irish Sea and adjacent areas. Geological Society Special Publication, 124, 277-296.

Waters, C. N., Browne, M. A. E., Dean, M. T., and Powell, J. H. (2007). Lithostratigraphic framework for Carboniferous succession of Great Britain (onshore). British Geological Survey Research Report, RR/07/01.

Weber, L. J., Francis, B. P., Harris, P. M., and Clark, M. (2003). Stratigraphy, lithofacies and reservoir distribution, Tengiz field, Kazakhstan. AAPG Memoir, 83, 351-394. https://doi.org/10.2110/pec.03.78

Wright, V. P. (1982). The recognition and interpretation of palaeokarsts: two examples from the Lower Carboniferous of South Wales. Journal of Sedimentary Petrology, 52, 83-94.

Wright, V. P. (1986). Facies sequences on a carbonate ramp: the Carboniferous of South Wales. Sedimentology, 33, 221-241.

Wright, V. P. (1987). The ecology of two early Carboniferous palaeosols. In: Miller, J., Adams, A. E., and Wright, V. P. (eds), European Dinantian Environments, 345-358.

Wygrala, B. P. (1991). Final Report. 1-D Modeling Study (Well O18-1). Report for Placid Oil. Juelich.

Yao, L., Aretz, M., Chen, J., Webb, G. E., and Wang, X. (2016). Global microbial carbonate proliferation after the end Devonian mass extinction: mainly controlled by the demise of skeletal bioconstructor. Scientific Reports, www.nature.com/scientificreports

Ziegler, P. A. (1988). Late Carboniferous to Permian Evolution of Arctic Basins, The Norwegian-Greenland Sea Rift and Permian Basins of West and Central Europe. AAPG Memoir, 43, 33-42. https://doi.org/10.1306/M43478C4

Ziegler, P. A. (1990). Geological Atlas of Western and Central Europe, 2nd edition. Geological Society Publishing House (Bath), 239 pp.

8. Appendix

The appendices, except for the confidential reports, are available via www.nlog.nl.

Appendix A:
1- Facies analysis and diagenetic evolution of the Dinantian carbonates in the Dutch subsurface: data and analyses well BHG-01
2- Facies analysis and diagenetic evolution of the Dinantian carbonates in the Dutch subsurface: data and analyses wells CAL-GT-01, 02, 03
3- Facies analysis and diagenetic evolution of the Dinantian carbonates in the Dutch subsurface: data and analyses well GVK-01
4- Facies analysis and diagenetic evolution of the Dinantian carbonates in the Dutch subsurface: data and analyses wells HEU-01 and HEU-01-S1
5- Facies analysis and diagenetic evolution of the Dinantian carbonates in the Dutch subsurface: data and analyses well KSL-DB123
6- Facies analysis and diagenetic evolution of the Dinantian carbonates in the Dutch subsurface: data and analyses well KSL-02
7- Facies analysis and diagenetic evolution of the Dinantian carbonates in the Dutch subsurface: data and analyses well KTG-01
8- Facies analysis and diagenetic evolution of the Dinantian carbonates in the Dutch subsurface: data and analyses well LTG-01
9- Facies analysis and diagenetic evolution of the Dinantian carbonates in the Dutch subsurface: data and analyses well MOL-GT-01 (confidential)
10- Facies analysis and diagenetic evolution of the Dinantian carbonates in the Dutch subsurface: data and analyses well Münsterland-1 (confidential)
11- Facies analysis and diagenetic evolution of the Dinantian carbonates in the Dutch subsurface: data and analyses well O18-01
12- Facies analysis and diagenetic evolution of the Dinantian carbonates in the Dutch subsurface: data and analyses well S02-02
13- Facies analysis and diagenetic evolution of the Dinantian carbonates in the Dutch subsurface: data and analyses well S05-01
14- Facies analysis and diagenetic evolution of the Dinantian carbonates in the Dutch subsurface: data and analyses well UHM-02
15- Facies analysis and diagenetic evolution of the Dinantian carbonates in the Dutch subsurface: data and analyses well WSK-01

Appendix B:

1- BHG-01 core log (Core 1)
2- BHG-01 core log (Core 2)
3- HEU-01 core log
4- HEU-01-S1 core log
5- KSL-02 core log
6- KTG-01 core log
7- LTG-01 core log (Core 1)
8- LTG-01 core log (Core 2)
9- O18-01 core log (Cores 3 and 4)
10- O18-01 core log (Core 5)
11- O18-01 core log (Core 6)
12- O18-01 core log (Core 7)
13- S02-02 core log (Cores 1 and 2)

14- S02-02 core log (Cores 3 and 4)
15- UHM-02 core log
16- WSK-01 core log

Appendix C:

Regional correlation: Includes the depositional cycles and regional correlation of the studied Dinantian wells

This page intentionally left blank

Onderzoek in de ondergrond voor aardwarmte